On the Performance of Free-Space Optical Systems over Generalized Atmospheric Turbulence Channels with Pointing Errors

Thesis by

Imran Shafique Ansari, B.Sc., M.Sc.

In Partial Fulfillment of the Requirements

For the Degree of

Doctor of Philosophy

(Electrical Engineering Program)

Division of Computer, Electrical, and Mathematical Sciences and Engineering

(CEMSE)

King Abdullah University of Science and Technology (KAUST)

Thuwal, Makkah Province, Kingdom of Saudi Arabia

February, 2015

The thesis of Imran Shafique Ansari is approved by the examination committee

Committee Chairperson: Prof. Mohamed-Slim Alouini

Committee Member: Prof. Moe. Z. Win

Committee Member: Prof. Boon S. Ooi

Committee Member: Dr. Basem Shihada

Committee Member: Dr. Tareq Al-Naffouri

King Abdullah University of Science and Technology

2015

ABSTRACT

On the Performance of Free-Space Optical Systems over Generalized Atmospheric Turbulence Channels with Pointing Errors

Imran Shafique Ansari

Generalized fading has been an imminent part and parcel of wireless communications. It not only characterizes the wireless channel appropriately but also allows its utilization for further performance analysis of various types of wireless communication systems. Under the umbrella of generalized fading channels, a unified performance analysis of a free-space optical (FSO) link over the Málaga ($\mathcal{M}$) atmospheric turbulence channel that accounts for pointing errors and both types of detection techniques (i.e. indirect modulation/direct detection (IM/DD) as well as heterodyne detection) is presented. Specifically, unified exact closed-form expressions for the probability density function (PDF), the cumulative distribution function (CDF), the moment generating function (MGF), and the moments of the end-to-end signal-to-noise ratio (SNR) of a single link FSO transmission system are presented, all in terms of the Meijer's G function except for the moments that is in terms of simple elementary functions. Then capitalizing on these unified results, unified exact closed-form expressions for various performance metrics of FSO link transmission systems are of-

fered, such as, the outage probability (OP), the higher-order amount of fading (AF), the average error rate for binary and M-ary modulation schemes, and the ergodic capacity (except for IM/DD technique, where closed-form lower bound results are presented), all in terms of Meijer's G functions except for the higher-order AF that is in terms of simple elementary functions. Additionally, the asymptotic results are derived for all the expressions derived earlier in terms of the Meijer's G function in the high SNR regime in terms of simple elementary functions via an asymptotic expansion of the Meijer's G function. Furthermore, new asymptotic expressions for the ergodic capacity in the low as well as high SNR regimes are derived in terms of simple elementary functions via utilizing moments. All the presented results are verified via computer-based Monte-Carlo simulations.

Besides addressing the pointing errors with zero boresight effects as has been addressed above, a unified capacity analysis of a FSO link that accounts for nonzero boresight pointing errors and both types of detection techniques (i.e. heterodyne detection as well as IM/DD) is also addressed. Specifically, an exact closed-form expression for the moments of the end-to-end SNR of a single link FSO transmission system is presented in terms of well-known elementary functions. Capitalizing on these new moments expressions, approximate and simple closed-form results for the ergodic capacity at high and low SNR regimes are derived for lognormal (LN), Rician-LN (RLN), and $\mathcal{M}$ atmospheric turbulences. All the presented results are verified via computer-based Monte-Carlo simulations.

Based on the fact that FSO links are cost-effective, license-free, and can provide even higher bandwidths compared to the traditional radio-frequency (RF) links, the performance analysis of a dual-hop relay system composed of asymmetric RF and FSO links is presented. This is complemented by the performance analysis of a dual-branch transmission system composed of a direct RF link and a dual-hop relay composed of asymmetric RF and FSO links. The performance of the later scenario

is evaluated under the assumption of the selection combining (SC) diversity and the maximal ratio combining (MRC) schemes. RF links are modeled by Rayleigh fading distribution whereas the FSO link is modeled by a unified GG fading distribution. More specifically, in this work, new exact closed-form expressions for the PDF, the CDF, the MGF, and the moments of the end-to-end SNR are derived. Capitalizing on these results, new exact closed-form expressions for the OP, the higher-order AF, the average error rate for binary and M-ary modulation schemes, and the ergodic capacity are offered.

Cognitive radio networks (CRN) have also proved to improve the performance of wireless communication systems and hence based on this, the hybrid system analyzed above is extended with CRN technology wherein the outage and error performance analysis of a dual-hop transmission system composed of asymmetric RF channel cascaded with a FSO link is presented. For the RF link, an underlay cognitive network is considered where the secondary users share the spectrum with licensed primary users. Indoor femtocells act as a practical example for such networks. Specifically, it is assumed that the RF link applies power control to maintain the interference at the primary network below a predetermined threshold. While the RF channel is modeled by the Rayleigh fading distribution, the FSO link is modeled by a unified Gamma-Gamma turbulence distribution. The FSO link accounts for pointing errors and both types of detection techniques (i.e. heterodyne detection as well as IM/DD). With this model, a new exact closed-form expression is derived for the OP and the error rate of the end-to-end SNR of these systems in terms of the Meijer's G function and the Fox's H functions under amplify-and-forward relay schemes. All new analytical results are verified via computer-based Monte-Carlo simulations and are illustrated by some selected numerical results.

ACKNOWLEDGMENTS

I would like to sincerely thank my supervisor Prof. Mohamed-Slim Alouini for his continuous guidance and encouragement throughout the course of this work. His enthusiasm and valuable feedback for research made my study very enjoyable and exciting and ultimately fruitful with rich experience. I would also like to thank him for providing me with an amazing research environment.

I would also like to thank Dr. Ferkan Yilmaz, Vodafone Technology in Turkey, for his great technical support. He has been there to support me in almost every hurdle during this journey and encourage and motivate me to get the work done with excellence and ahead of time.

I thank my parents for their continuous encouragement and my daughter, my wife, and my siblings for bearing with me for my negligence towards them during this journey and their deep moral support at all times.

Additionally, I would like to thank Prof. Alouini's research group members i.e. the inhabitants of Building 1, Level 3, 3139 area cubicles for making the environment very research friendly and exciting to work.

Lastly, I would like to thank the people at KAUST, Thuwal, Makkah Province, Saudi Arabia for providing support and resources for this research work.

TABLE OF CONTENTS

NOMENCLATURE

ACRONYMS

Symbol	Meaning
AF	Amount of fading
AWGN	Additive white Gaussian noise
BER	Bit error rate
CBFSK	Coherent binary frequency shift keying
CBPSK	Coherent binary phase shift keying
DBPSK	Differential binary phase shift keying
CDF	Cumulative distribution function
CEP	Conditional error probability
CF	Characteristic function
CSI	Channel state information
EC	Ergodic capacity
EGBMGF	Extended generalized bivariate Meijer's G function
EGC	Equal-gain combining
GK	Generalized-K
i.n.i.d.	Independent and non-identically distributed
i.i.d.	Independent and identically distributed
LOS	Line of sight
NBFSK	Non-coherent binary frequency shift keying
NLOS	Non-line of sight
MGF	Moment generating function
MIMO	Multiple-input multiple-output
MISO	Multiple-input single-output
MRC	Maximal ratio combining
OP	Outage probability
PDF	Probability density function
RV	Random variable
SC	Selection combining
SIMO	Single-input multiple-output
SISO	Single-input single-output
SNR	Signal-to-noise ratio
SER	Symbol error rate
TIMO	Two-input multiple-output

LIST OF SYMBOLS

Symbol	Meaning
$\overline{P}_b$	Average bit error rate (BER)
$\overline{P}_s$	Average symbol error rate (SER)
$\overline{C}$	Ergodic channel capacity
γ	Instantaneous power
$\Gamma(\cdot)$	Gamma function
${}_pF_q$	The generalized hypergeometric function for integers p and q
K_m	The modified Bessel function of second kind and order m
$\mathrm{H}_{p,q}^{m,n}$	The Fox's H function with parameters m, n, p, and q
$\bar{\mathrm{H}}_{p,q}^{m,n}$	The Fox's $\bar{\mathrm{H}}$ function with parameters m, n, p, and q
$\hat{\mathrm{H}}_{p,q}^{m,n}$	The extended Fox's $\bar{\mathrm{H}}$ ($\hat{\mathrm{H}}$) function with parameters m, n, p, and q
$\mathrm{G}_{p,q}^{m,n}$	The Meijer's G function with parameters m, n, p, and q
$\mathrm{S}[\cdot]$	The extended generalized bivariate Meijer's G function
$\mathrm{G}_{p_1,q_1:p_2,q_2:p_3,q_3}^{m_1,n_1:m_2,n_2:m_3,n_3}$	The extended generalized bivariate Meijer's G function with parameters m_1, n_1, m_2, n_2, m_3, n_3, p_1, q_1, p_2, q_2, p_3, and q_3
$\mathrm{H}_{p_1,q_1:p_2,q_2:p_3,q_3}^{m_1,n_1:m_2,n_2:m_3,n_3}$	The extended generalized bivariate Fox's H function with parameters m_1, n_1, m_2, n_2, m_3, n_3, p_1, q_1, p_2, q_2, p_3, and q_3

List of Figures

List of Tables

Chapter 1

Introduction

1.1 Wireless Communications

1.1.1 Wireless Channel Modeling and Various Diversity Schemes

Wireless communication is driven via a complicated phenomenon termed as radio-wave propagation. It is characterized by multiple effects including multipath fading and shadowing. The statistical behaviour of these effects is characterized by different turbulence models depending on the nature of the communication environment [1]. It is important to study such effects to encompass the practicality concern of the currently available turbulence channel models and beyond. Hence, it becomes very evident and attractive to study large-scale fading alongside small-scale fading as the multi-hop relay networks are emerging in the current times. The geographically distributed nodes experience different multipath fading and shadowing statistics [1]. Hence, modeling composite fading turbulence channels, where the multipath fading and shadowing are modeled together, is essential for the performance analysis of various communication systems.

The signal transmitted via the wireless channel mainly experiences three impair-

ments (i) pathloss, (ii) shadowing, and (iii) fading.

Pathloss

Pathloss is a large scale propagation effect and it characterizes the variation in the power of the transmitted signal over large distances [2]. Pathloss is a deterministic quantity and is usually modeled as a function of distance d. The general model for pathloss is $PL \propto d^{-\alpha}$, where α is the path loss exponent [2]. The signal power diminishes rapidly due to pathloss.

Shadowing

Another large scale propagation effect experienced by the signal is called shadowing and is caused by large obstructions. A common model used for shadowing is the log-normal shadowing model in which the received power at the receiver is assumed to be random with a log-normal distribution [2].

When a signal is transmitted in a wireless channel, multiple copies of the signal are received at the destination due to reflection and scattering. These multiple copies add constructively and destructively to cause abrupt variation in signal power. This rapid fluctuation of the signal power in a wireless channel is termed as fading [2].

Fading

Fading is a random phenomena and various random distributions have been proposed to model the effect of fading [3]. For example, in a multiple scattering environment, the fading envelop is modeled using Rayleigh distribution. If there exist a line of sight path from the transmitter to the receiver, Rician distribution is used to model fading. Various other distributions used for modelling fading are discussed in [3]. Fading can be further classified into following types:

- *Fast Fading:* In fast fading, the channel fading realization changes rapidly and varies from symbol to symbol.

- *Slow Fading:* In slow fading, the channel fading realization does not change rapidly and is constant over multiple symbols.

Fading greatly degrades the performance of the wireless communication systems. For example, in an additive white Gaussian noise (AWGN) channel for binary phase shift keying (BPSK), the error probability decreases exponentially with increasing transmit power. Thus, for fading channels a large amount of additional power is required to get the error rate performance of the AWGN channel.

1.1.2 Diversity Systems

In wireless systems, the base-stations (BSs) or access points communicate with small low power terminals. These terminals may be limited to a single transmit chain due to power complexity constraints [4]. On the other hand, multiple transmit and receive antenna systems i.e. Multiple-Input-Multiple-Output (MIMO) systems offer substantial performance improvement in wireless systems. This is possible by increasing their spectral efficiency and/or by reducing the effects of the channel impairments [5]. Additionally, one of the simplest and most efficient techniques to overcome the destructive effects of turbulence in wireless communication systems is diversity [4]. In this, the receiver processes the obtained diversity signals in such a way that maximizes the system's power efficiency. There are several diversity techniques such as equal-gain combining (EGC), maximal ratio combining (MRC), selection combining (SC), and a combination of MRC and SC referred to as generalized selection combining (GSC) among others.

An approach to overcome the severe effect of fading is to send multiple copies of the signal over the wireless channel such that each copy of the signal experiences

independent fading. The idea is that it is improbable that multiple independent paths experience deep fades at the same time. This technique is called diversity. Diversity can be achieved by multiple ways [2].

- *Time Diversity:* As the wireless channel is time varying, a simple technique to achieve diversity is to transmit the signal over multiple time slots where each time slot experiences independent fading i.e. the signal is transmitted in time slots separated by time greater than the coherence time of the channel.

- *Frequency Diversity:* Diversity can also be achieved by transmitting the same signal over different carrier frequencies that are separated by more than the coherence bandwidth of the channel and thus experience independent fading. This is termed as frequency diversity.

- *Space Diversity:* Diversity can also be achieved in space by transmitting the multiple copies of the signal using multiple antennas where each antenna experiences independent fading.

The multiple copies of the signal sent by the transmitter can be combined in various ways [3]. Some of the combining schemes that have been proposed are

- *Maximum Ratio Combining:* The received signals are combined after weighting the received copies proportional to the amplitude of the fading realization of the channel and compensating the phase.

- *Equal Gain Combining:* The received signals are combined after giving all the received copies equal weight and compensating the phase.

- *Selection Combining:* The signal with the maximum channel fading amplitude is selected.

In recent times, different diversity schemes have marked an important impact in the arena of wireless communication systems. The main reason behind this is that these different diversity schemes allow for multiple transmission and/or reception paths for the same signal [3, 6–8]. One of the optimal diversity combining scheme is the MRC diversity scheme where all the diversity branches are processed to obtain the best possible devised and improved single output that possibly stays above a certain specified threshold [3, 9, 10]. This results into extensive occurrence of the statistical distribution of the sum of squared envelopes of faded signals in several wireless communication systems [11]. Additionally, wireless communications are driven by a complicated phenomenon known as radio-wave propagation that is characterized by various effects such as fading, shadowing, and path-loss. The statistical behavior of these effects is described by different models depending on the nature of the communication environment.

1.1.3 Cooperative Relaying Technology

Utilizing mobile terminals as relay stations is an interesting concept that is emerging as a feasible option for overcoming the problems of the next generation wireless networks. There can be two relaying systems in broad sense: conventional relaying systems that use relays as pure forwarders whereas cooperative relays that tackle the fundamental features of wireless medium i.e. its broadcast nature, and its ability to provide independent channels [12]. Hence, this concept allows achievement of diversity. Cooperative networks benefit from the broadcast nature since once a signal is transmitted, it can be received and usefully forwarded via multiple terminals. Nevertheless, whichever type of relaying system one employs; it encompasses the concept of multiple scattering radio propagation channels [1]. This has been proved useful in many scientific fields of communications and it fits many propagation scenarios from the recent past.

The classical relay channel model has been around since the 1960ś [13, 14]. However, due to practical constraints little work was carried out on relays until recently [15–17]. Advances in wireless communications technology has now rekindled interest in cooperative relays. Cooperative relaying exploits spatial diversity by employing antennas distributed over multiple terminals. Hence, each terminal can have less number of antennas and less number of radio frequency (RF) chains. These terminals combined act as a distributed MIMO system [18].

In a cooperative relay system, a terminal called a relay receives information from the source, processes the information and then forwards it to the intended destination. In addition to achieving cooperative diversity, relays also provide the benefit of increasing coverage area [19]. There are two main types of relays found in literature [17]:

• *Amplify-and-Forward:* These relays first amplify the signal received from the source and then forward it to the destination. The advantage of amplify-and-forward relays is that they are simple to implement. However, the drawback of these relays is that they cannot detect errors in the received signal.

• *Decode-and-Forward:* These relays first decode the received signal. Then they re-encode the signal after which it is forwarded to the destination. As the relay decodes the signal, it can detect errors present in the signal. However, this comes at the cost of added complexity and it can be difficult to incorporate this in to relays that usually need to be simple and inexpensive.

Due to their low cost and ease of implementation, amplify-and-forward relays are commonly used in literature. They are currently used in signal repeaters [20]. Amplify-and-forward relays can be further sub-divided into two types:

• *Fixed Gain [21]:* The relay gain of these types of amplify-and-forward relays is set at the beginning of data transmission and does not change with time and channel conditions.

• *Variable Gain [22]:* The relay gain of these types of amplify-and-forward relays depends on the channel response of the source (S)-relay (R) link. As the channel response of the S-R link changes, so does the relay gain.

1.2 Free-Space Optics (FSO)

1.2.1 General Background

Wireless communication has taken a prime spot in our daily lives and at times it does gives us a feel of being a basic commodity of our life but wireless communication is a technology that has its own limits. As wireless communication continues to take such an essential space in our daily lives, the prime resource that successfully allows wireless communication to exist is reaching its limits, also termed as spectrum scarcity. Hence, spectrum scarcity has been the primary concern in the current times when the discussion falls in the arena of wireless communications. To overcome this issue, many possible solutions have been proposed and have been successful within their own limits and challenges. Some of the possible solutions include the cognitive radio network (CRN) technology and free-space optical (FSO) technology among others.

FSO communication has recently gained a growing interest for both commercial and military applications [23, 24]. Similar to fiber, FSO transmits data in form of a small conical shaped beam by means of low powered laser or light-emitting diode (LED) in Terahertz spectrum [25, 26]. Instead of enclosing the data stream in a glass fiber, it is transmitted through the air and it operates in near infrared (IR) band. FSO is all-optical, unlike the well-known RF wireless systems. So, one gets the speed of a fiber without the substantial costs of digging up sidewalks to install a fiber link. This technology does not require government licensing for installation [26]. It can be readily deployed as soon as the line-of-sight (LOS) link between the laser and the receiver becomes available. This implies no hassles, no backlog, and no intermediary

devices to the fiber backbone.

FSO becomes attractive technology where fiber installation and the right of way are very expensive. FSO addresses applications like metropolitan networks, inter-building communication, backhaul wireless systems, in-door links, fiber backup, service acceleration, security, military purposes, and satellite communications, etc. For deep space probes and inter-satellite communication, FSO is an excellent candidate because of the low loss links and small size antennas [26–33]. Commercial products are available for a data bandwidth of 100M up to 2.5Gbps. Furthermore, it is expected that this technology will observe fast growth in terms of number of wavelengths sharing the same space path [34]. It is expected to grow to hundreds of wavelengths per FSO transponder (transmitter and receiver). Future developments of this technology will potentially reach the tens of Terabit/sec range.

Since FSO link can be easily installed within 24 hours or less, there is a growing interest in military and homeland security applications. It is very practical to connect remote non-permanent sites, borders control and surveillance sites, difficult terrains, and battlefields with very high bandwidth links. In addition, FSO is rapidly becoming an important component in governments and large corporation's disaster recovery plans [35]. Furthermore, FSO is also getting a growing market share in active imaging and remote sensing applications [36]. These applications are particularly attractive for defense and homeland security. Moreover, there is a recent growing interest to exploit FSO in military and difficult terrain mobile networks despite the LOS stringent challenge [26]. Indeed the deployment of ubiquitous wireless commercial communications results in regulatory pressure and the spectrum available for military use is decreasing. Military applications need communication system with higher capacity because they need to exchange huge amount of voice, video, and data. In effect, new age wars and conflicts require a real time transfer of huge information directly from the field to center of command. Naval communications is also another potential

market for FSO communication technology [23].

For the past decade, there has been an increasing interest in FSO or terrestrial optical wireless communication systems due to their various characteristics. These include higher bandwidth and higher capacity relative to the traditional RF communication systems. In addition, FSO links are license-free and hence are cost-effective relative to the traditional RF links. FSO is a promising technology as it offers full-duplex Gigabit Ethernet throughput in certain applications and environment, ultimately offering a huge license-free spectrum, immunity to interference, and high security [25]. These features of FSO communication systems potentially enable solving the issues that the RF communication systems face due to the expensive and scarce spectrum. Additionally, advanced research and development (R&D) lab prototypes demonstrated the feasibility of up to 1.28 Terabits per second [8]. With the correct setup, much higher speeds may be possible as the approach utilizes multiple wavelengths acting like separate channels. Hence, in this concept, the signals are sent down a fibre and launched through the air (known as FSO) and then they travel through a lens before ending up back in fibre. Besides these nice characteristic features of FSO communication systems, over long distances of 1Km or longer, the atmospheric turbulence may lead to a significant degradation in the performance of the FSO communication systems [4, 12, 37–41].

Although there are many advantages of using FSO, the optical free space is affected by weather and atmospheric losses along the propagation path. This includes rain, dust particles, fog, snow, fading due to turbulence, etc. (see Fig. 1.1) [26, 42]. Fading might lead to short-term outages for a few milliseconds. These are caused by atmospheric turbulence-induced fading. It might also lead to long-term outages up to duration of a few seconds usually caused by LOS obstructions or pointing errors [42]. To mitigate these effects, various different approaches have been presented. They include physical and higher layer techniques. At the physical layer, forward er-

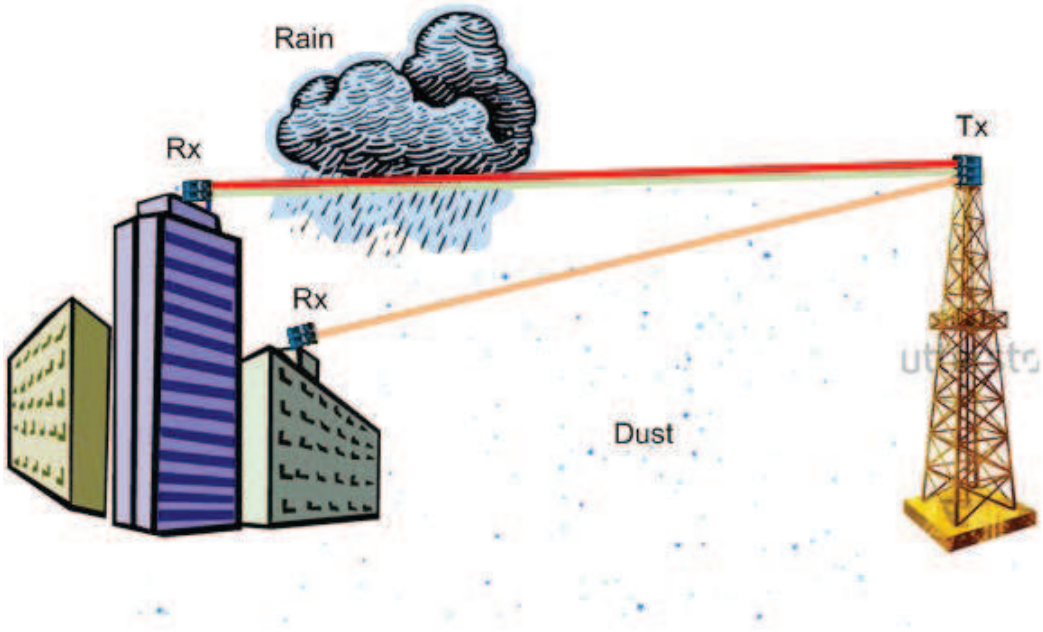

Figure 1.1: Environmental effects on a FSO system.

ror correction (FEC), dynamic thresholding, and time delayed diversity (TDD) have been proved to be acceptable solutions [42]. At higher layers, FEC has also been demonstrated to be a possible solution although it imposes a penalty on the channel throughput. For duplex communications, automatic repeat request (ARQ) protocols are proposed to be a more efficient solution [43]. Moreover, spatial diversity and channel coding are used to obtain improved performance over the turbulent link. An appropriate method that will reduce the probability of error for FSO communication system is Alamouti space time coding [44, 45]. MIMO techniques have gained more interest as means of combating turbulence and leveraging the performance of FSO links [46, 47].

Moreover, thermal expansion, dynamic wind loads, and weak earthquakes lead to the building sway phenomenon that causes vibration of the transmitter beam. This ultimately leads to a misalignment between the transmitter and the receiver termed as pointing error. These pointing errors may lead to additional performance degra-

dation and are a serious issue in urban areas, where the FSO equipment's are placed on high-rise buildings [48–50]. Furthermore, it is important to know that indirect modulation/direct detection (IM/DD) is the main mode of detection in FSO systems but coherent communications have also been proposed as an alternative detection mode. Heterodyne detection is a more complicated detection method though it has the ability to better overcome various turbulence effects (see [51, 52] and references therein).

1.2.2 Asymmetric RF-Free-Space Optical (FSO) Dual-Hop Communication Systems

For the past decade, FSO or optical wireless communication (OWC) systems have gained an increasing interest due to its various characteristics including higher bandwidth and higher capacity compared to the traditional RF communication systems. In addition, FSO links are license-free and hence are cost-effective relative to the traditional RF links. It is a promising technology as it offers full-duplex Gigabit Ethernet throughput in certain applications and environment offering a huge license-free spectrum, immunity to interference, and high security [37]. These features of FSO communication systems potentially enable solving the issues that the RF communication systems face due to the expensive and scarce spectrum [4, 12, 37–41]. Besides these nice characteristic features of FSO communication systems, over long distances of 1Km or longer, the atmospheric turbulence may lead to a significant degradation in the performance of the FSO communication systems [38]. Hence, as proposed in [53], a relaying system based on both FSO as well as RF characteristics can be expected to be more adaptive and constitute an effective communication system in a real-life environment.

Keeping RF as the prime band for transmission for the end users and combining

the channel modeling experience with a relatively newer technology i.e. utilizing laser light for fulfilling the purpose of data transmission, commonly termed as FSO communications and/or OWC, through the network to the internet back-haul/destination improves the system performance manifolds.

1.2.3 Cognitive Radio Networks (CRN) with FSO

Cognitive radio network (CRN) has been proposed as a promising solution for efficient utilization of the RF spectrum. A practical example for such networks are indoor femto-cells where the users are allowed to deploy femto BSs that have the capability to share the spectrum with macro-cell users. Such networks have proved to improve the performance of indoor users in terms of capacity [54].

The spectrum usage by cognitive (secondary) users is generally governed by the following three approaches (see [55] and references cited therein).

- *Interweave CRNs* wherein the primary and the secondary users are not allowed to operate simultaneously i.e. only when the primary users (PUs) are in idle mode, the secondary users (SUs) are allowed to access the spectrum.

- *Underlay CRNs* wherein the PUs are allocated a higher priority over the SUs in terms of spectrum usage. Hence, the PUs and SUs are allowed to coexist as long as the power of the SUs signals at the PUs receivers do not exceed a predefined interference threshold known also as interference temperature (IT).

- *Overlay CRNs* wherein PUs and SUs transmit concurrently with the assistance of advanced coding techniques.

Based on the benefits of CRN technology, it will be useful to combine the CRN technology with this asymmetric RF-FSO transmission system to give a chance of further overcoming the issue of spectrum scarcity.

1.3 Objectives and Contributions

The main objective of this thesis is to present advances in the field of FSO communications. This thesis presents advancement in FSO communications via utilizing other technologies along with the FSO technology to improve the performance of wireless communication systems.

The remainder of the thesis is organized as follows. Chapter 2 talks about FSO and its characteristics in brief followed by analyzing the performance of single FSO links over both types of detection techniques (i.e. heterodyne detection technique as well as IM/DD technique) in a unified fashion. This is followed by performing ergodic capacity analysis of various atmospheric turbulence models in composition with nonzero boresight pointing errors in Chapter 3 wherein it is proved that utilizing nonzero boresight pointing errors is a quite a challenge to analyze various FSO communication system.

Utilizing the single link analysis presented in Chapter 2, asymmetric RF-FSO and hybrid RF/RF-FSO transmission systems are introduced in Chapter 4. Specifically, Chapter 4 introduces the FSO channel model inclusive of zero boresight pointing errors in brief and presents the motivation behind employing such a mixed RF-FSO transmission systems followed by performance analysis of a mixed or an asymmetric RF-FSO dual-hop transmission system is presented. Chapter 4 also discusses the possibility of implementing diversity schemes on such an asymmetric RF-FSO transmission system along with a direct RF link in operation too. The performance analysis displayed is impressive and conforms with the characteristic features of a diverse system. It is important to note here that all the study performed on mixed or asymmetric RF-FSO and/or hybrid RF/RF-FSO transmission systems is done under amplify-and-forward relay schemes. Both types of amplify-and-forward scheme are employed i.e. fixed gain as well as variable gain.

Another development to the asymmetric RF-FSO transmission system is proposed

in Chapter 5 that includes the CRN technology. Specifically, the RF end is considered to be operating under the CRN technology followed by the FSO hop with the help of a relay. Similar analysis has been performed to such a transmission system as was tackled in Chapter 4 above.

Hence, the contributions of this thesis unfolds in the following streams:

- Unified performance analysis of FSO links over Málaga ($\mathcal{M}$) atmospheric turbulence channels with pointing errors.
- Ergodic capacity analysis of FSO links with nonzero boresight pointing errors.
- Performance analysis of asymmetric RF-FSO dual-hop and hybrid RF/RF-FSO transmission systems along with the impact of pointing errors on such systems.
- Performance analysis of underlay cognitive RF and FSO wireless channels.

As a summary, the flow-chart of this thesis is given in Fig. 1.2.

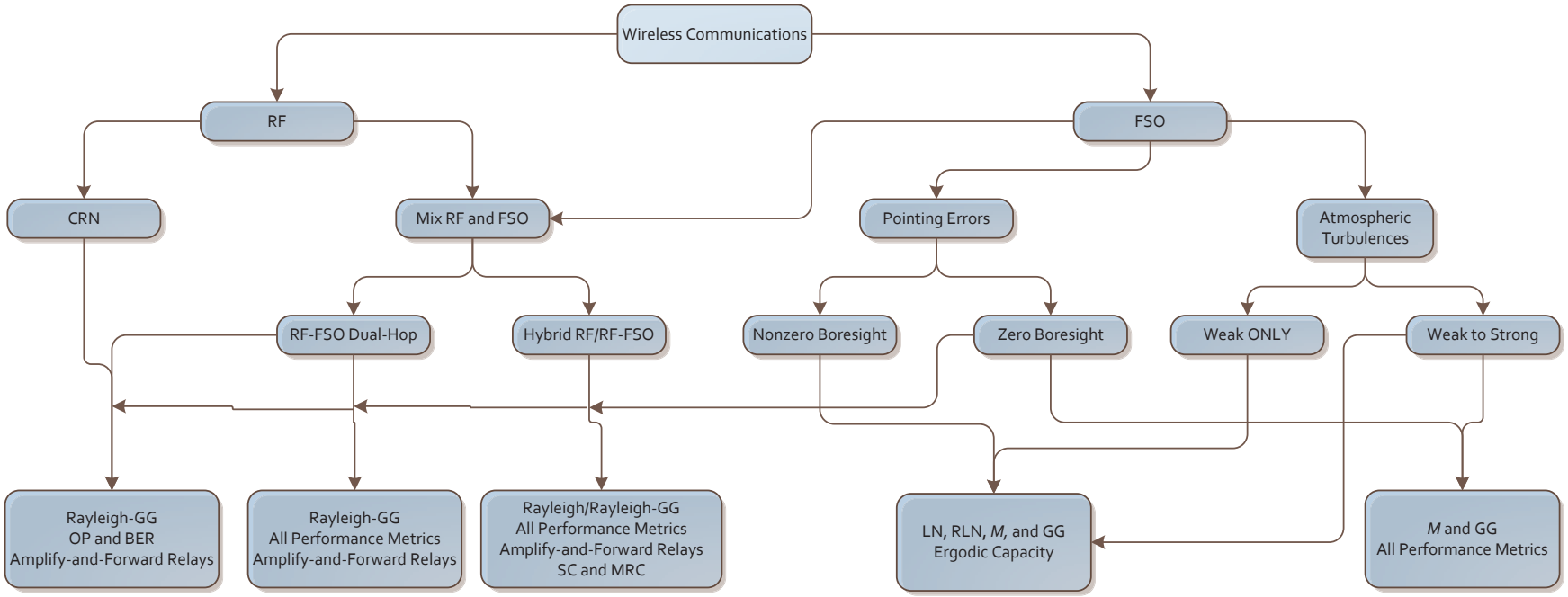

Figure 1.2: Thesis flow-chart.

Chapter 2

Performance Analysis of Free-Space Optical Links Over Málaga ($\mathcal{M}$) Turbulence Channels with Pointing Errors

2.1 Introduction

2.1.1 Motivation

Up until recent past, many irradiance probability density function (PDF) models have been utilized with different degrees of success out of which the most commonly utilized models are the lognormal and the Gamma-Gamma. The scope of lognormal model is restricted to weak turbulences whereas Gamma-Gamma PDF was suggested by Andrews *et. al.* in [38] as a reasonable alternative to Beckmann's PDF because of its much more tractable mathematical model [56]. Recently, a new and generalized statistical model, Málaga ($\mathcal{M}$) distribution, was proposed in [56] to model the

irradiance fluctuation of an unbounded optical wavefront (plane or spherical waves) propagating through a turbulent medium under all irradiance conditions in homogeneous, isotropic turbulence [57]. This $\mathcal{M}$ distribution unifies most of the proposed statistical models derived until now in the bibliography in a closed-form expression providing an excellent agreement with published simulation data over a wide range of turbulence conditions (weak to strong) [56]. Hence, both lognormal and Gamma-Gamma models are a special case of this newly proposed general model.

2.1.2 Contributions

The main contributions of this work are:

- The performance analysis for the $\mathcal{M}$ turbulence channel under the *heterodyne detection* technique in presence of the pointing errors is presented. To the best of our knowledge, these results are new in the literature.

- Some analysis has been presented in [57] for the $\mathcal{M}$ turbulence channel under the *IM/DD technique*. Hence, the work presented in [57] is complemented in this work. To the best of our knowledge, these complemented results are new in the open literature.

- Specifically, the probability density function (PDF), the cumulative distribution function (CDF), and the moment generating function (MGF) of a single $\mathcal{M}$ turbulent FSO link in exact closed-form in terms of Meijer's G function, and the moments in terms of simple elementary functions for both heterodyne and IM/DD detection techniques are derived. Then, the outage probability (OP), the bit-error rate (BER) of binary modulation schemes, the symbol error rate (SER) of M-ary amplitude modulation (M-AM), M-ary phase shift keying (M-PSK) and M-ary quadrature amplitude modulation (M-QAM), and the ergodic

capacity in terms of Meijer's G functions, and the higher-order amount of fading (AF) in terms of simple elementary functions, are derived.

- The *asymptotic expressions* for all expressions mentioned above are derived in terms of simple elementary functions via Meijer's G function expansion, and additionally, the ergodic capacity is also derived at low and high SNR regimes in terms of simple elementary functions by utilizing moments of the $\mathcal{M}$ distribution. With the help of these simple results, one can easily derive useful insights. Additionally, these simple results are easily tractable. These results are new in the open literature.

- The *diversity order and the coding gain* for $\mathcal{M}$ turbulence model under consideration are derived applicable to both the detection techniques under the presence of pointing error effects. These results are new in the open literature.

- Interestingly enough, all the above mentioned results are combined in a unified form i.e. the results for any statistical characteristic or any performance metric applicable to both the detection techniques are presented in a single unified expression. Such unified results are new in the open literature.

- Finally, we also derive the *mapping* between the lognormal distribution parameter and the $\mathcal{M}$ distribution parameters demonstrating the tightness of the approximation of lognormal distribution as a special case of $\mathcal{M}$ distribution.

2.1.3 Structure

The remainder of the chapter is organized as follows. Sections 2 presents a single unified FSO link system and channel model for the $\mathcal{M}$ turbulence distribution. The channel model accounts for pointing errors with both types of detection techniques (heterodyne detection as well as IM/DD). This is then followed by exact closed

form expressions and the asymptotic expressions for the statistical characteristics of a single unified FSO link including the CDF and the MGF, and the moments in terms of Meijer's G functions and simple elementary functions, respectively, in Section 3. Subsequently, the performance metrics under consideration, namely, the OP, the higher-order AF, the BER, the SER, and the ergodic capacity are also presented in terms of unified expressions and asymptotic expressions in Section 4. Finally, Section 5 presents some simulation results to validate these analytical results followed by concluding remarks in Section 6.

2.2 Channel and System Models

2.2.1 Málaga ($\mathcal{M}$) Atmospheric Turbulence Model

The $\mathcal{M}$ turbulence model [56] is based on a physical model that involves a LOS contribution, U_L, a component that is quasi-forward scattered by the eddies on the propagation axis and coupled to the LOS contribution, U_S^C, and another component, U_S^G, due to energy that is scattered to the receiver by off-axis eddies. U_S^C and U_S^G are statistically independent random processes and U_L and U_S^G are also independent random processes. The $\mathcal{M}$ turbulence model can be visually understood via [56, Fig. 1]. One of the main motivation to study this turbulence model is its generality i.e. $\mathcal{M}$ represents various other turbulence models as a special case as can be seen from [56, Table 1]. Hence, a FSO link is employed that experiences $\mathcal{M}$ turbulence for which the PDF of the irradiance I_a is given by [56, Eq. (24)]

$$f_a(I_a) = A \sum_{m=1}^{\beta} a_m \, I_a \, K_{\alpha-m}\left(2\sqrt{\frac{\alpha\,\beta\,I_a}{g\,\beta+\Omega'}}\right), \quad I_a > 0, \tag{2.1}$$

where

$$A \triangleq \frac{2\,\alpha^{\alpha/2}}{g^{1+\alpha/2}\Gamma(\alpha)} \left(\frac{g\,\beta}{g\,\beta+\Omega'}\right)^{\beta+\alpha/2},$$
$$a_m \triangleq \binom{\beta-1}{m-1} \frac{\left(g\,\beta+\Omega'\right)^{1-m/2}}{(m-1)!} \left(\frac{\Omega'}{g}\right)^{m-1} \left(\frac{\alpha}{\beta}\right)^{m/2}, \tag{2.2}$$

α is a positive parameter related to the effective number of large-scale cells of the scattering process, β is the amount of fading parameter and is a natural number [1], $g = \mathbb{E}\left[|U_S^G|^2\right] = 2\,b_0\,(1-\rho)$ denotes the average power of the scattering component received by off-axis eddies, $2\,b_0 = \mathbb{E}\left[|U_S^C|^2 + |U_S^G|^2\right]$ is the average power of the total scatter components, the parameter $0 \leq \rho \leq 1$ represents the amount of scattering power coupled to the LOS component, $\Omega' = \Omega + 2\,b_0\,\rho + 2\sqrt{2\,b_0\,\rho\,\Omega}\cos(\phi_A - \phi_B)$ represents the average power from the coherent contributions, $\Omega = \mathbb{E}\left[|U_L|^2\right]$ is the average power of the LOS component, ϕ_A and ϕ_B are the deterministic phases of the LOS and the coupled-to-LOS scatter terms, respectively, $\Gamma(.)$ is the Gamma function as defined in [58, Eq. (8.310)], and $K_v(.)$ is the v^{th}-order modified Bessel function of the second kind [58, Sec. (8.432)]. It is interesting to know here that $\mathbb{E}\left[|U_S^C|^2\right] = 2\,b_0\,\rho$ denotes the average power of the coupled-to-LOS scattering component and $\mathbb{E}\left[I_a\right] = \Omega + 2\,b_0$. [2]

2.2.2 Pointing Error Model

Pointing errors play an important role in channels fading characteristics. Hence, presence of the pointing error impairments is assumed for which the PDF of the

[1] A generalized expression of (2.1) is given in [56, Eq. (22)] for β being a real number though it is less interesting due to the high degree of freedom of the proposed distribution (Sec. III of [56]).

[2] Detailed information on the $\mathcal{M}$ distribution, its formation, and its random generation can be extracted from [56, Eqs. (13-21)].

irradiance I_p is given by [3] [59, Eq. (11)]

$$f_p(I_p) = \frac{\xi^2}{A_0^{\xi^2}} I_p^{\xi^2-1}, \qquad 0 \leq I_p \leq A_0, \tag{2.3}$$

where ξ is the ratio between the equivalent beam radius at the receiver and the pointing error displacement standard deviation (jitter) at the receiver [48, 50] (i.e. when $\xi \to \infty$, (2.5) converges to the non-pointing errors case), and A_0 is a constant term that defines the pointing loss.

2.2.3 Composite Atmospheric Turbulence-Pointing Error Model

The joint distribution of $I = I_a\, I_p$ can be derived by utilizing the relationship

$$f_I(I) = \int_{I/A_0}^{\infty} f_a(I_a)\, f_{I|I_a}(I|I_a) dI_a. \tag{2.4}$$

Hence, applying a simple random variable transformation on (2.3) and using (2.4), the PDF of the receiver irradiance I experiencing $\mathcal{M}$ turbulence in presence of pointing error impairments is obtained as [57, Eq. (21)]

$$f_I(I) = \frac{\xi^2 A}{2\, I} \sum_{m=1}^{\beta} b_m\, \mathrm{G}_{1,3}^{3,0}\left[\frac{\alpha\, \beta}{(g\, \beta + \Omega')} \frac{I}{A_0} \,\middle|\, \begin{matrix} \xi^2 + 1 \\ \xi^2, \alpha, m \end{matrix} \right], \tag{2.5}$$

where $b_m = a_m \left[\alpha\, \beta / \left(g\, \beta + \Omega'\right)\right]^{-(\alpha+m)/2}$ and G[.] is the Meijer's G function as defined in [58, Eq. (9.301)].

For the heterodyne detection technique case, the average SNR develops as $\mu_{\text{heterdoyne}} = \eta_e\, \mathbb{E}_I[I]/N_0 = A_0\, \eta_e\, \xi^2 (g + \Omega')/\left[(1 + \xi^2)\, N_0\right]$, [4] where η_e is the effective photoelectric

[3] For detailed information on the pointing error model and its subsequent derivation, one may refer to [59].

[4] $\mathbb{E}_I[I^n]$ can be easily derived directly utilizing (2.5) though the derived $\mathbb{E}_I[I^n]$ comes out to be as a summation as expected. Hence to avoid the summation, $\mathbb{E}_I[I^n]$ has been derived in simpler terms in [57, Eq. (34)] that is utilized here.

conversion ratio and N_0 symbolizes the AWGN sample. Alongside, with $\gamma = \eta_e\, I/N_0$, $I = A_0\, \xi^2 (g + \Omega^{'})\, \gamma / \left[\mu_{\text{heterodyne}}\, (\xi^2 + 1)\right]$ is obtained. On utilizing this simple random variable transformation, the resulting SNR PDF under the heterodyne detection technique is given as

$$f_{\gamma_{\text{heterodyne}}}(\gamma) = \frac{\xi^2 A}{2\,\gamma} \sum_{m=1}^{\beta} b_m\, \mathrm{G}_{1,3}^{3,0}\left[B \frac{\gamma}{\mu_{\text{heterodyne}}} \,\middle|\, \begin{matrix} \xi^2 + 1 \\ \xi^2, \alpha, m \end{matrix} \right], \tag{2.6}$$

where $B = \xi^2 \alpha\, \beta\, (g + \Omega^{'}) / [(\xi^2 + 1)\, (g\, \beta + \Omega^{'})]$ and $\mu_{\text{heterodyne}} = \mathbb{E}_{\gamma_{\text{heterodyne}}}[\gamma] = \overline{\gamma}_{\text{heterodyne}}$ is the average SNR of (2.6). This is the very first appearance of this PDF (in (2.6)) in the open literature.

Similarly, for the IM/DD detection technique case, the electrical SNR develops as $\mu_{\text{IM/DD}} = \eta_e^2\, \mathbb{E}_I^2[I]/N_0 = A_0^2\, \eta_e^2\, \xi^4 \left(g + \Omega^{'}\right)^2 / \left[(1 + \xi^2)^2\, N_0\right]$. With $\gamma = \eta_e^2\, I^2/N_0$, $I = \xi^2\, (g + \Omega^{'})\, A_0 / \left(\xi^2 + 1\right) \sqrt{\gamma / \mu_{\text{IM/DD}}}$ is obtained. On utilizing this simple random variable transformation, the resulting SNR PDF under the IM/DD technique is given as

$$f_{\gamma_{\text{IM/DD}}}(\gamma) = \frac{\xi^2 A}{4\,\gamma} \sum_{m=1}^{\beta} b_m\, \mathrm{G}_{1,3}^{3,0}\left[B \sqrt{\frac{\gamma}{\mu_{\text{IM/DD}}}} \,\middle|\, \begin{matrix} \xi^2 + 1 \\ \xi^2, \alpha, m \end{matrix} \right], \tag{2.7}$$

where

$$\begin{aligned} \mu_{\text{IM/DD}} &= \mathbb{E}_{\gamma_{\text{IM/DD}}}[\gamma]\, \mathbb{E}_I^2[I] / \mathbb{E}_I[I^2] \\ &= \frac{\xi^2\, (\xi^2 + 1)^{-2}\, (\xi^2 + 2)\, \left(g + \Omega^{'}\right)}{\alpha^{-1}\, (\alpha + 1)\, [2\, g\, (g + 2\, \Omega^{'}) + \Omega^{'2}\, (1 + 1/\beta)]}\, \overline{\gamma}_{\text{IM/DD}}, \end{aligned} \tag{2.8}$$

is the electrical SNR of (2.7), where $\mathbb{E}_I[I^2]/\mathbb{E}_I^2[I] - 1$ is defined as the scintillation index [60, Eq. (6)]. When $\xi^2\, (g + \Omega^{'}) / \left(\xi^2 + 1\right) = 1$, this PDF given in (2.7) comes in agreement with [61, Eq. (19)].

2.2.4 Unification

Both these PDFs in (2.6) and (2.7) can be easily combined yielding the unified expression for the $\mathcal{M}$ turbulence as

$$f_\gamma(\gamma) = \frac{\xi^2 A}{2^r\,\gamma} \sum_{m=1}^{\beta} b_m \, \mathrm{G}_{1,3}^{3,0}\left[B \left(\frac{\gamma}{\mu_r} \right)^{\frac{1}{r}} \middle| \begin{matrix} \xi^2+1 \\ \xi^2, \alpha, m \end{matrix} \right], \tag{2.9}$$

where r is the parameter defining the type of detection technique (i.e. $r = 1$ represents heterodyne detection and $r = 2$ represents IM/DD). More specifically, for μ_r, when $r = 1$, $\mu_1 = \mu_{\text{heterodyne}}$ and when $r = 2$, $\mu_2 = \mu_{\text{IM/DD}}$. Now, as a special case, when $\rho = 1$ and $\Omega^{'} = 1$ [56, Table 1], this PDF in (2.9) reduces to

$$f_\gamma(\gamma) = \frac{\xi^2}{r\,\gamma\,\Gamma(\alpha)\Gamma(\beta)} \, \mathrm{G}_{1,3}^{3,0}\left[\frac{\xi^2\,\alpha\,\beta}{\xi^2+1} \left(\frac{\gamma}{\mu_r} \right)^{\frac{1}{r}} \middle| \begin{matrix} \xi^2+1 \\ \xi^2, \alpha, \beta \end{matrix} \right]. \tag{2.10}$$

This expression in (2.10) represents the unified PDF for the Gamma-Gamma turbulence. For instance, for negligible pointing errors case under IM/DD technique (i.e. $\xi \to \infty$ and $r = 2$) and $\xi^2 >> 1$, (2.10) reduces to [50, Eq. (9)].

2.2.5 Important Outcomes

- It is important to note here that one may easily derive a PDF corresponding to a certain detection technique from the PDF of the other corresponding detection technique via simple random variable transformation. For instance, (2.7) can be easily derived from (2.6) by transforming the random variable, γ, in (2.6) to $\gamma^2\,\mu_{\text{IM/DD}}/\mu^2_{\text{heterodyne}}$ wherein this updated γ will represent the random variable of (2.7).

- There are two different expressions for the two different cases dependent on the type of receiver detection and these differ in various aspects though it is

important to be aware of the fact that this unification presented in this work is 'unified' in a rather notational point of view. This unification is classified in terms of having, inclusive within a single expression as in (2.9), the parameters that characterize the effects of turbulence i.e. α and β, the parameter that characterizes the effect of pointing errors i.e. ξ, the μ_r, and the ultimate unifying parameter (notationally speaking) r wherein when one places $r = 1$, it gives the PDF applicable to the heterodyne detection technique with its subsequent μ_1 and when one places $r = 2$, it gives the PDF applicable to the IM/DD technique with its subsequent μ_2.

- Emphasizing on the notational importance of this unified expression, it is clarified that for $r = 1$ case, μ_1 represents the average SNR for the heterodyne detection technique whereas for $r = 2$ case, μ_2 represents the electrical SNR for the IM/DD technique for which its relation with the average SNR is shared in (2.8).

2.3 Closed-Form Statistical Characteristics

In this section, we will derive the exact closed-form unified statistical characteristics for our model.

2.3.1 Cumulative Distribution Function

Exact Analysis

Using [62, Eq. (07.34.21.0084.01)] and some simple algebraic manipulations, the CDF for the $\mathcal{M}$ turbulence can be shown to be given by

$$F_\gamma(\gamma) = \int_0^\gamma f_\gamma(t)\, dt = D \sum_{m=1}^{\beta} c_m \, \mathrm{G}_{r+1,3r+1}^{3r,1}\left[E\frac{\gamma}{\mu_r} \middle| \begin{matrix} 1, \kappa_1 \\ \kappa_2, 0 \end{matrix} \right], \tag{2.11}$$

where $D = \xi^2 A / \left[2^r (2\,\pi)^{r-1}\right]$, $c_m = a_m\, b_m\, r^{\alpha+m-1}$, $E = B^{\,r}/r^{2\,r}$, $\kappa_1 = \frac{\xi^2+1}{r}, \ldots, \frac{\xi^2+r}{r}$ comprises of r terms, and $\kappa_2 = \frac{\xi^2}{r}, \ldots, \frac{\xi^2+r-1}{r}, \frac{\alpha}{r}, \ldots, \frac{\alpha+r-1}{r}, \frac{m}{r}, \ldots, \frac{m+r-1}{r}$ comprises of $3r$ terms. The above CDF in (2.11) reduces to the CDF of Gamma-Gamma turbulence as

$$F_\gamma(\gamma) = J\, \mathrm{G}_{r+1,3r+1}^{3r,1}\left[K \frac{\gamma}{\mu_r} \middle| \begin{matrix} 1, \kappa_1 \\ \kappa_3, 0 \end{matrix}\right], \tag{2.12}$$

where $J = r^{\alpha+\beta-2}\, \xi^2 / \left[(2\,\pi)^{r-1} \Gamma(\alpha)\Gamma(\beta)\right]$, $K = (\xi^2 \alpha\, \beta)^r / \left[(\xi^2+1)^{\,r}\, r^{2\,r}\right]$, and $\kappa_3 = \frac{\xi^2}{r}, \ldots, \frac{\xi^2+r-1}{r}, \frac{\alpha}{r}, \ldots, \frac{\alpha+r-1}{r}, \frac{\beta}{r}, \ldots, \frac{\beta+r-1}{r}$ comprises of $3r$ terms. This unified expression for the CDF of a single unified FSO link in (2.12) is in agreement (for $\xi^2 >> 1$) with the individual results presented in [63, Eq. (15)] (for $\xi \to \infty$ and $r = 2$), [48, Eq. (15)] and [64, Eq. (17)] (for $r = 1$), [65, Eq. (16)] and [51, Eq. (7)] (for $\xi \to \infty$ and $r = 1$), and references cited therein. All these special cases are even tabulated in Table 2.2. Mathematically, (2.12) can be easily derived from (2.11) by simply setting $\rho = 1$ and $\Omega^{'} = 1$ in (2.11) i.e. all the sum terms in (2.11) become 0 except for the term when $m = \beta$ [61]. Hence, with this and with some simple algebraic manipulations, (2.12) can be easily obtained from (2.11).

Asymptotic Analysis

Using [66, Eq. (6.2.2)] to invert the argument in the Meijer's G function in (2.11) and then applying (A.1) from the Appendix, the CDF for the $\mathcal{M}$ turbulence in (2.11) can be given asymptotically, at ***high SNR***, in a simpler form in terms of basic elementary functions as

$$F_\gamma(\gamma) \underset{\mu_r >> 1}{\approxeq} D \sum_{m=1}^{\beta} c_m \sum_{k=1}^{3r} \left(\frac{\mu_r}{E\,\gamma}\right)^{-\kappa_{2,k}} \frac{\prod_{l=1;\, l\neq k}^{3r} \Gamma(\kappa_{2,l} - \kappa_{2,k})}{\kappa_{2,k} \prod_{l=1}^{r} \Gamma(\kappa_{1,l} - \kappa_{2,k})}, \tag{2.13}$$

where $\kappa_{u,v}$ represents the v^{th}-term of κ_u. The asymptotic expression for the CDF in (2.13) is dominated by the $\min(\xi, \alpha, \beta)$ where ξ represents the 1^{st}-term, α represents the $(r+1)^{\text{th}}$-term, and β represents the $(2\,r+1)^{\text{th}}$-term in κ_2 i.e. when the difference

between the parameters is greater than 1 then the asymptotic expression for the CDF in (2.13) is dominated by a single term that has the least value among the above three parameters i.e. ξ, α, and β. On the other hand, if the difference between any two parameters is less than 1 then the asymptotic expression for the CDF in (2.13) is dominated by the summation of the two terms that have the least value among the above three parameters with a difference less than 1 and so on and so forth. As a special case, the asymptotic CDF of the Gamma-Gamma turbulence can be obtained as

$$F_{\gamma}(\gamma) \underset{\mu_r >> 1}{\approxeq} J \sum_{k=1}^{3r} \left(\frac{\mu_r}{K\,\gamma} \right)^{-\kappa_{3,k}} \frac{\prod_{l=1;\, l\neq k}^{3r} \Gamma(\kappa_{3,l} - \kappa_{3,k})}{\kappa_{3,k} \prod_{l=1}^{r} \Gamma(\kappa_{1,l} - \kappa_{3,k})}. \tag{2.14}$$

2.3.2 Moment Generating Function

Exact Analysis

The MGF defined as $\mathcal{M}_{\gamma}(s) \triangleq \mathbb{E}\left[e^{-\gamma s}\right]$, can be expressed, using integration by parts, in terms of CDF as

$$\mathcal{M}_{\gamma}(s) = s \int_{0}^{\infty} e^{-\gamma s} F_{\gamma}(\gamma) d\gamma. \tag{2.15}$$

By placing (2.11) into (2.15) and utilizing [58, Eq. (7.813.1)], after some manipulations the MGF for the $\mathcal{M}$ turbulence is obtained as

$$\mathcal{M}_{\gamma}(s) = D \sum_{m=1}^{\beta} c_m \, \mathrm{G}_{r+2,3r+1}^{3r,2} \left[\frac{E}{\mu_r \, s} \middle| \begin{matrix} 0, 1, \kappa_1 \\ \kappa_2, 0 \end{matrix} \right]. \tag{2.16}$$

As a special case, the MGF for the Gamma-Gamma turbulence is derived as

$$\mathcal{M}_{\gamma}(s) = J \, \mathrm{G}_{r+2,3r+1}^{3r,2} \left[\frac{K}{\mu_r \, s} \middle| \begin{matrix} 0, 1, \kappa_1 \\ \kappa_3, 0 \end{matrix} \right]. \tag{2.17}$$

This unified expression for the MGF of a single unified FSO link in (2.17) is in agreement (for $\xi^2 >> 1$) with the individual result presented in [67, Eq. (3)] (for

$\xi \to \infty$ and $r = 2$), and references cited therein.

Asymptotic Analysis

Similar to the CDF, the MGF for the $\mathcal{M}$ turbulence can be expressed asymptotically, at ***high SNR***, as

$$\mathcal{M}_{\gamma}(s) \underset{\mu_r >> 1}{\approxeq} D \sum_{m=1}^{\beta} c_m \sum_{k=1}^{3r} \left(\frac{s}{E}\,\mu_r\right)^{-\kappa_{2,k}} \frac{\prod_{l=1;\, l\neq k}^{3r} \Gamma(\kappa_{2,l} - \kappa_{2,k}) \prod_{l=1}^{2} \Gamma(1 + \kappa_{2,k} - \kappa_{1,l})}{\Gamma(1 + \kappa_{2,k}) \prod_{l=1}^{r} \Gamma(\kappa_{1,l} - \kappa_{2,k})}, \tag{2.18}$$

for the Gamma-Gamma turbulence as

$$\mathcal{M}_{\gamma}(s) \underset{\mu_r >> 1}{\approxeq} J \sum_{k=1}^{3r} \left(\frac{s}{K}\,\mu_r\right)^{-\kappa_{3,k}} \frac{\prod_{l=1;\, l\neq k}^{3r} \Gamma(\kappa_{3,l} - \kappa_{3,k}) \prod_{l=1}^{2} \Gamma(1 + \kappa_{3,k} - \kappa_{1,l})}{\Gamma(1 + \kappa_{3,k}) \prod_{l=1}^{r} \Gamma(\kappa_{1,l} - \kappa_{3,k})}, \tag{2.19}$$

and can be further expressed via only the dominant term(s) based on a similar explanation to the one given for the CDF case earlier.

2.3.3 Moments

The moments are defined as $\mathbb{E}\left[\gamma^n\right]$. Placing (2.1) into the definition and utilizing [58, Eq. (7.811.4)], to the best of our knowledge, a new expression for the moments of the $\mathcal{M}$ turbulence is derived in exact closed-form and in terms of simple elementary functions as

$$\mathbb{E}\left[\gamma^n\right] = \frac{r\,\xi^2\,A\,\Gamma(r\,n + \alpha)}{2^r\ (r\,n + \xi^2)\ B^{r\,n}} \sum_{m=1}^{\beta} b_m\,\Gamma(r\,n + m)\,\mu_r^n, \tag{2.20}$$

and of the Gamma-Gamma turbulence as

$$\mathbb{E}\left[\gamma^n\right] = \frac{\xi^2\,(\xi^2 + 1)^{r\,n}\,\Gamma(r\,n + \alpha)\Gamma(r\,n + \beta)}{(\xi^2 \alpha\,\beta)^{r\,n}\,(r\,n + \xi^2)\,\Gamma(\alpha)\Gamma(\beta)}\,\mu_r^n. \tag{2.21}$$

It is worthwhile to note that this simple result for the moments is particularly useful to conduct asymptotic analysis of the ergodic capacity in the later part of this work.

2.4 Applications

2.4.1 Outage Probability

When the instantaneous output SNR γ falls below a given threshold γ_{th}, a situation labeled as outage is encountered and it is an important feature to study the OP of a system. Hence, another important fact worth stating here is that the expressions derived in (2.11), (2.12), (2.13), and (2.14) also serve the purpose for the results of the OP for a FSO channel or in other words, the probability that the SNR falls below a predetermined protection ratio γ_{th} can be simply expressed by replacing γ with γ_{th} in (2.11), (2.12), (2.13), and (2.14) as $P_{\text{out}}(\gamma_{\text{th}}) = F_{\gamma}(\gamma_{\text{th}})$.

2.4.2 Higher-Order Amount of Fading

The AF is an important measure for the performance of a wireless communication system as it can be utilized to parameterize the distribution of the SNR of the received signal. In particular, the n^{th}-order AF for the instantaneous SNR γ is defined as $AF_{\gamma}^{(n)} = \frac{\mathbb{E}[\gamma^n]}{\mathbb{E}[\gamma]^n} - 1$ [68]. Now, substituting (2.20) into this definition, the n^{th}-order AF and the classical AF can be easily obtained.

2.4.3 Average BER

Exact Analysis

Substituting (2.11) into [69, Eq. (12)] and utilizing [58, Eq. (7.813.1)], the average BER $\overline{P}_b$ of a variety of binary modulations for the $\mathcal{M}$ turbulence is obtained as

$$\overline{P}_b = \frac{D}{2\,\Gamma(p)} \sum_{m=1}^{\beta} c_m \, \mathrm{G}_{r+2,3r+1}^{3r,2} \left[\frac{E}{\mu_r \, q} \middle| \begin{matrix} 1-p, 1, \kappa_1 \\ \kappa_2, 0 \end{matrix} \right], \tag{2.22}$$

Table 2.1: BER Parameters of Binary Modulations

Modulation	p	q
Coherent Binary Frequency Shift Keying (CBFSK)	0.5	0.5
Coherent Binary Phase Shift Keying (CBPSK)	0.5	1
Non-Coherent Binary Frequency Shift Keying (NBFSK)	1	0.5
Differential Binary Phase Shift Keying (DBPSK)	1	1

and for the Gamma-Gamma turbulence as

$$\overline{P}_b = \frac{J}{2\,\Gamma(p)}\,\mathrm{G}_{r+2,3r+1}^{3r,2}\left[\frac{K}{\mu_r\,q}\,\middle|\,\begin{matrix}1-p,1,\kappa_1\\ \kappa_3,0\end{matrix}\right], \tag{2.23}$$

where the parameters p and q account for different modulation schemes. For an extensive list of modulation schemes represented by these parameters, one may look into [69–73] or refer to Table 2.1. This unified expression for the BER of a single unified FSO link in (2.23) is in agreement (for $\xi^2 >> 1$) with the individual results presented in [74, Eq. (5)] (for $r = 2$), [48, Eq. (24)] (for $r = 1$), [51, Eq. (10)] and [75, Eq. (7)] (for $\xi \to \infty$ and $r = 1$), and references cited therein. All these special cases are even tabulated in Table 2.2.

Asymptotic Analysis

Similar to the CDF, the BER can be expressed asymptotically for the $\mathcal{M}$ turbulence, at ***high SNR***, as

$$\overline{P}_b \underset{\mu_r >>1}{\approxeq} \frac{D}{2\,\Gamma(p)}\sum_{m=1}^{\beta} c_m \sum_{k=1}^{3r}\left(\frac{q}{E}\,\mu_r\right)^{-\kappa_{2,k}} \frac{\prod_{l=1;\,l\neq k}^{3r}\Gamma(\kappa_{2,l}-\kappa_{2,k})\prod_{l=1}^{2}\Gamma(1+\kappa_{2,k}-\kappa_{1,l})}{\Gamma(1+\kappa_{2,k})\prod_{l=1}^{r}\Gamma(\kappa_{1,l}-\kappa_{2,k})}, \tag{2.24}$$

for the Gamma-Gamma turbulence as

$$\overline{P}_b \underset{\mu_r >>1}{\approxeq} \frac{J}{2\,\Gamma(p)} \sum_{k=1}^{3r} \left(\frac{q}{K}\,\mu_r\right)^{-\kappa_{3,k}} \frac{\prod_{l=1;\,l\neq k}^{3r} \Gamma(\kappa_{3,l}-\kappa_{3,k}) \prod_{l=1}^{2} \Gamma(1+\kappa_{3,k}-\kappa_{1,l})}{\Gamma(1+\kappa_{3,k}) \prod_{l=1}^{r} \Gamma(\kappa_{1,l}-\kappa_{3,k})}, \tag{2.25}$$

and can be further expressed via only the dominant term(s) based on a similar explanation to the one given for the CDF case earlier.

Diversity Order and Coding Gain

Utilizing $\overline{P}_b \approx (G_c\,\mu_r)^{-G_d}$ [76, Eq. (1)], it can be easily derived for the $\mathcal{M}$ turbulence, the diversity order is $G_d = \min(\xi^2/r, \alpha/r, \beta/r) \underset{\alpha>\beta}{=} \min(\xi^2/r, \beta/r)$ and the coding gain is

$$G_c = q/E \left(D/\left(2\,\Gamma(p)\right) \sum_{m=1}^{\beta} c_m \frac{\prod_{l=1;\,l\neq k}^{3\,r} \Gamma(\kappa_{2,l}-\kappa_{2,k}) \prod_{l=1}^{2} \Gamma(1+\kappa_{2,k}-\kappa_{1,l})}{\Gamma(1+\kappa_{2,k}) \prod_{l=1}^{r} \Gamma(\kappa_{1,l}-\kappa_{2,k})} \right)^{-\frac{1}{\kappa_{2,k}}}. \tag{2.26}$$

Similarly, for the Gamma-Gamma turbulence, the diversity order outcomes as $G_d = \min(\xi^2/r, \alpha/r, \beta/r) \underset{\alpha>\beta}{=} \min(\xi^2/r, \beta/r)$ and the coding gain as

$$G_c = q/K \left(J/\left(2\,\Gamma(p)\right) \frac{\prod_{l=1;\,l\neq k}^{3\,r} \Gamma(\kappa_{3,l}-\kappa_{3,k}) \prod_{l=1}^{2} \Gamma(1+\kappa_{3,k}-\kappa_{1,l})}{\Gamma(1+\kappa_{3,k}) \prod_{l=1}^{r} \Gamma(\kappa_{1,l}-\kappa_{3,k})} \right)^{-\frac{1}{\kappa_{3,k}}}. \tag{2.27}$$

The authors in [77, Eqs. (18) and (19)] have also derived the diversity order and the coding gain for the Gamma-Gamma turbulence FSO channels though applicable to the IM/DD technique under negligible pointing errors. Hence, the results for the coding gain and the diversity order in this work are applicable to even the heterodyne detection technique and also for non-negligible pointing error effects for both types of detection techniques.

2.4.4 Average SER

In [78], the conditional SER has been presented in a desirable form and utilized to obtain the average SER of M-AM, M-PSK, and M-QAM. For example, for M-PSK the average SER $\overline{P}_s$ over generalized fading channels is given by [78, Eq. (41)]. Similarly, for M-AM and M-QAM, the average SER $\overline{P}_s$ over generalized fading channels is given by [78, Eq. (45)] and [78, Eq. (48)] respectively. On substituting (2.16) into [78, Eq. (41)], [78, Eq. (45)], and [78, Eq. (48)], one can obtain the SER of M-PSK, M-AM, and M-QAM, respectively. The analytical SER performance expressions obtained via the above substitutions are exact and can be easily estimated accurately by utilizing the Gauss-Chebyshev Quadrature (GCQ) formula [79, Eq. (25.4.39)] that converges rapidly, requiring only few terms for an accurate result [80].

2.4.5 Ergodic Capacity

Exact Analysis

The ergodic channel capacity $\overline{C}$ is defined as $\overline{C} \triangleq \mathbb{E}\left[\log_2(1 + c\,\gamma)\right]$ where c is a constant term such that $c = 1$ for heterodyne detection and $c = e/(2\,\pi)$ for IM/DD [81, Eq. (26)], [82, Eq. (7.43)]. Utilizing this equation by substituting (2.9) in it, representing $\ln(1 + c\,\gamma)$ in terms of Meijer's G function as $\mathrm{G}_{2,2}^{1,2}\left[c\,\gamma \,\middle|\, {1,1 \atop 1,0}\right]$, and using [83, Eq. (21)], the ergodic capacity for the $\mathcal{M}$ turbulence can be expressed as

$$\overline{C} = \frac{D}{\ln(2)} \sum_{m=1}^{\beta} c_m \, \mathrm{G}_{r+2,3r+2}^{3r+2,1}\left[\frac{E}{\mu_r^{\sim}} \,\middle|\, {0, 1, \kappa_1 \atop \kappa_2, 0, 0}\right], \tag{2.28}$$

and for the Gamma-Gamma turbulence as

$$\overline{C} = \frac{J}{\ln(2)} \, \mathrm{G}_{r+2,3r+2}^{3r+2,1}\left[\frac{K}{\mu_r^{\sim}} \,\middle|\, {0, 1, \kappa_1 \atop \kappa_3, 0, 0}\right], \tag{2.29}$$

where $\mu_r^{\sim} = c\,\mu_r$. Specifically, $\mu_1^{\sim} = \mu_1$ for the heterodyne detection technique (i.e. $r = 1$) and $\mu_2^{\sim} = e/(2\,\pi)\ \mu_2$ for the IM/DD technique (i.e. $r = 2$). This unified expression for the ergodic capacity of a single unified FSO link in (2.29) is in agreement (for $\xi^2 >> 1$) with the individual results presented in [50, Eq. (22)] (for $r = 2$), [63, Eq. (21)] and [50, Eq. (11)] (for $\xi \to \infty$ and $r = 2$), [84, Eq. (10)] (for $r = 1$), [85, Eq. (16)] and [86, Eq. (3)] (for $\xi \to \infty$ and $r = 1$), and references cited therein. All these special cases are even tabulated in Table 2.2.

For readers clarification, the Shannon ergodic capacity given as $\overline{C} \triangleq \mathbb{E}\left[\log_2(1 + c\,\gamma)\right]$ is true as an exact expression for deriving the respective ergodic capacity for heterodyne detection technique whereas for IM/DD technique, it acts as a lower bound as given in [81, Eq. (26)] and [82, Eq. (7.43)]. Hence, it can be safely claimed that the ergodic capacity's derived in (2.28) and (2.29) above are an exact solution for the heterodyne detection technique (i.e. $r = 1$) whereas for the IM/DD technique (i.e. $r = 2$), these solutions (as per above mentioned references) act as a lower bound.

Asymptotic Analysis

Similar to the CDF, the ergodic capacity for the $\mathcal{M}$ turbulence can be expressed asymptotically via utilizing the Meijer's G function expansion given in the Appendix, at ***high SNR***, as

$$\overline{C} \underset{\mu_r >>1}{\approxeq} \frac{D}{\ln(2)} \sum_{m=1}^{\beta} c_m \sum_{k=1}^{3r+2} \left(\frac{\mu_r^{\sim}}{E}\right)^{-\kappa_{2,k}} \frac{\Gamma(1+\kappa_{2,k}) \prod_{l=1;\, l\neq k}^{3r+2} \Gamma(\kappa_{2,l} - \kappa_{2,k})}{\Gamma(1-\kappa_{2,k}) \prod_{l=1}^{r} \Gamma(\kappa_{1,l} - \kappa_{2,k})}. \tag{2.30}$$

Similarly, the asymptotic expression for the Gamma-Gamma turbulence is derived as

$$\overline{C} \underset{\mu_r >>1}{\approxeq} \frac{J}{\ln(2)} \sum_{k=1}^{3r+2} \left(\frac{\mu_r^{\sim}}{K}\right)^{-\kappa_{3,k}} \frac{\Gamma(1+\kappa_{3,k}) \prod_{l=1;\, l\neq k}^{3r+2} \Gamma(\kappa_{3,l} - \kappa_{3,k})}{\Gamma(1-\kappa_{3,k}) \prod_{l=1}^{r} \Gamma(\kappa_{1,l} - \kappa_{3,k})}, \tag{2.31}$$

and can be further expressed via only the dominant term(s) based on the similar explanation as has been given for the CDF case earlier in Section II.3.1 except with $\min(\xi, \alpha, \beta, 1, 1+\epsilon)$ instead of $\min(\xi, \alpha, \beta)$, where ϵ is a very small error introduced so as not to violate the conditions given in the Appendix, required to utilize (A.1).

Alternatively, a ***high SNR*** asymptotic analysis may also be done by utilizing the moments as [68, Eqs. (8) and (9)]

$$\overline{C} \underset{\mu_r >>1}{\approxeq} \log(\mu_r) + \zeta, \tag{2.32}$$

where

$$\zeta = \frac{\partial}{\partial n} A F_{\gamma}^{(n)} \bigg|_{n=0}. \tag{2.33}$$

The expression in (2.32) can be simplified to

$$\begin{aligned}
\overline{C} &\underset{\mu_r >>1}{\approxeq} \log(\mu_r) + \frac{\partial}{\partial n} A F_{\gamma}^{(n)} \bigg|_{n=0} \\
&= \log(\mu_r) + \frac{\partial}{\partial n} \left(\frac{\mathbb{E}\left[\gamma^n\right]}{\mathbb{E}\left[\gamma\right]^n} - 1 \right) \bigg|_{n=0} \\
&= \log(\mu_r) + \left(\frac{1}{\mathbb{E}\left[\gamma\right]^n} \frac{\partial}{\partial n} \mathbb{E}\left[\gamma^n\right] + \mathbb{E}\left[\gamma^n\right] \frac{\partial}{\partial n} \frac{1}{\mathbb{E}\left[\gamma\right]^n} \right) \bigg|_{n=0} \\
&= \log(\mu_r) + \left(\frac{1}{\mathbb{E}\left[\gamma\right]^n} \frac{\partial}{\partial n} \mathbb{E}\left[\gamma^n\right] - \frac{\mathbb{E}\left[\gamma^n\right]}{\mathbb{E}\left[\gamma\right]^n} \log\left(\mathbb{E}\left[\gamma\right]\right) \right) \bigg|_{n=0} \\
&= \log(\mu_r) + \left(\frac{1}{\mathbb{E}\left[\gamma\right]^n} \frac{\partial}{\partial n} \mathbb{E}\left[\gamma^n\right] - \frac{\mathbb{E}\left[\gamma^n\right]}{\mathbb{E}\left[\gamma\right]^n} \log\left(\mu_r\right) \right) \bigg|_{n=0} = \frac{\partial}{\partial n} \mathbb{E}\left[\gamma^n\right] \bigg|_{n=0}.
\end{aligned} \tag{2.34}$$

Hence, it is required to evaluate the first derivative of the moments in (2.20) at $n = 0$ for high SNR asymptotic approximation to the ergodic capacity in (2.28). The first derivative of the moments is given as

$$\begin{aligned}
\frac{\partial}{\partial n} \mathbb{E}\left[\gamma^n\right] = \frac{r\,\xi^2\,A\,\Gamma(r\,n+\alpha)}{2^r\ (r\,n+\xi^2)\ B^{r\,n}} \sum_{m=1}^{\beta} b_m\,\Gamma(r\,n+m) \\
\times \left\{ r\left[\psi(r\,n+\alpha) + \psi(r\,n+m) - \log(B)\right] + \log(\mu_r) - r/\left(r\,n+\xi^2\right) \right\} \tilde{\mu_r^{\,n}},
\end{aligned} \tag{2.35}$$

where $\psi(.)$ is the digamma (psi) function [79, Eq. (6.3.1)], [58, Eq. (8.360.1)]. Evaluating (2.35) at $n = 0$,

$$\overline{C} \underset{\mu_r >>1}{\approxeq} \frac{r\, A\, \Gamma(\alpha)}{2^r} \sum_{m=1}^{\beta} b_m\, \Gamma(m) \left\{ r \left[-1/\xi^2 - \log(B) + \psi(\alpha) + \psi(m) \right] + \log(\mu_r^{\sim}) \right\}, \tag{2.36}$$

is obtained. Hence, (2.36) gives the required expression for $\overline{C}$ for the $\mathcal{M}$ turbulent channel at high SNR in terms of simple elementary functions. A similar expression is derived for the Gamma-Gamma turbulent channel as

$$\overline{C} \underset{\mu_r >>1}{\approxeq} \log(\mu_r^{\sim}) + r \left[-\frac{1}{\xi^2} - \log\left(\frac{\xi^2}{\xi^2 + 1} \right) - \log(\alpha\, \beta) + \psi(\alpha) + \psi(\beta) \right]. \tag{2.37}$$

Furthermore, for ***low SNR*** asymptotic analysis, it can be easily shown that the ergodic capacity can be asymptotically approximated by the first moment. Now, utilizing (2.20) via placing $n = 1$ in it to obtain the ergodic capacity approximate at low SNR. Hence the ergodic capacity of a single FSO link under $\mathcal{M}$ turbulence can be approximated at low SNR in closed-form in terms of simple elementary functions as

$$\overline{C} \underset{\mu_r <<1}{\approxeq} \mathbb{E}\left[\gamma^{n=1}\right] = \frac{r\, \xi^2\, A\, \Gamma(r + \alpha)}{2^r\ (r + \xi^2)\ B^r} \sum_{m=1}^{\beta} b_m\, \Gamma(r + m)\, \mu_r^{\sim}, \tag{2.38}$$

and under Gamma-Gamma turbulence as

$$\overline{C} \underset{\mu_r <<1}{\approxeq} \mathbb{E}\left[\gamma^{n=1}\right] = \frac{\xi^2\, (\xi^2 + 1)^r\ \Gamma(r + \alpha)\Gamma(r + \beta)}{(\xi^2 \alpha\, \beta)^r\, (r + \xi^2)\, \Gamma(\alpha)\Gamma(\beta)}\, \mu_r^{\sim}. \tag{2.39}$$

2.5 Numerical Results and Discussion

The FSO link is modeled as $\mathcal{M}$ turbulent channel with the effects of atmosphere as ($\alpha = 2.296$; $\beta = 2$), ($\alpha = 4.2$; $\beta = 3$) and ($\alpha = 8$; $\beta = 4$), ($\Omega = 1.3265$, $b_0 = 0.1079$),

$\rho = 0.596$, and $\phi_A - \phi_B = \pi/2$.[5] In MATLAB, a $\mathcal{M}$ turbulent channel random variable was generated via squaring the absolute value of a Rician-shadowed random variable [56]. Additionally, please note that the Eq. (.) numbers referred to in all of the following figures represent the equations in this chapter.

The OP is presented in Fig. 2.1 for both types of detection techniques (i.e. IM/DD and heterodyne) across the normalized electrical SNR with fixed effect of the pointing error ($\xi = 1$). It can be observed from Fig. 2.1 that the simulation results provide

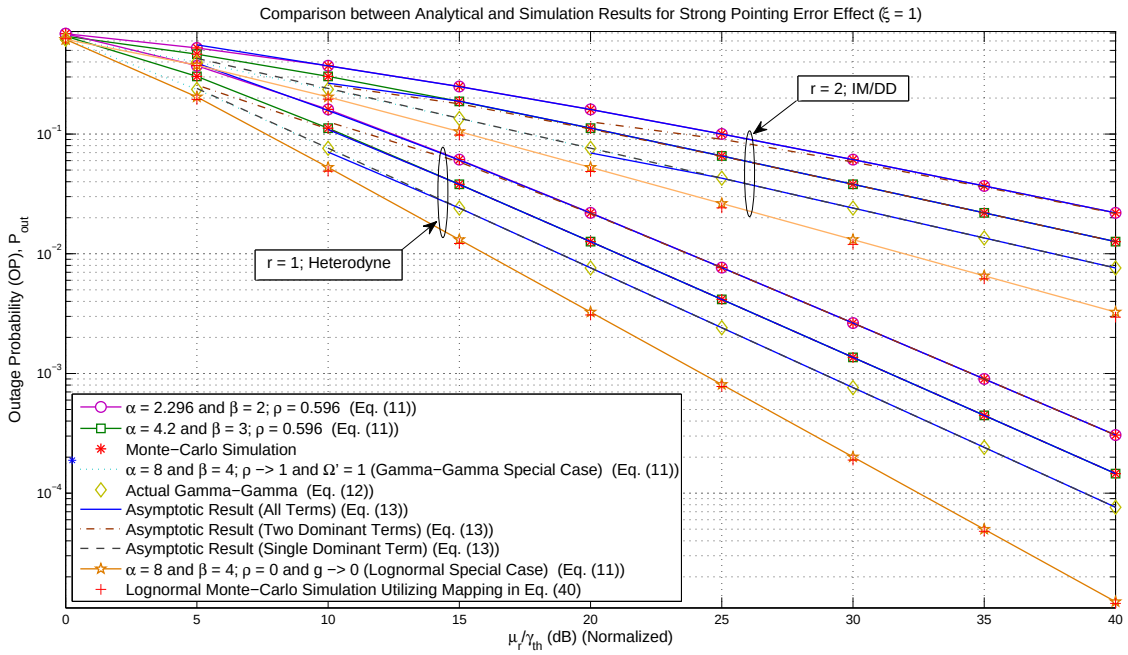

Figure 2.1: OP showing the performance of both the detection techniques (heterodyne and IM/DD) under different turbulence conditions.

a perfect match to the analytical results obtained in this work. Additionally, it can be observed that as the effect of atmospheric turbulence decreases, the performance improves. It can be seen that at high SNR, the asymptotic expression derived in (2.13) (i.e. utilizing all the terms in the summation) converges quite fast to the exact result

[5]It is important to note here that these values for the parameters were selected from [56, 57, 61] subject to the standards to prove the validity of the obtained results and hence other specific values can be used to obtain the required results by design communication engineers before deployment. Also, for all cases, 10^6 realizations of the random variable were generated to perform the Monte-Carlo simulations in MATLAB.

proving this asymptotic approximation to be tight enough. Based on the effects of the turbulence parameters and the pointing error, the appropriate dominant term(s) can be selected as has been discussed earlier under the CDF subsection. Hence, it can be seen that these respective dominant term(s) also converge though relatively slower, specially for the IM/DD technique. More importantly, it can be observed that once $\rho = 1$ and $\Omega^{'} = 1$ is applied, the $\mathcal{M}$ turbulence matches exactly the special case of the Gamma-Gamma turbulence. This can be depicted from the case wherein ($\alpha = 8$; $\beta = 4$).

Furthermore, on applying $\rho = 0$ and $g \to 0$ to $\mathcal{M}$ atmospheric turbulence, one can obtain an approximation to weak lognormal atmospheric turbulence [56]. Hence, to analyze this, we derived the mapping for the lognormal parameter σ, where σ^2 is defined as the scintillation index [60], in terms of the parameters of $\mathcal{M}$ atmospheric turbulence i.e. in terms of $\alpha, \beta, \xi, m, \Omega^{'}$, and g. Specifically, σ was obtained via the moment matching method. The moments of lognormal turbulence are very well known to be given as $\mathbb{E}\left[I^n\right]_{LN} = \frac{\xi^{2(1-n)}}{(\xi^2+n)(\xi^2+1)^{-n}} \exp\left\{\frac{n\,\sigma^2}{2}\,(n-1)\right\}$ [60] and the moments for the $\mathcal{M}$ turbulence can be easily extracted from (2.20). On matching the third moment, we obtained the mapping for σ as

$$\sigma = \sqrt{\frac{1}{6}\ln\left\{\frac{\xi^{12}\,A\,\Gamma\left(\alpha+4\right)}{2\,\left(\xi^2+1\right)^4\,B^4}\sum_{m=1}^{\beta} b_m\,\Gamma\left(m+4\right)\right\}}. \tag{2.40}$$

The plot for this scenario can be easily depicted in Fig. 2.1 from the case wherein ($\alpha = 8$; $\beta = 4$). It must be noted that the curve signified by the second last entry in the legend depicts the lognormal special case approximate plotted via utilizing the unified exact closed-form OP analytical expression in (2.11). The last entry in the legend of Fig. 2.1 depicts the Monte-Carlo simulation/generation for lognormal random variable with σ acquiring values from (2.40). It can be clearly observed that this approximation of $\mathcal{M}$ turbulence to lognormal is quite tight. Moreover, we had

obtained expressions for σ via matching the second moment as well and it was realized that the expression derived via matching the third moment gave tighter approximate results. Based on this, we can easily conclude that the higher moments we utilize to derive the mapping expression for σ, the tighter approximate may be obtained.

Additionally, another important outcome must be observed that the heterodyne detection technique, being more complex method of detection technique, performs better than the IM/DD technique. For instance, for $\alpha = 2.296$, $\beta = 2$, and $\rho = 0.596$, at an electrical SNR of 15 dB, the heterodyne detection technique outperforms the IM/DD technique in terms of the OP by $1.8852 * 10^{-1}$. On the other hand, for $\alpha = 8$, $\beta = 4$, $\rho \to 1$, and $\Omega' = 1$, for a desired OP i.e. lets say for $P_{\text{out}} = 7.6 * 10^{-3}$, the heterodyne detection technique outperforms the IM/DD technique by 20 dB.

Similarly, Fig. 2.2 presents the OP for varying effects of pointing error (ξ = 1 and 6.7) under the IM/DD technique. It can be observed that for lower effect

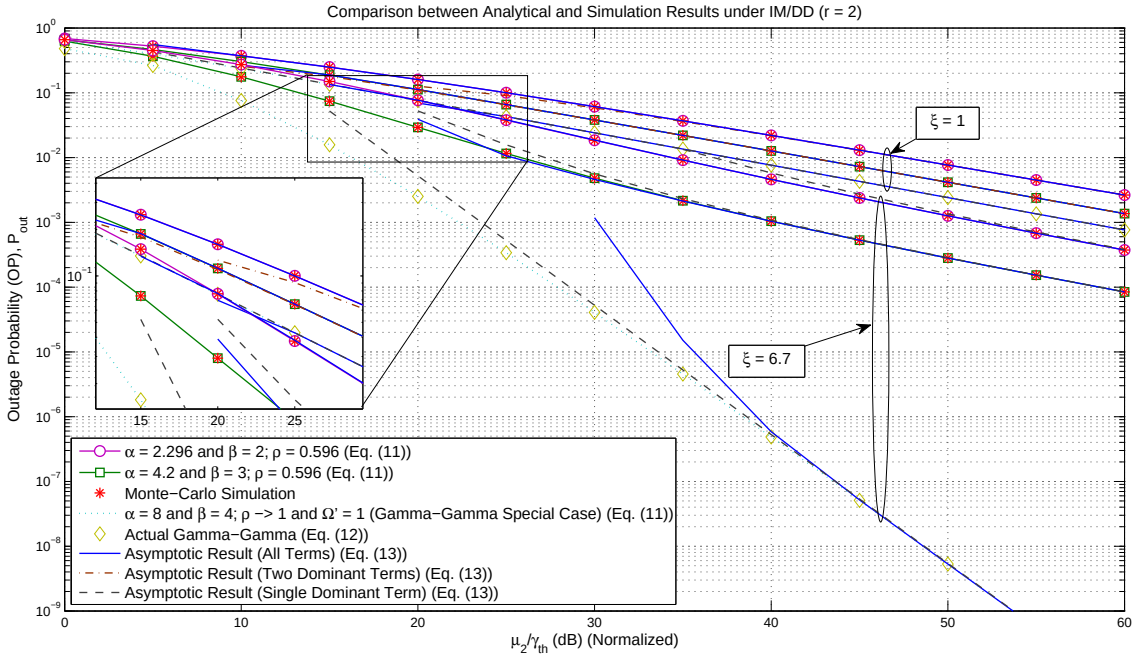

Figure 2.2: OP showing the performance of IM/DD technique under different turbulence conditions with varying effects of pointing error.

of the pointing error (i.e. higher value of ξ), the respective performance gets better

manifolds. Other outcomes, specially for the asymptotic approximations, can be observed similar to Fig. 2.1 above except when the atmospheric effects get weaker and weaker wherein the single dominant term of the asymptotic result converges faster than the sum of all terms in the asymptotic result.

The average BER performance of DBPSK binary modulation scheme is presented in Fig. 2.3. The effect of pointing error is fixed at $\xi = 1$. Similar results can be ob-

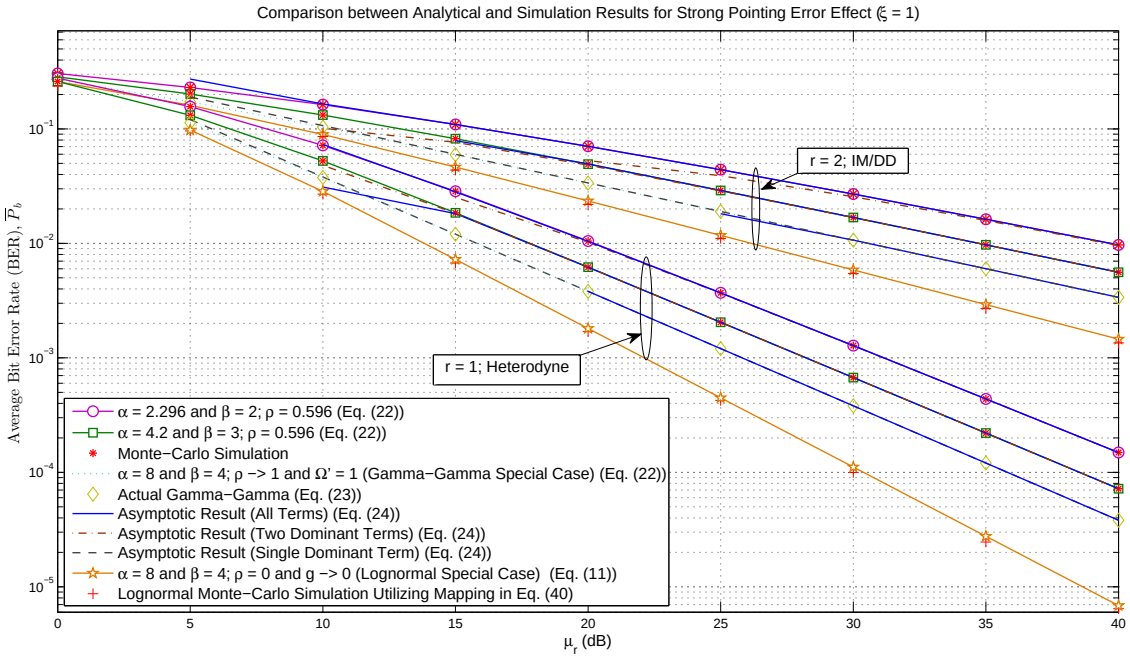

Figure 2.3: Average BER of DBPSK binary modulation scheme showing the performance of both the detection techniques (heterodyne and IM/DD) under different turbulence conditions.

served as were observed for Fig. 2.1. Similarly, Fig. 2.4 presents the average BER for varying effects of pointing error ($\xi = 1$ and 6.7) under the IM/DD technique. It can be observed that for lower effect of the pointing error ($\xi \to \infty$), the respective performance gets better. Other outcomes, specially for the asymptotic approximations, can be observed similar to Fig. 2.2 above.

In Fig. 2.5 and Fig. 2.6, the lower bound ergodic capacity of FSO channel in operation under IM/DD technique is demonstrated for varying effects of pointing

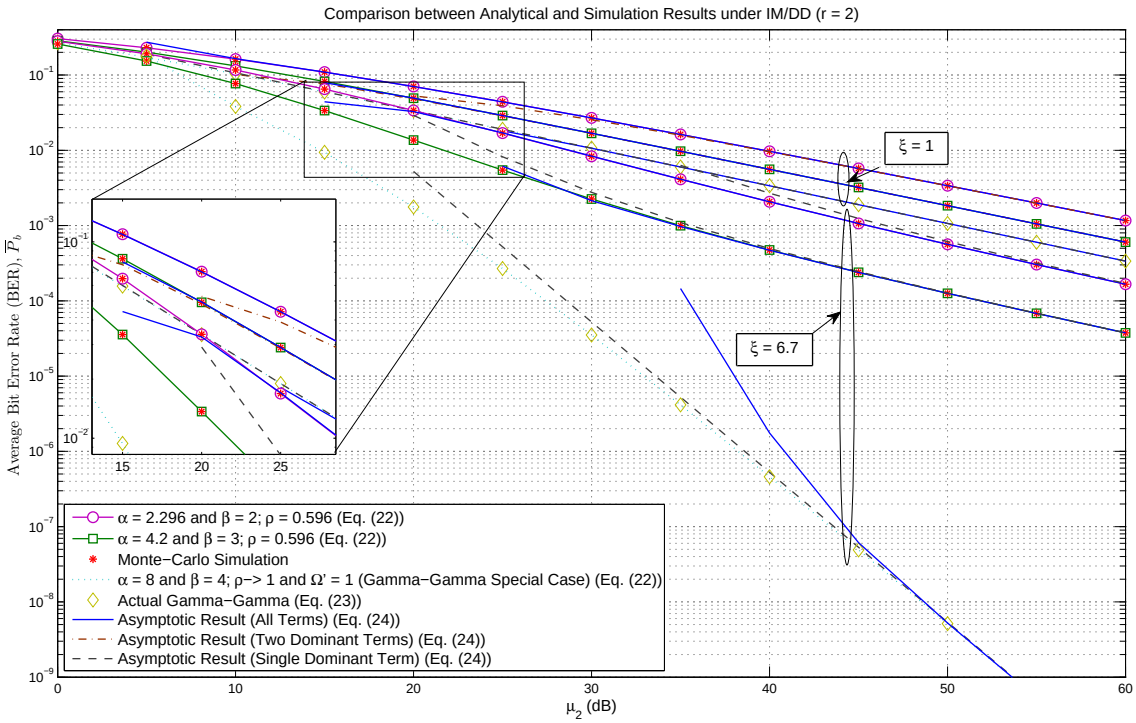

Figure 2.4: Average BER of DBPSK binary modulation scheme showing the performance of IM/DD technique under different turbulence conditions for varying effects of pointing error.

error, $\xi = 1$ and 6.7. Expectedly, as the atmospheric turbulence conditions get severe and/or as the pointing error gets severe, the ergodic capacity starts decreasing (i.e. the higher the values of α and β, and/or ξ, the higher will be the ergodic capacity). One of the most important outcomes of Fig. 2.5 and Fig. 2.6 are the asymptotic results for the ergodic capacity via two different methods. It can be seen that at high SNR, the asymptotic expression, via Meijer's G function expansion, derived in (2.30) (i.e. utilizing all the terms in the summation) converges rather slowly. Based on the effects of the turbulent parameters and the pointing error, the appropriate dominant term(s) are selected and it can be seen that these respective dominant term(s) also converge though relatively quite faster than the case where all the terms are employed. On the other hand, the asymptotic expression, via utilizing moments, derived in (2.36) gives very tight asymptotic results in high SNR regime. Interestingly enough, it can be

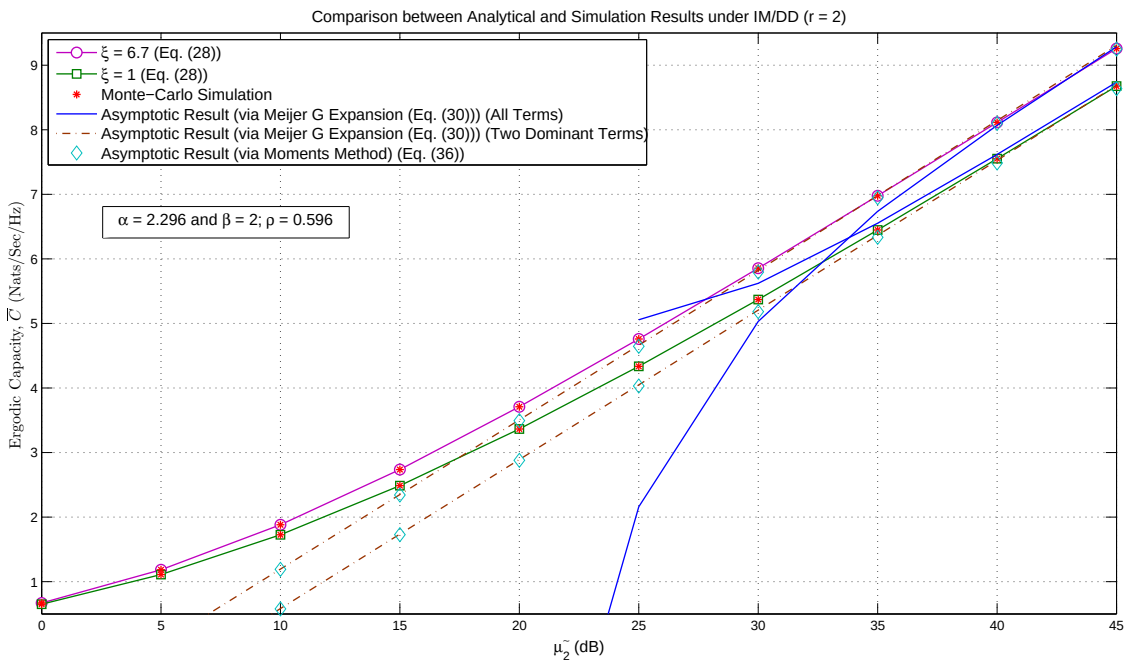

Figure 2.5: Ergodic capacity results for the IM/DD technique for varying pointing errors along with the asymptotic results in high SNR regime.

clearly seen that the two-dominant terms of (2.30) (derived via Meijer's G function expansion) signified by the two 1's present in the Meijer's G function of the lower bound ergodic capacity results in (2.28) and (2.36) (derived via moments) overlap. Fig. 2.7 presents tight asymptotic results for the ergodic capacity in low SNR regime derived in (2.38).

Finally in Fig. 2.8, the relative performance of $\mathcal{M}$ turbulent channels with Gamma-Gamma turbulent channels is demonstrated. It is interesting to see how ρ and Ω' behave. It can be observed that ρ has a significant effect on the performance though as the Ω' increases much beyond 60 dB, the effect of ρ nullifies. Similar trend is observed for the variations with Ω' itself.

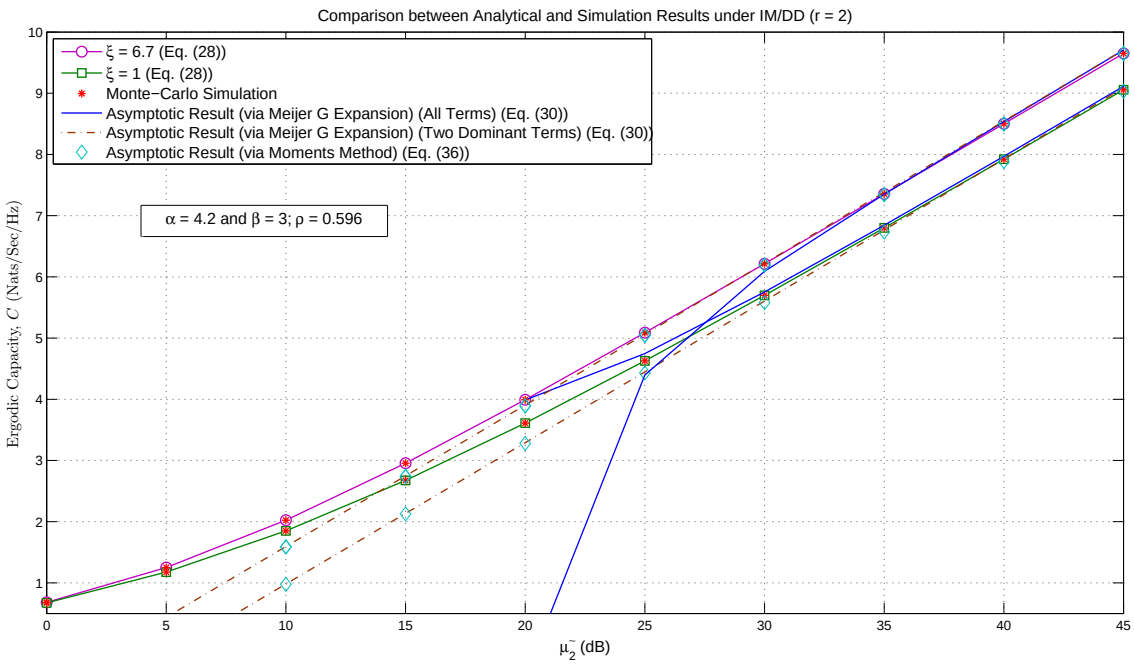

Figure 2.6: Ergodic capacity results for the IM/DD technique for varying pointing errors along with the asymptotic results in high SNR regime.

2.6 Concluding Remarks

Unified expressions for the PDF, the CDF, the MGF, and the moments of the average SNR of a FSO link operating over $\mathcal{M}$ turbulence were presented. Capitalizing on these expressions, new unified formulas were presented for various performance metrics including the OP, the higher-order AF, the error rate of a variety of modulation schemes, and the ergodic capacity in terms of Meijer's G function except for the higher-order AF that was in terms of simple elementary functions. Further, novel asymptotic expressions were derived and presented for the OP, the average BER, and the ergodic capacity in terms of basic elementary functions via utilizing Meijer's G function expansion given in the Appendix and via utilizing moments too for the ergodic capacity asymptotes. In addition, all the special cases of the Gamma-Gamma atmospheric turbulence scenario are presented in Table 2.2. Finally, this work presented simulation examples to validate and illustrate the mathematical formulation

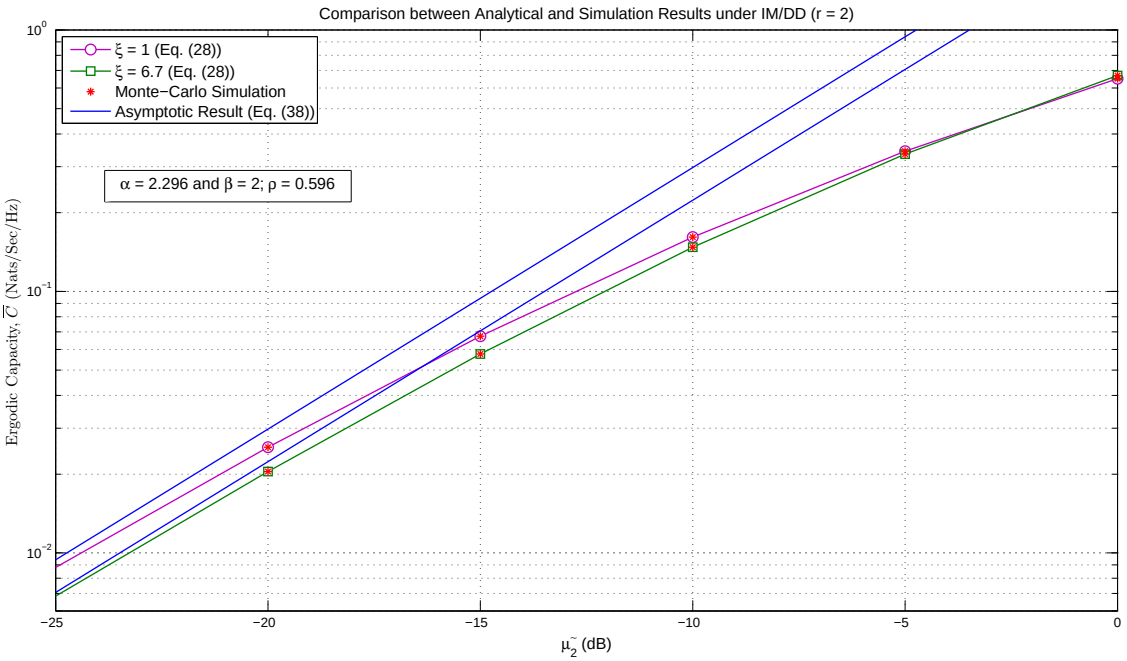

Figure 2.7: Ergodic capacity results for the IM/DD technique for varying pointing errors along with the asymptotic results in low SNR regime.

developed in this work and to show the effect of the atmospheric turbulence conditions severity and the pointing errors severity on the system performance.

These results demonstrate the unification of various FSO turbulent scenarios into a single expression allowing one to utilize this unified expression and derive the required expression for one's objective. Additionally, one can easily utilize the unified analysis over the $\mathcal{M}$ FSO turbulent channels to obtain many other atmospheric turbulence channels, as per need, as its special case. Furthermore, having these unified asymptotic results opens door for simpler further analysis over more complex systems undergoing these FSO turbulence channels.

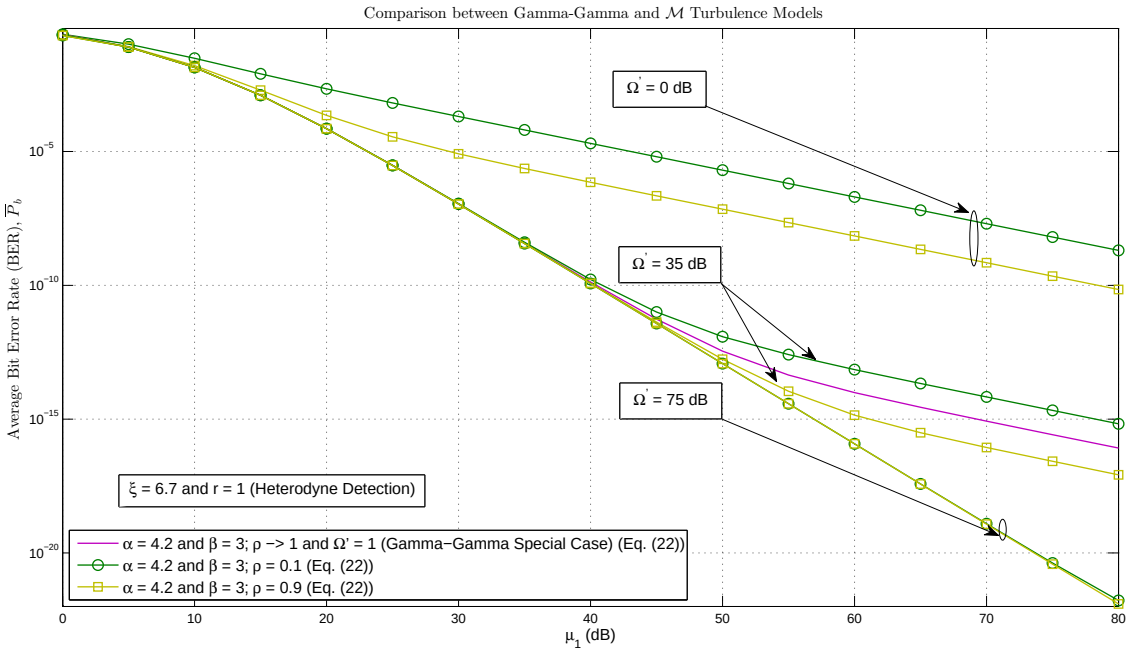

Figure 2.8: Comparison of the FSO link performance with Gamma-Gamma and $\mathcal{M}$ turbulent channels with fixed α, β, and ξ.

Table 2.2: Special Cases for Gamma-Gamma Atmospheric Turbulence Performance Metrics

Performance Metric	**Heterodyne Detection** ($r = 1$) **With Pointing Errors**	**Heterodyne Detection** ($r = 1$) **Without Pointing Errors** ($\xi \to \infty$)	**IM/DD** ($r = 2$) **With Pointing Errors**	**IM/DD** ($r = 2$) **Without Pointing Errors** ($\xi \to \infty$)
Outage Probability (OP)	$F_\gamma(\gamma) = J\, \mathrm{G}_{2,4}^{3,1}\left[K\frac{\gamma}{\mu_1}\middle\vert\begin{smallmatrix}1,\kappa_1\\ \kappa_3,0\end{smallmatrix}\right]$ $J = \xi^2/\left[\Gamma(\alpha)\Gamma(\beta)\right]$ $K = \xi^2\alpha\,\beta/\left(\xi^2+1\right)$ $\kappa_1 = \xi^2+1$ $\kappa_3 = \xi^2, \alpha, \beta$ [48, Eq. (15)], [64, Eq. (17)]	$F_\gamma(\gamma) = J\, \mathrm{G}_{1,3}^{2,1}\left[K\frac{\gamma}{\mu_1}\middle\vert\begin{smallmatrix}1\\ \kappa_3,0\end{smallmatrix}\right]$ $J = 1/\left[\Gamma(\alpha)\Gamma(\beta)\right]$ $K = \alpha\,\beta$ $\kappa_3 = \alpha, \beta$ [65, Eq. (16)], [51, Eq. (7)]	$F_\gamma(\gamma) = J\, \mathrm{G}_{3,7}^{6,1}\left[K\frac{\gamma}{\mu_2}\middle\vert\begin{smallmatrix}1,\kappa_1\\ \kappa_3,0\end{smallmatrix}\right]$ $J = 2^{\alpha+\beta-2}\,\xi^2/\left[(2\,\pi)\Gamma(\alpha)\Gamma(\beta)\right]$ $K = (\xi^2\alpha\,\beta)^2/\left[16\,\left(\xi^2+1\right)^2\right]$ $\kappa_1 = \frac{\xi^2+1}{2}, \frac{\xi^2+2}{2}$ $\kappa_3 = \frac{\xi^2}{2}, \frac{\xi^2+1}{2}, \frac{\alpha}{2}, \frac{\alpha+1}{2}, \frac{\beta}{2}, \frac{\beta+1}{2}$	$F_\gamma(\gamma) = J\, \mathrm{G}_{1,5}^{4,1}\left[K\frac{\gamma}{\mu_2}\middle\vert\begin{smallmatrix}1\\ \kappa_3,0\end{smallmatrix}\right]$ $J = 2^{\alpha+\beta-2}/\left[(2\,\pi)\Gamma(\alpha)\Gamma(\beta)\right]$ $K = (\alpha\,\beta)^2/16$ $\kappa_3 = \frac{\alpha}{2}, \frac{\alpha+1}{2}, \frac{\beta}{2}, \frac{\beta+1}{2}$ [63, Eq. (15)]
Bit-Error Rate (BER)	$\overline{P}_b = \frac{J}{2\,\Gamma(p)}\, \mathrm{G}_{3,4}^{3,2}\left[\frac{K}{\mu_1\, q}\middle\vert\begin{smallmatrix}1-p,1,\kappa_1\\ \kappa_3,0\end{smallmatrix}\right]$ [48, Eq. (24)]	$\overline{P}_b = \frac{J}{2\,\Gamma(p)}\, \mathrm{G}_{2,3}^{2,2}\left[\frac{K}{\mu_1\, q}\middle\vert\begin{smallmatrix}1-p,1\\ \kappa_3,0\end{smallmatrix}\right]$ [51, Eq. (10)], [75, Eq. (7)]	$\overline{P}_b = \frac{J}{2\,\Gamma(p)}\, \mathrm{G}_{4,7}^{6,2}\left[\frac{K}{\mu_2\, q}\middle\vert\begin{smallmatrix}1-p,1,\kappa_1\\ \kappa_3,0\end{smallmatrix}\right]$ [74, Eq. (5)]	$\overline{P}_b = \frac{J}{2\,\Gamma(p)}\, \mathrm{G}_{2,5}^{4,2}\left[\frac{K}{\mu_2\, q}\middle\vert\begin{smallmatrix}1-p,1,\kappa_1\\ \kappa_3,0\end{smallmatrix}\right]$
Ergodic Capacity	$\overline{C} = \frac{J}{\ln(2)}\, \mathrm{G}_{3,5}^{5,1}\left[\frac{K}{\mu_1^{\sim}}\middle\vert\begin{smallmatrix}0,1,\kappa_1\\ \kappa_3,0,0\end{smallmatrix}\right]$ [84, Eq. (10)]	$\overline{C} = \frac{J}{\ln(2)}\, \mathrm{G}_{2,4}^{4,1}\left[\frac{K}{\mu_1^{\sim}}\middle\vert\begin{smallmatrix}0,1\\ \kappa_3,0,0\end{smallmatrix}\right]$ [85, Eq. (16)], [86, Eq. (3)]	$\overline{C} = \frac{J}{\ln(2)}\, \mathrm{G}_{4,8}^{8,1}\left[\frac{K}{\mu_2^{\sim}}\middle\vert\begin{smallmatrix}0,1,\kappa_1\\ \kappa_3,0,0\end{smallmatrix}\right]$ [50, Eq. (22)]	$\overline{C} = \frac{J}{\ln(2)}\, \mathrm{G}_{2,6}^{6,1}\left[\frac{K}{\mu_2^{\sim}}\middle\vert\begin{smallmatrix}0,1\\ \kappa_3,0,0\end{smallmatrix}\right]$ [63, Eq. (21)], [50, Eq. (11)]

Chapter 3

Ergodic Capacity Analysis of Free-Space Optical Links with Nonzero Boresight Pointing Errors

3.1 Introduction

3.1.1 Motivation

Over the last couple of decades, a good amount of work has been done on studying the performance of a single FSO link operating over weak turbulence channels modeled by lognormal (LN) distribution (see [87–91] and references cited therein), operating over composite turbulence channels (such as Rician-lognormal (RLN) (see [92–95] and references cited therein)), and operating over generalized turbulence channels modeled by Málaga ($\mathcal{M}$) distribution (see [56, 96, 97] and references therein) and Gamma-Gamma (GG) distribution (as a special case to $\mathcal{M}$ distribution) (see [12, 37–41, 52, 98, 99] and references therein). All the above referred analysis has been done under heterodyne detection as well as IM/DD techniques, though independently.

However, as per authors best knowledge, there are no unified exact expressions nor asymptotic expressions that capture the ergodic capacity performance of both these detection techniques with nonzero boresight pointing errors under such turbulence channels.

3.1.2 Contributions

The key contributions of this chapter are stated as follows.

- The integrals are setup for the ergodic capacity of the LN, the RLN, and the $\mathcal{M}$ (also GG as a special case of $\mathcal{M}$) turbulence models in composition with nonzero boresight pointing errors. On analyzing these integrals, it is realized that most of these *integrals are very complex to solve* and to the authors best knowledge, an exact closed-form solution to most of these integrals is not achievable. Hence, it is required to look into alternative solutions to analyze the ergodic capacity for such turbulence models.

- A *unified approach for the calculation of the moments* of a single FSO link is presented in exact closed-form in terms of simple elementary functions for the LN, the RLN, and the $\mathcal{M}$ (also GG as a special case of $\mathcal{M}$) turbulence models. These unified moments are then utilized, as an alternative solution, to perform the ergodic capacity analysis for such turbulence models.

- A *general methodology* is presented for simplifying the ergodic capacity analysis of composite FSO turbulence models by independently integrating the various constituents of the composite turbulence model thereby trying to reduce the number of integrals. If we are able to reduce to a single integral (that is not solvable further) then various techniques such as Gauss-Hermite formula can be utilized to obtain the required results.

- *Asymptotic closed-form expressions* for the ergodic capacity of the LN, the RLN, and the $\mathcal{M}$ (also GG as a special case of $\mathcal{M}$) FSO turbulence models, applicable at high as well as low SNR regimes, are derived in terms of simple elementary functions via utilizing the derived unified moments.

3.1.3 Structure

The remainder of the chapter is organized as follows. Section 2 presents the channel and system model inclusive of the nonzero boresight pointing error model and the various turbulence models applicable to both the types of detection techniques (i.e. heterodyne detection and IM/DD) utilized in this work. Section 3 presents the derivation of the exact closed-form channel statistic in terms of the moments in simple elementary functions for the various turbulence models introduced in Section 2 under the effects of nonzero boresight effects. Ergodic capacity analysis in terms of approximate though closed-form expressions is presented along with some simulation results to validate these analytical results in Section 4 for these turbulence channels in terms of simple elementary functions. Finally Section 5 makes some concluding remarks.

3.2 Channel and System Model

A FSO system with either of the two types of detection techniques i.e. heterodyne detection (denoted in the formulas by $r = 1$) or IM/DD (denoted in the formulas by $r = 2$) is considered. The transmitted data propagates through an atmospheric turbulence channel in the presence of pointing errors. The received optical power is converted into an electrical signal through either of the two types of detection techniques (i.e. heterodyne detection or IM/DD) at the photodetector. Assuming

AWGN N for the thermal/shot noise, the received signal y can be expressed as

$$y = I\,x + N, \tag{3.1}$$

where x is the transmit intensity and I is the channel gain. Following [59, 95], the off-axis scintillation is assumed to vary slowly near the spot of boresight displacement and uses a constant value of scintillation index to characterize the atmospheric turbulence. Hence, the atmospheric turbulence and the pointing error are independent. Subsequently, the channel gain can be expressed as $I = I_l\, I_a\, I_p$, where I_l is the path loss that is a constant in a given weather condition and link distance, I_a is a random variable that signifies the atmospheric turbulence loss factor, and I_p is another random variable that represents the pointing error loss factor.

3.2.1 Pointing Error Models

Nonzero Boresight Pointing Error Model

Pointing error impairments are assumed and employed to be present for which the PDF of the irradiance I_p with nonzero boresight effects is given by [1] [95, Eq. (5)]

$$\begin{aligned} f_p(I_p) = {} & \xi^2 / A_0^{\xi^2} \, \exp\left\{-s^2 / \left(2\,\sigma_s^2\right)\right\} \, I_p^{\xi^2 - 1} \\ & \times I_0\left(s/\sigma_s \sqrt{-2\,\xi^2 \, \ln\left\{I_p/A_0\right\}}\right), \qquad 0 \le I_p \le A_0, \end{aligned} \tag{3.2}$$

where ξ is the ratio between the equivalent beam radius at the receiver and the pointing error displacement standard deviation (jitter) σ_s at the receiver, A_0 is a constant term that defines the pointing loss, s is the boresight displacement, and $I_v\,(.)$ represents the v^{th}-order modified Bessel functions of an imaginary argument of the first kind [58, Sec. (8.431)].

[1] For detailed information on this model of the pointing error and its subsequent derivation, one may refer to [95].

Zero Boresight Pointing Error Model

The PDF of the irradiance I_p with zero boresight effects (i.e. $s = 0$ in (3.2)) is given by [2] [59, Eq. (11)]

$$f_p(I_p) = \xi^2 \, I_p^{\xi^2 - 1} / A_0^{\xi^2}, \qquad 0 \leq I_p \leq A_0. \tag{3.3}$$

3.2.2 Atmospheric Turbulence Models

Lognormal (LN) Turbulence Scenario

The optical turbulence can be modeled as LN distribution when the optical channel is considered as a clear-sky atmospheric turbulence channel [88]. Hence, for weak turbulence conditions, reference [38] suggested a LN PDF to model the irradiance that is the power density of the optical beam. Employing weak turbulence conditions, with a log-scale parameter λ, the LN PDF of the irradiance I_{a_L} is given by (please refer to [38, 88] and references therein)

$$f_L(I_{a_L}) = \frac{1}{I_{a_L}\sqrt{2\,\pi}\,\sigma} \, \exp\left\{ -\frac{\left[\ln\left(I_{a_L}\right) - \lambda\right]^2}{2\,\sigma^2} \right\}, \quad I_{a_L} > 0, \tag{3.4}$$

where $\sigma^2 = \mathbb{E}_I[I^2]/\mathbb{E}_I^2[I] - 1 < 1$ is defined as the scintillation index [88, Eq. (1)] or the Rytov variance σ_R^2 and is related to the log-amplitude variance by $\sigma_X^2 = \sigma_R^2/4 = \sigma^2/4$, and λ is the log-scale parameter [88].

Now, the joint distribution of $I_{LN} = I_l \, I_{a_L} \, I_p$ can be derived by utilizing

$$\begin{aligned} f(I_{LN}) &= \int_{I_{LN}/A_0}^{\infty} f_{I_{LN}|I_{a_L}}(I_{LN}|I_{a_L}) \, f_L(I_{a_L}) \, dI_{a_L} \\ &= \int_{I_{LN}/A_0}^{\infty} \frac{1}{I_l \, I_{a_L}} \, f_p\left(\frac{I_{LN}}{I_l \, I_{a_L}}\right) \, f_L(I_{a_L}) \, dI_{a_L}. \end{aligned} \tag{3.5}$$

On substituting (3.4) and (3.2) appropriately into the integral in (3.5), the following

[2] For detailed information on this model of the pointing error and its subsequent derivation, one may refer to [59].

PDF under the influence of nonzero boresight effects is obtained as [95, Eq. (10)]

$$f(I_{LN}) = \xi^2 / \left[2\ (I_l\, A_0)^{\xi^2}\right]\ I_{LN}^{\xi^2-1}\ \exp\left\{\xi^2\left[\xi^2\,\sigma^2/2 - \lambda\right] + s^2/\sigma_s^2\right\} \times \operatorname{erfc}\left\{\frac{\xi^2\,\sigma^2 - \lambda + \frac{3\,s}{2\,\xi^2\,\sigma_s^2} + \ln\left\{\frac{I_{LN}}{I_l\,A_0}\right\}}{\sqrt{2\left(\frac{s^2}{\sigma_s^2\,\xi^4} + \sigma^2\right)}}\right\}, \tag{3.6}$$

where erfc $\{.\}$ is the complementary error function [79, Eq. (7.1.2)]. As a special case, for $s = 0$, the integral in (3.5) results into the PDF that corresponds to the absence of the boresight effects as

$$f(I_{LN}) = \xi^2 / \left[2\ (I_l\, A_0)^{\xi^2}\right]\ I_{LN}^{\xi^2-1}\ \exp\left\{\xi^2\left[\xi^2\,\sigma^2/2 - \lambda\right]\right\} \times \operatorname{erfc}\left\{\left[\xi^2\,\sigma^2 - \lambda + \ln\left\{I_{LN}/\left(I_l\,A_0\right)\right\}\right] / \left[\sqrt{2}\,\sigma\right]\right\}. \tag{3.7}$$

Rician-Lognormal (RLN) Turbulence Scenario

In FSO communication environments, the received signals can also be modeled as the product of two independent random processes i.e. a Rician small-scale turbulence process and a lognormal large-scale turbulence process [92, 93]. The Rician PDF (amplitude PDF) of the irradiance I_{a_R} is given by [3, Eq. (2.16)]

$$f_R\left(I_{a_R}\right) = \left(k^2+1\right)/\Omega\ \exp\left\{-k^2 - \left[\left(k^2+1\right)/\Omega\right]\ I_{a_R}\right\} \times I_0\left(2\,k\,\sqrt{\left(k^2+1\right)/\Omega\, I_{a_R}}\right), \qquad I_{a_R} > 0, \tag{3.8}$$

where Ω is the mean-square value or the average power of the irradiance being considered and $0 < k < \infty$ is the turbulence parameter. This parameter k is related to the Rician K factor by $K = k^2$ that corresponds to the ratio of the power of the LOS (specular) component to the average power of the scattered component. The LN PDF is as given in (3.4).

Now, with the presence of the nonzero boresight pointing errors whose PDF is

given in (3.2), the combined PDF of $I_{RLN} = I_l\, I_{a_R}\, I_{a_L}\, I_p$ is given as

$$\begin{aligned} f\left(I_{RLN}\right) = {} & \left(k^2+1\right)\, \xi^2 / \left[2\, \left(I_l\, A_0\right)^{\xi^2}\right]\, \exp\left\{-k^2\right\} \\ & \times \exp\left\{\xi^2 \left[\frac{\xi^2\, \sigma^2}{2} - \lambda\right] + \frac{s^2}{\sigma_s^2}\right\} \int_0^\infty \frac{1}{z^{\,\xi^2}}\, \exp\left\{-\frac{k^2+1}{z}\, I_{RLN}\right\} \\ & \times I_0\left(2\, k \sqrt{\frac{k^2+1}{z}\, I_{RLN}}\right) \operatorname{erfc}\left\{\frac{\xi^2\, \sigma^2 - \lambda + \frac{3\, s}{2\, \xi^2\, \sigma_s^2} + \ln\left\{\frac{z}{I_l\, A_0}\right\}}{\sqrt{2\left(\frac{s^2}{\sigma_s^2\, \xi^4} + \sigma^2\right)}}\right\} dz. \end{aligned} \tag{3.9}$$

Similarly, the combined PDF of $I_{RLN} = I_l\, I_{a_R}\, I_{a_L}\, I_p$, in presence of zero boresight pointing errors whose PDF is given in (3.3), is given as

$$\begin{aligned} f\left(I_{RLN}\right) = {} & \left(k^2+1\right)\, \xi^2 / \left[2\, \left(I_l\, A_0\right)^{\xi^2}\right]\, \exp\left\{-k^2\right\} \\ & \times \exp\left\{\xi^2 \left[\frac{\xi^2\, \sigma^2}{2} - \lambda\right]\right\} \int_0^\infty \frac{1}{z^{\,\xi^2}}\, \exp\left\{-\frac{k^2+1}{z}\, I_{RLN}\right\} \\ & \times I_0\left(2\, k \sqrt{\frac{k^2+1}{z}\, I_{RLN}}\right) \operatorname{erfc}\left\{\frac{\xi^2\, \sigma^2 - \lambda - \ln\left\{\frac{z}{I_l\, A_0}\right\}}{\sqrt{2}\, \sigma}\right\} dz. \end{aligned} \tag{3.10}$$

The integrals in (3.9) and (3.10) are not easy to solve and hence the analysis will be resorted based on moments as will be seen in the upcoming sections.

Málaga ($\mathcal{M}$) Turbulence Scenario

The optical turbulence can be modeled as $\mathcal{M}$ distribution when the irradiance fluctuating of an unbounded optical wavefront (plane or spherical waves) propagates through a turbulent medium under all irradiance conditions in homogeneous, isotropic turbulence [56]. As a special case, the optical turbulence can be modeled as GG distribution when the optical channel is considered as a cloudy/foggy-sky atmospheric turbulence channel [48–51, 100]. Hence, employing generalized turbulence conditions,

the PDF of the irradiance I_{a_M} is given by [56]

$$f_M(I_{a_M}) = A \sum_{m=1}^{\beta} a_m \, I_{a_M} \, K_{\alpha-m}\left(2\sqrt{\frac{\alpha\,\beta\,I_{a_M}}{g\,\beta+\Omega'}}\right), \quad I_{a_M} > 0, \tag{3.11}$$

where all the parameters [3] in (3.11) have been defined in Section 2.2.1 [4].

Now, with the presence of the nonzero boresight pointing errors whose PDF is given in (3.2), the combined PDF of $I_M = I_l \, I_{a_M} \, I_p$ is given as

$$\begin{aligned} f\left(I_M\right) = & \frac{\xi^2 \, A \, I_M^{\xi^2-1}}{I_l^{\xi^2} \, A_0^{\xi^2}} \, \exp\left\{-\frac{s^2}{2\,\sigma_s^2}\right\} \sum_{m=1}^{\beta} \int_{I/A_0}^{\infty} I_{aM}^{1-\xi^2} \\ & \times I_0\left(\frac{s}{\sigma_s}\sqrt{-2\,\xi^2 \, \ln\left\{\frac{I_M}{I_l \, I_{a_M} \, A_0}\right\}}\right) \, K_{\alpha-m}\left(2\sqrt{\frac{\alpha\,\beta\,I_{a_M}}{g\,\beta+\Omega'}}\right) dI_{a_M}. \end{aligned} \tag{3.12}$$

The integral in (3.12) is not easy to solve in closed-form and hence the analysis will be resorted based on moments as will be seen in the upcoming sections. Similarly, the combined PDF of $I_M = I_l \, I_{a_M} \, I_p$, in presence of zero boresight pointing errors (i.e. $s = 0$ in (3.12)) whose PDF is given in (3.3), is known to be given by [56]

$$f(I_M) = \frac{\xi^2 A}{2\,I_M} \sum_{m=1}^{\beta} b_m \, \mathrm{G}_{1,3}^{3,0}\left[\frac{\alpha\,\beta}{(g\,\beta+\Omega')}\frac{I_M}{A_0}\,\middle|\,\begin{matrix}\xi^2+1\\ \xi^2, \alpha, m\end{matrix}\right], \tag{3.13}$$

where $b_m = a_m \left[\alpha\,\beta/\left(g\,\beta+\Omega'\right)\right]^{-(\alpha+m)/2}$ and G[.] is the Meijer's G function as defined in [58, Eq. (9.301)].

[3] A generalized expression of (3.11) is given in [56, Eq. (22)] for real β number though it is less interesting due to the high degree of freedom of the proposed distribution (Sec. III of [56]).

[4] Detailed information on the $\mathcal{M}$ distribution, its formation, and its random generation can be found in [56, Eqs. (13-21)].

3.2.3 Important Outcomes and Further Motivations

To the best of our knowledge, it is quite tedious to manipulate the expressions in (3.6)-(3.13) [5]. As will be shown in Section 3.4, it is in most cases not possible or challenging to deal with such expressions to obtain some further exact closed-form results for the ergodic capacity of such a FSO channel. Therefore, the capacity analysis of such FSO link is carried out utilizing moments as will be derived in the following section.

3.3 Exact Closed-Form Moments

As has seen above that it is quite a challenge to obtain closed-form PDF and even if it is possible to find one, the expression(s) are not simple enough to be utilized further for the analysis of the ergodic capacity as will be seen in the following section. Hence, the analysis is resorted to moments based for which the moments for the various turbulence scenarios discussed in the previous section are derived here.

For the heterodyne detection technique case, the instantaneous SNR $\gamma = \eta_e\, I/N_0$ and the average SNR [6] develops as $\mu_{\text{heterdoyne}} = \mathbb{E}_{\gamma_{\text{heterodyne}}}[\gamma] = \overline{\gamma}_{\text{heterodyne}} = \eta_e\, \mathbb{E}_I[I]/N_0$, where η_e is the effective photoelectric conversion ratio, N_0 symbolizes the AWGN sample, and $\mathbb{E}\,[.]$ denotes the expectation operator.

Similarly, for the IM/DD technique, $\gamma = \eta_e^2\, I^2/N_0$ and the electrical SNR [7] devel-

[5] Similar results corresponding to (3.12) and (3.13) have also been derived for the GG turbulence scenario though those have not been presented here as GG turbulence is a special case of $\mathcal{M}$ turbulence.

[6] $\overline{\gamma}_{\text{heterodyne}}$ is the average SNR for coherent/heterodyne FSO systems given by $\overline{\gamma}_{\text{heterodyne}} = C_c$ [60, Eq. (7)], where $C_c = 2\,R^2 A\,P_{LO}/\left[2\,q\,R\,\Delta f\,P_{LO} + 2\,\Delta f\,(q\,R\,A\,I_b + 2\,k_b\,T_k\,F_n/R_L)\right] \approx R\,A/\left(q\,\Delta f\right)$ is a multiplicative constant for a given heterodyne/coherent system, where R is the photodetector responsivity, A is the photodetector area, P_{LO} is the local oscillator power, Δf denotes the noise equivalent bandwidth of a FSO receiver, q is the electronic charge, I_b is the background light irradiance, k_b is Boltzmann's constant, T_k is the temperature in Kelvin, F_n represents a thermal noise enhancement factor due to amplifier noise, and R_L is the load resistance. It is evident that $C_c = \mu_{\text{heterodyne}}$ in this work.

[7] $\overline{\gamma}_{\text{IM/DD}}$ is the average SNR for IM/DD FSO systems given by $\overline{\gamma}_{\text{IM/DD}} = C_s\,\mathbb{E}_I[I^2]/\mathbb{E}_I^2[I]$, where $C_s = \left(R\,A\,\xi\right)^2/\left[2\,\Delta f\,(q\,R\,A\,I_b + 2\,k_b\,T_k\,F_n/R_L)\right]$ [60] is a multiplicative constant for a given IM/DD system. It is evident that $C_s = \mu_{\text{IM/DD}}$ in this work.

ops as $\mu_{\text{IM/DD}} = \mathbb{E}_{\gamma_{\text{IM/DD}}}[\gamma]\,\mathbb{E}_I^2[I]/\mathbb{E}_I[I^2] = \overline{\gamma}_{\text{IM/DD}}\,\mathbb{E}_I^2[I]/\mathbb{E}_I[I^2] = \eta_e^2\,\mathbb{E}_I^2[I]/N_0$ [50].

Now, on combining the SNR expressions above for both the detection types, $\gamma_r = \eta_e^r\, I^r/N_0$ and $\mu_r = \eta_e^r\,\mathbb{E}_I^r[I]/N_0$ are obtained. Since, I_a and I_p are independent random variables, the unified moments are defined as [8, 9]

$$\begin{aligned}\mathbb{E}\left[\gamma_r^n\right] &= \eta_e^{r\,n}\,\mathbb{E}\left[I^{r\,n}\right]/N_0^n = \mu_r^n\,\mathbb{E}\left[\left(I_a\,I_p\right)^{r\,n}\right]/\mathbb{E}^{r\,n}[I_a\,I_p] \\ &= \mu_r^n\,\mathbb{E}\left[I_a^{r\,n}\right]\mathbb{E}\left[I_p^{r\,n}\right]/\left(\mathbb{E}^{r\,n}[I_a]\,\mathbb{E}^{r\,n}[I_p]\right).\end{aligned} \tag{3.14}$$

3.3.1 Lognormal (LN) Turbulence Scenario

The unified moments for this particular scenario are defined as

$$\begin{aligned}\mathbb{E}\left[\gamma_r^n\right]_{LN} &= \eta_e^{r\,n}\,\mathbb{E}\left[I^{r\,n}\right]/N_0^n = \mu_r^n\,\mathbb{E}\left[\left(I_{a_L}\,I_p\right)^{r\,n}\right]/\mathbb{E}^{r\,n}[I_{a_L}\,I_p] \\ &= \mu_r^n\,\mathbb{E}\left[I_{a_L}^{r\,n}\right]\mathbb{E}\left[I_p^{r\,n}\right]/\left(\mathbb{E}^{r\,n}[I_{a_L}]\,\mathbb{E}^{r\,n}[I_p]\right).\end{aligned} \tag{3.15}$$

Utilizing the definition of the moments, $\mathbb{E}\left[I_{a_L}^{r\,n}\right]$ and $\mathbb{E}\left[I_p^{r\,n}\right]$ for nonzero boresight pointing errors are easily obtained after some manipulations as $\mathbb{E}\left[I_{a_L}^{r\,n}\right] = \exp\left\{r\,n\,\lambda + \left(r\,n\,\sigma\right)^2/2\right\}$ and $\mathbb{E}\left[I_p^{r\,n}\right] = A_0^{r\,n}\,\xi^2/\left(\xi^2 + r\,n\right)\exp\left\{-r\,n\,s^2/\left[2\,\sigma_s^2\left(\xi^2 + r\,n\right)\right]\right\}$ [95, Eq. (6)], respectively. Substituting these back into (3.15), the unified exact closed-form moments for LN atmospheric turbulence in presence of nonzero boresight pointing errors are obtained as

$$\begin{aligned}\mathbb{E}\left[\gamma_r^n\right]_{LN} = \frac{\xi^{2(1-r\,n)}}{\left(\xi^2 + r\,n\right)\left(\xi^2+1\right)^{-r\,n}}\,\exp\Bigg\{&\frac{r\,n\,\sigma^2}{2}\left(r\,n - 1\right) \\ &+ r\,n\,s^2/\left(2\,\sigma_s^2\right)\left[1/\left(\xi^2+1\right) - 1/\left(\xi^2 + r\,n\right)\right]\Bigg\}\,\mu_r^n.\end{aligned} \tag{3.16}$$

[8] I_l, A_0, and λ cancel out being deterministic parameters.

[9] $\overline{\gamma}_1$ is the first moment (i.e. $n = 1$) for the heterodyne ($r = 1$) case as can be seen from (3.14). Based on this substitution, we obtain $\overline{\gamma}_1 = \mu_1$ signifying that $\overline{\gamma}_1$ and μ_1 are the same quantity defined as the average SNR for the heterodyne FSO systems. Similarly, $\overline{\gamma}_2$ is the first moment (i.e. $n = 1$) for the IM/DD ($r = 2$) case as can be seen from (3.14). Based on this substitution, we obtain $\overline{\gamma}_2 = \mathbb{E}\left[I_a^2\right]\mathbb{E}\left[I_p^2\right]/\left(\mathbb{E}^2[I_a]\,\mathbb{E}^2[I_p]\right)\,\mu_2 = \mathbb{E}\left[I^2\right]/\mathbb{E}^2[I]\,\mu_2$ or $\mu_2 = \mathbb{E}^2[I_a]\,\mathbb{E}^2[I_p]/\left(\mathbb{E}\left[I_a^2\right]\mathbb{E}\left[I_p^2\right]\right)\,\overline{\gamma}_2 = \mathbb{E}^2[I]/\mathbb{E}\left[I^2\right]\overline{\gamma}_2$ signifying that $\overline{\gamma}_2$ and μ_2 are different quantities defined as the average SNR and the electrical SNR for the IM/DD FSO systems, respectively [60].

Similarly, when considering zero boresight pointing errors (i.e. special case with $s = 0$), the $\mathbb{E}\left[I_p^{r\,n}\right] = A_0^{r\,n}\,\xi^2/\left(\xi^2 + r\,n\right)$ and the corresponding unified exact closed-form moments for LN atmospheric turbulence in presence of zero boresight pointing errors are obtained as

$$\mathbb{E}\left[\gamma_r^n\right]_{LN} = \frac{\xi^{2(1-r\,n)}}{\left(\xi^2 + r\,n\right)\left(\xi^2+1\right)^{-r\,n}}\,\exp\left\{\frac{r\,n\,\sigma^2}{2}\left(r\,n-1\right)\right\}\,\mu_r^n. \tag{3.17}$$

3.3.2 Rician-Lognormal (RLN) Turbulence Scenario

Since I_{a_R}, I_{a_L}, and I_p are independent random variables, the unified moments for RLN turbulence scenario are defined as

$$\begin{aligned}\mathbb{E}\left[\gamma_r^n\right]_{RLN} &= \eta_e^{r\,n}\,\mathbb{E}\left[I^{r\,n}\right]/N_0^n = \mu_r^n\,\mathbb{E}\left[\left(I_{a_R}\,I_{a_L}\,I_p\right)^{r\,n}\right]/\mathbb{E}^{r\,n}[I_{a_R}\,I_{a_L}\,I_p] \\ &= \mu_r^n\,\mathbb{E}\left[I_{a_R}^{r\,n}\right]\mathbb{E}\left[I_{a_L}^{r\,n}\right]\mathbb{E}\left[I_p^{r\,n}\right]/\left(\mathbb{E}^{r\,n}[I_{a_R}]\,\mathbb{E}^{r\,n}[I_{a_L}]\,\mathbb{E}^{r\,n}[I_p]\right).\end{aligned} \tag{3.18}$$

Utilizing the definition of the moments, $\mathbb{E}\left[I_{a_L}^{r\,n}\right]$ and $\mathbb{E}\left[I_p^{r\,n}\right]$ for nonzero boresight pointing errors were easily obtained in previous subsection i.e. Section 3.3.1 whereas $\mathbb{E}\left[I_{a_R}^{r\,n}\right] = \left[\Omega/\left(k^2+1\right)\right]^{r\,n}\,\Gamma\left(r\,n+1\right)\,{}_1F_1\left[-r\,n;1;-k^2\right]$ [3, Eq. (2.18)], where ${}_pF_q\left[.;.;.\right]$ represents the generalized hypergeometric F function [58, Eq. (9.14.1)] and more specifically, ${}_1F_1\left[.;.;.\right]$ represents the confluent hypergeometric F function [58, Eq. (9.210.1)]. Substituting these back into (3.18), the unified exact closed-form moments for RLN turbulence under nonzero boresight pointing errors are obtained as [10]

$$\begin{aligned}\mathbb{E}\left[\gamma_r^n\right]_{RLN} &= \xi^{2(1-r\,n)}/\left[\left(\xi^2+r\,n\right)\left(\xi^2+1\right)^{-r\,n}\right] \\ &\quad\times\exp\left\{\frac{r\,n\,\sigma^2}{2}\left(r\,n-1\right)+\frac{r\,n\,s^2}{2\,\sigma_s^2}\left(\frac{1}{\xi^2+1}-\frac{1}{\xi^2+r\,n}\right)\right\} \\ &\quad\times\Gamma\left(r\,n+1\right)\,{}_1F_1\left[-r\,n;1;-k^2\right]/\left(k^2+1\right)^{r\,n}\,\mu_r^n.\end{aligned} \tag{3.19}$$

[10] It must be noted that ${}_1F_1\left[-1;1;-k^2\right] = k^2+1$.

Similarly, when considering zero boresight pointing errors (i.e. special case with $s = 0$), the corresponding unified exact closed-form moments for RLN atmospheric turbulence in presence of zero boresight pointing errors are obtained as

$$\begin{aligned}\mathbb{E}\left[\gamma_r^n\right]_{RLN} &= \xi^{2(1-r\,n)} / \left[\left(\xi^2 + r\,n\right)\left(\xi^2+1\right)^{-r\,n}\right] \\ &\times \exp\left\{\frac{r\,n\,\sigma^2}{2}\left(r\,n-1\right)\right\} \frac{{}_1F_1\left[-r\,n;1;-k^2\right]}{\left(k^2+1\right)^{r\,n}\,\Gamma\left(r\,n+1\right)^{-1}}\,\mu_r^n.\end{aligned} \tag{3.20}$$

3.3.3 Málaga ($\mathcal{M}$) Turbulence Scenario

Since I_{a_M} and I_p are independent random variables, the unified moments for $\mathcal{M}$ turbulence scenario are defined as

$$\begin{aligned}\mathbb{E}\left[\gamma_r^n\right]_M &= \eta_e^{r\,n}\,\mathbb{E}\left[I^{r\,n}\right]/N_0^n = \mu_r^n\,\mathbb{E}\left[\left(I_{a_M}\,I_p\right)^{r\,n}\right]/\mathbb{E}^{r\,n}[I_{a_M}\,I_p] \\ &= \mu_r^n\,\mathbb{E}\left[I_{a_M}^{r\,n}\right]\mathbb{E}\left[I_p^{r\,n}\right]/\left(\mathbb{E}^{r\,n}[I_{a_M}]\,\mathbb{E}^{r\,n}[I_p]\right).\end{aligned} \tag{3.21}$$

Utilizing the definition of the moments, $\mathbb{E}\left[I_p^{r\,n}\right]$ for nonzero boresight pointing errors was easily obtained in previous subsection i.e. Section 3.3.1 whereas $\mathbb{E}\left[I_{a_M}^{r\,n}\right]/\mathbb{E}^{r\,n}[I_{a_M}]$ $= r\,A\,\Gamma(r\,n+\alpha)\sum_{m=1}^{\beta} b_m\,\Gamma(r\,n+m)/\left(2^r\,B^{r\,n}\right)$ where $B = \alpha\,\beta\,(g+\Omega')/(g\,\beta+\Omega')$. Substituting these back into (3.21), the unified exact closed-form moments for $\mathcal{M}$ turbulence under nonzero boresight pointing errors are obtained as

$$\begin{aligned}\mathbb{E}\left[\gamma_r^n\right]_M &= \xi^{2(1-r\,n)} / \left[\left(\xi^2 + r\,n\right)\left(\xi^2+1\right)^{-r\,n}\right] \\ &\times \exp\left\{r\,n\,s^2/\left(2\,\sigma_s^2\right)\left[1/\left(\xi^2+1\right) - 1/\left(\xi^2+r\,n\right)\right]\right\} \\ &\times r\,A\,\Gamma(r\,n+\alpha)/\left(2^r\,B^{r\,n}\right)\sum_{m=1}^{\beta} b_m\,\Gamma(r\,n+m)\,\mu_r^n.\end{aligned} \tag{3.22}$$

As a special case, the unified exact closed-form moments for GG turbulence under nonzero boresight pointing errors are obtained as

$$\begin{aligned}\mathbb{E}\left[\gamma_r^n\right]_{GG} = &\frac{\xi^{2(1-r\,n)}\ \left(\xi^2+1\right)^{r\,n}\ \Gamma\left(r\,n+\alpha\right)\ \Gamma\left(r\,n+\beta\right)}{\left(\xi^2+r\,n\right)\ \left(\alpha\,\beta\right)^{r\,n}\ \Gamma\left(\alpha\right)\ \Gamma\left(\beta\right)} \\ &\times\ \exp\left\{r\,n\,s^2/\left(2\,\sigma_s^2\right)\left[1/\left(\xi^2+1\right)-1/\left(\xi^2+r\,n\right)\right]\right\}\ \mu_r^n.\end{aligned} \tag{3.23}$$

Similarly, when considering zero boresight pointing errors (i.e. special case with $s = 0$), the corresponding unified exact closed-form moments for $\mathcal{M}$ atmospheric turbulence in presence of zero boresight pointing errors are obtained as

$$\mathbb{E}\left[\gamma_r^n\right]_M = \frac{r\,\xi^2\,A\,\Gamma(r\,n+\alpha)}{2^r\ \left(r\,n+\xi^2\right)\ B^{r\,n}}\sum_{m=1}^{\beta} b_m\,\Gamma(r\,n+m)\,\mu_r^n. \tag{3.24}$$

As a special case, the corresponding unified exact closed-form moments for GG atmospheric turbulence in presence of zero boresight pointing errors are obtained as

$$\mathbb{E}\left[\gamma_r^n\right]_{GG} = \frac{\xi^{2(1-r\,n)}\ \left(\xi^2+1\right)^{r\,n}\ \Gamma(r\,n+\alpha)\Gamma(r\,n+\beta)}{\left(\xi^2+r\,n\right)\ \left(\alpha\,\beta\right)^{r\,n}\,\Gamma(\alpha)\,\Gamma(\beta)}\,\mu_r^n. \tag{3.25}$$

3.3.4 Important Outcomes and Further Motivations

- Interestingly enough and expectedly, the expressions in (3.16), (3.17), (3.19), (3.20), and (3.22)-(3.25) reduce to simply μ_1^n for $r = 1$ (heterodyne detection technique case) which is in line with the difference between the definitions of average SNR vs. electrical SNR.

- It is worthy to note that these simple results for the moments can be directly plugged into [68, Eq. (3)] to obtain the n^{th}-order AF for the instantaneous SNR, γ. These interesting results can be then utilized to parameterize the distribution of the SNR of the received signal.

- More importantly, these simple results for the moments are useful to conduct

asymptotic analysis of the ergodic capacity as shown in the following section of this work.

3.4 Ergodic Capacity

3.4.1 General Methodology

The ergodic channel capacity $\overline{C}$ is defined as [81, Eq. (26)], [82, Eq. (7.43)]

$$\overline{C} \triangleq \mathbb{E}\left[\ln\left\{1 + c\,\gamma\right\}\right], \tag{3.26}$$

where c is a constant term such that $c = 1$ for heterodyne detection giving an exact result and $c = e/\left(2\,\pi\right)$ for IM/DD giving a lower-bound result [81,82] [11]. Additionally, knowing that I_a and I_p are independent random variables, the definition of the ergodic capacity can be re-written as

$$\begin{aligned}\overline{C} &= \mathbb{E}\left[\ln\left\{1 + \frac{c\,\left(\eta_e\,I\right)^r}{N_0}\right\}\right] = \int_0^{\infty} \ln\left\{1 + \frac{c\,\left(\eta_e\,I\right)^r}{N_0}\right\}\,f\left(I\right)\,dI \\ &= \int_0^{\infty}\int_0^{A_0} \ln\left\{1 + \frac{c\,\left(\eta_e\,I_l\,I_a\,I_p\right)^r}{N_0}\right\}\,f_a\left(I_a\right)\,f_p\left(I_p\right)\,dI_p\,dI_a.\end{aligned} \tag{3.27}$$

Since, I_p is the common random variable in all the different atmospheric turbulence scenarios, (3.27) can possibly be solved for the two types of pointing errors. By substituting (3.2) into (3.27), to the best of our knowledge, it is not possible to find an exact closed-form solution for the inner integral. On the other hand, if (3.3) is

[11] For readers clarification, to the best of the authors knowledge based on the open literature, there does not exists any actual mathematical formulation for analyzing the ergodic capacity of such FSO channels.

placed into (3.27), we obtain

$$\begin{aligned}\overline{C} &= \int_0^{\infty}\int_0^{A_0} \ln\left\{1+\frac{c\,(\eta_e\,I_l\,I_a\,I_p)^r}{N_0}\right\}\,\xi^2\,I_p^{\xi^2-1}/A_0^{\xi^2}\,dI_p\,f_a\,(I_a)\,dI_a \\ &= \int_0^{\infty}\left[\ln\left\{\frac{c\,(\eta_e\,A_0\,I_l\,I_a)^r}{N_0}+1\right\}-\frac{c\,(\eta_e\,A_0\,I_l\,I_a)^r}{N_0}\right. \\ &\left.\times\,\Phi\left(-\frac{c\,(\eta_e\,A_0\,I_l\,I_a)^r}{N_0},1,\frac{\xi^2+r}{r}\right)\right]f_a\,(I_a)\,dI_a,\end{aligned} \tag{3.28}$$

where $\Phi\,(.)$ is the LerchPhi function [62, Eq. (10.06.02.0001.01)].

If an exact closed-form is not obtainable via either (3.26) and/or (3.27) and/or (3.28), the ergodic capacity can be analyzed utilizing the moments. At ***high SNR***, an asymptotic analysis can be done by utilizing the moments yielding an asymptotically tight lower bound given by [12] [68, Eqs. (8) and (9)]

$$\overline{C} \underset{\mu_r>>1}{\approxeq} \log(c\,\mu_r)+\zeta, \tag{3.29}$$

where

$$\zeta = \partial/\partial n\,(\mathbb{E}\,[\gamma_r^n]/\mathbb{E}\,[\gamma_r]^n-1)|_{n=0}\,. \tag{3.30}$$

This expression can be simplified to

$$\overline{C} \underset{\mu_r>>1}{\approxeq} \log(c\,\mu_r)+\frac{\partial}{\partial n}\left(\frac{\mathbb{E}\,[\gamma_r^n]}{\mathbb{E}\,[\gamma_r]^n}-1\right)\bigg|_{n=0} = \frac{\partial}{\partial n}\,\mathbb{E}\,[\gamma_r^n]\bigg|_{n=0}. \tag{3.31}$$

Similarly, at ***low SNR***, it can be easily shown that the ergodic capacity can be asymptotically approximated by the first moment.

[12] For readers clarification, it is possible to use SNR moments as an efficient tool for deriving even higher order ergodic capacity statistics utilizing [68, Eq. (6)]

3.4.2 Lognormal (LN) Turbulence Scenario

Exact Analysis

For LN atmospheric turbulence scenario under nonzero boresight pointing errors and zero boresight pointing errors, (3.6) and (3.7) are respectively substituted in (3.26). Both the above scenarios can not be solved in exact closed-form.

Additionally, a conclusion has already been obtained that it is not possible to solve the inner integral for nonzero boresight pointing errors in (3.27) with (3.2). Alternatively, by substituting (3.4) in (3.27), the outer integral for LN PDF $f_L\left(I_{a_L}\right)$ in (3.27) does not lead to possible exact closed-form results. On the other hand, the inner integral for zero boresight pointing errors in (3.27) with (3.3) was successfully solved to obtain (3.28) and hence on placing the LN PDF $f_L\left(I_{a_L}\right)$ (3.4) into (3.28),

$$\begin{aligned}\overline{C} = & \frac{1}{\sqrt{2\,\pi}\,\sigma}\int_0^{\infty}\frac{1}{I_{a_L}}\,\exp\left\{-\left[\frac{\ln\left\{I_{a_L}\right\}-\lambda}{\sqrt{2}\,\sigma}\right]^2\right\} \\ & \times\left[\ln\left\{\frac{c\,\left(\eta_e\,A_0\,I_l\,I_{a_L}\right)^r}{N_0}+1\right\}-\frac{c\,\left(\eta_e\,A_0\,I_l\,I_{a_L}\right)^r}{N_0}\right. \\ & \left.\times\,\Phi\left(-\frac{c\,\left(\eta_e\,A_0\,I_l\,I_{a_L}\right)^r}{N_0},1,\frac{\xi^2+r}{r}\right)\right]\,dI_{a_L}.\end{aligned} \tag{3.32}$$

is obtained. On applying simple change of random variable $x=\left(\ln\left\{I_{a_L}\right\}-\lambda\right)/\left(\sqrt{2}\,\sigma\right)$, we get $I_{a_L}=\exp\left\{\sqrt{2}\,\sigma\,x+\lambda\right\}$ and $dI_{a_L}=\sqrt{2}\,\sigma\,\exp\left\{\sqrt{2}\,\sigma\,x+\lambda\right\}\,dx$ and we can write

$$\overline{C}=\frac{1}{\sqrt{\pi}}\int_{-\infty}^{\infty}\exp\left\{-x^2\right\}\,f_x\left(x\right)\,dx, \tag{3.33}$$

where

$$\begin{aligned}f_x\left(x\right) = & \ln\left\{\frac{c\,\left(\eta_e\,A_0\,I_l\right)^r}{N_0}\,\exp\left\{r\left(\sqrt{2}\,\sigma\,x+\lambda\right)\right\}+1\right\} \\ & -\frac{c\,\left(\eta_e\,A_0\,I_l\right)^r}{N_0}\,\exp\left\{r\left(\sqrt{2}\,\sigma\,x+\lambda\right)\right\} \\ & \times\,\Phi\left(-\frac{c\,\left(\eta_e\,A_0\,I_l\right)^r}{N_0}\,\exp\left\{r\left(\sqrt{2}\,\sigma\,x+\lambda\right)\right\},1,\frac{\xi^2+r}{r}\right).\end{aligned} \tag{3.34}$$

The integral in (3.33) is solvable with the help of $N = 20$-point Gauss-Hermite formula [79, Eq. (25.4.46)] leading to

$$\overline{C} \cong \frac{1}{\sqrt{\pi}} \sum_{i=1}^{N} w_i \, f_x \left(x_i \right), \tag{3.35}$$

where w_i and x_i are the weights and the abscissas that can be acquired from [79, Table 25.10].

Approximate Analysis

Reverting back to LN atmospheric turbulence under nonzero boresight pointing errors, since it is not feasible to obtain an exact closed-form solution, the moments derived earlier are utilized to deduce the asymptotic results. Hence, based on (3.31), the first derivative of the moments in (3.16) is required to be evaluated at $n = 0$ for high SNR asymptotic approximation to the ergodic capacity. The first derivative of the moments in (3.16) is given as

$$\begin{aligned} \partial/\partial n \, \mathbb{E}\left[\gamma_r^n\right] = {} & \xi^{2(1-r\,n)} / \left[\left(\xi^2 + r\,n \right) \left(\xi^2 + 1 \right)^{-r\,n} \right] \\ & \times \exp\left\{ \frac{r\,n\,\sigma^2}{2} \left(r\,n - 1 \right) + \frac{r\,n\,s^2}{2\,\sigma_s^2} \left(\frac{1}{\xi^2 + 1} - \frac{1}{\xi^2 + r\,n} \right) \right\} \\ & \times \left\{ r\,\sigma^2 \left(r\,n - \frac{1}{2} \right) + \frac{r\,s^2}{2\,\sigma_s^2} \left[\frac{r\,n}{\left(\xi^2 + r\,n \right)^2} + \frac{1}{\xi^2 + 1} - \frac{1}{\xi^2 + r\,n} \right] \right. \\ & \left. - \, r / \left(r\,n + \xi^2 \right) - r \, \ln\left\{ \xi^2 / \left(\xi^2 + 1 \right) \right\} + \ln\left\{ c\,\mu_r \right\} \right\} \left(c\,\mu_r \right)^n, \end{aligned} \tag{3.36}$$

and at $n = 0$, it evaluates to

$$\overline{C} \underset{\mu_r >> 1}{\approx} \ln\left\{ c\,\mu_r \right\} - r \left[\frac{1}{\xi^2} + \frac{\sigma^2}{2} + \frac{s^2}{2\,\sigma_s^2\,\xi^2\,\left(\xi^2 + 1 \right)} + \ln\left\{ \xi^2 / \left(\xi^2 + 1 \right) \right\} \right]. \tag{3.37}$$

Similarly, for LN atmospheric turbulence under zero boresight pointing errors (i.e. for $s = 0$), the asymptotic approximation to the ergodic capacity at high SNR is derived

as

$$\overline{C} \underset{\mu_r >>1}{\approxeq} \ln\left\{c\,\mu_r\right\} - r\left[1/\xi^2 + \sigma^2/2 + \ln\left\{\xi^2/\left(\xi^2+1\right)\right\}\right]. \tag{3.38}$$

Similarly, for LN atmospheric turbulence under no pointing errors (i.e. for $s = 0$ and $\xi \to \infty$), the asymptotic approximation to the ergodic capacity at high SNR is derived as

$$\overline{C} \underset{\mu_r >>1}{\approxeq} \ln\left\{c\,\mu_r\right\} - r\,\sigma^2/2. \tag{3.39}$$

Furthermore, for ***low SNR*** asymptotic analysis, it can be easily shown that the ergodic capacity can be asymptotically approximated by the first moment. Utilizing (3.16) via placing $n = 1$ in it, the ergodic capacity of a single FSO link under LN turbulence effected by nonzero boresight pointing errors can be approximated at low SNR in closed-form in terms of simple elementary functions by

$$\begin{aligned}\overline{C} \underset{\mu_r <<1}{\approxeq} \frac{\xi^{2(1-r)}}{\left(\xi^2+r\right)\left(\xi^2+1\right)^{-r}} \exp\Bigg\{\frac{r\,\sigma^2}{2}\left(r-1\right) \\ + r\,s^2/\left(2\,\sigma_s^2\right)\left[1/\left(\xi^2+1\right) - 1/\left(\xi^2+r\right)\right]\Bigg\}\, c\,\mu_r.\end{aligned} \tag{3.40}$$

Similarly, for LN atmospheric turbulence under zero boresight pointing errors (i.e. for $s = 0$), the asymptotic approximation to the ergodic capacity at low SNR is obtained as

$$\overline{C} \underset{\mu_r <<1}{\approxeq} \frac{\xi^{2(1-r)}}{\left(\xi^2+r\right)\left(\xi^2+1\right)^{-r}} \exp\left\{\frac{r\,\sigma^2}{2}\left(r-1\right)\right\}\, c\,\mu_r. \tag{3.41}$$

Similarly, for LN atmospheric turbulence under zero pointing errors (i.e. for $s = 0$ and $\xi \to \infty$), the asymptotic approximation to the ergodic capacity at low SNR is obtained as

$$\overline{C} \underset{\mu_r <<1}{\approxeq} \exp\left\{r\,\sigma^2\left(r-1\right)/2\right\}\, c\,\mu_r. \tag{3.42}$$

Results and Discussion

As an illustration of the mathematical formalism presented above, simulation and numerical results for the ergodic capacity of a single FSO link transmission system under LN turbulent channels are presented as follows.

The FSO link is modeled as a LN turbulence channel with nonzero boresight pointing errors. The dotted lines marked as simulation in the figures represent the Monte-Carlo generation for the exact results to observe the asymptotic tightness of the approximated results and to prove their validity. The ergodic capacity of the FSO channel in operation under heterodyne detection technique as well as IM/DD technique is presented in Fig. 3.1 and Fig. 3.2, respectively, for high SNR scenario. Subsequently, the ergodic capacity of the FSO channel in operation under IM/DD

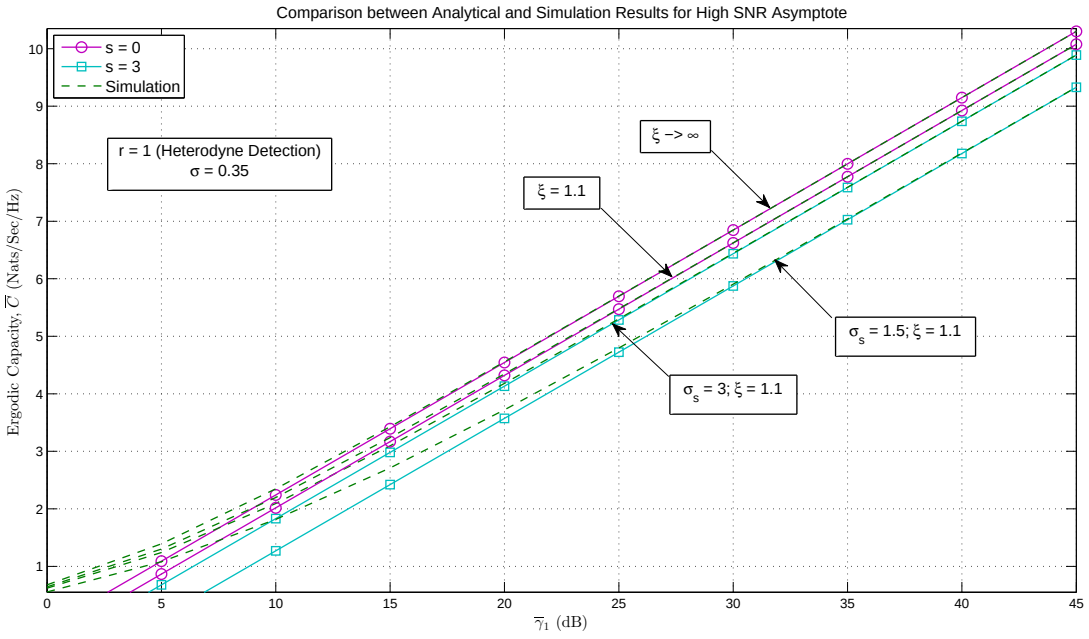

Figure 3.1: Ergodic capacity results for varying pointing errors at high SNR regime for LN turbulence under heterodyne detection technique ($r = 1$).

technique is presented in Fig. 3.3 for low SNR scenario [13]. These figures demonstrate

[13]For readers clarification, the low SNR asymptote in (3.40) is actually the average SNR and hence the plot in Fig. 3.3 is against the electrical SNR.

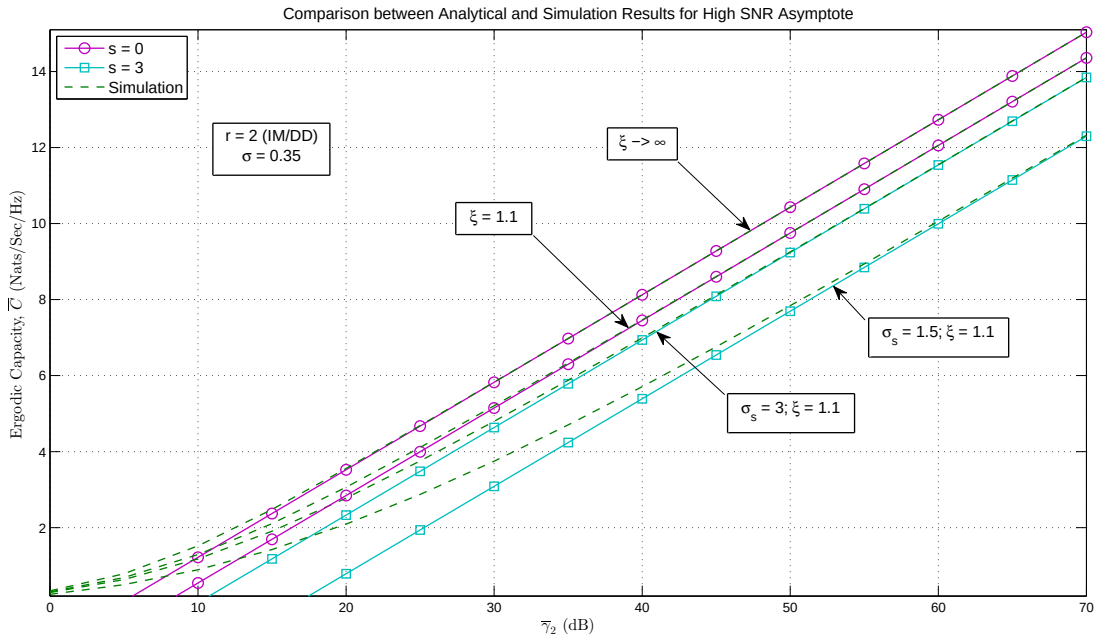

Figure 3.2: Ergodic capacity results for varying pointing errors at high SNR regime for LN turbulence under IM/DD technique ($r = 2$).

the obtained results for varying effects of pointing errors with $\sigma = 0.35$.[14]

Expectedly, for high SNR regime (i.e. Fig. 3.1 and Fig. 3.2), as the pointing error gets severe, the ergodic capacity starts decreasing (i.e. the lower the value of s and/or the higher the value of ξ, the higher will be the ergodic capacity). Interestingly, for low SNR regime (i.e. Fig. 3.3), as the pointing error gets severe, the ergodic capacity starts increasing (i.e. the lower the value of s and/or the higher the value of ξ, the lower will be the ergodic capacity). This can be explained by the dominant nature of the pointing error effects in (3.40) i.e. the pointing error inversely effects the ergodic capacity in the low SNR regime relative to the high SNR regime. Hence, we can conclude that under such given scenarios, the pointing error effects in low SNR regime assist to have a better ergodic capacity performance.

[14]It is important to note here that these values for the parameters were selected from the cited references subject to the standards to prove the validity of the obtained results and hence other specific values can be used to obtain the required results by design communication engineers before deployment.

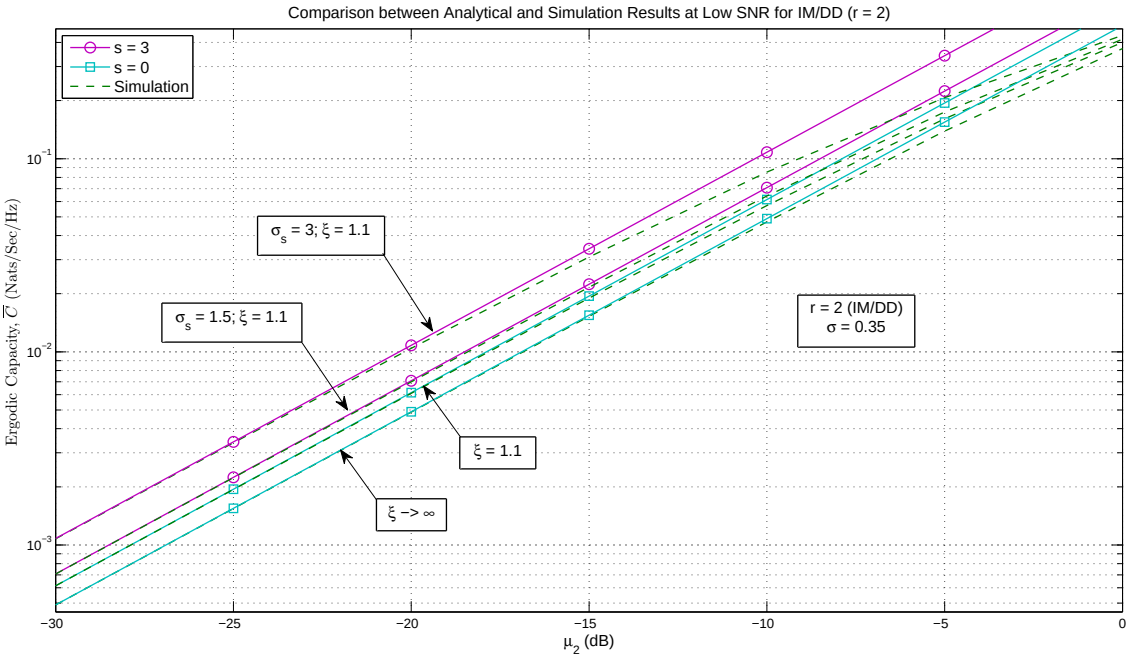

Figure 3.3: Ergodic capacity results for varying pointing errors at low SNR regime for LN turbulence under IM/DD technique ($r = 2$).

Furthermore, it can be seen that at high SNR, the asymptotic expression derived in (3.37) via utilizing moments gives very tight asymptotic results in high SNR regime and the same can be observed for the low SNR regime too corresponding to (3.40). Fig. 3.4 presents the effect of varying scintillation index parameter $\sigma = 0.1, 0.2, 0.3, 0.4, 0.5$. The pointing error effect is fixed at $s = 0$ and $\xi = 1.1$, and the ergodic capacity is plotted for the IM/DD technique (i.e. $r = 2$). It can be observed that as the scintillation index increases, the ergodic capacity degrades.

3.4.3 Rician-Lognormal (RLN) Turbulence Scenario

Exact Analysis

For RLN atmospheric turbulence scenario under nonzero boresight pointing errors and zero boresight pointing errors, (3.9) and (3.10) are respectively substituted in (3.26). To the best of our knowledge, both the above scenarios can not be solved in

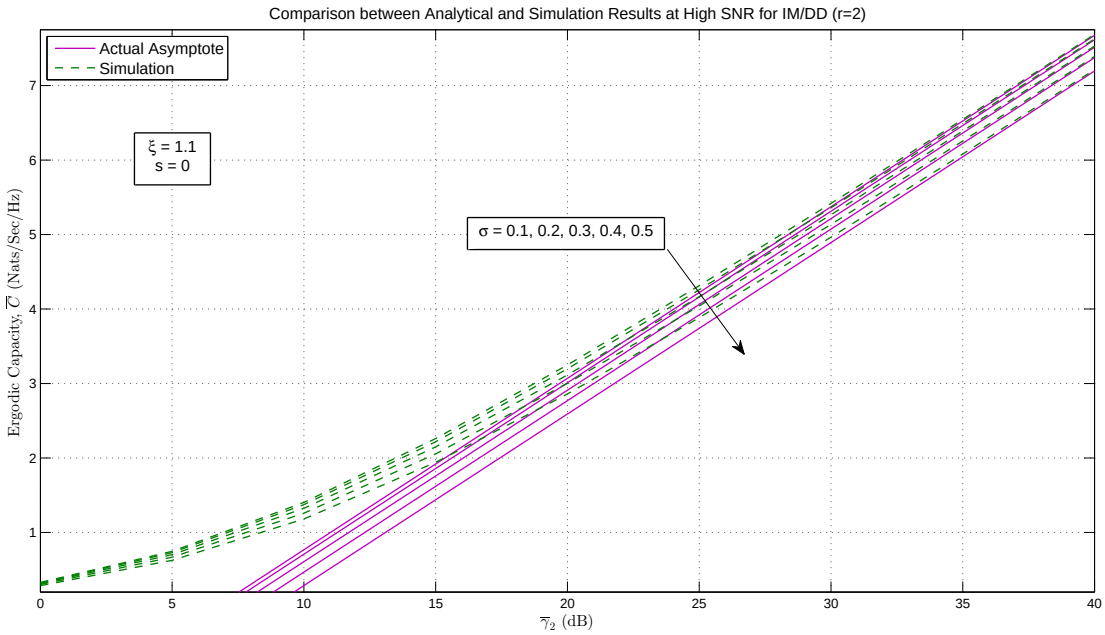

Figure 3.4: Ergodic capacity results for IM/DD technique and varying σ at high SNR regime for LN turbulence.

exact closed-form.

Additionally, a conclusion has already been obtained that it is not possible to solve the inner integral for nonzero boresight pointing errors in (3.27) with (3.2). Hence, a three-integral expression is encountered involving the I_{a_R} and I_{a_L} independently. It was already learned from the previous subsection that the middle integral for LN PDF $f_L\left(I_{a_L}\right)$ in (3.27) with (3.4) does not lead to possible exact closed-form results and similarly the outer integral for the Rician PDF $f_R\left(I_{a_R}\right)$ in (3.27) with (3.8) also does not lead to possible exact closed-form results.

On the other hand, although the inner integral has been solved for zero boresight pointing errors in (3.27) with (3.3) to obtain (3.28) but on placing the LN PDF $f_L\left(I_{a_L}\right)$ (3.4) and the Rician PDF $f_R\left(I_{a_R}\right)$ (3.8) into (3.28), a double integral is obtained. To the best of our knowledge, this double integral does not has an exact closed-form solution nor this double integral can be reduced further to a single integral for other possible solutions. Therefore, the ergodic capacity is analyzed utilizing the

moments derived in previous section.

Approximate Analysis

Based on (3.31), the first derivative of the moments derived in (3.19) is obtained as

$$\begin{aligned}\frac{\partial}{\partial n}\mathbb{E}\left[\gamma_r^n\right] = & \frac{\xi^{2(1-r\,n)}\,\Gamma\left(r\,n+1\right)}{\left(\xi^2+r\,n\right)\left(\xi^2+1\right)^{-r\,n}\,\left(1+k^2\right)^{r\,n}} \\ & \times \exp\left\{\frac{r\,n\,\sigma^2}{2}\left(r\,n-1\right)+\frac{r\,n\,s^2}{2\,\sigma_s^2}\left(\frac{1}{\xi^2+1}-\frac{1}{\xi^2+r\,n}\right)\right\} \\ & \times \left\{{}_1F_1\left[-r\,n;1;-k^2\right]\left[-r/\left(\xi^2+r\,n\right)+r\,\sigma^2\left(r\,n-1/2\right)\right.\right. \\ & + r\,s^2/\left(2\,\sigma_s^2\right)\left[r\,n/\left(\xi^2+r\,n\right)^2+1/\left(\xi^2+1\right)-1/\left(\xi^2+r\,n\right)\right] \\ & - r\,\ln\left\{\xi^2/\left(\xi^2+1\right)\right\}+r\,\psi\left(r\,n+1\right)-r\,\ln\left\{k^2+1\right\} \\ & \left.\left.+\ln\left\{c\,\mu_r\right\}\right]-r\,\partial/\partial n\,{}_1F_1\left[-r\,n;1;-k^2\right]\right\}\left(c\,\mu_r\right)^n.\end{aligned} \tag{3.43}$$

It can be seen from (3.43) that the last term is in form of derivative definition. The derivative of $\partial/\partial a\,{}_1F_1\left[a;b;z\right]$ or $\partial/\partial b\,{}_1F_1\left[a;b;z\right]$ is not available in the open mathematical literature though this can be solved for the special case when the variable being derived with respect to, is set to 0 i.e. $\partial/\partial a\,{}_1F_1\left[a;b;z\right]|_{a=0}$ or $\partial/\partial b\,{}_1F_1\left[a;b;z\right]|_{b=0}$ [101, App. A]. Hence, $\partial/\partial n\,{}_1F_1\left[-r\,n;1;-k^2\right]|_{n=0}$ can be solved as [102, Eq. (38a)]

$$\partial/\partial n\,{}_1F_1\left[-r\,n;1;-k^2\right]|_{n=0} = -k^2\,{}_2F_2\left[1,1;2,2;-k^2\right]. \tag{3.44}$$

Now, substituting (3.44) into (3.43) and evaluating (3.43) at $n=0$ yields

$$\begin{aligned}\overline{C} \underset{\mu_r>>1}{\approxeq} & \ln\left\{c\,\mu_r\right\}-r\left[\frac{1}{\xi^2}+\frac{\sigma^2}{2}+\frac{s^2}{2\,\sigma_s^2\,\xi^2\,\left(\xi^2+1\right)}\right. \\ & \left.+\ln\left\{\frac{\xi^2}{\xi^2+1}\right\}+\ln\left\{k^2+1\right\}+\gamma_E-k^2\,{}_2F_2\left[1,1;2,2;-k^2\right]\right],\end{aligned} \tag{3.45}$$

where $\gamma_E \cong 0.577216$ denotes the Euler-Mascheroni constant/Euler's Gamma/Euler's constant [103]. This can be further simplified to

$$\overline{C} \underset{\mu_r >>1}{\cong} \ln\{c\,\mu_r\} - r\left[\frac{1}{\xi^2} + \frac{\sigma^2}{2} + \frac{s^2}{2\,\sigma_s^2\,\xi^2\,(\xi^2+1)} + \ln\left\{\xi^2/\left(\xi^2+1\right)\right\} - \ln\left\{k^2/\left(k^2+1\right)\right\} - \Gamma\left(0,k^2\right)\right]. \tag{3.46}$$

Equation (3.46) can be further simplified via utilizing [79, Eq. (6.5.15)] to obtain

$$\overline{C} \underset{\mu_r >>1}{\cong} \ln\{c\,\mu_r\} - r\left[\frac{1}{\xi^2} + \frac{\sigma^2}{2} + \frac{s^2}{2\,\sigma_s^2\,\xi^2\,(\xi^2+1)} + \ln\left\{\xi^2/\left(\xi^2+1\right)\right\} - \ln\left\{k^2/\left(k^2+1\right)\right\} - E_1\left(k^2\right)\right], \tag{3.47}$$

where $E_n(z)$ is an exponential integral [79, Sec. 5.1]. Hence, eq. (3.47) gives the required expression for the ergodic capacity $\overline{C}$ at high SNR in terms of simple elementary functions for RLN FSO turbulent channels under the effect of boresight pointing errors. Similarly, for RLN atmospheric turbulence under zero boresight pointing errors (i.e. for $s = 0$), the asymptotic approximation to the ergodic capacity at high SNR is derived as

$$\overline{C} \underset{\mu_r >>1}{\cong} \ln\{c\,\mu_r\} - r\left[\frac{1}{\xi^2} + \frac{\sigma^2}{2} + \ln\left\{\frac{\xi^2}{\xi^2+1}\right\} - \ln\left\{\frac{k^2}{1+k^2}\right\} - E_1\left(k^2\right)\right]. \tag{3.48}$$

Similarly, for RLN atmospheric turbulence under no pointing errors (i.e. for $s = 0$ and $\xi \to \infty$), the asymptotic approximation to the ergodic capacity at high SNR is derived as

$$\overline{C} \underset{\mu_r >>1}{\cong} \ln\{c\,\mu_r\} - r\left[\sigma^2/2 - \ln\left\{k^2/\left(1+k^2\right)\right\} - E_1\left(k^2\right)\right]. \tag{3.49}$$

Furthermore, for ***low SNR*** asymptotic analysis, it can be easily shown that the ergodic capacity can be asymptotically approximated by the first moment. Utilizing

(3.19) via placing $n = 1$ in it, the ergodic capacity of a single FSO link under RLN FSO turbulence effected by nonzero boresight pointing errors can be approximated at low SNR in closed-form in terms of simple elementary functions by

$$\overline{C} \underset{\mu_r << 1}{\approx} \frac{\xi^{2(1-r)}}{(\xi^2 + r)(\xi^2 + 1)^{-r}} \exp\left\{\frac{r\,\sigma^2}{2}(r-1) + \frac{r\,s^2}{2\,\sigma_s^2}\left(\frac{1}{\xi^2+1} - \frac{1}{\xi^2+r}\right)\right\} \times \Gamma(r+1)\ {}_1F_1\left[-r;1;-k^2\right] / \left(k^2+1\right)^r\ c\,\mu_r. \tag{3.50}$$

Similarly, for RLN atmospheric turbulence under zero boresight pointing errors (i.e. for $s = 0$), the asymptotic approximation to the ergodic capacity at low SNR is obtained as

$$\overline{C} \underset{\mu_r << 1}{\approx} \frac{\xi^{2(1-r)}}{(\xi^2 + r)(\xi^2 + 1)^{-r}} \exp\left\{\frac{r\,\sigma^2}{2}(r-1)\right\} \frac{\Gamma(r+1)\ {}_1F_1\left[-r;1;-k^2\right]}{(1+k^2)^r}\, c\,\mu_r. \tag{3.51}$$

Similarly, for RLN atmospheric turbulence under zero pointing errors (i.e. for $s = 0$ and $\xi \to \infty$), the asymptotic approximation to the ergodic capacity at low SNR is obtained as

$$\overline{C} \underset{\mu_r << 1}{\approx} \exp\left\{\frac{r\,\sigma^2}{2}(r-1)\right\} \frac{\Gamma(r+1)\ {}_1F_1\left[-r;1;-k^2\right]}{(1+k^2)^r}\, c\,\mu_r. \tag{3.52}$$

Results and Discussion

As an illustration of the mathematical formalism presented above, simulation and numerical results for the ergodic capacity of a single FSO link transmission system under RLN turbulent channels is presented as follows.

The FSO link is modeled as composite RLN turbulent channel. The ergodic capacity of the FSO channel in operation under heterodyne detection technique as well as IM/DD technique is presented in Fig. 3.5 and Fig. 3.6, respectively, for high SNR scenario. Subsequently, the ergodic capacity of the FSO channel in operation

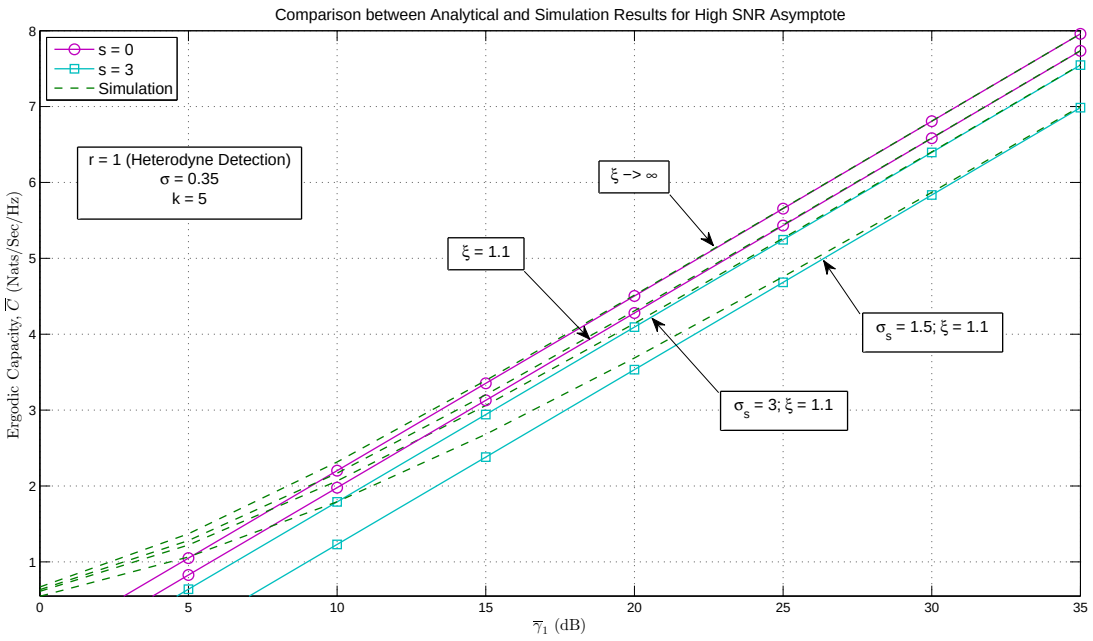

Figure 3.5: Ergodic capacity results for varying pointing errors at high SNR regime for RLN turbulence under heterodyne detection technique ($r = 1$).

under IM/DD technique is presented in Fig. 3.7 for low SNR scenario [15]. These figures demonstrate the obtained results for varying effects of pointing error with $k = 5$ and $\sigma = 0.35$. [16] Similar trend in results can be observed here as were observed for the LN only scenario in Fig. 3.1, Fig. 3.2, and Fig. 3.3. Fig. 3.8 presents the effect of varying k turbulence parameter $k \to \infty, 4, 2, 1$. The pointing error effect is fixed at $s = 0$ and $\xi = 1.1$, and the LN scintillation index is fixed at $\sigma = 0.35$. The ergodic capacity is plotted for the IM/DD technique (i.e. $r = 2$). It can be observed that as the turbulence parameter k increases, the ergodic capacity improves and ultimately matches with LN turbulence (signified with a diamond shape symbol in Fig. 3.8) as $k \to \infty$ (i.e. Rician turbulence becomes negligible).

[15] For readers clarification, the low SNR asymptote in (3.50) is actually the average SNR and hence the plot in Fig. 3.7 is against the electrical SNR.

[16] It is important to note here that these values for the parameters were selected from the cited references subject to the standards to prove the validity of the obtained results and hence other specific values can be used to obtain the required results by design communication engineers before deployment.

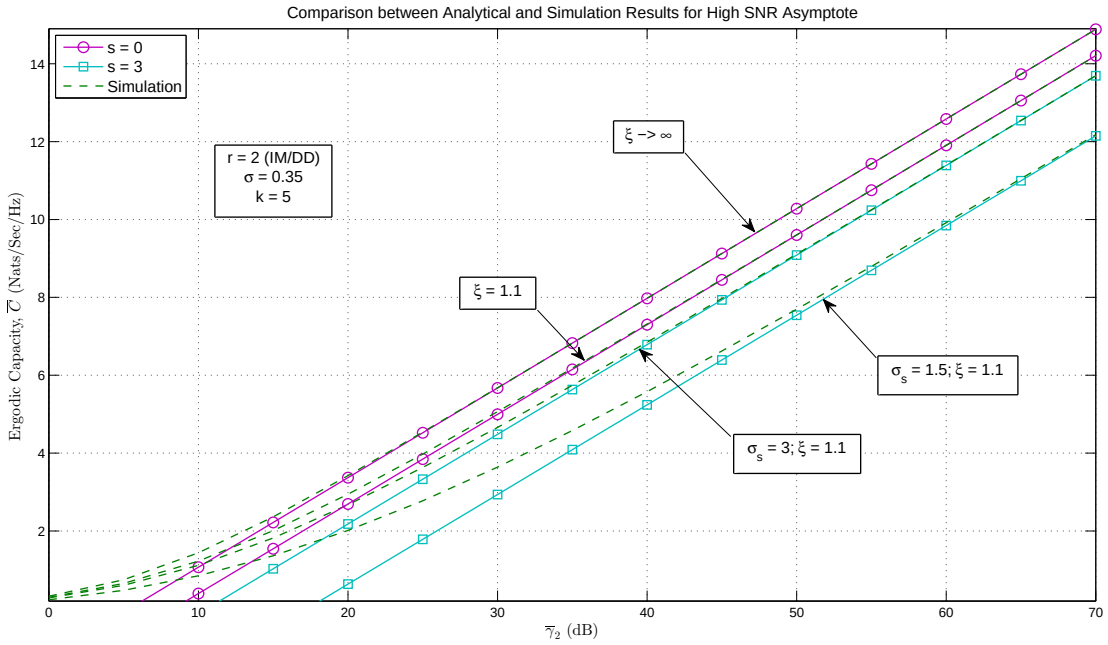

Figure 3.6: Ergodic capacity results for varying pointing errors at high SNR regime for RLN turbulence under IM/DD technique ($r = 2$).

Moreover, it is important to note that these plots are very useful to easily obtain the approximation error of the asymptotic results obtained by the proposed moments-based approximation method or in other words to find the accuracy of the proposed moments-based approximation method. For instance, let us refer to the third curve from the top that corresponds to $s = 3$, $\sigma_s = 3$, and $\xi = 1.1$ in Fig. 3.6. Let us assume that we want to control the approximation error to, lets say, around 3.9% or less. Now, we can easily deduce the channel performance i.e. at $\overline{\gamma} = 30$ dB; $\overline{C} = \{4.66$ (exact), 4.482 (simulaiton)$\}$ with approximation error = 3.8197%. Based on this, we can easily conclude that for an acceptable approximation error of 3.9% or less, our average SNR must be at least $\overline{\gamma} = 30$ dB or more. Similarly, if we want to look at this in another way i.e. our system is operating at a certain average SNR and we would like find out the accuracy of our approximation then this can also be obtained easily as follows. We can easily deduce that at $\overline{\gamma} = 30$ dB, $\overline{C} = \{4.66$ (exact), 4.482 (simulaiton)$\}$ that leads to an approximation error = 3.8197%. Similarly, at

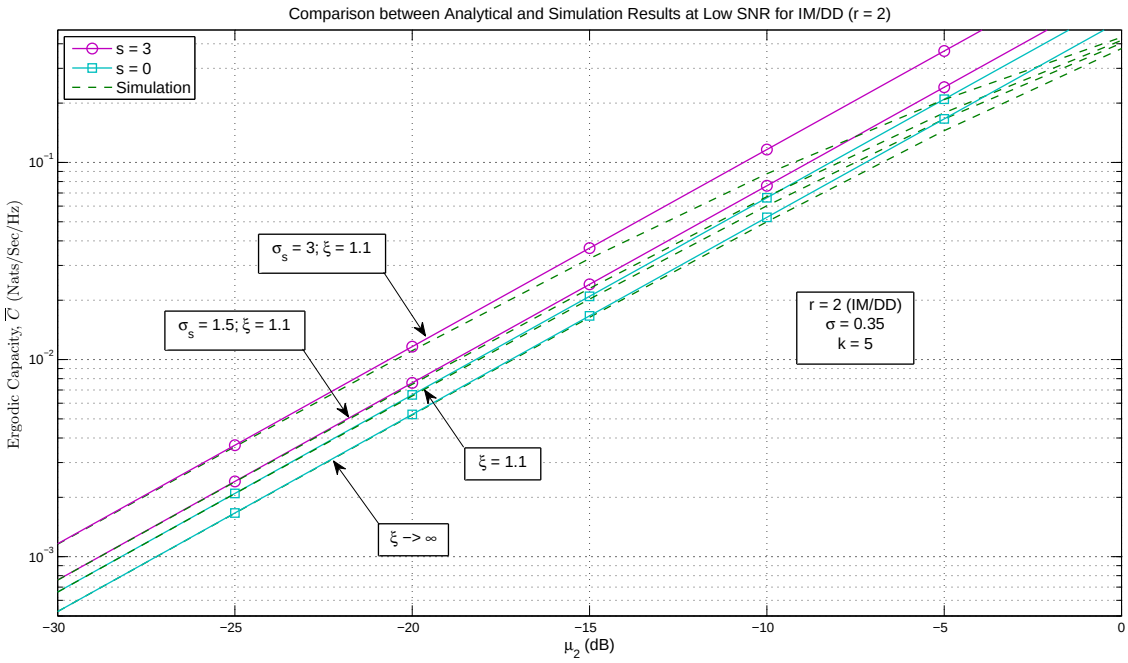

Figure 3.7: Ergodic capacity results for varying pointing errors at low SNR regime for RLN turbulence under IM/DD technique ($r = 2$).

$\overline{\gamma} = 35$ dB; $\overline{C} = \{5.741$ (exact), 5.633 (simulaiton)$\}$ leads to an approximation error $= 1.8812\%$, and at $\overline{\gamma} = 40$ dB; $\overline{C} = \{6.849$ (exact), 6.784 (simulaiton)$\}$ leads to an approximation error $= 0.949\%$.

3.4.4 Málaga ($\mathcal{M}$) Turbulence Scenario

Exact Analysis

For $\mathcal{M}$ atmospheric turbulence scenario under nonzero boresight pointing errors, (3.12) and (3.13) are respectively substituted in (3.26). To the best of our knowledge, both the above scenarios can not be solved in exact closed-form.

Additionally, a conclusion has already been obtained that it is not possible to solve the inner integral for nonzero boresight pointing errors in (3.27) with (3.2). Hence, a double-integral expression is encountered involving the I_{a_M}. The integral with respect

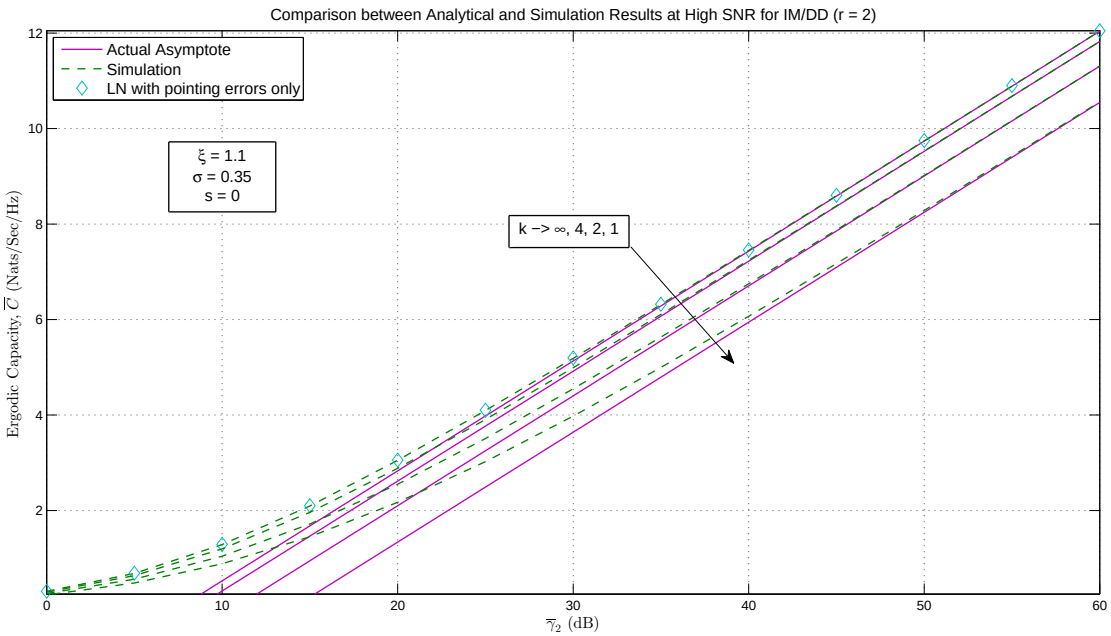

Figure 3.8: Ergodic capacity results for IM/DD technique and varying k at high SNR regime for RLN turbulence.

to I_{a_M} can be solved in exact closed-form to obtain

$$\begin{aligned}\overline{C} &= \int_0^{A_0}\int_0^{\infty} \ln\left\{1+\frac{c\left(\eta_e\, I_l\, I_{a_M}\, I_p\right)^r}{N_0}\right\} f_M\left(I_{a_M}\right)\, f_p\left(I_p\right)\, dI_{a_M}\, dI_p \\ &= \xi^2\, A\, r^3 / \left[2\, A_0^{\xi^2}\, (2\,\pi)^{r-1}\right]\, \left[\left(g\,\beta+\Omega'\right)/\left(\alpha\,\beta\right)\right]^2 \exp\left\{-s^2/\left(2\,\sigma_s^2\right)\right\} \\ &\times \sum_{m=1}^{\beta} a_m \int_0^{A_0} I_p^{\xi^2-1}\, I_0\left(s/\sigma_s\,\sqrt{-2/\xi^{-2}\,\ln\left\{I_p/A_0\right\}}\right) \\ &\times \mathrm{G}_{2\,r+2,2}^{1,2\,r+2}\left[\frac{c\left(\eta_e\, I_l\, I_p\right)^r\, \left(g\,\beta+\Omega'\right)^r}{r^{-2\,r}\, N_0\, \left(\alpha\,\beta\right)^r}\,\middle|\, \begin{matrix}1, 1, \kappa_0\\ 1, 0\end{matrix}\right] dI_p,\end{aligned} \tag{3.53}$$

where $\kappa_0 = \frac{-1-(\alpha-m)/2}{r}, \ldots, \frac{-2-(\alpha-m)/2+r}{r}, \frac{-1-(m-\alpha)/2}{r}, \ldots, \frac{-2-(m-\alpha)/2+r}{r}$ comprises of $2r$ terms. To the best of our knowledge, this single integral in (3.53) does not have an exact closed-form solution [17].

On the other hand, for $\mathcal{M}$ atmospheric turbulence under zero boresight pointing

[17] Please note that similar integral results/outcomes were obtained for GG turbulence scenario under nonzero boresight pointing errors.

errors, utilizing (3.26) by placing (3.11) in it results into an exact closed-form result as (2.28)

$$\overline{C} = \frac{D}{\ln(2)} \sum_{m=1}^{\beta} c_m \, \mathrm{G}_{r+2,3r+2}^{3r+2,1}\left[\frac{E}{c\,\mu_r} \middle| \begin{matrix} 0, 1, \kappa_1 \\ \kappa_2, 0, 0 \end{matrix} \right], \tag{3.54}$$

where $D = \xi^2 A / \left[2^r (2\,\pi)^{r-1}\right]$, $c_m = a_m \, b_m \, r^{\alpha+m-1}$, $E = \left(B\,\xi^2\right)^r / \left[\left(\xi^2+1\right)^r r^{2\,r}\right]$, $\kappa_1 = \frac{\xi^2+1}{r}, \ldots, \frac{\xi^2+r}{r}$ comprises of r terms, and $\kappa_2 = \frac{\xi^2}{r}, \ldots, \frac{\xi^2+r-1}{r}, \frac{\alpha}{r}, \ldots, \frac{\alpha+r-1}{r}, \frac{m}{r}, \ldots, \frac{m+r-1}{r}$ comprises of $3r$ terms. Similarly, as a special case, an exact closed-form result for the moments of GG atmospheric turbulence under zero boresight pointing errors is obtained as (2.29)

$$\overline{C} = \frac{J}{\ln(2)} \, \mathrm{G}_{r+2,3r+2}^{3r+2,1}\left[\frac{K}{c\,\mu_r} \middle| \begin{matrix} 0, 1, \kappa_1 \\ \kappa_3, 0, 0 \end{matrix} \right], \tag{3.55}$$

where $J = r^{\alpha+\beta-2}\,\xi^2 / \left[(2\,\pi)^{r-1}\,\Gamma(\alpha)\,\Gamma(\beta)\right]$, $K = (\xi^2 \alpha\,\beta)^r / \left[\left(\xi^2+1\right)^r r^{2\,r}\right]$, and $\kappa_3 = \frac{\xi^2}{r}, \ldots, \frac{\xi^2+r-1}{r}, \frac{\alpha}{r}, \ldots, \frac{\alpha+r-1}{r}, \frac{\beta}{r}, \ldots, \frac{\beta+r-1}{r}$ comprises of $3r$ terms.

Approximate Analysis

Reverting back to $\mathcal{M}$ atmospheric turbulence under nonzero boresight pointing errors, since it is not feasible to obtain an exact closed-form solution, the moments derived earlier are utilized to deduce the asymptotic results. Hence, based on (3.31), the first derivative of the moments in (3.22) is required to be evaluated at $n = 0$ for high SNR asymptotic approximation to the ergodic capacity. The first derivative of the moments in (3.22) is given as

$$\begin{aligned} \frac{\partial}{\partial n} \mathbb{E}\left[\gamma_r^n\right] = & \frac{\xi^{2(1-r\,n)}\, r\, A\, \Gamma\left(r\,n+\alpha\right)}{\left(\xi^2+r\,n\right)\,\left(\xi^2+1\right)^{-r\,n}\,2^r\,B^{r\,n}} \sum_{m=1}^{\beta} b_m\, \Gamma\left(r\,n+m\right) \\ & \times \exp\left\{ r\,n\,s^2 / \left(2\,\sigma_s^2\right) \left[1/\left(\xi^2+1\right) - 1/\left(\xi^2+r\,n\right) \right] \right\} \\ & \times \left[-r/\left(\xi^2+r\,n\right) - r\,\ln\left\{ \xi^2/\left(\xi^2+1\right) \right\} - r\,\ln\left\{B\right\} \right. \\ & + r\,s^2/\left(2\,\sigma_s^2\right) \left[r\,n/\left(\xi^2+r\,n\right)^2 + 1/\left(\xi^2+1\right) - 1/\left(\xi^2+r\,n\right) \right] \\ & \left. + r\,\psi\left(r\,n+\alpha\right) + r\,\psi\left(r\,n+m\right) + \ln\left\{c\,\mu_r\right\} \right] \left(c\,\mu_r\right)^n . \end{aligned} \tag{3.56}$$

and at $n = 0$, it evaluates to

$$\overline{C} \underset{\mu_r >>1}{\approxeq} \frac{r\,A\,\Gamma(\alpha)}{2^r} \sum_{m=1}^{\beta} b_m\,\Gamma(m)\,\left\{r\left[-1/\xi^2 - \ln(B) + \psi(\alpha) \right.\right. \\ \left.\left. -\ \frac{s^2\,\sigma_s^{-2}}{2\,\xi^2\,(\xi^2+1)} - \ln\left\{\frac{\xi^2}{\xi^2+1}\right\} + \psi(m)\right] + \ln(c\,\mu_r)\right\}. \tag{3.57}$$

For GG atmospheric turbulence, as a special case to $\mathcal{M}$ turbulence, the first derivative, evaluated at $n = 0$, of the moments in (3.23) is derived as

$$\overline{C} \underset{\mu_r >>1}{\approxeq} \ln\{c\,\mu_r\} - r\left[\frac{1}{\xi^2} + \frac{s^2\,\sigma_s^{-2}}{2\,\xi^2\,(\xi^2+1)} + \ln\left\{\frac{\xi^2}{\xi^2+1}\right\} + \ln\{\alpha\,\beta\} - \psi(\alpha) - \psi(\beta)\right]. \tag{3.58}$$

Now, for $\mathcal{M}$ and GG atmospheric turbulences under zero boresight pointing errors (i.e. for $s = 0$), the asymptotic approximations to the respective ergodic capacity's at high SNR are derived as

$$\overline{C} \underset{\mu_r >>1}{\approxeq} \frac{r\,A\,\Gamma(\alpha)}{2^r} \sum_{m=1}^{\beta} b_m\,\Gamma(m)\,\left\{r\left[-1/\xi^2 - \ln(B) \right.\right. \\ \left.\left. -\ \ln\left\{\frac{\xi^2}{\xi^2+1}\right\} + \psi(\alpha) + \psi(m)\right] + \ln(c\,\mu_r)\right\}, \tag{3.59}$$

and

$$\overline{C} \underset{\mu_r >>1}{\approxeq} \ln\{c\,\mu_r\} - r\left[\frac{1}{\xi^2} + \ln\left\{\frac{\xi^2}{\xi^2+1}\right\} + \ln\{\alpha\,\beta\} - \psi(\alpha) - \psi(\beta)\right]. \tag{3.60}$$

Alternatively, for $\mathcal{M}$ and GG atmospheric turbulences under zero boresight pointing errors (i.e. for $s = 0$), the ergodic capacity's in (3.54) and (3.55) can be expressed asymptotically via utilizing the Meijer's G function expansion as (2.30)

$$\overline{C} \underset{\mu_r >>1}{\approxeq} \frac{D}{\ln(2)} \sum_{m=1}^{\beta} c_m \sum_{k=1}^{3r+2} \left(\frac{c\,\mu_r}{E}\right)^{-\kappa_{2,k}} \frac{\Gamma(1+\kappa_{2,k}) \prod_{l=1;\,l\neq k}^{3r+2} \Gamma(\kappa_{2,l} - \kappa_{2,k})}{\Gamma(1-\kappa_{2,k}) \prod_{l=1}^{r} \Gamma(\kappa_{1,l} - \kappa_{2,k})}, \tag{3.61}$$

and (2.31)

$$\overline{C} \underset{\mu_r >>1}{\approxeq} \frac{A}{\ln(2)} \sum_{k=1}^{3r+2} \left(\frac{c\,\mu_r}{B}\right)^{-\kappa_{3,k}} \frac{\Gamma(1+\kappa_{3,k}) \prod_{l=1;\, l\neq k}^{3r+2} \Gamma(\kappa_{3,l}-\kappa_{3,k})}{\Gamma(1-\kappa_{3,k}) \prod_{l=1}^{r} \Gamma(\kappa_{1,l}-\kappa_{3,k})}, \tag{3.62}$$

respectively, where $\kappa_{u,v}$ represents the v^{th}-term of κ_u. Similarly, for $\mathcal{M}$ atmospheric turbulence under zero pointing errors (i.e. for $s = 0$ and $\xi \to \infty$), the asymptotic approximation to the ergodic capacity at high SNR is derived as

$$\overline{C} \underset{\mu_r >>1}{\approxeq} \frac{r\,A\,\Gamma(\alpha)}{2^r} \sum_{m=1}^{\beta} b_m\,\Gamma(m)\,\left\{r\left[-\ln(B)+\psi(\alpha)+\psi(m)\right]+\ln(c\,\mu_r)\right\}, \tag{3.63}$$

and

$$\overline{C} \underset{\mu_r >>1}{\approxeq} \ln\left\{c\,\mu_r\right\} - r\left[\ln\left\{\alpha\,\beta\right\} - \psi\left(\alpha\right) - \psi\left(\beta\right)\right]. \tag{3.64}$$

Furthermore, for ***low SNR*** asymptotic analysis, it can be easily shown that the ergodic capacity can be asymptotically approximated by the first moment. Utilizing (3.23) and (3.22) via placing $n = 1$ in them, the ergodic capacity's of a single FSO link under $\mathcal{M}$ and GG FSO turbulences effected by nonzero boresight pointing errors can be approximated at low SNR in closed-form in terms of simple elementary functions by

$$\begin{aligned}\overline{C} \underset{\mu_r <<1}{\approxeq} & \xi^{2(1-r)} / \left[\left(\xi^2+r\right)\left(\xi^2+1\right)^{-r}\right] \exp\left\{r\,s^2/\left(2\,\sigma_s^2\right)\left[1/\left(\xi^2+1\right)-1/\left(\xi^2+r\right)\right]\right\} \\ & \times r\,A\,\Gamma(r+\alpha)/\left(2^r\,B^r\right) \sum_{m=1}^{\beta} b_m\,\Gamma(r+m)\,c\,\mu_r,\end{aligned} \tag{3.65}$$

and

$$\begin{aligned}\overline{C} \underset{\mu_r <<1}{\approxeq} & \frac{\xi^{2(1-r)}\,\left(\xi^2+1\right)^r\,\Gamma\left(r+\alpha\right)\,\Gamma\left(r+\beta\right)}{\left(\xi^2+r\right)\,\left(\alpha\,\beta\right)^r\,\Gamma\left(\alpha\right)\,\Gamma\left(\beta\right)} \\ & \times \exp\left\{r\,s^2/\left(2\,\sigma_s^2\right)\left[1/\left(\xi^2+1\right)-1/\left(\xi^2+r\right)\right]\right\}\,c\,\mu_r,\end{aligned} \tag{3.66}$$

respectively. Similarly, for $\mathcal{M}$ and GG atmospheric turbulences under zero bore-

sight pointing errors (i.e. for $s = 0$), the asymptotic approximations to the ergodic capacity's at low SNR are obtained, respectively, as

$$\overline{C} \underset{\mu_r << 1}{\approx} \xi^{2(1-r)} / \left[\left(\xi^2 + r \right) \left(\xi^2 + 1 \right)^{-r} \right] r \, A \, \Gamma(r + \alpha) / \left(2^r \, B^r \right) \sum_{m=1}^{\beta} b_m \, \Gamma(r + m) \, c \, \mu_r, \tag{3.67}$$

and

$$\overline{C} \underset{\mu_r << 1}{\approx} \frac{\xi^{2(1-r)} \, \left(\xi^2 + 1 \right)^r \, \Gamma\left(r + \alpha \right) \, \Gamma\left(r + \beta \right)}{\left(\xi^2 + r \right) \, \left(\alpha \, \beta \right)^r \, \Gamma\left(\alpha \right) \, \Gamma\left(\beta \right)} \, c \, \mu_r. \tag{3.68}$$

Similarly, for $\mathcal{M}$ and GG atmospheric turbulences under zero pointing errors (i.e. for $s = 0$ and $\xi \to \infty$), the asymptotic approximations to the ergodic capacity's at low SNR are obtained, respectively, as

$$\overline{C} \underset{\mu_r << 1}{\approx} r \, A \, \Gamma(r + \alpha) / \left(2^r \, B^r \right) \sum_{m=1}^{\beta} b_m \, \Gamma(r + m) \, c \, \mu_r, \tag{3.69}$$

and

$$\overline{C} \underset{\mu_r << 1}{\approx} \frac{\Gamma\left(r + \alpha \right) \, \Gamma\left(r + \beta \right)}{\left(\alpha \, \beta \right)^r \, \Gamma\left(\alpha \right) \, \Gamma\left(\beta \right)} \, c \, \mu_r. \tag{3.70}$$

Results and Discussion

As an illustration of the mathematical formalism presented above, simulation and numerical results for the ergodic capacity of a single FSO link transmission system under $\mathcal{M}$ turbulence channels is presented as follows. The FSO link is modeled as $\mathcal{M}$ turbulence channel with the effects of atmosphere as ($\alpha = 2.296$; $\beta = 2$), ($\alpha = 4.2$; $\beta = 3$) and ($\alpha = 8$; $\beta = 4$), ($\Omega = 1.3265$, $b_0 = 0.1079$), $\rho = 0.596$, and $\phi_A - \phi_B = \pi/2$ unless stated otherwise. [18] In MATLAB, a $\mathcal{M}$ turbulent channel random variable was generated via squaring the absolute value of a Rician-shadowed random variable [56].

[18] It is important to note here that these values for the parameters were selected from [56] subject to the standards to prove the validity of the obtained results and hence other specific values can be used to obtain the required results by design communication engineers before deployment. Also, for all cases, 10^6 realizations of the random variable were generated to perform the Monte-Carlo simulations in MATLAB.

The ergodic capacity of the FSO channel in operation under heterodyne detection technique as well as IM/DD technique is presented in Fig. 3.9 and Fig. 3.10, respectively, for high SNR scenario. Subsequently, the ergodic capacity of the FSO channel

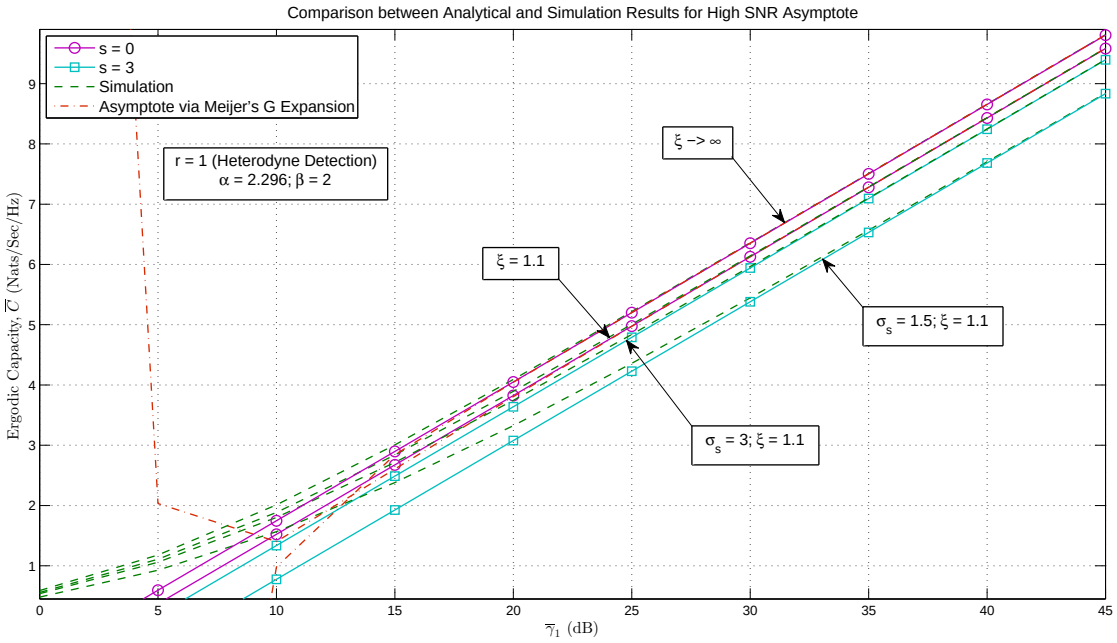

Figure 3.9: Ergodic capacity results for varying pointing errors at high SNR regime for M turbulence under heterodyne detection technique ($r = 1$).

in operation under IM/DD technique is presented in Fig. 3.11 for low SNR scenario [19]. These figures demonstrate the obtained results for varying effects of pointing error with $\alpha = 2.296$ and $\beta = 2$. Similar trend in results can be observed here as were observed for the LN only and the RLN scenarios in Fig. 3.1, Fig. 3.2, Fig. 3.3, Fig. 3.5, Fig. 3.6, and Fig. 3.7. Additionally, Fig. 3.9 and Fig. 3.10 plots the new Meijer's G function expansion based ergodic capacity approximate for the zero boresight pointing error case under the $\mathcal{M}$ turbulence scenario where the exact closed-form ergodic capacity involves the Meijer's G function that is given in (3.61). The plots confirm that both the approaches i.e. the moments-based approach and the Meijer's G

[19]For readers clarification, the low SNR asymptote in (3.65) is actually the average SNR and hence the plot in Fig. 3.11 is against the electrical SNR.

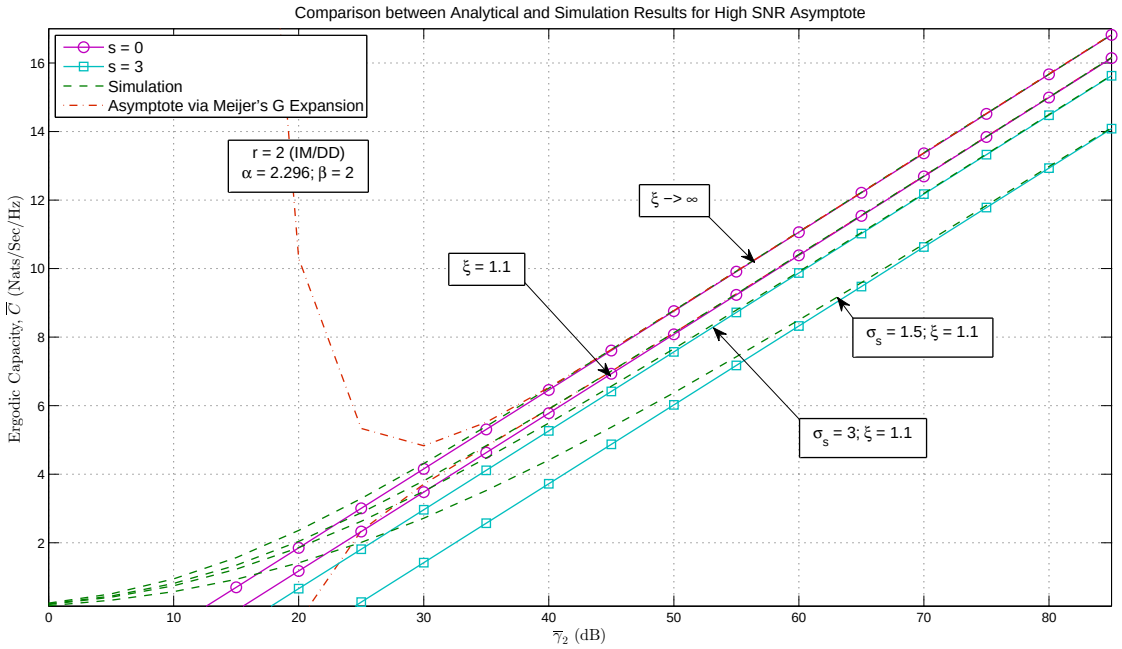

Figure 3.10: Ergodic capacity results for varying pointing errors at high SNR regime for M turbulence under IM/DD technique ($r = 2$).

function expansion based approach provide similar results for the ergodic capacity of such FSO atmospheric turbulence channel as the curves from both these approaches overlap simultaneously with the simulation curves nearly at a similar average SNR. Fig. 3.12 presents the effect of varying atmospheric turbulences (i.e. varying α's and β's). The pointing error effect is fixed at $s = 3$, $\sigma_s = 1.5$, and $\xi = 1.1$. The ergodic capacity is plotted for the IM/DD technique (i.e. $r = 2$). It can be observed that as the turbulence gets severs, the ergodic capacity degrades and vice versa. An important observation is that it can be observed that once $\rho \to 1$ and $\Omega' = 1$ are applied, the $\mathcal{M}$ turbulence matches exactly the special case of the Gamma-Gamma turbulence. This can be depicted from the case wherein ($\alpha = 8$; $\beta = 4$).

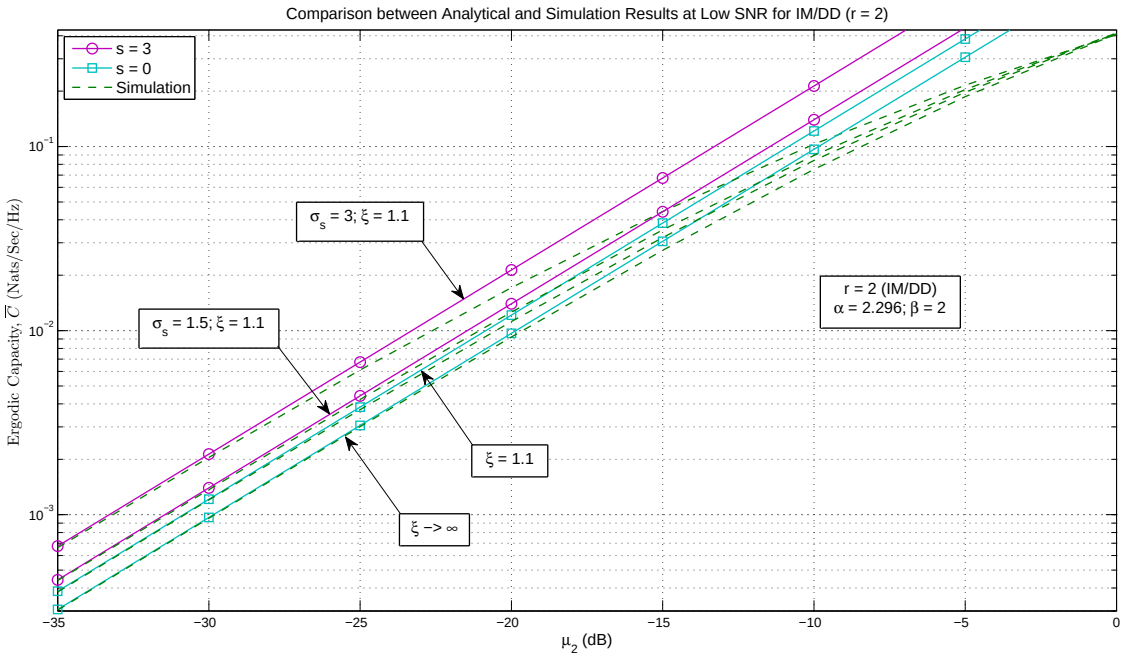

Figure 3.11: Ergodic capacity results for varying pointing errors at low SNR regime for M turbulence under IM/DD technique ($r = 2$).

3.4.5 Important Outcomes and Further Motivations

- Hence, eqs. (3.37), (3.47), and (3.57) give the required expressions for the ergodic capacity $\overline{C}$ at high SNR in terms of simple elementary functions.
- Some special cases of these ergodic capacity results are presented in Table 3.1.
- Furthermore, at high SNR, the ergodic capacity for the optimal rate adaptation (ORA) policy and the optimal joint power and rate adaptation (OPRA) policy perform similarly. Therefore, these ergodic capacity results are applicable to both the ergodic capacity policies (i.e. ORA as well as OPRA).
- Interestingly, the low SNR asymptotic ergodic capacity for the heterodyne detection technique (i.e. $r = 1$ case) in (3.40)-(3.42), (3.50)-(3.52), and (3.65)-(3.70) is actually the average SNR i.e. $\overline{C} \underset{\mu_1 << 1}{\approx} \overline{\gamma}_1 = \mu_1$.

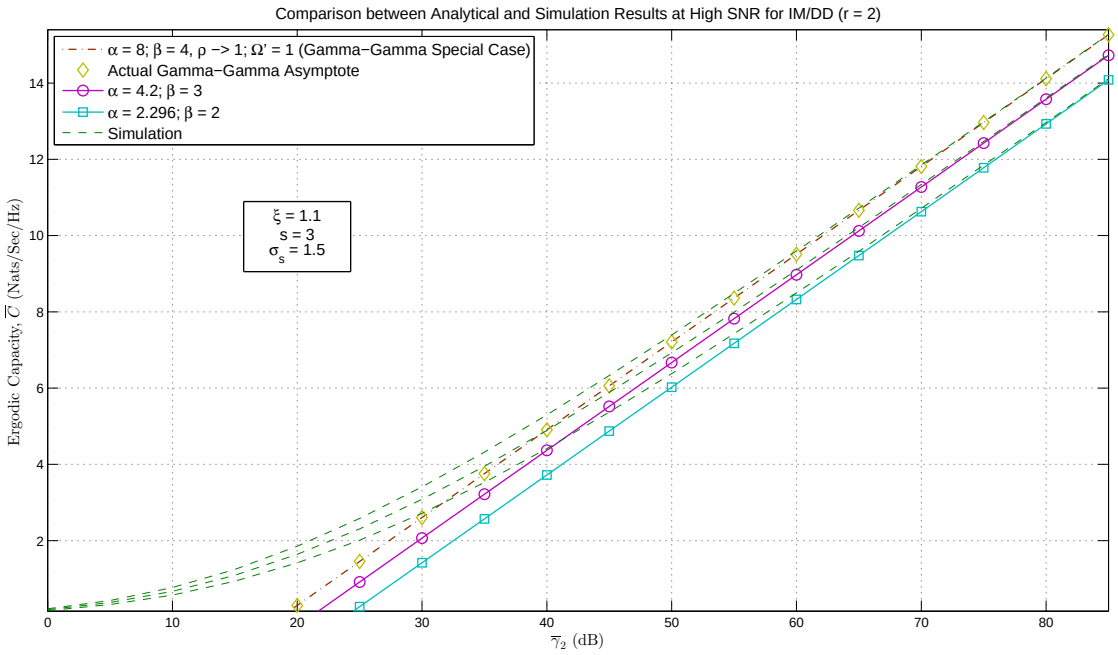

Figure 3.12: Ergodic capacity results for IM/DD technique and varying atmospheric turbulence effects at high SNR regime for M turbulence.

3.5 Concluding Remarks

Unified expression for the moments of the average SNR of a FSO link operating over the LN, the RLN, and the $\mathcal{M}$ atmospheric turbulences under nonzero and zero boresight pointing errors were derived. Capitalizing on these expressions, new unified asymptotic formulas were presented that are applicable in high and low SNR regimes for the ergodic capacity in terms of simple elementary functions for the respective turbulence models. Subsequently, some special cases were also summarized in Table 3.1. In addition, this work presented simulation examples to validate and illustrate the mathematical formulations developed in this work and to show the effect of the scintillation index, the pointing errors, and the respective turbulence parameters severity on the system performance.

Table 3.1: Special Cases for LN, RLN, and $\mathcal{M}$ Atmospheric Turbulent High SNR Ergodic Capacities

Turbulence Model	**With Nonzero Boresight Pointing Errors**	**With Zero Boresight Pointing Errors** ($s = 0$)	**Without Pointing Errors** ($s = 0; \xi \to \infty$)
Lognormal (LN) ($k \to \infty$)	$\ln\{c\,\mu_r\} - r\left[\frac{1}{\xi^2} + \frac{\sigma^2}{2} + \frac{s^2}{2\,\sigma_s^2\,\xi^2\,(\xi^2+1)} + \ln\left\{\frac{\xi^2}{\xi^2+1}\right\}\right]$	$\ln\{c\,\mu_r\} - r\left[\frac{1}{\xi^2} + \frac{\sigma^2}{2} + \ln\left\{\frac{\xi^2}{\xi^2+1}\right\}\right]$	$\ln\{c\,\mu_r\} - r\,\frac{\sigma^2}{2}$
Rician-LN (RLN)	$\ln\{c\,\mu_r\} - r\left[\frac{1}{\xi^2} + \frac{\sigma^2}{2} + \frac{s^2}{2\,\sigma_s^2\,\xi^2\,(\xi^2+1)} + \ln\left\{\frac{\xi^2}{\xi^2+1}\right\} - \ln\left\{\frac{k^2}{k^2+1}\right\} - E_1\left(k^2\right)\right]$	$\ln\{c\,\mu_r\} - r\left[\frac{1}{\xi^2} + \frac{\sigma^2}{2} + \ln\left\{\frac{\xi^2}{\xi^2+1}\right\} - \ln\left\{\frac{k^2}{1+k^2}\right\} - E_1\left(k^2\right)\right]$	$\ln\{c\,\mu_r\} - r\left[\frac{\sigma^2}{2} - \ln\left\{\frac{k^2}{1+k^2}\right\} - E_1\left(k^2\right)\right]$
Rician ($\sigma \to 0$)	$\ln\{c\,\mu_r\} - r\left[\frac{1}{\xi^2} + \frac{s^2}{2\,\sigma_s^2\,\xi^2\,(\xi^2+1)} + \ln\left\{\frac{\xi^2}{\xi^2+1}\right\} - \ln\left\{\frac{k^2}{k^2+1}\right\} - E_1\left(k^2\right)\right]$	$\ln\{c\,\mu_r\} - r\left[\frac{1}{\xi^2} + \ln\left\{\frac{\xi^2}{\xi^2+1}\right\} - \ln\left\{\frac{k^2}{1+k^2}\right\} - E_1\left(k^2\right)\right]$	$\ln\{c\,\mu_r\} - r\left[\ln\left\{\frac{1+k^2}{k^2}\right\} - E_1\left(k^2\right)\right]$
Rayleigh-LN ($k \to 0$)	$\ln\{c\,\mu_r\} - r\left[\frac{1}{\xi^2} + \frac{\sigma^2}{2} + \frac{s^2}{2\,\sigma_s^2\,\xi^2\,(\xi^2+1)} + \ln\left\{\frac{\xi^2}{\xi^2+1}\right\} + \gamma_E\right]$	$\ln\{c\,\mu_r\} - r\left[\frac{1}{\xi^2} + \frac{\sigma^2}{2} + \ln\left\{\frac{\xi^2}{\xi^2+1}\right\} + \gamma_E\right]$	$\ln\{c\,\mu_r\} - r\left[\frac{\sigma^2}{2} + \gamma_E\right]$
Rayleigh ($k \to 0; \sigma \to 0$)	$\ln\{c\,\mu_r\} - r\left[\frac{1}{\xi^2} + \frac{s^2}{2\,\sigma_s^2\,\xi^2\,(\xi^2+1)} + \ln\left\{\frac{\xi^2}{\xi^2+1}\right\} + \gamma_E\right]$	$\ln\{c\,\mu_r\} - r\left[\frac{1}{\xi^2} + \ln\left\{\frac{\xi^2}{\xi^2+1}\right\} + \gamma_E\right]$	$\ln\{c\,\mu_r\} - r\,\gamma_E$
Málaga ($\mathcal{M}$)	$\frac{r\,A\,\Gamma(\alpha)}{2^r}\sum_{m=1}^{\beta} b_m\,\Gamma(m)\left\{r\left[-1/\xi^2 - \ln(B) - \frac{s^2\,\sigma_s^{-2}}{2\,\xi^2\,(\xi^2+1)} - \ln\left\{\frac{\xi^2}{\xi^2+1}\right\} + \psi(\alpha) + \psi(m)\right] + \ln(c\,\mu_r)\right\}$	$\frac{r\,A\,\Gamma(\alpha)}{2^r}\sum_{m=1}^{\beta} b_m\,\Gamma(m)\left\{r\left[-1/\xi^2 - \ln(B) - \ln\left\{\frac{\xi^2}{\xi^2+1}\right\} + \psi(\alpha) + \psi(m)\right] + \ln(c\,\mu_r)\right\}$	$\frac{r\,A\,\Gamma(\alpha)}{2^r}\sum_{m=1}^{\beta} b_m\,\Gamma(m)\left\{r\left[-\ln(B) + \psi(\alpha) + \psi(m)\right] + \ln(c\,\mu_r)\right\}$
Gamma-Gamma (GG) $\left(\rho \to 1,\, \Omega' = 1\right)$	$\ln\{c\,\mu_r\} - r\left[\frac{1}{\xi^2} + \frac{s^2}{2\,\sigma_s^2\,\xi^2\,(\xi^2+1)} + \ln\left\{\frac{\xi^2}{\xi^2+1}\right\} + \ln\{\alpha\,\beta\} - \psi(\alpha) - \psi(\beta)\right]$	$\ln\{c\,\mu_r\} - r\left[\frac{1}{\xi^2} + \ln\left\{\frac{\xi^2}{\xi^2+1}\right\} + \ln\{\alpha\,\beta\} - \psi(\alpha) - \psi(\beta)\right]$	$\ln\{c\,\mu_r\} - r\left[\ln\{\alpha\,\beta\} - \psi(\alpha) - \psi(\beta)\right]$

Chapter 4

On the Performance of Mixed RF and FSO Transmission Systems

4.1 Asymmetric RF-FSO Dual-Hop Relay Transmission Systems

4.1.1 Introduction

Motivation

Relaying technology has gained enormous attention for quite a while now since it not only provides wider and energy-efficient coverage but also an increased capacity for wireless communication systems. As such, many efforts have been made to study the relay system performance under various fading conditions [21, 80, 104, 105]. These independent studies consider symmetric channel conditions i.e. the links at the hops are similar in terms of the fading distributions though it is more practical to experience different/asymmetric link conditions at different hops i.e. each link may differ in the channel conditions from the other link [53, 67, 106–108]. This is due to the fact that

the signals on each hop are transmitted either via different communication systems or the signals might have to commute through physically different paths. For instance, as proposed in [53], a relaying system based on both radio frequency (RF) as well as free-space optical (FSO) characteristics can be expected to be more adaptive and constitute an effective communication system in a real-life environment.

Another aspect considering an uplink scenario, besides all the advantages of FSO over RF, that very much motivates this work is the concept of multiplexing i.e. RF users can be multiplexed into a single FSO link. This comes with the reasoning that there exists a connectivity gap between the backbone network and the last-mile access network and hence this last mile connectivity can be delivered via high-speed FSO links [109]. For instance, in developing countries where there might not be much of a fiber optic structure and hence to increase its reach and bandwidth to the last mile, it will require huge amount of economic resources to dig up the current brown-field. It will be much better to simply install FSO transmitters and detectors on the high-rise buildings and cover the last mile by having the users with RF capability to communicate via their respective RF bands and let the rest be taken care of by the FSO links to get it through to the backbone as can be observed from Fig. 4.1. In Fig. 4.1, there exists no fiber optics structure between the buildings. Since similar optical transmitters and detectors are used for FSO and fiber optics, similar bandwidth capabilities are achievable [109]. Therefore, this will get the required job done saving numerous amount of economic resources by utilizing FSO instead of digging up the current brown-field to install fiber optics between the different buildings. In another instance, we can think of a building floor (femto-cell in a heterogeneous network) where the users can send and receive through the backbone via FSO transmitter and detector respectively, placed at one of the corners of that floor. This FSO transmitter/detector can communicate with other such devices over other high-rise buildings and ultimately hop to the backbone. Above all, having FSO

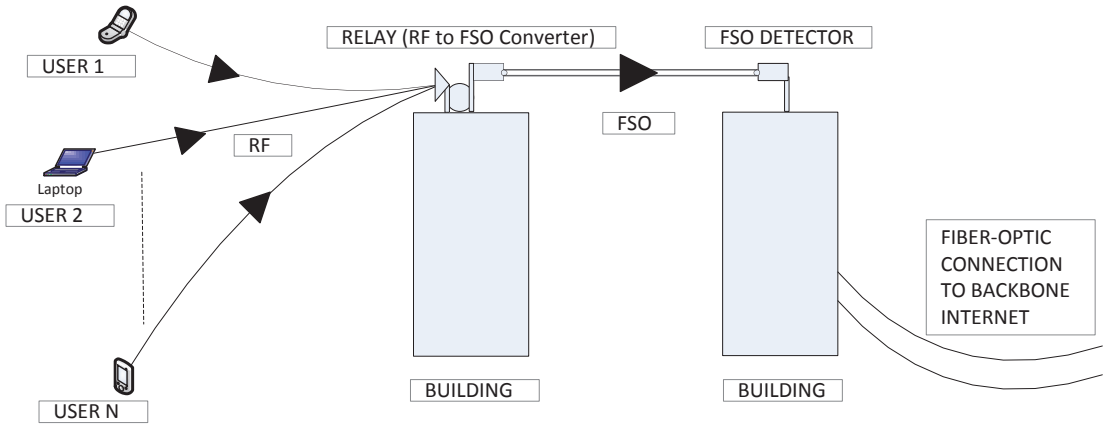

Figure 4.1: System model block diagram of an asymmetric RF-FSO dual-hop uplink transmission system.

will avoid any sort of interference(s) due to its point-to-point transmission feature unlike RF where the transmission is a broadcast leading to possible interference(s).

Recently, some work has been published on the asymmetric relay networks (so-called mixed fading channels) that have different fading channel distributions for each link [53, 106, 107]. The RF link is assumed to be operating over Rayleigh fading environment [3] whereas the FSO link is considered to be operating over Gamma-Gamma fading environment [37, 39] under the effect of pointing errors. Here, an amplify-and-forward (fixed gain and variable gain) relay scheme system is considered. For the amplify-and-forward relay system, a subcarrier intensity modulation (SIM) scheme is adopted to convert the input RF signals at the relay to the optical signals for retransmissions from the relay [67, 108]. However, the results presented in [53] were derived under the assumption of non-pointing errors in the FSO link with intensity modulation/direct detection (IM/DD) technique only. In this work, the model presented in [53] is built upon to study the impact of pointing errors on the performance of asymmetric RF-FSO dual-hop transmission systems with amplify-and-forward relays including the heterodyne detection technique and the IM/DD technique.

Contributions

The key contributions of this chapter are:

- *Statistical characterizations* of the end-to-end signal-to-noise ratio (SNR) of the asymmetric RF-FSO transmission system is studied. This includes the cumulative distribution function (CDF), the probability density function (PDF), the moment generating function (MGF), and the moments of SNR of such asymmetric RF-FSO dual-hop transmission systems are derived for fixed gain relays as well variable gain relays.

- This statistical characterization of the SNR is then applied to derive the exact closed-form expressions for the *performance metrics* such as the outage probability (OP), the higher-order amount of fading (AF), the average bit-error rate (BER) of binary modulation schemes, the average symbol error rate (SER) of M-ary amplitude modulation (M-AM), M-ary phase shift keying (M-PSK) and M-ary quadrature amplitude modulation (M-QAM), and the ergodic capacity in terms of Meijer's G functions for both types of amplify-and-forward relay schemes.

Organization

The remainder of the chapter is organized as follows. Subsection 2 introduces the channel and systems models. Subsection 3 presents the statistical characterizations and the performance analysis of fixed gain relay asymmetric RF-FSO dual-hop transmission systems whereas Subsection 4 presents the similar study for variable gain relays. Specifically, the statistical characterizations include the PDF, the CDF, the MGF, and the moments and the performance metrics include, namely, the OP, the higher-order AF, the BER, the SER, and the ergodic capacity. Subsection 5 presents some simulation results to validate these analytical results followed by concluding

remarks in Section 3.

4.1.2 Channel and System Models

A single user/RF link is assumed along with an amplify-and-forward relay leading to a FSO link to destination as can be seen from the Fig. 4.1. The Source(S)-Relay(R) link experiences Rayleigh fading which is most frequently used to model the multipath fading with non-line-of-sight path in the RF propagation environments [3, 21]. Similarly, Relay(R)-Destination(D) link experiences Gamma-Gamma fading distribution that is widely used to model the atmospheric turbulence in the FSO communication environments [37, 39, 40] for negligible pointing errors case and under the effect of pointing errors for non-negligible pointing errors case.

Therefore, the received signal at the relay R can be expressed as

$$y_{SR} = h_{SR}\, x + n_{SR}, \tag{4.1}$$

where h_{SR} is the fading amplitude of the Rayleigh fading channel for the S-R link, x is the transmitted RF signal from the source S, and n_{SR} is the AWGN with the power spectral density (PSD) of $N_{o_{SR}}$. Now, when the SIM scheme is applied in the relay, the transmitted optical signal at the relay R will be

$$x_{optical} = G(1 + \eta\, y_{SR}), \tag{4.2}$$

where G is the fixed relay gain at the relay R, and η is the electrical-to-optical conversion coefficient. The received optical signal at the destination D can be written as

$$y_{RD} = A_o\ I\{G[1 + \eta(h_{SR}\, x + n_{SR})]\} + n_{RD}, \tag{4.3}$$

where A_o is the constant for propagation, I is a stationary random variable following

the Gamma-Gamma distribution for the FSO link, and n_{RD} is the AWGN with the PSD of $N_{o_{RD}}$. Now, when the direct current (DC) component is filtered out at the destination, the received signal becomes as

$$y_{RD} = I\,G\,\eta(h_{SR}\,x + n_{SR}) + n_{RD}. \tag{4.4}$$

Therefore, the overall SNR at the destination D can be expressed as [21]

$$\gamma = \frac{I^2\,G^2\,\eta^2\,h_{SR}^2\,P_{SR}}{I^2\,G^2\,\eta^2\,N_{o_{SR}} + N_{o_{RD}}} = \frac{\frac{h_{SR}^2\,P_{SR}}{N_{o_{SR}}}\frac{I^2\,\eta^2}{N_{o_{RD}}}}{\frac{I^2\,\eta^2}{N_{o_{RD}}} + \frac{1}{G^2\,N_{o_{SR}}}}, \tag{4.5}$$

where the P_{SR} is the power transmitted at the source S.

For fixed gain amplify-and-forward relay, it can be assumed that $(G^2\,N_{o_{SR}})^{-1} = C$. Also, the SNRs of each hop can be equated as $\gamma_{SR} = \frac{h_{SR}^2\,P_{SR}}{N_{o_{SR}}}$ and $\gamma_{RD} = \frac{I^2\,\eta^2}{N_{o_{RD}}}$. So, (4.5) can now be written as

$$\gamma = \frac{\gamma_{SR}\,\gamma_{RD}}{\gamma_{RD} + C}, \tag{4.6}$$

where γ_{SR} represents the SNR of the RF hop i.e. S-R link, γ_{RD} represents the SNR of the FSO hop i.e. R-D link, and C is a fixed relay gain [3, 21, 53].

Similarly, for variable gain amplify-and-forward, the end-to-end SNR can be given as

$$\gamma = \frac{\gamma_{SR}\,\gamma_{RD}}{\gamma_{SR} + \gamma_{RD} + 1}. \tag{4.7}$$

Since the closed-from analysis of the statistical characteristics of γ is complicated, the standard approximation $\gamma = \frac{\gamma_{SR}\,\gamma_{RD}}{\gamma_{SR}+\gamma_{RD}+1} \approxeq \min(\gamma_{SR}\,\gamma_{RD})$ [106, 110, 111] is utilized.

Therefore, the RF link (i.e. S-R link) is assumed to follow Rayleigh fading whose SNR follows an exponential distribution, parameterized by the average SNR $\overline{\gamma}_{SR}$ of

the S-R link, with a PDF given by [3]

$$f_{\gamma_{SR}}(\gamma_{SR}) = 1/\overline{\gamma}_{SR} \exp(-\gamma_{SR}/\overline{\gamma}_{SR}). \tag{4.8}$$

On the other hand, it is assumed that the FSO link (i.e. R-D link) experiences Gamma-Gamma fading with pointing error impairments whose SNR PDF is given by

$$f_{\gamma_{RD}}(\gamma_{RD}) = \frac{\xi^2}{r\,\gamma_{RD}\,\Gamma(\alpha)\,\Gamma(\beta)}\,\mathrm{G}_{1,3}^{3,0}\left[\alpha\,\beta\left(\frac{\gamma_{RD}}{\mu_{RD}^{(r)}}\right)^{\frac{1}{r}}\,\middle|\,\begin{matrix}\xi^2+1\\ \xi^2,\alpha,\beta\end{matrix}\right], \tag{4.9}$$

where $\mu_{RD}^{(r)}$ is the electrical SNR of the FSO link, α and β are the fading parameters related to the atmospheric turbulence conditions [37, 39] with lower values of α and β indicating severe atmospheric turbulence conditions, ξ is the ratio between the equivalent beam radius at the receiver and the pointing error displacement standard deviation (jitter) at the receiver [59] (i.e. when $\xi \to \infty$, (4.9) converges to the non-pointing errors case), r is the parameter defining the type of detection technique (i.e. $r = 1$ represents heterodyne detection and $r = 2$ represents IM/DD), $\Gamma(.)$ is the Gamma function as defined in [58, Eq. (8.310)], and G(.) is the Meijer's G function as defined in [58, Eq. (9.301)].

4.1.3 Fixed-Gain Relay System

This section presents exact closed-form results on the statistical characteristics including the CDF, the PDF, the MGF, and the moments of the asymmetric dual-hop RF-FSO relay transmission systems in terms of the Meijer's G functions. Additionally, this section also presents new performance analysis results, in particular the OP, the higher-order AF, the BER analysis, the SER analysis, and the ergodic capacity of asymmetric dual-hop RF-FSO relay transmission systems with fixed gain relay.

Closed-Form Statistical Characteristics

Cumulative Distribution Function: The CDF is given by [21]

$$F_{\gamma}(\gamma) = \Pr\left[\frac{\gamma_{SR}\,\gamma_{RD}}{\gamma_{RD}+C} < \gamma\right], \tag{4.10}$$

which can be written as

$$F_{\gamma}(\gamma) = \int_{0}^{\infty} \Pr\left[\frac{\gamma_{SR}\,\gamma_{RD}}{\gamma_{RD}+C} < \gamma | \gamma_{RD}\right] f_{\gamma_{RD}}(\gamma_{RD})\, d\gamma_{RD}. \tag{4.11}$$

Using [62, Eq. (07.34.03.0228.01)], $\exp\left(-\gamma\, C/\left(\gamma_{RD}\,\overline{\gamma}_{SR}\right)\right)$ can be re-written as $\mathrm{G}_{0,1}^{1,0}\left[\frac{\gamma\, C}{\gamma_{RD}\,\overline{\gamma}_{SR}}\,\middle|_{\,0}\right]$. Further using [66, Eq. (6.2.2)], $\mathrm{G}_{0,1}^{1,0}\left[\frac{\gamma\, C}{\gamma_{RD}\,\overline{\gamma}_{SR}}\,\middle|_{\,0}\right]$ can be alternated to $\mathrm{G}_{1,0}^{0,1}\left[\frac{\gamma_{RD}\,\overline{\gamma}_{SR}}{\gamma\, C}\,\middle|^{\,1}\right]$. Now, along with the above modifications, applying [83, Eq. (21)] to (4.11), and with some simple algebraic manipulations along with utilizing [66, Eq. (6.2.4)], the CDF of γ can be shown to be given by

$$F_{\gamma}(\gamma) = 1 - A\exp\left(-\gamma/\overline{\gamma}_{SR}\right)\mathrm{G}_{r,3r+1}^{3r+1,0}\left[\frac{B\,C}{\overline{\gamma}_{SR}\,\mu_{RD}^{(r)}}\,\gamma\,\middle|\,\begin{matrix}\kappa_1\\ \kappa_2, 0\end{matrix}\right], \tag{4.12}$$

where $A = \frac{r^{\alpha+\beta-2}\,\xi^2}{(2\,\pi)^{r-1}\Gamma(\alpha)\,\Gamma(\beta)}$, $B = \frac{(\alpha\,\beta)^r}{r^{2\,r}}$, $\kappa_1 = \frac{\xi^2+1}{r}, \ldots, \frac{\xi^2+r}{r}$ comprises of r terms, and $\kappa_2 = \frac{\xi^2}{r}, \ldots, \frac{\xi^2+r-1}{r}, \frac{\alpha}{r}, \ldots, \frac{\alpha+r-1}{r}, \frac{\beta}{r}, \ldots, \frac{\beta+r-1}{r}$ comprises of $3\,r$ terms. The above result presented in (4.12) reduces to [53, Eq. (15)] when $\xi \to \infty$ and $r = 2$.

Probability Density Function: Differentiating (4.12) with respect to γ, using the product rule then utilizing [62, Eq. (07.34.20.0001.01)], after some algebraic manipulations the PDF in exact closed-form is obtained in terms of Meijer's G functions

as

$$f_{\gamma}(\gamma) = \frac{A\, r^{2(1-r)}}{2^{1-r}\, \gamma\, \overline{\gamma}_{SR}} \exp\left(-\gamma/\overline{\gamma}_{SR}\right) \left(r\, \overline{\gamma}_{SR}\, \mathrm{G}_{0,2r+1}^{2r+1,0}\left[\frac{B\, C}{\overline{\gamma}_{SR}\, \mu_{RD}^{(r)}}\, \gamma \,\middle|\, \begin{matrix} - \\ \kappa_3 \end{matrix} \right] + (r\, \gamma - \xi^2\, \overline{\gamma}_{SR})\, \mathrm{G}_{r,3r+1}^{3r+1,0}\left[\frac{B\, C}{\overline{\gamma}_{SR}\, \mu_{RD}^{(r)}}\, \gamma \,\middle|\, \begin{matrix} \kappa_1 \\ \kappa_2, 0 \end{matrix} \right] \right), \tag{4.13}$$

where $\kappa_3 = \frac{\alpha}{r}, \ldots, \frac{\alpha+r-1}{r}, \frac{\beta}{r}, \ldots, \frac{\beta+r-1}{r}, 0$ comprises of $2\,r+1$ terms. Additionally, the PDF was also derived by placing (4.9) into $f_{\gamma}(\gamma) = \int_0^{\infty} f_{\gamma_{SR}}(\gamma|\gamma_{RD}) f_{\gamma_{RD}}(\gamma_{RD})\, d\gamma_{RD}$, utilizing [62, Eq. (0.34.03.0228.01)], using [66, Eq. (6.2.2)], using [83, Eq. (21)], and obtaining after some simple algebraic manipulations

$$f_{\gamma}(\gamma) = \frac{A}{\overline{\gamma}_{SR}}\, \exp\left(-\gamma/\overline{\gamma}_{SR}\right) \times \left(\mathrm{G}_{r,3r+1}^{3r+1,0}\left[\frac{B\, C}{\overline{\gamma}_{SR}\, \mu_{RD}^{(r)}}\, \gamma \,\middle|\, \begin{matrix} \kappa_1 \\ \kappa_2, 0 \end{matrix} \right] + \frac{\overline{\gamma}_{SR}}{\gamma}\, \mathrm{G}_{r,3r+1}^{3r+1,0}\left[\frac{B\, C}{\overline{\gamma}_{SR}\, \mu_{RD}^{(r)}}\, \gamma \,\middle|\, \begin{matrix} \kappa_1 \\ \kappa_2, 1 \end{matrix} \right] \right). \tag{4.14}$$

The exact closed-form PDF expressions in (4.13) and (4.14) are numerically equivalent and hence further validating the derived results.

Moment Generating Function: The MGF is defined as

$$\mathcal{M}_{\gamma}(s) \triangleq \mathbb{E}\left[e^{-\gamma s}\right] = \int_0^{\infty} e^{-\gamma s} f_{\gamma}(\gamma) d\gamma. \tag{4.15}$$

Using integration by parts, MGF can be defined in terms of CDF as

$$\mathcal{M}_{\gamma}(s) = s \int_0^{\infty} e^{-\gamma s} F_{\gamma}(\gamma) d\gamma. \tag{4.16}$$

Placing (4.12) into (4.16) and utilizing [58, Eq. (7.813.1)], after some manipulations the MGF of γ is obtained as

$$\mathcal{M}_{\gamma}(s) = 1 - \frac{s\, A}{(s + 1/\overline{\gamma}_{SR})}\, \mathrm{G}_{r+1,3r+1}^{3r+1,1}\left[\frac{B\, C}{\mu_{RD}^{(r)}(s\, \overline{\gamma}_{SR} + 1)} \,\middle|\, \begin{matrix} 0, \kappa_1 \\ \kappa_2, 0 \end{matrix} \right]. \tag{4.17}$$

Moments: The moments are defined by

$$\mathbb{E}\left[\gamma^n\right] = \int_0^\infty \gamma^n f_\gamma(\gamma) d\gamma. \tag{4.18}$$

Using integration by parts (with $u = \gamma^n$, $dv = f_\gamma(\gamma)\, d\gamma$, and $v = F_\gamma(\gamma) - 1$), (4.18) can be presented in terms of the CDF of γ as

$$\mathbb{E}\left[\gamma^n\right] = n \int_0^\infty \gamma^{n-1} F_\gamma^c(\gamma)\, d\gamma, \tag{4.19}$$

where, $F_\gamma^c(\gamma) = 1 - F_\gamma(\gamma)$ is the complementary CDF (CCDF) of γ. Now, placing (4.12) into (4.19) and utilizing [58, Eq. (7.813.1)], the moments are obtained as

$$\mathbb{E}\left[\gamma^n\right] = n\, A\, \overline{\gamma}_{SR}^n\, \mathrm{G}_{r+1,3r+1}^{3r+1,1}\left[\frac{B\, C}{\mu_{RD}^{(r)}}\middle|\begin{matrix}1-n, \kappa_1 \\ \kappa_2, 0\end{matrix}\right]. \tag{4.20}$$

Applications to the Performance of Asymmetric RF-FSO Dual-Hop Relay Transmission Systems with Fixed Gain Relay

Outage Probability: When the instantaneous output SNR γ falls below a given threshold γ_{th}, a situation labeled as outage is encountered and it is an important feature to study OP of a system. Hence, another important fact worth stating here is that the expression derived in the (4.12) also serves the purpose for the expression of OP for the system or in other words, the probability that the SNR falls below a predetermined protection ratio γ_{th} can be simply expressed by replacing γ with γ_{th} in (4.12) as

$$P_{\mathrm{out}}(\gamma_{\mathrm{th}}) = F_\gamma(\gamma_{\mathrm{th}}). \tag{4.21}$$

Higher-Order Amount of Fading: The AF is an important measure for the

performance of a wireless communication system as it can be utilized to parameterize the distribution of the SNR of the received signal. In particular, the n^{th}-order AF for the instantaneous SNR γ is defined as [68]

$$AF_{\gamma}^{(n)} = \frac{\mathbb{E}\left[\gamma^{n}\right]}{\mathbb{E}\left[\gamma\right]^{n}} - 1. \tag{4.22}$$

The n^{th}-order AF for the instantaneous SNR γ can be obtained by utilizing (4.22). On substituting (4.20) into (4.22), the n^{th}-order AF is obtained as

$$AF_{\gamma}^{(n)} = n\, A^{1-n} \mathrm{G}_{r+1,3r+1}^{3r+1,1}\left[\frac{B\,C}{\mu_{RD}^{(r)}}\middle|\begin{matrix}1-n,\kappa_1\\ \kappa_2,0\end{matrix}\right] \mathrm{G}_{r+1,3r+1}^{3r+1,1}\left[\frac{B\,C}{\mu_{RD}^{(r)}}\middle|\begin{matrix}0,\kappa_1\\ \kappa_2,0\end{matrix}\right]^{-n} - 1. \tag{4.23}$$

For $n = 2$, as a special case, the classical AF [112] is obtained as

$$AF = AF_{\gamma}^{(2)} = 2\,A^{-1}\,\mathrm{G}_{r+1,3r+1}^{3r+1,1}\left[\frac{B\,C}{\mu_{RD}^{(r)}}\middle|\begin{matrix}-1,\kappa_1\\ \kappa_2,0\end{matrix}\right] \mathrm{G}_{r+1,3r+1}^{3r+1,1}\left[\frac{B\,C}{\mu_{RD}^{(r)}}\middle|\begin{matrix}0,\kappa_1\\ \kappa_2,0\end{matrix}\right]^{-2} - 1. \tag{4.24}$$

Average BER: Substituting (4.12) into [69, Eq. (12)] and utilizing [58, Eq. (7.813.1)], the average BER $\overline{P}_b$ is obtained for a variety of binary modulations as

$$\overline{P}_b = \frac{1}{2} - \frac{A\,q^{p}\,\Gamma(p)^{-1}}{2\,(q+1/\overline{\gamma}_{SR})^{p}}\,\mathrm{G}_{r+1,3r+1}^{3r+1,1}\left[\frac{B\,C}{\mu_{RD}^{(r)}(q\,\overline{\gamma}_{SR}+1)}\middle|\begin{matrix}1-p,\kappa_1\\ \kappa_2,0\end{matrix}\right], \tag{4.25}$$

where the parameters p and q account for different modulation schemes as discussed earlier in Chapter 2.

Average SER: In [78], the conditional SER has been presented in a desirable form and utilized to obtain the average SER of M-AM, M-PSK, and M-QAM. For example, for M-PSK the average SER $\overline{P}_s$ over generalized fading channels is given by [78, Eq. (41)]. Similarly, for M-AM and M-QAM, the average SER $\overline{P}_s$ over generalized fading channels is given by [78, Eq. (45)] and [78, Eq. (48)] respectively. On substituting

(4.17) into [78, Eq. (41)], [78, Eq. (45)], and [78, Eq. (48)], the SER of M-PSK, M-AM, and M-QAM, respectively can be obtained.

Ergodic Capacity: The ergodic channel capacity $\overline{C}$ is given by

$$\overline{C} = \frac{1}{\ln(2)} \int_0^\infty \ln(1+\gamma) f_\gamma(\gamma) d\gamma. \tag{4.26}$$

Alternatively, using integration by parts (with $u = \ln(1+\gamma)$, $dv = f_\gamma(\gamma)d\gamma$, and $v = F_\gamma(\gamma) - 1$), $\overline{C}$ can also be presented in terms of CDF as [113, Eq. (15)]

$$\overline{C} = \frac{1}{\ln(2)} \int_0^\infty \frac{F_\gamma^c(\gamma)}{1+\gamma} d\gamma. \tag{4.27}$$

Utilizing (4.27) by exploiting the identity [114, p. 152] $(1+az)^{-b} = \frac{1}{\Gamma(b)} \mathrm{G}_{1,1}^{1,1}\left[az \,\middle|\, {1-b \atop 0}\right]$ in it and using the integral identity [69, Eq. (20)], the ergodic capacity can be expressed in terms of the extended generalized bivariate Meijer's G function (EGBMGF) (see [69] and references therein) as

$$\overline{C} = \frac{A\,\overline{\gamma}_{SR}}{\ln(2)} \mathrm{G}_{1,0:1,1:\,\mathrm{r},3\mathrm{r}+1}^{1,0:1,1:\,3\mathrm{r}+1,0} \left[\begin{array}{c|c|c|c} 1 & \begin{matrix} 0 \\ 0 \end{matrix} & \kappa_1 & \overline{\gamma}_{\mathrm{SR}}, \dfrac{\mathrm{B\,C}}{\mu_{\mathrm{RD}}^{(\mathrm{r})}} \\ & & \kappa_2, 0 & \end{array} \right]. \tag{4.28}$$

The expression in (4.28) can be easily and efficiently evaluated by utilizing the MATHEMATICA® implementation of the EGBMGF given in [69, Table II].

4.1.4 Variable-Gain Relay System

This section presents exact closed-form results on the statistical characteristics including the CDF, the PDF, the MGF, and the moments of the asymmetric dual-hop RF-FSO relay transmission systems in terms of the Meijer's G functions. Additionally, this section also presents new performance analysis results, in particular the OP, the higher-order AF, the BER analysis, the SER analysis, and the ergodic capacity

of asymmetric dual-hop RF-FSO relay transmission systems with variable gain relay.

Closed-Form Statistical Characteristics

Cumulative Distribution Function: It is well known that the CDF of $\gamma = \min(\gamma_{SR}, \gamma_{RD})$ can be expressed as

$$F_{\gamma}(\gamma) = \Pr(\min(\gamma_{SR}, \gamma_{RD}) < \gamma). \tag{4.29}$$

The expression in (4.29) can be re-written as [115, Eq. (4)]

$$F_{\gamma}(\gamma) = F_{\gamma_{SR}}(\gamma_{SR}) + F_{\gamma_{RD}}(\gamma_{RD}) - F_{\gamma_{SR}}(\gamma_{SR})\, F_{\gamma_{RD}}(\gamma_{RD}). \tag{4.30}$$

Now, using $F_{\gamma_{SR}}(\gamma_{SR}) = 1 - \exp(-\gamma/\overline{\gamma}_{SR})$ as the CDF of the Rayleigh channel, (2.12) (with $\gamma = \gamma_{RD}$ and $\mu_r = \mu_{RD}^{(r)}$), and some simple algebraic manipulations, the CDF of γ can be shown to be given after some simplifications by

$$F_{\gamma}(\gamma) = 1 - \exp\left(-\gamma/\overline{\gamma}_{SR}\right) \left(1 - A\, \mathrm{G}_{r+1,3r+1}^{3r,1}\left[\frac{B}{\mu_{RD}^{(r)}}\gamma \,\middle|\, \begin{matrix} 1, \kappa_1 \\ \kappa_2, 0 \end{matrix}\right]\right). \tag{4.31}$$

Probability Density Function: Differentiating (4.31) with respect to γ, using the product rule then utilizing [62, Eq. (07.34.20.0001.01)], after some algebraic manipulations the PDF is obtained in terms of Meijer's G functions as

$$\begin{aligned} f_{\gamma}(\gamma) = \exp\left(-\gamma/\overline{\gamma}_{SR}\right) \Bigg[\frac{1}{\overline{\gamma}_{SR}} + \frac{A}{\gamma\, \overline{\gamma}_{SR}} \Bigg(\overline{\gamma}_{SR}\, \mathrm{G}_{r,3r}^{3r,0}\left[\frac{B}{\mu_{RD}^{(r)}}\gamma \,\middle|\, \begin{matrix} \kappa_1 \\ \kappa_2 \end{matrix}\right] \\ -\gamma\, \mathrm{G}_{r+1,3r+1}^{3r,1}\left[\frac{B}{\mu_{RD}^{(r)}}\gamma \,\middle|\, \begin{matrix} 1, \kappa_1 \\ \kappa_2, 0 \end{matrix}\right]\Bigg)\Bigg]. \end{aligned} \tag{4.32}$$

Moment Generating Function: Substituting (4.31) into (4.16) and utilizing [58,

Eq. (7.813.1)], after some manipulations the MGF of γ is obtained as

$$\mathcal{M}_{\gamma}(s) = 1 - \frac{s}{s + 1/\overline{\gamma}_{SR}} \left(1 - A\, \mathrm{G}_{r+2,3r+1}^{3r,2} \left[\frac{B}{\mu_{RD}^{(r)}(s + 1/\overline{\gamma}_{SR})} \middle| \begin{matrix} 0, 1, \kappa_1 \\ \kappa_2, 0 \end{matrix} \right] \right). \tag{4.33}$$

Moments: Placing (4.31) into (4.19) and utilizing [58, Eq. (7.813.1)], the moments are obtained as

$$\mathbb{E}\left[\gamma^n\right] = n\, \overline{\gamma}_{SR}^{n} \left(\Gamma(n) - A\, \mathrm{G}_{r+2,3r+1}^{3r,2} \left[\frac{B\, \overline{\gamma}_{SR}}{\mu_{RD}^{(r)}} \middle| \begin{matrix} 1-n, 1, \kappa_1 \\ \kappa_2, 0 \end{matrix} \right] \right). \tag{4.34}$$

Applications to the Performance of Asymmetric RF-FSO Dual-Hop Relay Transmission Systems with Variable Gain Relay

Outage Probability: Similar to the OP derived earlier for the fixed gain relay scenario, utilizing (4.31), the required OP of a variable gain relay system can be obtained.

Higher-Order Amount of Fading: Utilizing (4.22) by substituting (4.34) into it, the n^{th}-order AF is obtained as

$$AF_{\gamma}^{(n)} = \frac{n \left(\Gamma(n) - A\, \mathrm{G}_{r+2,3r+1}^{3r,2} \left[\frac{B\, \overline{\gamma}_{SR}}{\mu_{RD}^{(r)}} \middle| \begin{matrix} 1-n, 1, \kappa_1 \\ \kappa_2, 0 \end{matrix} \right] \right)}{\left(1 - A\, \mathrm{G}_{r+2,3r+1}^{3r,2} \left[\frac{B\, \overline{\gamma}_{SR}}{\mu_{RD}^{(r)}} \middle| \begin{matrix} 0, 1, \kappa_1 \\ \kappa_2, 0 \end{matrix} \right] \right)^{n}} - 1. \tag{4.35}$$

For $n = 2$, as a special case, the classical AF [112] is obtained as

$$AF = AF_{\gamma}^{(2)} = \frac{2 \left(1 - A\, \mathrm{G}_{r+2,3r+1}^{3r,2} \left[\frac{B\, \overline{\gamma}_{SR}}{\mu_{RD}^{(r)}} \middle| \begin{matrix} -1, 1, \kappa_1 \\ \kappa_2, 0 \end{matrix} \right] \right)}{\left(1 - A\, \mathrm{G}_{r+2,3r+1}^{3r,2} \left[\frac{B\, \overline{\gamma}_{SR}}{\mu_{RD}^{(r)}} \middle| \begin{matrix} 0, 1, \kappa_1 \\ \kappa_2, 0 \end{matrix} \right] \right)^{2}} - 1. \tag{4.36}$$

Average BER: Substituting (4.31) into [69, Eq. (12)] and utilizing [58, Eq. (7.813.1)],

the average BER $\overline{P}_b$ is obtained for a variety of binary modulations as

$$\overline{P}_b = \frac{1}{2} - \frac{q^p}{2\left(q + 1/\overline{\gamma}_{SR}\right)^p} \left(1 - \frac{A}{\Gamma(p)} \, \mathrm{G}_{r+2,3r+1}^{3r,2} \left[\frac{B}{\mu_{RD}^{(r)}(q + 1/\overline{\gamma}_{SR})} \middle| \begin{matrix} 1-p, 1, \kappa_1 \\ \kappa_2, 0 \end{matrix} \right] \right). \tag{4.37}$$

Average SER: Substituting (4.33) into [78, Eq. (41)], [78, Eq. (45)], and [78, Eq. (48)], the SER of M-PSK, M-AM, and M-QAM, respectively can be obtained.

Ergodic Capacity: Utilizing (4.27) by exploiting the identity [114, p. 152] $(1 + az)^{-b} = \frac{1}{\Gamma(b)} \, \mathrm{G}_{1,1}^{1,1}\left[az \middle| \begin{smallmatrix} 1-b \\ 0 \end{smallmatrix}\right]$ in it and using the integral identity [69, Eq. (20)], the ergodic capacity can be expressed in terms of the EGBMGF (see [69] and references therein) as

$$\begin{aligned} \overline{C} = {} & \frac{1}{\ln(2)} \left(\mathrm{E}_1(1/\overline{\gamma}_{SR}) \exp(1/\overline{\gamma}_{SR}) - A\,\overline{\gamma}_{SR}\right. \\ & \left. \times \mathrm{G}_{1,0:1,1:\,r+1,3r+1}^{1,0:1,1:\,3r,1} \left[\begin{matrix} 1 \\ \end{matrix} \middle| \begin{matrix} 0 \\ 0 \end{matrix} \middle| \begin{matrix} \kappa_1 \\ \kappa_2 \end{matrix} \middle| \overline{\gamma}_{\mathrm{SR}}, \frac{\mathrm{B}\,\overline{\gamma}_{\mathrm{SR}}}{\mu_{\mathrm{RD}}^{(\mathrm{r})}} \right] \right), \end{aligned} \tag{4.38}$$

where $\mathrm{E}_1(.)$ is an exponential integral [79, Eq. (5.1.45)].

4.1.5 Results and Discussion

Fixed-Gain Relay System

As an illustration of the mathematical formalism, simulation results for different performance metrics of an asymmetric dual-hop RF-FSO fixed gain relay transmission system with pointing errors are presented in this section. The RF link (i.e. the S-R link) is modeled as Rayleigh fading channel and the FSO link (i.e. the R-D link) is modeled as Gamma-Gamma fading channel with atmospheric turbulence parameters $\alpha = 2.1$ and $\beta = 3.5$. The relay is set such as $C = 0.6$ and the pointing error is set such as $\xi = 1.2$. The average SNR per bit per hop in all the scenarios discussed is assumed to be equal.

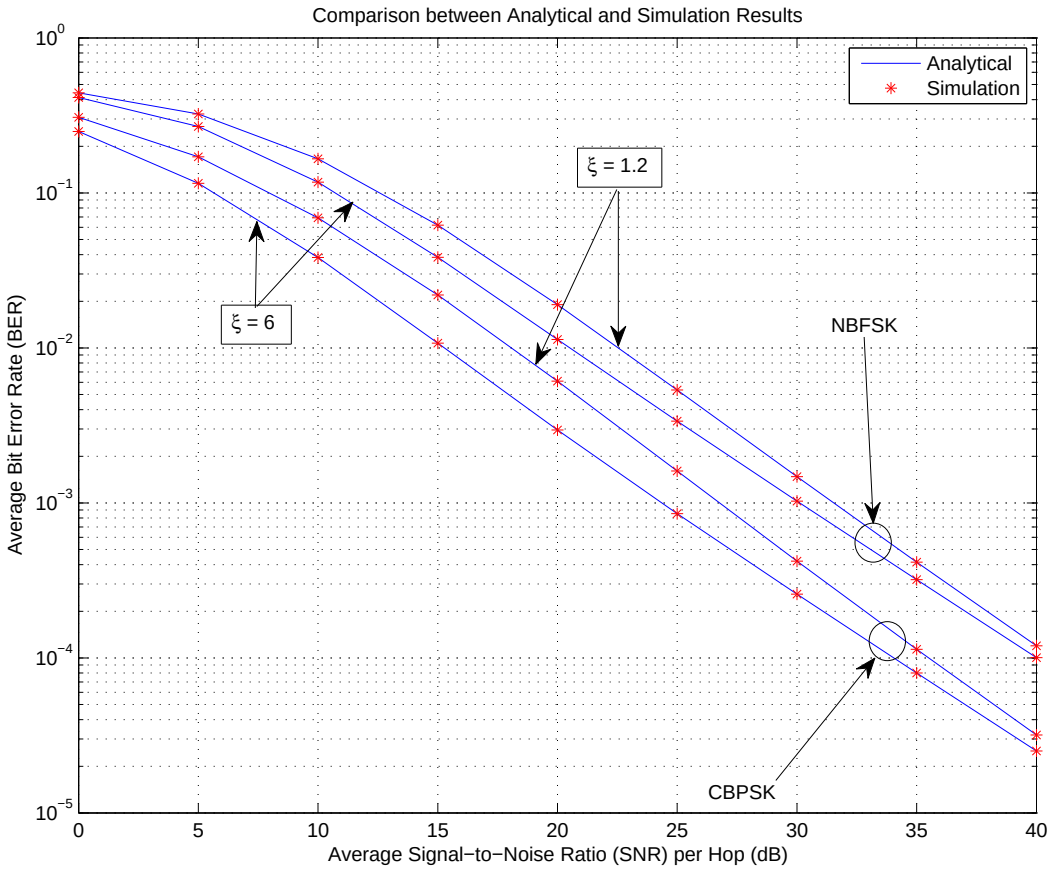

Figure 4.2: Average BER of different binary modulation schemes showing impact of pointing errors (varying ξ) with fading parameters $\alpha = 2.1$, $\beta = 3.5$, and $C = 0.6$.

The average BER performance of different digital binary modulation schemes are presented in Fig. 4.2 based on the values of p and q as presented in Table 2.1 where $p = 0.5$ and $q = 1$ represents CBPSK, $p = 1$ and $q = 1$ represents DBPSK, CBFSK is represented by $p = 0.5$ and $q = 0.5$, and NBFSK is represented by $p = 1$ and $q = 0.5$. Hence, it can be observed from Fig. 4.2 that the simulation results provide a perfect match to the analytical results obtained in this work. Also, the results are as expected i.e. the BER decreases as the SNR increases. It is important to note here that these values for the parameters were selected arbitrarily to prove the validity of the obtained results and hence specific values based on the standards can be used to

obtain the required results. It can be seen from Fig. 4.2 that, as expected, CBPSK outperforms NBFSK. Also, the effect of pointing error can be observed in Fig. 4.2 i.e. as the effect of pointing error (as the value of ξ increases, the effect of pointing error decreases) increases, the BER deteriorates and vice versa. It can be shown that as the atmospheric turbulence conditions get severe i.e. as the values of α and β start dropping, the BER starts deteriorating and vice versa. Additionally, PSK in general performs better than FSK, as expected. Similar results for any other binary modulations schemes and any other values of α's, β's, c's, and ξ's can be observed.

Also, in Fig. 4.3, it can be observed that as the atmospheric turbulence conditions get severe i.e. as the values of α and β start dropping, the BER starts deteriorating and vice versa. Similarly, in Fig. 4.4, as the atmospheric turbulence conditions get severe, the ergodic capacity starts decreasing (i.e. the higher the values of α and β, the higher will be the ergodic capacity). Also, the effect of pointing error can be observed in Fig. 4.4. Note that as the value of ξ increases (i.e. the effect of pointing error decreases) the ergodic capacity decreases.

Variable-Gain Relay System

As an illustration of the mathematical formalism, simulation results for different performance metrics of an asymmetric dual-hop RF-FSO variable gain relay transmission system are presented in this section. For the asymmetric RF-FSO relay transmission systems with variable gain scenario, the RF link (i.e. the S-R link) is modeled as Rayleigh fading channel and the FSO link (i.e. the R-D link) is modeled as Gamma-Gamma fading channel with atmospheric turbulence parameters $\alpha = 2.1$ and $\beta = 3.5$. The average SNR per bit per hop in all the scenarios discussed is assumed to be equal. The average BER performance of DBPSK with heterodyne detection and CBPSK with IM/DD are presented in Fig. 4.5 with varying effects of pointing error ($\xi = 1.2, 1.6, \text{and } 6.7$). It can be observed from Fig. 4.5 that the simulation

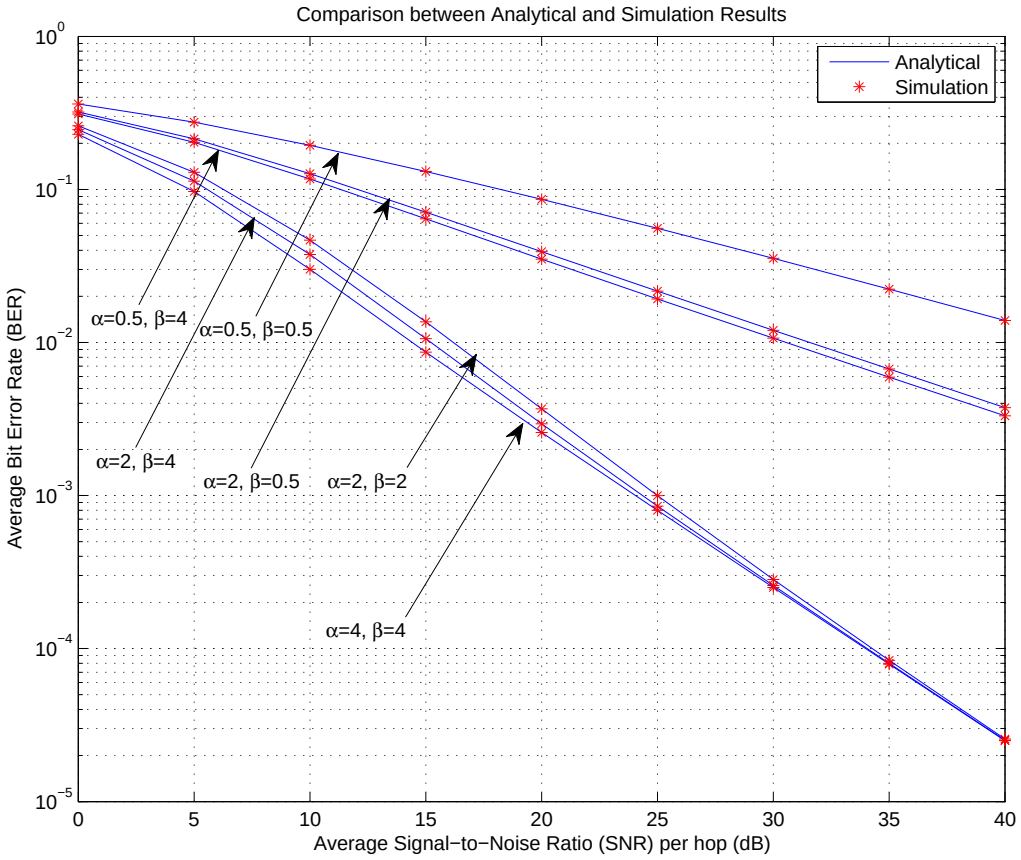

Figure 4.3: Average BER of CBPSK modulation scheme with varying fading parameters α's and β's.

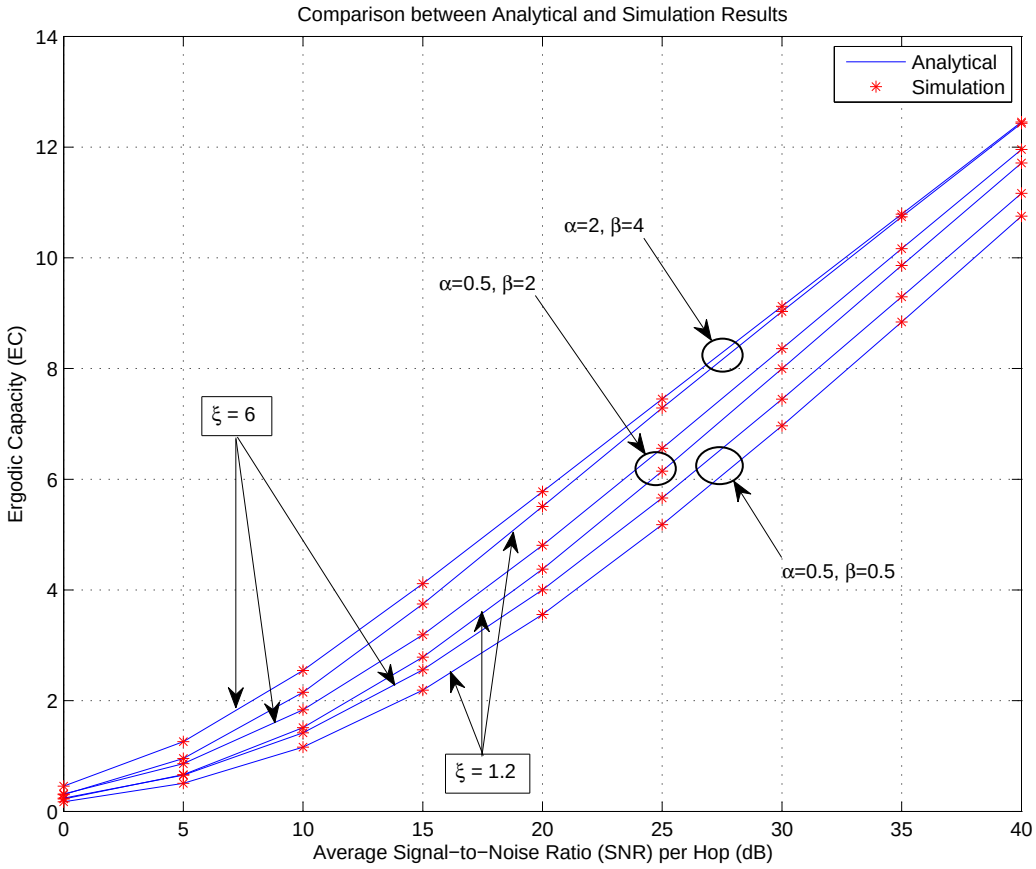

Figure 4.4: Effect of pointing errors (varying ξ) on the ergodic capacity with varying fading parameters α's and β's, and $C = 0.6$.

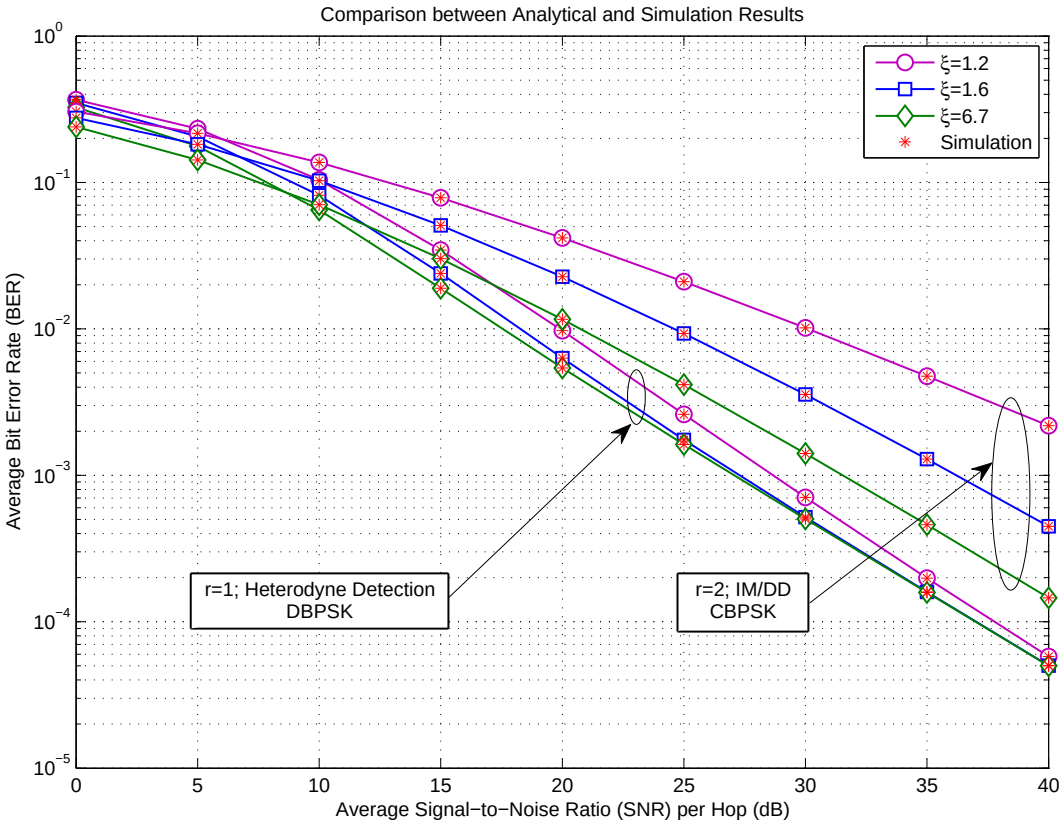

Figure 4.5: Average BER of variable gain relay dual-hop for different binary modulation schemes showing the performance of both the detection techniques (heterodyne and IM/DD) with varying effects of pointing error and with fading parameters $\alpha = 1.2$ and $\beta = 3.5$.

results provide a perfect match to the analytical results obtained in this work. It is observed that as the effects of pointing error get severe, BER starts increasing (i.e. the higher the values of ξ, the lower will be the BER). It is important to note here that these values for the parameters were selected arbitrarily to prove the validity of the obtained results and hence specific values based on the standards can be used to obtain the required results by design communication engineers before deployment.

Similarly, in Fig. 4.6, the effect of pointing error is set such that $\xi = 2.1$ to see the effect of varying fading parameters. It can be seen that as the atmospheric turbulence conditions get severe, BER starts increasing (i.e. the higher the values of α and β, the lower will be the BER). Also, similar results on the ergodic capacity can be observed for heterodyne detection and IM/DD techniques as were seen above in Fig. 4.5 and Fig. 4.6 for the BER case.

4.2 Hybrid RF/RF-FSO Transmission Systems

4.2.1 Introduction

Motivation

In this work, a dual-path transmission system is considered utilizing a SC diversity receiver. It involves a direct RF link/path and an asymmetric RF-FSO dual-hop path as can be seen from Fig. 4.1. The motivation behind such a system involves a fact that the users are mostly mobile and with only RF capabilities (no FSO capabilities). Installing FSO capability on these mobile users does not seem to be a justified approach. Another source of motivation is the fact that we fall short of bandwidth (BW) every now and then. Hence, to save on BW and to save on the economic resources by avoiding unnecessary modifications to the current mobile devices, such a system is introduced wherein the users remain as is with RF only capability(s) and yet can

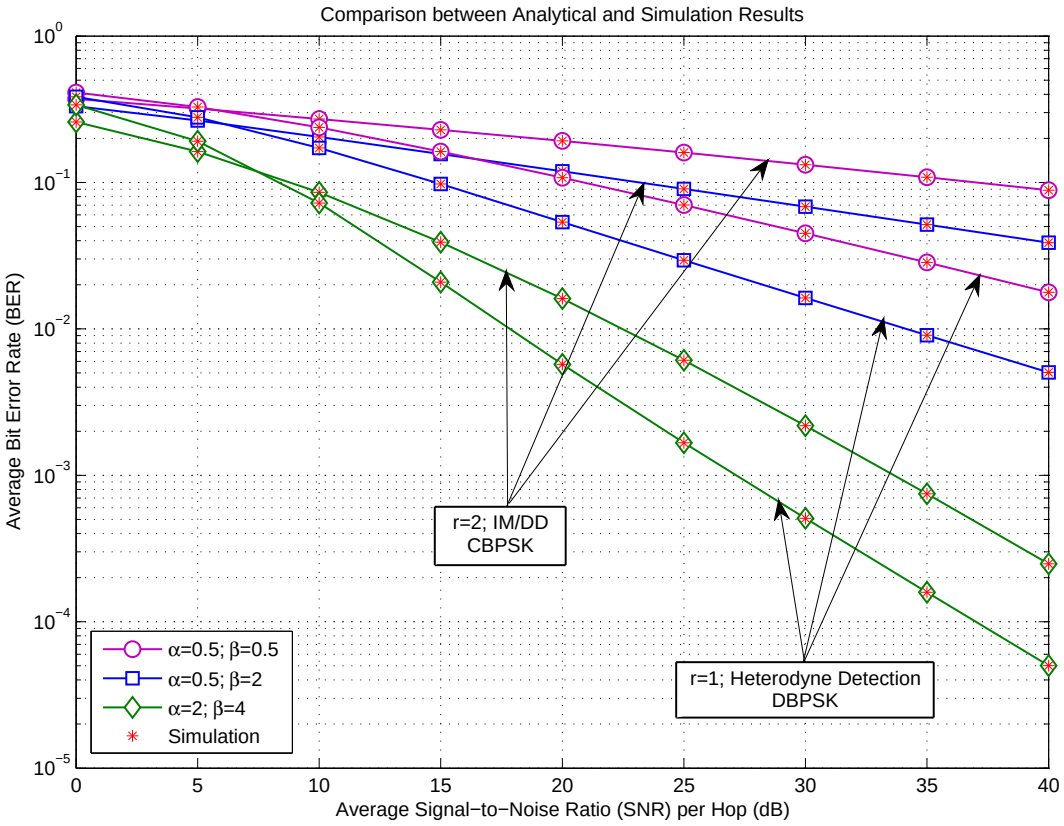

Figure 4.6: Average BER for variable gain relay dual-hop for different binary modulation schemes showing the performance of both the detection techniques (heterodyne and IM/DD) with varying fading parameters α's and β's and with effect of pointing error $\xi = 2.1$.

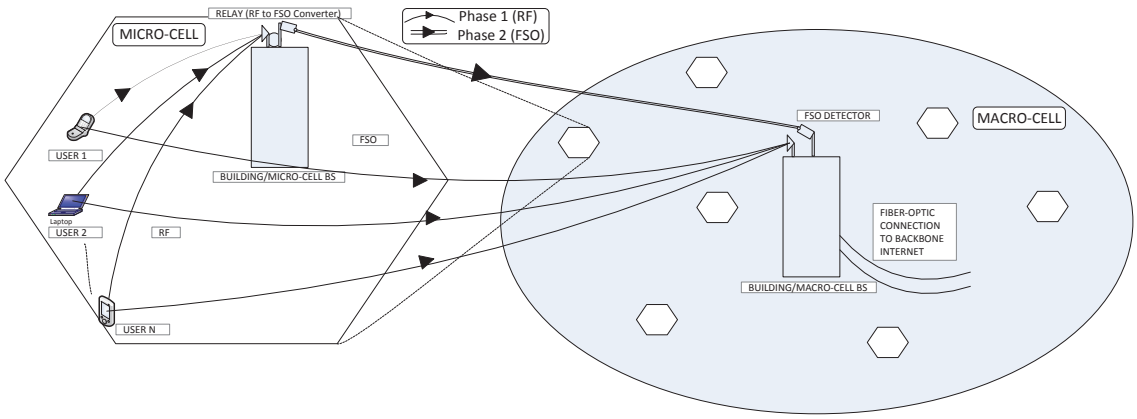

Figure 4.7: System model block diagram of a hybrid RF/RF-FSO uplink transmission system.

be part of and/or make use of the FSO featured network. Essentially, as can be seen from Fig. 4.1, mobile devices/users with RF only capability will be transmitting in phase 1 that shall be heard by the relay and the destination. During phase 2, the relay will be transmitting the RF converted to FSO and shall be heard by the destination. Then both these messages received in phase 1 and phase 2 at the destination will be dealt with under SC diversity scheme. Furthermore, the performance measures of the system under the SC diversity scheme are compared with the maximal ratio combining (MRC) diversity, which is an optimal diversity combining scheme where all the diversity branches are processed to obtain the best possible devised and improved single output that possibly stays above a certain specified threshold [3, 9, 10]. An important point to note here is that during phase 2, the RF BW is completely free from the systems current use and hence can still be utilized by surrounding users/devices as it will cause no interference to the FSO simultaneous transmission.

Recently, some work has been published on the asymmetric relay networks (so-called mixed fading channels) that have different fading channel distributions for each link [53, 106, 107] but to the best of the authors knowledge, no work involves performance study of a dual-branch diversity system with a direct RF link and an

asymmetric relay link. The main objective of this work is to bring forth the essence of utilizing FSO technology in the current traditional RF based communication systems thereby increasing the performance of the system manifolds. In this proposed work, the asymmetric RF-FSO link is up and being utilized at all times along with the direct RF link. In this way, the asymmetric RF-FSO is always complementing the direct RF link via SC or MRC diversity schemes thereby improving the performance relative to the current traditional systems. On the other hand, as can be seen from the Fig. 4.1, RF user(s) being part of the macro-cell might at times be far away from the macro-cell BS and the received signal might not be good enough. This RF user(s), also being part of the micro-cell with a micro-cell BS in its much closer vicinity, is being heard by the micro-cell BS. This micro-cell BS is ultimately connected to the macro-cell BS via FSO technology and is assisting the RF user(s) message to reach the macro-cell BS via SC or MRC diversity scheme. Therefore, such a proposed hybrid system will always be beneficial and more specifically when the direct RF link is weak.

Interestingly enough, having FSO technology on the second link of the RF-FSO link also provides a solution to the current traditional communication system in case when the direct RF link is reaching a saturation in terms of its BW. In such a situation, the RF link of the asymmetric RF-FSO link can combine/multiplex multiple RF users to its maximum capability in a single instance and send all through the FSO link to the other end. In this way, the major advantage of FSO technology of having much higher BW is also utilized, again as a great benefit to the current traditional systems.

In this work, the authors consider a RF based communication system i.e. RF is the main mode of communication though the receiver benefits from the presence of the diverse asymmetric RF-FSO channel too. This RF-FSO asymmetric link utilizes the FSO technology and as discussed earlier in detail, this can prove to be handy manifolds. In this work, the RF links are assumed to be operating over Rayleigh fading environment [3] whereas the FSO link is considered to be operating over unified

Gamma-Gamma fading environment [37, 39, 40] under the effect of pointing errors. Here, the authors would like to bring to the notice of the readers that this Gamma-Gamma model is unified in terms of inculcating both types detection techniques (i.e. heterodyne and IM/DD) and additionally also includes the effects of pointing error. Indeed, this unified model increases the complexity and hence providing a comprehensive study on such a proposed hybrid system makes this an interesting problem to study. Such a unified model, to the authors best knowledge, has not been seen in the literature for the study of such proposed hybrid communication systems.

Contributions

The key contributions of this work are stated as follows.

- The *statistical characterizations* such as the CDF, the PDF, the MGF, and the moments of the end-to-end SNR of such hybrid RF/RF-FSO transmission systems are derived for fixed gain relays as well variable gain relays.

- This statistical characterization of the SNR is then applied to derive the exact closed-form expressions for the *performance metrics* such as the OP, the higher-order AF, the average BER of binary modulation schemes, the average SER of M-AM, M-PSK and M-QAM, and the ergodic capacity in terms of Meijer's G functions for both types of amplify-and-forward relay schemes.

Organization

The remainder of the chapter is organized as follows. Subsection 2 introduces the channel and systems models. Subsection 3 presents the statistical characterizations and the performance analysis of fixed gain relay hybrid RF/RF-FSO transmission systems in collaboration with the SC diversity scheme whereas Subsection 4 presents the similar study for variable gain relays in collaboration with the SC as well as

the MRC diversity schemes. Specifically, the statistical characterizations include the PDF, the CDF, the MGF, and the moments and the performance metrics include, namely, the OP, the higher-order AF, the BER, the SER, and the ergodic capacity. Subsection 5 presents some simulation results to validate these analytical results followed by concluding remarks in Section 3.

4.2.2 Channel and System Models

Based on the discussion earlier in the Introduction and Fig. 4.7, a dual-path transmission system model is employed with a direct RF link that indicates mobile users/devices with RF only capabilities (no FSO capability) and a relay consisting RF-FSO branch. This signifies that the buildings/base stations (BSs) near these mobile users/devices have FSO capability too and so do all the subsequent BSs ultimately reaching the internet backbone. Also, it is worthwhile to assume that the RF BW is getting scarce and there is no additional availability of RF BW thus leading to the utility of freely available FSO features. The SNR of the direct RF link is denoted by γ_{SD}.

Now, the end-to-end SNR of the fixed gain relay branch can be given as

$$\gamma_{SRD} = \frac{\gamma_{SR}\gamma_{RD}}{\gamma_{RD} + C}, \tag{4.39}$$

where S, R, and D refer to source, relay, and destination respectively and C is a fixed relay gain [3, 21, 53].

Similarly, for variable gain amplify-and-forward, the end-to-end SNR can be given as

$$\gamma_{SRD} = \frac{\gamma_{SR}\,\gamma_{RD}}{\gamma_{SR} + \gamma_{RD} + 1}. \tag{4.40}$$

Since the closed-from analysis of the statistical characteristics of γ_{SRD} is complicated, the standard approximation $\gamma_{SRD} = \frac{\gamma_{SR}\,\gamma_{RD}}{\gamma_{SR}+\gamma_{RD}+1} \approxeq \min(\gamma_{SR}\,\gamma_{RD})$ [106, 110, 111] is

utilized.

The RF links (i.e. S-R link and S-D link) are independent and non-identically distributed (i.n.i.d.) and are assumed to follow Rayleigh fading whose SNR follows an exponential distribution, parameterized by the average SNR $\overline{\gamma}_{SR}$ of the S-R link and $\overline{\gamma}_{SD}$ of the S-D link, with a PDF given by [3]

$$f_{\gamma_{SD}}(\gamma_{SD}) = 1/\overline{\gamma}_{SD} \exp(-\gamma_{SD}/\overline{\gamma}_{SD}), \tag{4.41}$$

for S-D link and similarly for S-R link by replacing the subscripts SD with SR in the above given PDF [3]. On the other hand, it is assumed that the FSO link (i.e. R-D link) experiences Gamma-Gamma fading with pointing error impairments whose SNR PDF is given by (4.9).

4.2.3 Fixed-Gain Relay System

This section presents exact closed-form results on the statistical characteristics including the CDF, the PDF, the MGF, and the moments of the hybrid RF/RF-FSO transmission systems in terms of the Meijer's G functions. Additionally, this section also presents new performance analysis results, in particular the OP, the higher-order AF, the BER analysis, the SER analysis, and the ergodic capacity of hybrid RF/RF-FSO transmission systems with fixed gain relay in presence of SC diverse receiver.

Closed-Form Statistical Characteristics

Cumulative Distribution Function: In SC diversity scheme, the highest SNR branch is selected. In this case, for dual-branch diversity, the end-to-end SNR γ is given by

$$\gamma = \max(\gamma_{SD}, \gamma_{SRD}). \tag{4.42}$$

The CDF of γ is given by

$$F(\gamma) = \Pr(\max(\gamma_{SD}, \gamma_{SRD} \leq \gamma)) = F_{\gamma_{SD}}(\gamma)\, F_{\gamma_{SRD}}(\gamma). \tag{4.43}$$

Using

$$F_{\gamma_{SD}}(\gamma) = 1 - \exp(-\gamma/\overline{\gamma}_{SD}), \tag{4.44}$$

as the CDF of the Rayleigh channel,

$$F_{\gamma_{SRD}}(\gamma) = 1 - A \exp(-\gamma/\overline{\gamma}_{SR})\, \mathrm{G}_{r,3r+1}^{3r+1,0}\left[\frac{B\,C}{\overline{\gamma}_{SR}\mu_{RD}^{(r)}}\gamma \,\middle|\, \begin{matrix}\kappa_1 \\ \kappa_2, 0\end{matrix}\right], \tag{4.45}$$

from (4.12), and some simple algebraic manipulations, the CDF of γ can be shown to be given by

$$\begin{aligned} F_{\gamma}(\gamma) &= 1 - \exp\left(-\gamma/\overline{\gamma}_{SD}\right) - A \exp\left(-\gamma/\overline{\gamma}_{SR}\right)\left(1 - \exp\left(-\gamma/\overline{\gamma}_{SD}\right)\right) \\ &\quad \times \mathrm{G}_{r,3r+1}^{3r+1,0}\left[\frac{B\,C}{\overline{\gamma}_{SR}\,\mu_{RD}^{(r)}}\,\gamma \,\middle|\, \begin{matrix}\kappa_1 \\ \kappa_2, 0\end{matrix}\right]. \end{aligned} \tag{4.46}$$

Probability Density Function: Differentiating (4.46) with respect to γ, using the product rule then utilizing [62, Eq. (07.34.20.0001.01)], after some algebraic manipulations the PDF is obtained in exact closed-form in terms of Meijer's G functions as

$$\begin{aligned} f_{\gamma}(\gamma) &= \frac{\exp\left(-\gamma/\overline{\gamma}_{SD}\right)}{\overline{\gamma}_{SD}} + \frac{A}{\gamma}\, \mathrm{G}_{0,2r+1}^{\,2r+1,0}\left[\frac{B\,C}{\overline{\gamma}_{SR}\,\mu_{RD}^{(r)}}\,\gamma \,\middle|\, \begin{matrix}- \\ \kappa_3, 0\end{matrix}\right] \left(\exp\left(-\gamma/\overline{\gamma}_{SR}\right)\right. \\ &\quad \left. - \exp\left(-\gamma/\overline{\gamma}_{SD} - \gamma/\overline{\gamma}_{SR}\right)\right) - A\left\{\left(\frac{1}{\overline{\gamma}_{SD}} + \frac{1}{\overline{\gamma}_{SR}} - \frac{\xi^2}{r\,\gamma}\right)\exp\left(-\gamma/\overline{\gamma}_{SD} - \gamma/\overline{\gamma}_{SR}\right)\right. \\ &\quad \left. - \left[1/\overline{\gamma}_{SR} - \xi^2/\left(r\,\gamma\right)\right]\exp\left(-\gamma/\overline{\gamma}_{SR}\right)\right\} \mathrm{G}_{r,3r+1}^{3r,0}\left[\frac{B\,C}{\overline{\gamma}_{SR}\,\mu_{RD}^{(r)}}\,\gamma \,\middle|\, \begin{matrix}\kappa_1 \\ \kappa_2, 0\end{matrix}\right]. \end{aligned} \tag{4.47}$$

Moment Generating Function: The MGF can be defined in terms of CDF as given in (4.16). Placing (4.46) into (4.16) and utilizing [58, Eq. (7.813.1)], after some manipulations the MGF of γ is obtained as

$$\begin{aligned}\mathcal{M}_{\gamma}(s) = 1 - \frac{s}{s+1/\overline{\gamma}_{SD}} - \frac{s\,A}{s+1/\overline{\gamma}_{SR}}\mathrm{G}_{r+1,3r+1}^{3r+1,1}\left[\frac{B\,C}{\mu_{RD}^{(r)}(s\,\overline{\gamma}_{SR}+1)}\middle|\begin{matrix}0,\kappa_1\\ \kappa_2,0\end{matrix}\right] \\ + \frac{s\,A}{s+1/\overline{\gamma}_{SD}+1/\overline{\gamma}_{SR}}\mathrm{G}_{r+1,3r+1}^{3r+1,1}\left[\frac{B\,C}{\mu_{RD}^{(r)}(s\,\overline{\gamma}_{SR}+\overline{\gamma}_{SR}/\overline{\gamma}_{SD}+1)}\middle|\begin{matrix}0,\kappa_1\\ \kappa_2,0\end{matrix}\right].\end{aligned} \tag{4.48}$$

Moments: The moments defined as $\mathbb{E}\left[\gamma^n\right]$ can be expressed in terms of the CCDF as givein in (4.19). Now, placing (4.46) into (4.19) and utilizing [58, Eq. (7.813.1)], the moments are obtained as

$$\begin{aligned}\mathbb{E}\left[\gamma^n\right] = n\,\overline{\gamma}_{SD}^{n}\,\Gamma(n) + n\,A\,\overline{\gamma}_{SR}^{n}\,\mathrm{G}_{r+1,3r+1}^{3r+1,1}\left[\frac{B\,C}{\mu_{RD}^{(r)}}\middle|\begin{matrix}1-n,\kappa_1\\ \kappa_2,0\end{matrix}\right] \\ - \frac{n\,A}{\left(1/\overline{\gamma}_{SD}+1/\overline{\gamma}_{SR}\right)^{n}}\,\mathrm{G}_{r+1,3r+1}^{3r+1,1}\left[\frac{B\,C}{\mu_{RD}^{(r)}\left(\overline{\gamma}_{SR}/\overline{\gamma}_{SD}+1\right)}\middle|\begin{matrix}1-n,\kappa_1\\ \kappa_2,0\end{matrix}\right].\end{aligned} \tag{4.49}$$

Applications to the Performance of Hybrid RF/RF-FSO Transmission Systems under Fixed Gain Relay

Outage Probability: Similar to the OP derivation presented earlier in Section 4.1.3, the required OP of a dual-branch system comprising of a fixed gain relay is obtained as (4.46).

Higher-Order Amount of Fading: The n^{th}-order AF for the instantaneous SNR γ is defined in [68, Eq. (3)] or in (4.22). Now, utilizing this equation by substituting (4.49) into it, the n^{th}-order AF can be obtained. Similarly, for $n = 2$ as a special case, the classical AF can be obtained [112].

Average BER: Substituting (4.46) into [69, Eq. (12)] and utilizing [58, Eq. (7.813.1)],

the average BER $\overline{P}_b$ of a variety of binary modulations is obtained as

$$\overline{P}_b = \frac{1}{2} - \frac{q^p}{2\,(q+1/\overline{\gamma}_{SD})^p} - \frac{A\,q^p}{2\,\Gamma(p)\,(q+1/\overline{\gamma}_{SR})^p}\,\mathrm{G}_{r+1,3r+1}^{3r+1,1}\left[\frac{B\,C}{\mu_{RD}^{(r)}(q\,\overline{\gamma}_{SR}+1)}\,\middle|\,\begin{matrix}1-p,\kappa_1\\ \kappa_2,0\end{matrix}\right] + \frac{A\,q^p}{2\,\Gamma(p)\,(q+1/\overline{\gamma}_{SD}+1/\overline{\gamma}_{SR})^p}\,\mathrm{G}_{r+1,3r+1}^{3r+1,1}\left[\frac{B\,C}{\mu_{RD}^{(r)}(q\,\overline{\gamma}_{SR}+\overline{\gamma}_{SR}/\overline{\gamma}_{SD}+1)}\,\middle|\,\begin{matrix}1-p,\kappa_1\\ \kappa_2,0\end{matrix}\right]. \tag{4.50}$$

Average SER: Substituting (4.48) into [78, Eq. (41)], [78, Eq. (45)], and [78, Eq. (48)], the SER of M-PSK, M-AM, and M-QAM, respectively can be obtained.

Ergodic Capacity: The ergodic channel capacity can be expressed in terms of the CCDF of γ as (4.27). Utilizing (4.27) by exploiting the identity [114, p. 152] $(1+az)^{-b} = \frac{1}{\Gamma(b)}\,\mathrm{G}_{1,1}^{1,1}\big[az\,\big|\,\begin{smallmatrix}1-b\\ 0\end{smallmatrix}\big]$ in it, using [79, Eq. (5.1.28)], and using the integral identity [69, Eq. (20)], the ergodic capacity can be expressed in terms of the EGBMGF (see [69] and references therein) as

$$\begin{aligned}\overline{C} = {} & 1/\ln(2)\,(\mathrm{E}_1(1/\overline{\gamma}_{SD})\,\exp(1/\overline{\gamma}_{SD}) + A\,\overline{\gamma}_{SR} \\ & \times \mathrm{G}_{1,0:1,1:\,3r+1,0}^{1,0:1,1:\,3r+1,0}\left[\begin{matrix}1\\ \\ \end{matrix}\,\middle|\,\begin{matrix}0\\ 0\end{matrix}\,\middle|\,\begin{matrix}\kappa_1\\ \kappa_2,0\end{matrix}\,\middle|\,\overline{\gamma}_{\mathrm{SR}},\frac{\mathrm{B\,C}}{\mu_{\mathrm{RD}}^{(\mathrm{r})}}\right] - \mathrm{A}/\,(1/\overline{\gamma}_{\mathrm{SD}}+1/\overline{\gamma}_{\mathrm{SR}}) \\ & \times \mathrm{G}_{1,0:1,1:\,3r+1,0}^{1,0:1,1:\,3r+1,0}\left[\begin{matrix}1\\ \\ \end{matrix}\,\middle|\,\begin{matrix}0\\ 0\end{matrix}\,\middle|\,\begin{matrix}\kappa_1\\ \kappa_2,0\end{matrix}\,\middle|\,\frac{1}{1/\overline{\gamma}_{\mathrm{SD}}+1/\overline{\gamma}_{\mathrm{SR}}},\frac{\mathrm{B\,C}}{\mu_{\mathrm{RD}}^{(\mathrm{r})}\,(\overline{\gamma}_{\mathrm{SR}}/\overline{\gamma}_{\mathrm{SD}}+1)}\right]\Bigg).\end{aligned} \tag{4.51}$$

4.2.4 Variable-Gain Relay System

This section presents exact closed-form results on the statistical characteristics including the CDF, the PDF, the MGF, and the moments of the hybrid RF/RF-FSO transmission systems in terms of the Meijer's G functions. Additionally, this section also presents new performance analysis results, in particular the OP, the higher-order

AF, the BER analysis, the SER analysis, and the ergodic capacity of hybrid RF/RF-FSO transmission systems with variable gain relay in presence of SC diverse receiver as well as MRC diverse receiver.

PERFORMANCE OVER SC DIVERSITY SCHEME

Closed-Form Statistical Characteristics

Cumulative Distribution Function: It is well known that the CDF of $\gamma_{SRD} = \min(\gamma_{SR}, \gamma_{RD})$ can be expressed as

$$F_{\gamma_{SRD}}(\gamma) = \Pr(\min(\gamma_{SR}, \gamma_{RD}) < \gamma). \tag{4.52}$$

The expression in (4.52) can be re-written as [115, Eq. (4)]

$$F_{\gamma_{SRD}}(\gamma) = F_{\gamma_{SR}}(\gamma) + F_{\gamma_{RD}}(\gamma) - F_{\gamma_{SR}}(\gamma)\, F_{\gamma_{RD}}(\gamma). \tag{4.53}$$

The result of (4.53) is given by (4.31)

$$F_{\gamma_{SRD}}(\gamma) = 1 - \exp(-\gamma/\overline{\gamma}_{SR}) \left(1 - A\, \mathrm{G}_{r+1,3r+1}^{3r,1}\left[\frac{B}{\mu_{RD}^{(r)}}\gamma \,\middle|\, \begin{matrix} 1, \kappa_1 \\ \kappa_2, 0 \end{matrix}\right]\right). \tag{4.54}$$

Now, substituting $F_{\gamma_{SD}}(\gamma)$ and $F_{\gamma_{SRD}}(\gamma)$ into (4.43), and with some simple algebraic manipulations, the CDF of γ can be shown to be given after some simplifications by

$$\begin{aligned} F_{\gamma}(\gamma) = {} & 1 - 2\exp\left(-\gamma/\overline{\gamma}_{SD}\right) + \exp\left(-\gamma/\overline{\gamma}_{SD} - \gamma/\overline{\gamma}_{SR}\right) \\ & + A\exp\left(-\gamma/\overline{\gamma}_{SR}\right)\left(1 - \exp\left(-\gamma/\overline{\gamma}_{SD}\right)\right) \mathrm{G}_{r+1,3r+1}^{3r,1}\left[\frac{B}{\mu_{RD}^{(r)}}\gamma \,\middle|\, \begin{matrix} 1, \kappa_1 \\ \kappa_2, 0 \end{matrix}\right]. \end{aligned} \tag{4.55}$$

Probability Density Function: Differentiating (4.55) with respect to γ, using

the product rule then utilizing [62, Eq. (07.34.20.0001.01)], after some algebraic manipulations the PDF is obtained in terms of Meijer's G functions as

$$\begin{aligned} f_{\gamma}(\gamma) &= 2/\overline{\gamma}_{SD} \exp\left(-\gamma/\overline{\gamma}_{SD}\right) - \left(1/\overline{\gamma}_{SD} + 1/\overline{\gamma}_{SR}\right) \exp\left(-\gamma/\overline{\gamma}_{SD} - \gamma/\overline{\gamma}_{SR}\right) \\ &\quad - A \exp\left(-\gamma/\overline{\gamma}_{SR}\right) \left[1/\overline{\gamma}_{SR} - \exp\left(-\gamma/\overline{\gamma}_{SD}\right) \left(1/\overline{\gamma}_{SR} + 1/\overline{\gamma}_{SD}\right)\right] \\ &\quad \times \mathrm{G}_{r+1,3r+1}^{3r,1}\left[\frac{B}{\mu_{RD}^{(r)}}\,\gamma \,\middle|\, \begin{matrix} 1, \kappa_1 \\ \kappa_2, 0 \end{matrix}\right] + A/\gamma \, \exp\left(-\gamma/\overline{\gamma}_{SR}\right) \\ &\quad \times \left(1 - \exp\left(-\gamma/\overline{\gamma}_{SD}\right)\right) \, \mathrm{G}_{r,3r}^{3r,0}\left[\frac{B}{\mu_{RD}^{(r)}}\,\gamma \,\middle|\, \begin{matrix} \kappa_1 \\ \kappa_2 \end{matrix}\right]. \end{aligned} \tag{4.56}$$

Moment Generating Function: Substituting (4.55) into (4.16) and utilizing [58, Eq. (7.813.1)], after some manipulations the MGF of γ is obtained as

$$\begin{aligned} \mathcal{M}_{\gamma}(s) &= 1 - \frac{2\,s}{s + 1/\overline{\gamma}_{SD}} + \frac{s}{s + 1/\overline{\gamma}_{SD} + 1/\overline{\gamma}_{SR}} + \frac{A\,s}{s + 1/\overline{\gamma}_{SR}} \\ &\quad \times \mathrm{G}_{r+2,3r+1}^{3r,2}\left[\frac{B}{\mu_{RD}^{(r)}(s + 1/\overline{\gamma}_{SR})} \,\middle|\, \begin{matrix} 0, 1, \kappa_1 \\ \kappa_2, 0 \end{matrix}\right] - \frac{A\,s}{s + 1/\overline{\gamma}_{SD} + 1/\overline{\gamma}_{SR}} \\ &\quad \times \mathrm{G}_{r+2,3r+1}^{3r,2}\left[\frac{B}{\mu_{RD}^{(r)}(s + 1/\overline{\gamma}_{SD} + 1/\overline{\gamma}_{SR})} \,\middle|\, \begin{matrix} 0, 1, \kappa_1 \\ \kappa_2, 0 \end{matrix}\right]. \end{aligned} \tag{4.57}$$

Moments: Placing (4.55) into (4.19) and utilizing [58, Eq. (7.813.1)], the moments are obtained as

$$\begin{aligned} \mathbb{E}\left[\gamma^n\right] &= n\,\Gamma(n)\left[2\,\overline{\gamma}_{SD}^{\,n} - \frac{1}{\left(1/\overline{\gamma}_{SD} + 1/\overline{\gamma}_{SR}\right)^n}\right] - A\,n\,\overline{\gamma}_{SR}^{\,n}\,\mathrm{G}_{r+2,3r+1}^{3r,2}\left[\frac{B\,\overline{\gamma}_{SR}}{\mu_{RD}^{(r)}} \,\middle|\, \begin{matrix} 1-n, 1, \kappa_1 \\ \kappa_2, 0 \end{matrix}\right] \\ &\quad + \frac{A\,n}{\left(1/\overline{\gamma}_{SD} + 1/\overline{\gamma}_{SR}\right)^n}\,\mathrm{G}_{r+2,3r+1}^{3r,2}\left[\frac{B}{\mu_{RD}^{(r)}\left(1/\overline{\gamma}_{SD} + 1/\overline{\gamma}_{SR}\right)} \,\middle|\, \begin{matrix} 1-n, 1, \kappa_1 \\ \kappa_2, 0 \end{matrix}\right]. \end{aligned} \tag{4.58}$$

Applications to the Performance of Hybrid RF/RF-FSO Transmission Systems under Variable Gain Relay and SC diversity receiver

Outage Probability: Tthe required OP of a dual-branch system comprising of a variable gain relay link can be obtained as (4.55).

Higher-Order Amount of Fading: On substituting (4.58) into [68, Eq. (3)], the n^{th}-order AF can be obtained. Similarly, for $n = 2$ as a special case, the classical AF [112] can be obtained.

Average BER: Substituting (4.55) into [69, Eq. (12)] and utilizing [58, Eq. (7.813.1)], the average BER $\overline{P}_b$ of a variety of binary modulations is obtained as

$$\begin{aligned}\overline{P}_b = \frac{1}{2} - \frac{q^p}{(q+1/\overline{\gamma}_{SD})^p} + \frac{q^p}{2\,(q+1/\overline{\gamma}_{SD}+1/\overline{\gamma}_{SR})^p} + \frac{A\,q^p}{2\,\Gamma(p)\,(q+1/\overline{\gamma}_{SR})^p} \\ \times \mathrm{G}_{r+2,3r+1}^{3r,2}\left[\frac{B}{\mu_{RD}^{(r)}(q+1/\overline{\gamma}_{SR})}\,\middle|\,\begin{matrix}1-p,1,\kappa_1\\ \kappa_2,0\end{matrix}\right] - \frac{A\,q^p}{2\,\Gamma(p)\,(q+1/\overline{\gamma}_{SD}+1/\overline{\gamma}_{SR})^p} \\ \times \mathrm{G}_{r+2,3r+1}^{3r,2}\left[\frac{B}{\mu_{RD}^{(r)}(q+1/\overline{\gamma}_{SD}+1/\overline{\gamma}_{SR})}\,\middle|\,\begin{matrix}1-p,1,\kappa_1\\ \kappa_2,0\end{matrix}\right].\end{aligned} \tag{4.59}$$

Average SER: Substituting (4.57) into [78, Eq. (41)], [78, Eq. (45)], and [78, Eq. (48)], the SER of M-PSK, M-AM, and M-QAM, respectively can be obtained.

Ergodic Capacity: Utilizing (4.27) by exploiting the identity [114, p. 152] $(1+az)^{-b} = \frac{1}{\Gamma(b)}\,\mathrm{G}_{1,1}^{1,1}\big[az\,\big|\,\begin{smallmatrix}1-b\\ 0\end{smallmatrix}\big]$ in it, using [79, Eq. (5.1.28)], and using the integral identity [69, Eq. (20)], the ergodic capacity can be expressed in terms of the EGBMGF

(see [69] and references therein) as

$$\overline{C} = 1/\ln(2)[\,(2\,\mathrm{E}_1(1/\overline{\gamma}_{SD})\,\exp(1/\overline{\gamma}_{SD}) - \mathrm{E}_1(1/\overline{\gamma}_{SD}+1/\overline{\gamma}_{SR})\,\exp(1/\overline{\gamma}_{SD}+1/\overline{\gamma}_{SR}))$$
$$- A\,\overline{\gamma}_{SR}\,\mathrm{G}^{1,0:1,1:3r,1}_{1,0:1,1:r+1,3r+1}\left[\begin{array}{c|c|c|c} 1 & \begin{array}{c}0\\0\end{array} & \begin{array}{c}1,\kappa_1\\ \kappa_2,0\end{array} & \overline{\gamma}_{\mathrm{SR}},\dfrac{\mathrm{B}\,\overline{\gamma}_{\mathrm{SR}}}{\mu^{(\mathrm{r})}_{\mathrm{RD}}}\end{array}\right] + \frac{A}{1/\overline{\gamma}_{SD}+1/\overline{\gamma}_{SR}}$$
$$\times\mathrm{G}^{1,0:1,1:3r,1}_{1,0:1,1:r+1,3r+1}\left[\begin{array}{c|c|c|c} 1 & \begin{array}{c}0\\0\end{array} & \begin{array}{c}1,\kappa_1\\ \kappa_2,0\end{array} & \dfrac{1}{1/\overline{\gamma}_{\mathrm{SD}}+1/\overline{\gamma}_{\mathrm{SR}}},\dfrac{\mathrm{B}}{\mu^{(\mathrm{r})}_{\mathrm{RD}}\,(1/\overline{\gamma}_{\mathrm{SD}}+1/\overline{\gamma}_{\mathrm{SR}})}\end{array}\right]\Bigg] \tag{4.60}$$

PERFORMANCE OVER MRC DIVERSITY SCHEME

For the sake of comparison, in this section, the MGF of such a system employed under MRC diverse receiver at the destination is derived and utilized to study various performance metrics, namely, the OP, the BER analysis, the SER analysis, and the ergodic capacity.

Closed-Form Statistical Characteristics

In MRC diversity scheme, the SNRs of all the branches are added to achieve the end-to-end SNR of the system. In this case, for dual-branch diversity, the end-to-end SNR γ is given by

$$\gamma = \gamma_{SD} + \gamma_{SRD}. \tag{4.61}$$

Deriving the CDF and/or the PDF of the above given end-to-end SNR in (4.61) can prove to be very complicated and cumbersome yet not certain to have a useful result. Hence, the MGF of this end-to-end SNR is derived and further utilized to derive various performance metrics.

Under the independence assumption between γ_{SD} and γ_{SRD}, the MGF of (4.61)

can be easily attained by

$$\mathcal{M}_{\gamma}(s) = \mathcal{M}_{\gamma_{SD}}(s)\,\mathcal{M}_{\gamma_{SRD}}(s). \tag{4.62}$$

It is well known that the MGF of a Rayleigh (S-D link) channel is given by $1/(1 + s\,\overline{\gamma}_{SD})$. The MGF of the RF-FSO path (S-R-D link) can be obtained by placing (4.54) in (4.16) as

$$\begin{aligned}\mathcal{M}_{\gamma_{SRD}}(s) = s \int_0^{\infty} e^{-s\,\gamma_{SRD}}\,[1 - \exp(-\gamma_{SRD}/\overline{\gamma}_{SR}) \\ \times \left(1 - A\,\mathrm{G}_{r+1,3r+1}^{3r,1}\left[\frac{B}{\mu_{RD}^{(r)}}\,\gamma_{SRD}\,\middle|\,\begin{matrix}1, \kappa_1 \\ \kappa_2, 0\end{matrix}\right]\right)\Bigg]\, d\gamma_{SRD}.\end{aligned} \tag{4.63}$$

On utilizing [58, Eq. (7.813.1)] along with some simple algebraic manipulations, $\mathcal{M}_{\gamma_{SRD}}(s)$ is derived as (4.33)

$$\mathcal{M}_{\gamma_{SRD}}(s) = 1 - s/\,(s + 1/\overline{\gamma}_{SR})\left(1 - A\,\mathrm{G}_{r+2,3r+1}^{3r,2}\left[\frac{B}{\mu_{RD}^{(r)}(s + 1/\overline{\gamma}_{SR})}\,\middle|\,\begin{matrix}0, 1, \kappa_1 \\ \kappa_2, 0\end{matrix}\right]\right). \tag{4.64}$$

To get the end-to-end MGF at the receivers end, the product of both the required MGF's given above is obtained to get

$$\begin{aligned}\mathcal{M}_{\gamma}(s) = [1/\,(1 + s\,\overline{\gamma}_{SD})]\,[1 - s/\,(s + 1/\overline{\gamma}_{SR}) \\ \times \left(1 - A\,\mathrm{G}_{r+2,3r+1}^{3r,2}\left[\frac{B}{\mu_{RD}^{(r)}(s + 1/\overline{\gamma}_{SR})}\,\middle|\,\begin{matrix}0, 1, \kappa_1 \\ \kappa_2, 0\end{matrix}\right]\right)\Bigg].\end{aligned} \tag{4.65}$$

Applications to the Performance of Hybrid RF/RF-FSO Transmission Systems under Variable Gain Relay and MRC diversity receiver

Outage Probability: The MGF-based approach proposed in [116, Eq. (11)] is utilized to derive the OP of the MRC diverse system in closed form. By placing (4.65) in the above reference, the required result is derived. The obtained result was successfully tested via Monte-Carlo simulations for its validity and correctness.

Average BER: Resorting to MGF-based approach as described and presented in [117], the BER expression in terms of MGF is given as [117, Eq. (33)]

$$\overline{P}_b = 1/\pi \int_0^{\pi/2} \mathcal{M}_\gamma(-g/\sin^2(\phi))\,\mathrm{d}\phi, \tag{4.66}$$

where, $g = 1$ for CBPSK. Now, substituting (4.65) into (4.66), the desired BER expression for CBPSK modulation scheme applicable to the proposed system under the MRC diversity scheme is successfully derived.

Average SER: On substituting (4.65) into [78, Eq. (41)], [78, Eq. (45)], and [78, Eq. (48)], the SER of M-PSK, M-AM, and M-QAM, respectively can be obtained. The analytical SER performance expressions obtained via the above substitutions are exact and can be easily estimated accurately by utilizing the Gauss-Chebyshev Quadrature (GCQ) formula [79, Eq. (25.4.39)] that converges rapidly, requiring only few terms for an accurate result [80].

Ergodic Capacity: The ergodic capacity is given in terms of MGF as [118, Eq. (7)], [119, Eq. (8)]

$$\overline{C} = 1/\ln(2) \int_0^{\infty} \mathrm{E}_i(-s)\,\mathcal{M}_\gamma^{(1)}(s) ds, \tag{4.67}$$

where, $\mathrm{E}_i(.)$ is the exponential integral function as defined in [79, Eq. (5.1.2)]. Based on (4.67), the first derivative of the MGF in (4.65) is derived as

$$\begin{aligned}
\mathcal{M}_\gamma^{(1)}(s) = &-\frac{\overline{\gamma}_{SD}}{\left(1+s\,\overline{\gamma}_{SD}\right)^2} - \frac{\overline{\gamma}_{SR}}{\left(1+s\,\overline{\gamma}_{SD}\right)\left(1+s\,\overline{\gamma}_{SR}\right)} \\
&\times \{[1 - s\,\overline{\gamma}_{SD}/\left(1+s\,\overline{\gamma}_{SD}\right) - s\,\overline{\gamma}_{SR}/\left(1+s\,\overline{\gamma}_{SR}\right)] \\
&- A\left[\left(1 - \frac{s\,\overline{\gamma}_{SD}}{1+s\,\overline{\gamma}_{SD}} - \frac{s\,\overline{\gamma}_{SR}}{1+s\,\overline{\gamma}_{SR}} - \frac{\xi^2 s\,\overline{\gamma}_{SR}}{r\left(1+s\,\overline{\gamma}_{SR}\right)}\right)\right. \\
&\times \mathrm{G}_{r+1,3r}^{3r,1}\left[\frac{B}{\mu_{RD}^{(r)}(s+1/\overline{\gamma}_{SR})}\,\middle|\,\begin{matrix}1,\kappa_1\\ \kappa_2\end{matrix}\right] \\
&\left.+\frac{s\,\overline{\gamma}_{SR}}{1+s\,\overline{\gamma}_{SR}}\,\mathrm{G}_{1,2r}^{2r,1}\left[\frac{B}{\mu_{RD}^{(r)}(s+1/\overline{\gamma}_{SR})}\,\middle|\,\begin{matrix}1\\ \kappa_3\end{matrix}\right]\right]\Bigg\}.
\end{aligned} \tag{4.68}$$

Now, by placing (4.68) in (4.67), the desired ergodic capacity is obtained.

4.2.5 Results and Discussion

As an illustration of the mathematical formalism, simulation results for different performance metrics of a dual-branch transmission system comprising of a RF direct link and an asymmetric dual-hop RF-FSO relay branch with fixed gain relay as well as variable gain relay are presented in this section.

Fixed Gain Relay Scenario

The RF links (i.e. the S-D link and the S-R link) are modeled as Rayleigh fading channel and the FSO link (i.e. the R-D link) is modeled as unified Gamma-Gamma fading channel. The average SNR per bit per hop in all the scenarios discussed is assumed to be equal. The different binary modulation schemes utilized here for demonstration are based on the values of p and q as presented in Table 2.1. The average BER performance of DBPSK with heterodyne detection and CBPSK with IM/DD are presented in Fig. 4.8 for fixed gain relay. The effect of pointing error is set such that $\xi = 2.1$ to see the effect of varying fading parameters. It can be seen that as the atmospheric turbulence conditions get severe, BER starts increasing (i.e. the higher the values of α and β, the lower will be the BER). Also, similar results on the ergodic capacity can be observed for heterodyne detection and IM/DD techniques as was seen above in Fig. 4.8. It can be observed from Fig. 4.8 that the simulation results provide a perfect match to the analytical results obtained in this work. It is important to note here that these values for the parameters were selected arbitrarily to prove the validity of the obtained results and hence specific values based on the standards can be used to obtain the required results by design communication engineers before deployment.

Finally, Fig. 4.9 demonstrates varying effects of pointing error ($\xi = 1.2, 1.6,$ and 6.7),

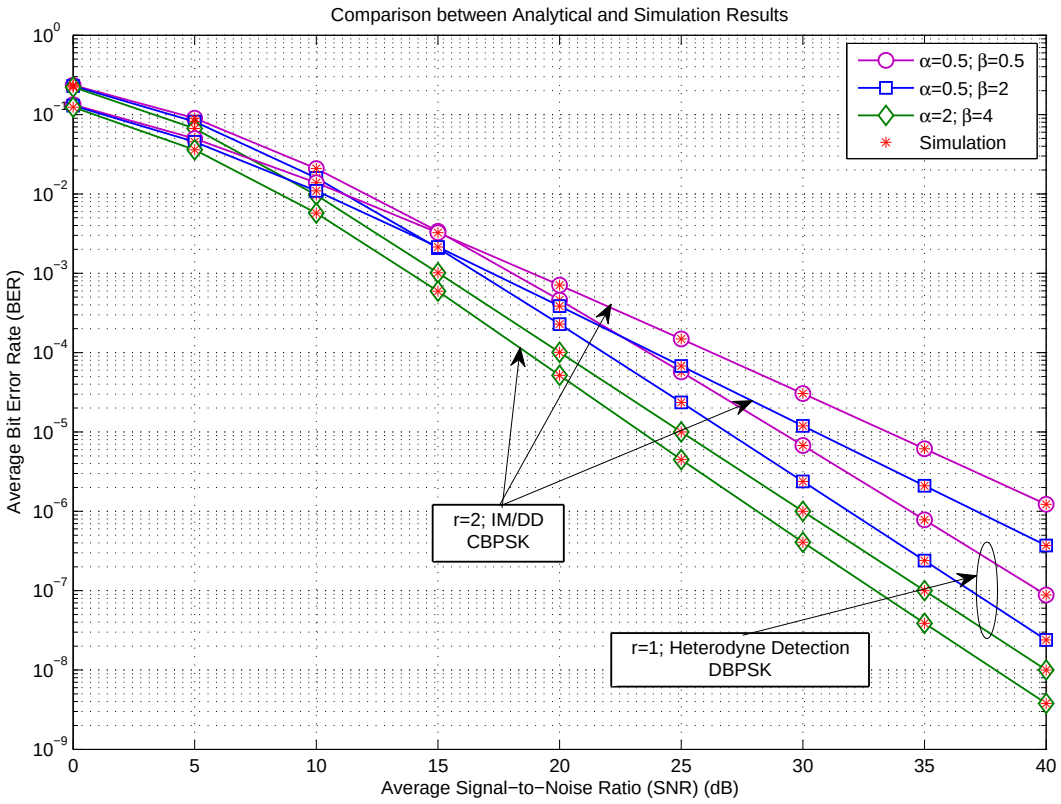

Figure 4.8: Average BER of different binary modulation schemes showing the performance of both the detection techniques (heterodyne and IM/DD) over fixed gain relay with varying fading parameters α's and β's and with effect of pointing error $\xi = 2.1$.

with fixed fading parameters $\alpha = 2.1$ and $\beta = 3.5$ for fixed gain relay and variable gain relay, respectively. For fixed gain scenario, the relay is set such as $C = 1.1$. The graphical presentations also demonstrate the comparison in performance between this proposed diverse system and the traditional simple RF (S-D) link. Also, the average SNRs of each link is different i.e. the average SNR between the relay and the destination (R-D link) is fixed at $\overline{\gamma}_{RD} = 20$ dB, and the average SNR from the source to relay (S-R link) depends on the average SNR from the source to the destination (S-D link) as $\overline{\gamma}_{SR} = \overline{\gamma}_{SD} + 6$ dB. It is observed that as the effects of pointing error get severe, BER starts increasing (i.e. the higher the values of ξ, the lower will be the

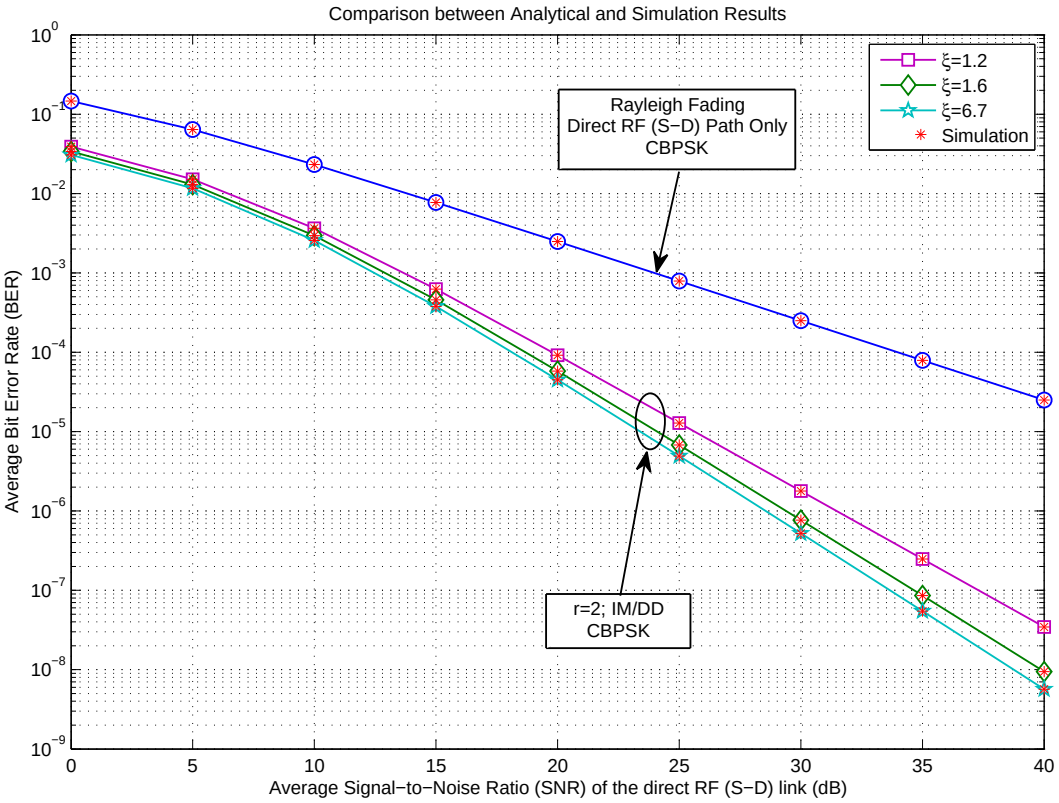

Figure 4.9: Average BER of CBPSK modulation scheme comparing the performance of a simple Rayleigh fading scenario and an IM/DD technique over fixed gain relay with varying effects of pointing error on the current system, with fading parameters $\alpha = 1.2$ and $\beta = 3.5$. $\overline{\gamma}_{RD}$ is fixed at 20 dB and $\overline{\gamma}_{SR} = \overline{\gamma}_{SD} + 6$ dB.

BER). As can be seen from Fig. 4.9 for fixed gain relay, the proposed diverse system performs way better than the traditional RF path only.

Variable Gain Relay Scenario

The RF links (i.e. the S-D link and the S-R link) are modeled as Rayleigh fading channel and the FSO link (i.e. the R-D link) is modeled as Gamma-Gamma fading channel. The electrical and average SNRs of each link are different i.e. the electrical SNR $\mu_{RD}^{(r)}$ between the relay and the destination (R-D link) is fixed at $\mu_{RD}^{(r)} = 20$ dB, and the average SNR from the source to relay (S-R link) depends on the average SNR from the source to the destination (S-D link) as $\overline{\gamma}_{SR} = \overline{\gamma}_{SD} + 6$ dB. The different binary modulation schemes utilized here for demonstration are based on the values of p and q as presented in Table 2.1. The average BER performance of DBPSK with heterodyne detection and with IM/DD are presented in Fig. 4.10 with varying effects of pointing error ($\xi = 1.1$ and 6.7) under moderate turbulence conditions (i.e. $\alpha = 2.296$ and $\beta = 1.822$) [120, Table I]. It can be observed from Fig. 4.10 that the simulation results provide a perfect match to the analytical results obtained in this work. It is observed that as the effects of pointing error get severe, BER starts increasing (i.e. the higher the values of ξ, the lower will be the BER). [1]

Similarly, in Fig. 4.11, the effect of pointing error is set such that $\xi = 2.1$ to see the effect of varying turbulence conditions. It can be seen that as the atmospheric turbulence conditions get severe, BER starts increasing (i.e. the higher the values of α and β, the lower will be the BER). Similar results on the ergodic capacity can be observed for heterodyne detection and IM/DD techniques as were seen above in Fig. 4.10 and Fig. 4.11 for the BER case.

Fig. 4.12 demonstrates the comparison in performance between the proposed sys-

[1] It is important to note here that these values for the parameters were selected from the cited references subject to the standards to prove the validity of the obtained results and hence other specific values can be used to obtain the required results by design communication engineers before deployment.

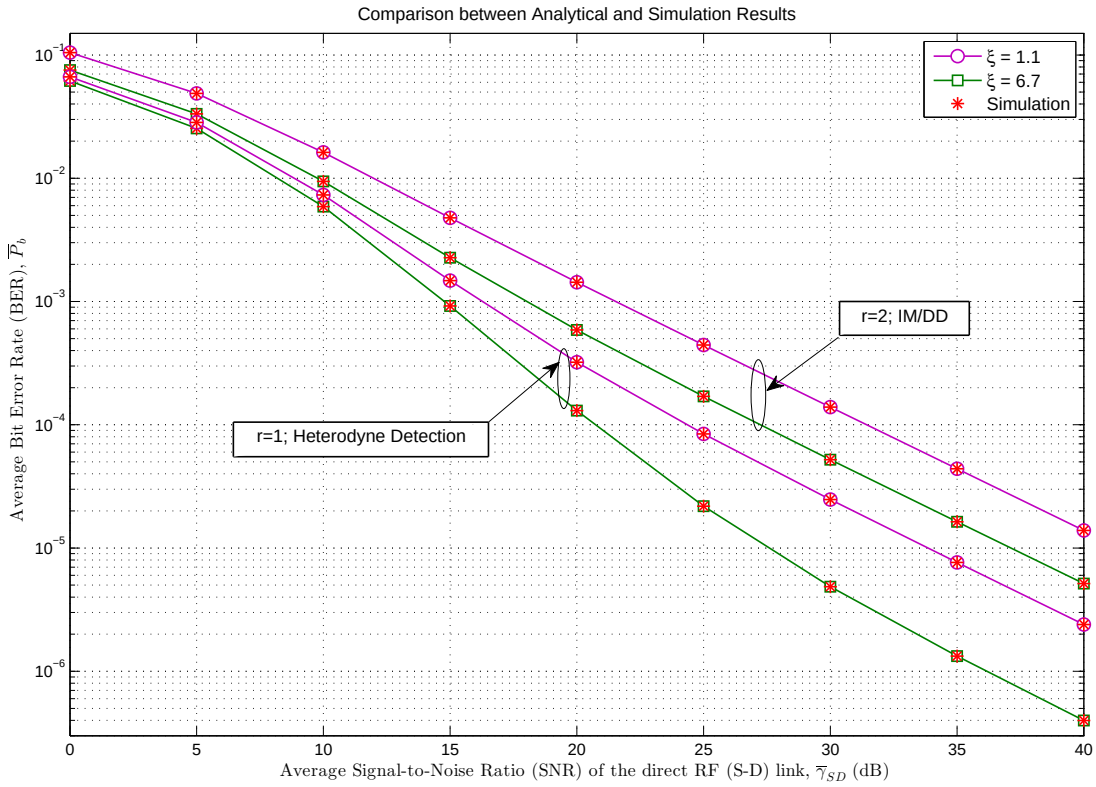

Figure 4.10: Average BER of DBPSK modulation scheme showing the performance of both the detection techniques (heterodyne and IM/DD) over variable gain relay with varying effects of pointing error under moderate turbulence conditions.

tem and the traditional simple RF link. The turbulence conditions are considered to be moderate with the pointing error effect varying ($\xi = 1.1, 1.6,$ and 6.7). As can be seen from Fig. 4.12, the diverse system performs way better than the traditional RF path only. Utilizing similar configuration as in Fig. 4.12, Fig. 4.13 presents an additional comparison of the SC diverse system with the performance of MRC diverse system thereby proving that the later outperforms the former.

Finally, Fig. 4.14 presents a performance comparison between both the diverse schemes i.e. SC as well as MRC in terms of the ergodic capacity. The turbulence conditions are considered to be moderate. The curves are plotted with varying effects of pointing errors as shown in the figure. The outcome is expectedly such that the

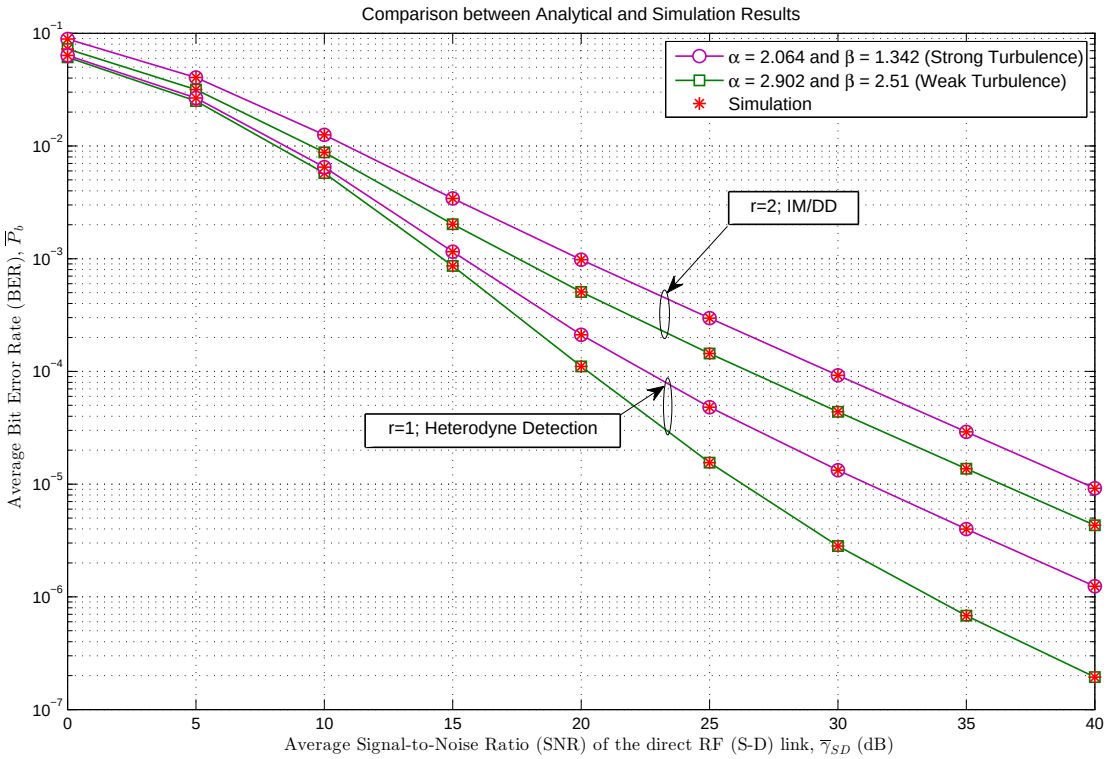

Figure 4.11: Average BER of DBPSK modulation scheme showing the performance of both the detection techniques (heterodyne and IM/DD) over variable gain relay with varying turbulence conditions with effect of pointing error fixed at $\xi = 2.1$.

MRC diversity scheme outperforms the SC diversity scheme.

4.3 Concluding Remarks

Novel exact closed-form expressions were derived for the CDF, the PDF, the MGF, and the moments of an asymmetric dual-hop RF-FSO relay transmission system composed of both RF and FSO environments with fixed gain relays as well as variable gain relays in terms of Meijer's G functions. Further, analytical expressions were derived for various performance metrics of such a transmission system including the OP, the higher-order AF, the error rate of a variety of modulation schemes, and the ergodic capacity in terms of Meijer's G functions.

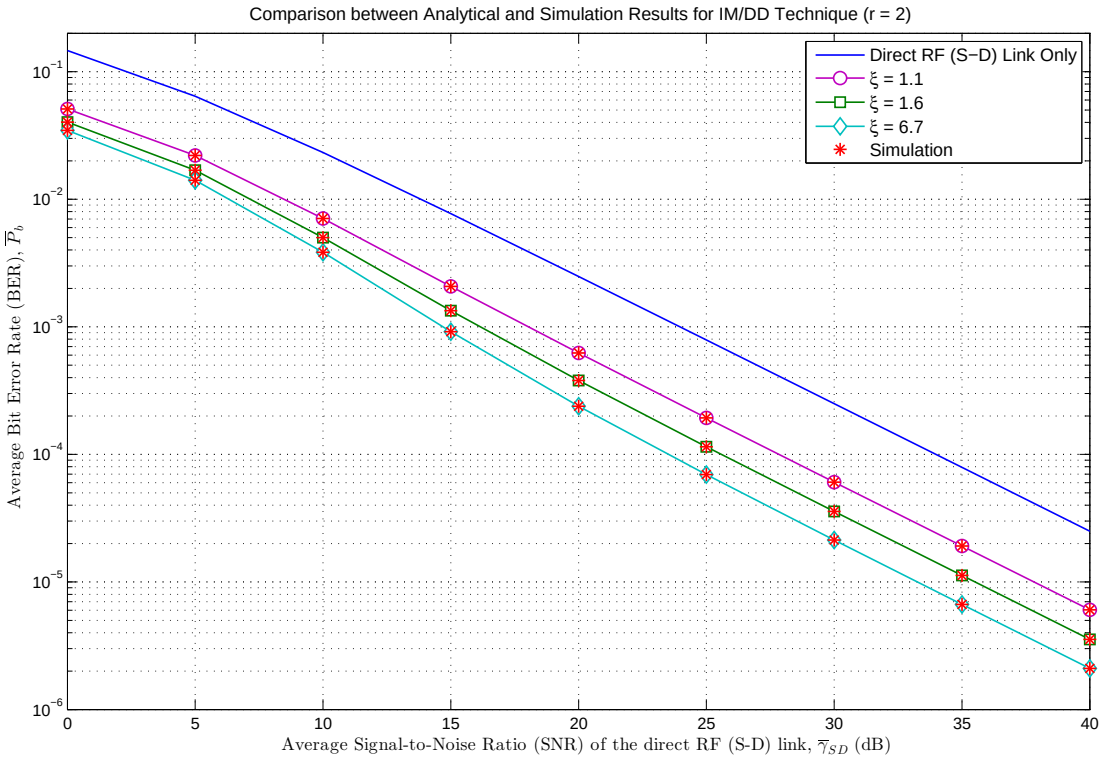

Figure 4.12: Average BER of CBPSK modulation scheme comparing the performance of a simple Rayleigh fading scenario and an IM/DD technique over variable gain relay with varying effects of pointing error on the current system under moderate turbulence conditions.

Additionally, novel exact closed-form expressions for the CDF, the PDF, the MGF, and the moments of a dual-branch transmission system comprising of a RF direct branch and an asymmetric RF-FSO dual-hop relay branch were derived. The asymmetric dual-hop RF-FSO relay branch is composed of both RF and FSO environments with fixed gain relays as well as variable gain relays in terms of Meijer's G functions. Further, analytical expressions were derived for various performance metrics of such a dual-branch transmission system under the influence of SC diversity scheme including the OP, the higher-order AF, the error rate of a variety of modulation schemes, and the ergodic capacity in terms of Meijer's G functions.

Furthermore, the MGF expression was derived for the proposed system under the

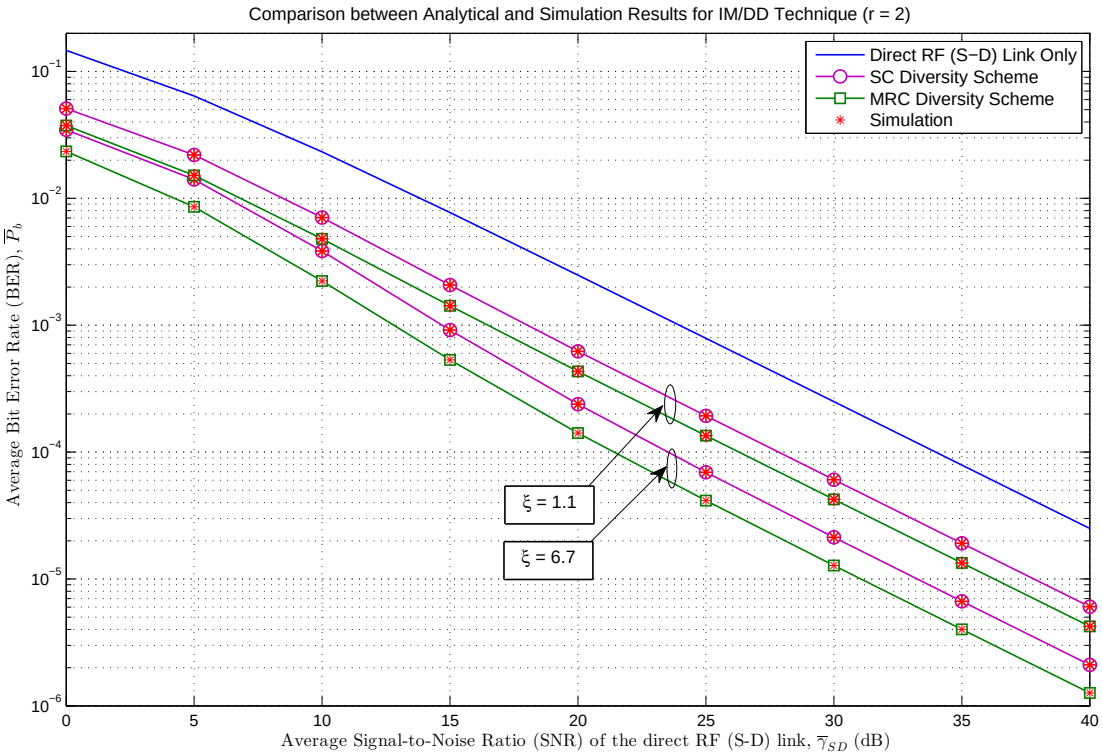

Figure 4.13: Average BER of CBPSK modulation scheme comparing the performance of a simple Rayleigh fading scenario and an IM/DD technique over variable gain relay with varying effects of pointing error on the current system under the effect of SC and MRC diversity schemes under moderate turbulence conditions.

influence of MRC diversity scheme and it was capitalized to derive various performance metrics, such as, the OP, the error rate of a variety of modulation schemes, and the ergodic capacity leading to a fine comparison between the two diversity schemes i.e. the SC and the MRC, expectedly resulting in later outperforming the former. This work also presented simulation examples to validate and illustrate the mathematical formulations developed in this work and to show the effects of the atmospheric turbulence conditions severity and pointing errors in the FSO link on the overall system performance.

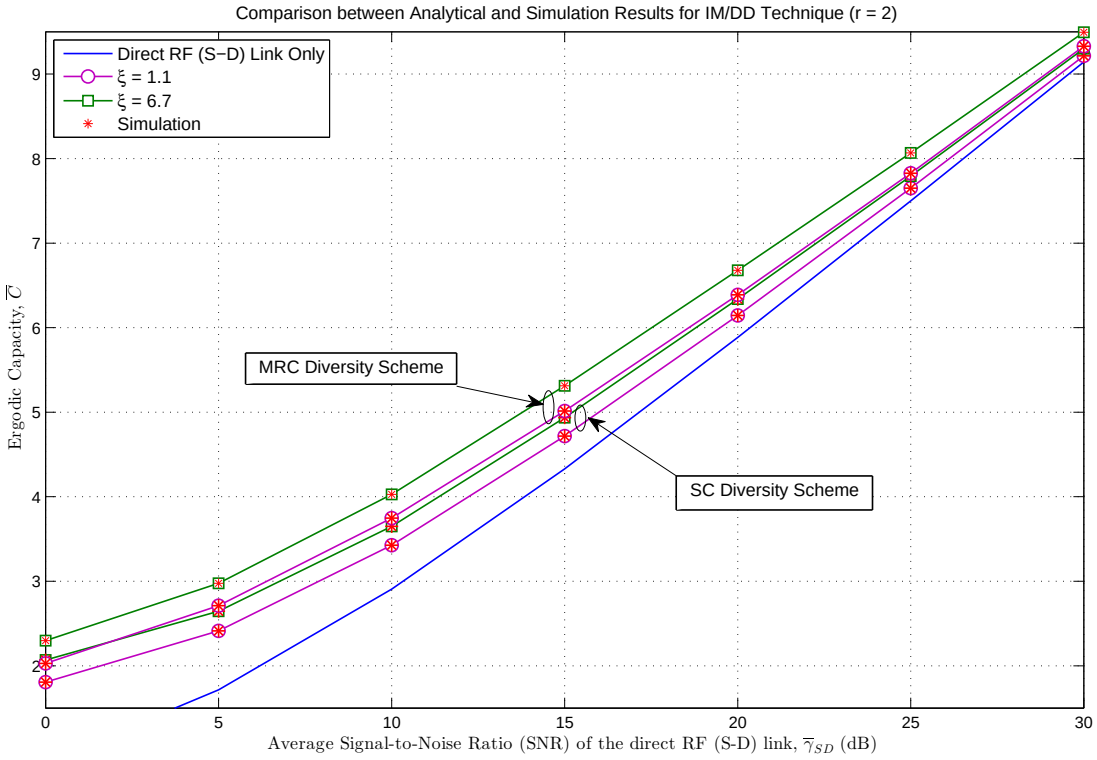

Figure 4.14: Ergodic capacity comparing the performance of a simple Rayleigh fading scenario and an IM/DD technique over variable gain relay with varying effects of pointing error on the current system under the effect of SC and MRC diversity schemes under moderate turbulence conditions.

Chapter 5

Performance Analysis of Mixed Underlay Cognitive RF and FSO Wireless Fading Channels

5.1 Introduction

5.1.1 Motivation

In cognitive radio networks (CRNs), an underlay network setting is considered where the secondary users (SUs) are allowed to share the spectrum with the primary users (PUs) under the condition that the interference observed at the PU is below a predetermined threshold. As can be seen from Fig. 5.1, where it is assumed that there exists no fiber optics structure between the buildings, a dual-hop transmission system is proposed with an asymmetric relay link wherein the first link is applying power control to maintain the interference at the primary network within a predetermined threshold (i.e. the underlay/secondary/cognitive radio user transmission) and the second link is trailed by free-space optical (FSO) technology. Recently, some work

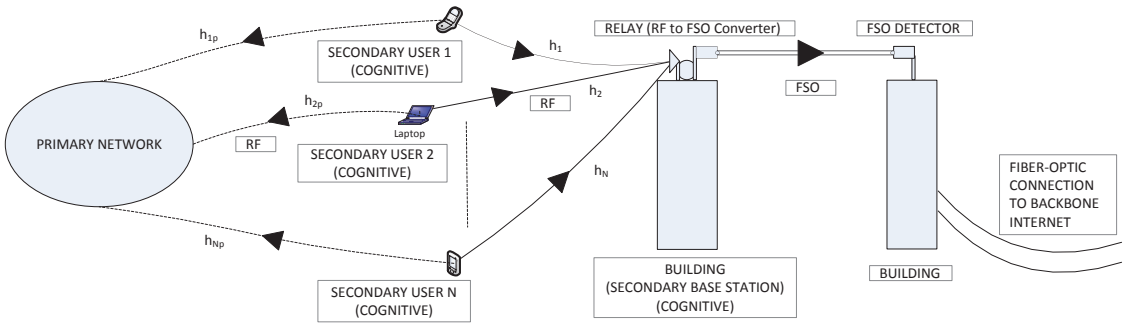

Figure 5.1: System model block diagram of an asymmetric mixed RF-FSO dual-hop transmission system wherein the desired (cognitive/secondary) users transmit to the secondary base station using the resources of the primary network.

has been published on the asymmetric relay networks (so-called mixed fading channels) that have different fading channel distributions for each link [106] but to the best of the authors knowledge, no work has been seen involving performance study of such a proposed system in Fig. 5.1.

Hence, the main objective of this work is to bring forth the essence of utilizing FSO technology in the CRN based communication systems thereby increasing the performance of the system manifolds. In this proposed work, unlike previously published literature, the secondary radio frequency (RF) user/link can not transmit at its maximum power as its transmit power must be adjusted to maintain the interference at the primary network below a pre-specified threshold. To the best of the authors knowledge, an outage analysis of such a novel proposed system, where in the secondary RF user's/link's transmission is dependent on the resources of the primary network and ultimately is relayed to the destination or to the internet back-haul via FSO technology, has not been seen in the open literature.

5.1.2 Contributions

The key contributions of this work are stated as follows.

- *Outage analysis* is carried out via deriving the cumulative distribution function (CDF) for such a proposed system model when the relay is governed by fixed gain amplify-and-forward scheme.

- The *statistical characterizations* such as the CDF, the probability density function (PDF), the moment generating function (MGF), and the moments of the end-to-end signal-to-noise ratio (SNR) of such asymmetric RF-FSO dual-hop transmission system are derived for variable gain relay scenario.

- This statistical characterization of the SNR is then applied to derive the exact closed-form expressions for the *performance metrics* such as the outage probability (OP), the higher-order amount of fading (AF), the average bit-error rate (BER) of binary modulation schemes, and the average symbol error rate (SER) of M-ary amplitude modulation (M-AM), M-ary phase shift keying (M-PSK) and M-ary quadrature amplitude modulation (M-QAM) in terms of Meijer's G functions for variable gain amplify-and-forward relay scheme.

5.1.3 Structure

The remainder of the chapter is organized as follows. Section 2 introduces the system and channel models followed by the evaluation of the statistical characteristics of the end-to-end SNR of such systems inclusive of the CDF for the fixed gain as well as the variable gain scenarios whereas the PDF, the MGF, and the moments applicable for the variable gain scenario, all in Section 3. All these expressions are derived in terms of the Meijer's G function and the Fox's H functions. Then, in Section 4, this statistical characterization of the SNR is applied to derive closed-form expressions of the OP for both the fixed gain and the variable gain scenarios whereas the higher-order AF, the average BER of binary modulation schemes, and the average SER of M-AM, M-PSK and M-QAM are derived for the variable gain scenario. All these

expressions are derived in terms of Meijer's G functions. Finally, some results are demonstrated in Section 5 along with concluding remarks in Section 6.

5.2 Channel and System Models

In this work, the underlay cognitive RF links are assumed to be operating over Rayleigh fading whereas the FSO link is considered to be operating within a Gamma-Gamma turbulence environment and is subject to the effect of pointing errors.

As shown in Fig. 5.1, a primary network is considered that consists of M PUs along side their primary BS and a secondary network that consists of N SUs along side their secondary BS, respectively. To maintain the quality of service (QoS) requirements of the primary network, the peak interference power levels caused by SU-transmitters at the primary base station (BS) must not exceed a predefined value (ψ), referred to as the interference temperature (IT), for each PU [55]. Additionally, it is assumed that the SU-transmitters employ a peak transmission power, P_n, and hence the SU transmit power can be written as follows

$$\overline{\gamma}_{SR} = \begin{cases} P_n, & \text{if } \psi \geq P_n\, h_{np} \\ \frac{\psi}{h_{np}}, & \text{if } \psi < P_n\, h_{np} \end{cases} = \min\left\{P_n, \frac{\psi}{h_{np}}\right\}, \tag{5.1}$$

where h_{np} is the channel power gain between the SU-transmitter and the PU-receiver as can be seen in Fig. 5.1.

In this work, a dual-hop transmission system model is employed with the first hop being a cognitive RF link that indicates mobile users/devices (i.e. SUs) with RF only capabilities (no FSO capability) and the second hop utilizing the FSO technology. This signifies that the BSs near these SUs have FSO capability too and so do all the subsequent BSs ultimately reaching the internet backbone. The RF link (i.e. Source(S)-Relay(R) link) is assumed to follow Rayleigh fading and hence the

respective channel power gains will be exponentially distributed. The received SNR for the RF link (i.e. the respective SU) follows (in absence of interference caused by the primary network)

$$\gamma_{SR} = \frac{h_n \, \overline{\gamma}_{SR}}{\eta}. \tag{5.2}$$

where h_n is the channel between the SU-transmitter and the SU-receiver as can be seen in Fig. 5.1, $\overline{\gamma}_{SR}$ is the average SNR of the S-R link as defined in (5.1), and η is the thermal additive white Gaussian noise (AWGN).

On the other hand, it is assumed that the FSO link (i.e. R-Destination(D) link) experiences Gamma-Gamma turbulence with pointing error impairments whose SNR PDF is given by (2.10)

$$f_{\gamma_{RD}}(\gamma_{RD}) = \frac{\xi^2}{r \, \gamma_{RD} \, \Gamma(\alpha) \, \Gamma(\beta)} \, \mathrm{G}_{1,3}^{3,0}\left[\alpha \, \beta \left(\frac{\gamma_{RD}}{\mu_{RD}} \right)^{\frac{1}{r}} \middle| \begin{matrix} \xi^2 + 1 \\ \xi^2, \alpha, \beta \end{matrix} \right], \tag{5.3}$$

where $\overline{\gamma}_{RD} = \mu_{RD}$ is the average SNR when $r = 1$ of the FSO link, $\overline{\gamma}_{RD} = \mu_{RD} \; (\alpha + 1) \; (\beta + 1) \; \xi^2 / \left[\alpha \, \beta \; (\xi^2 + 2) \right]$ is the average SNR when $r = 2$ [1] of the FSO link, α and β are the scintillation parameters [48, 50, 75] [2] related to the atmospheric turbulence conditions with lower values of α and β indicating severe atmospheric turbulence conditions, ξ is the ratio between the equivalent beam radius at the receiver and

[1] In (5.3), $\overline{\gamma}_{RD}$ is the average SNR either for IM/DD FSO systems (when $r = 2$) or for heterodyne FSO systems (when $r = 1$). In case of IM/DD FSO systems, the average SNR is given by $\overline{\gamma}_{RD} = C_s \, (\alpha + 1) \, (\beta + 1) \, / \, (\alpha\beta)$ [60, Eq. (8)], where $C_s = (R \, A \, \xi)^2 \, / \, [2 \, \Delta f \, (q \, R \, A \, I_b + 2 \, k_b \, T_k \, F_n / R_L)]$ is a multiplicative constant for a given IM/DD system, where R is the photodetector responsivity, A is the photodetector area, Δf denotes the noise equivalent bandwidth of a FSO receiver, q is the electronic charge, I_b is the background light irradiance, k_b is Boltzmann's constant, T_k is the temperature in Kelvin, F_n represents a thermal noise enhancement factor due to amplifier noise, and R_L is the load resistance. On the other hand, the average SNR for coherent/heterodyne FSO systems is given by $\overline{\gamma}_{RD} = C_c$ [60, Eq. (7)], where $C_c = 2 \, R^2 A \, P_{LO} / \left[2 \, q \, R \, \Delta f \, P_{LO} + 2 \, \Delta f \, (q \, R \, A \, I_b + 2 \, k_b \, T_k \, F_n / R_L) \right] \approx R \, A / \left(q \, \Delta f \right)$ is a multiplicative constant for a given heterodyne/coherent system, where P_{LO} is the local oscillator power.

[2] Note that the parameters α and β vary depending on the type (plane or spherical) of wave propagation being assumed. Hence, α and β are not chosen arbitrarily instead they can be determined from the Rytov variance [60]. In case of plane wave propagation, α and β may be determined via [48, Eq. (3)] whereas in case of spherical wave propagation, α and β may be determined utilizing [50, Eqs. (4) and (5)].

the pointing error displacement standard deviation (jitter) at the receiver [49] (i.e. when $\xi \to \infty$, (5.3) converges to the non-pointing errors case), r is the parameter defining the type of detection technique (i.e. $r = 1$ represents heterodyne detection and $r = 2$ represents intensity modulation/direct detection (IM/DD)), $\Gamma(.)$ is the Gamma function as defined in [58, Eq. (8.310)], and G(.) is the Meijer's G function as defined in [58, Eq. (9.301)].

Here, fixed gain as well as variable gain amplify-and-forward relay schemes are considered. For the amplify-and-forward relay system, a subcarrier intensity modulation (SIM) scheme [37] is adopted to convert the input RF signals at the relay to the optical signals for retransmissions from the relay.

For fixed gain scenario, the end-to-end SNR of the system can be given as

$$\gamma = \frac{\gamma_{SR}\,\gamma_{RD}}{\gamma_{RD} + C}, \tag{5.4}$$

where C is the fixed relay gain [21].

For variable gain scenario, the end-to-end SNR of the system can be given as

$$\gamma_{SRD} = \frac{\gamma_{SR}\,\gamma_{RD}}{\gamma_{SR} + \gamma_{RD} + 1}, \tag{5.5}$$

where [3, 21, 53]. Since the closed-from analysis of the statistical characteristics of γ_{SRD} is complicated, the standard approximation

$$\gamma_{SRD} = \frac{\gamma_{SR}\,\gamma_{RD}}{\gamma_{SR} + \gamma_{RD} + 1} \cong \min(\gamma_{SR}, \gamma_{RD}) = \gamma, \tag{5.6}$$

is utilized.

5.3 Closed-Form Statistical Characterization

5.3.1 Fixed Gain Relay Scenario

Cumulative Distribution Function

When the instantaneous output SNR γ falls below a given threshold, a situation labeled as outage is encountered and it is an important feature to study the OP of a system that is usually quantified by the CDF. Hence, the CDF is given by [21]

$$F_{\gamma}(\gamma) = \Pr\left[\frac{\gamma_{SR}\,\gamma_{RD}}{\gamma_{RD}+C} < \gamma\right], \tag{5.7}$$

which can be written as

$$F_{\gamma}(\gamma) = \int_{0}^{\infty} \Pr\left[\frac{\gamma_{SR}\,\gamma_{RD}}{\gamma_{RD}+C} < \gamma\right] f_{\gamma_{RD}}(\gamma_{RD})\, d\gamma_{RD}, \tag{5.8}$$

where $\Pr\left[\frac{\gamma_{SR}\,\gamma_{RD}}{\gamma_{RD}+C} < \gamma\right] = F_{\gamma_{SR}}\left(\frac{\gamma\,(\gamma_{RD}+C)}{\gamma_{RD}}\right)$. The CDF of the first hop $F_{\gamma_{SR}}(\gamma_{SR})$, under the assumption that $\eta = 1$, is given as [55, Eq. (5)]

$$F_{\gamma_{SR}}(\gamma_{SR}) = 1 - e^{-\gamma_{SR}/P_n} + \gamma_{SR}/\left(\psi+\gamma_{SR}\right) e^{-(\gamma_{SR}+\psi)/P_n}. \tag{5.9}$$

Now, on placing (5.9) into (5.8), the following is obtained

$$\begin{aligned} F_{\gamma}(\gamma) = {} & \underbrace{\int_{0}^{\infty} f_{\gamma_{RD}}(\gamma_{RD})\, d\gamma_{RD}}_{\mathcal{I}_1} - \underbrace{e^{-\frac{\gamma}{P_n}} \int_{0}^{\infty} e^{-\frac{\gamma\,C}{P_n}\gamma_{RD}^{-1}} f_{\gamma_{RD}}(\gamma_{RD})\, d\gamma_{RD}}_{\mathcal{I}_2} \\ & + \underbrace{e^{-\frac{\psi+\gamma}{P_n}} \int_{0}^{\infty} \frac{\gamma\,\gamma_{RD}}{\gamma_{RD}\left(\psi+\gamma\right)+\gamma\,C} e^{-\frac{\gamma\,C}{P_n}\gamma_{RD}^{-1}} f_{\gamma_{RD}}(\gamma_{RD})\, d\gamma_{RD}}_{\mathcal{I}_3} \\ & + \underbrace{e^{-\frac{\psi+\gamma}{P_n}} \int_{0}^{\infty} \frac{\gamma\,C}{\gamma_{RD}\left(\psi+\gamma\right)+\gamma\,C} e^{-\frac{\gamma\,C}{P_n}\gamma_{RD}^{-1}} f_{\gamma_{RD}}(\gamma_{RD})\, d\gamma_{RD}}_{\mathcal{I}_4}. \end{aligned} \tag{5.10}$$

The integral in $\mathcal{I}_1$ simply reduces to 1 as it is the CDF evaluated at ∞.

For the integral in $\mathcal{I}_2$, $e^{-\frac{\gamma C}{P_n}\gamma_{RD}^{-1}}$ is altered to an appropriate Meijer's G function representation via the usage of [62, Eq. (07.34.03.0228.01)] and [66, Eq. (6.2.2)] yielding

$$e^{-\frac{\gamma C}{P_n}\gamma_{RD}^{-1}} = \mathrm{G}_{1,0}^{0,1}\left[\frac{P_n}{\gamma C}\gamma_{RD}\middle|\begin{matrix}1\\-\end{matrix}\right]. \tag{5.11}$$

With this alteration, the integral in $\mathcal{I}_2$ now has the product of two Meijer's G functions along with the random variable being integrated over itself that can be easily solved utilizing [83, Eq. (21)] to get

$$\mathcal{I}_2 = A_1\, e^{-\frac{\gamma}{P_n}}\, \mathrm{G}_{r,3r+1}^{3r+1,0}\left[B_1\,\gamma\middle|\begin{matrix}\kappa_1\\ \kappa_2, 0\end{matrix}\right], \tag{5.12}$$

where $A_1 = \frac{r^{\alpha+\beta-2}\xi^2}{(2\pi)^{r-1}\Gamma(\alpha)\,\Gamma(\beta)}$, $B_1 = \frac{(\alpha\,\beta)^r\,C}{r^{2r}\,P_n\,\overline{\gamma}_{RD}}$, $\kappa_1 = \frac{\xi^2+1}{r}, \ldots, \frac{\xi^2+r}{r}$ comprises of r terms, and $\kappa_2 = \frac{\xi^2}{r}, \ldots, \frac{\xi^2+r-1}{r}, \frac{\alpha}{r}, \ldots, \frac{\alpha+r-1}{r}, \frac{\beta}{r}, \ldots, \frac{\beta+r-1}{r}$ comprises of $3r$ terms.

Now, for the integrals in $\mathcal{I}_3$ and $\mathcal{I}_4$, the exponential term is represented alternatively, similar to as was done earlier for the integral in $\mathcal{I}_2$, to an appropriate Meijer's G function representation followed by representing the fractional part, $\gamma\,C/\left[(\psi+\gamma)\,\gamma_{RD}+\gamma\,C\right]$, in terms of Meijer's G function as

$$\gamma\,C/\left[(\psi+\gamma)\,\gamma_{RD}+\gamma\,C\right] = \mathrm{G}_{1,1}^{1,1}\left[\frac{\psi+\gamma}{\gamma\,C}\gamma_{RD}\middle|\begin{matrix}0\\0\end{matrix}\right], \tag{5.13}$$

via the exploitation of the identity $(1+az)^{-b} = \frac{1}{\Gamma(b)}\,\mathrm{G}_{1,1}^{1,1}\left[az\,\middle|\,\begin{matrix}1-b\\0\end{matrix}\right]$ [114, pg. 152]. Subsequently, all the Meijer's G functions in the integral present in $\mathcal{I}_3$ and $\mathcal{I}_4$ are altered to Fox's H functions via the utilization of [66, Eqs. (6.2.8) and (6.2.3)] to give an integral with three Fox's H functions. This is solved using [121, Eq. (2.3)] to, respectively, get $\mathcal{I}_3$ and $\mathcal{I}_4$ in terms of extended generalized bivariate Fox's H function

(EGBFHF) (see [121] and references therein) as

$$\mathcal{I}_3 = A_2\, e^{-\frac{\psi+\gamma}{P_n}}\, \mathrm{H}^{3,0:1,1:0,1}_{3,1:1,1:1,0}\left[\begin{array}{c|c|c|c} \kappa_3 & (0,1) & (1,1) & \frac{B_2}{\gamma}, \frac{B_3}{\gamma} \\ \kappa_4 & (0,1) & - & \end{array}\right], \tag{5.14}$$

where $A_2 = \frac{\xi^2\, \overline{\gamma}_{RD}}{(\alpha\, \beta)^r\, C\, \Gamma(\alpha)\, \Gamma(\beta)}$, $\kappa_3 = (1-\xi^2-r, r; r), (1-\alpha-r, r; r), (1-\beta-r, r; r)$, $\kappa_4 = (-\xi^2-r, r; r)$, $B_2 = \frac{(\psi+\gamma)\, \overline{\gamma}_{RD}}{(\alpha\, \beta)^r\, C}$, and $B_3 = \frac{P_n\, \overline{\gamma}_{RD}}{(\alpha\, \beta)^r\, C}$ and

$$\mathcal{I}_4 = A_3\, e^{-\frac{\psi+\gamma}{P_n}}\, \mathrm{H}^{3,0:1,1:0,1}_{3,1:1,1:1,0}\left[\begin{array}{c|c|c|c} \kappa_5 & (0,1) & (1,1) & \frac{B_2}{\gamma}, \frac{B_3}{\gamma} \\ \kappa_6 & (0,1) & - & \end{array}\right], \tag{5.15}$$

where $A_3 = \frac{\xi^2}{\Gamma(\alpha)\, \Gamma(\beta)}$, $\kappa_5 = (1-\xi^2, r; r), (1-\alpha, r; r), (1-\beta, r; r)$, and $\kappa_6 = (-\xi^2, r; r)$. The expressions in (5.14) and (5.15) can be easily and efficiently evaluated by utilizing the MATLAB® implementation given in [122] and/or by extrapolating and utilizing the MATHEMATICA® implementation of the extended generalized bivariate Meijer's G function (EGBMGF) (see [69] and references therein) given in [69, Table II].

Now, on combining $\mathcal{I}_1 = 1$, $\mathcal{I}_2$ from (5.12), $\mathcal{I}_3$ from (5.14), and $\mathcal{I}_4$ from (5.15), the desired exact closed-form expression for the CDF of the proposed system, $F_\gamma(\gamma)$ is attained in (5.10), in terms of extended generalized bivariate Fox's G functions (EGBFHFs). As a special case, for heterodyne detection case (i.e. when $r = 1$), after altering the representations of the exponential and the fractional terms to Meijer's G functions in $\mathcal{I}_3$ and $\mathcal{I}_4$, the respective integral with three Meijer's G functions can be solved directly via utilizing [123, Eq. (12)] to get the required exact closed-form expression for the CDF, $F_\gamma(\gamma)$, of the proposed system in a rather simpler form in terms of EGBMGFs.

In the absence of IT (i.e. non-cognitive scenario on the RF link wherein the user is always transmitting with constant (peak) power, P_n), the CDF in (5.10) simplifies

to (4.12). This can be easily deduced as follows. When $\psi \to \infty$, $e^{-\psi/P_n} \to 0$ and hence the expression for the CDF, $F_\gamma(\gamma)$ in (5.10) simply reduces to the non-CRN case as $\mathcal{I}_3 \to 0$ and $\mathcal{I}_4 \to 0$. Additionally, for the IM/DD scheme (i.e. when $r = 2$) under non-CRN case, $F_\gamma(\gamma)$ in (5.10) reduces to [124, Eq. (2)] and further in the absence of pointing errors (i.e. when $\xi \to \infty$), $F_\gamma(\gamma)$ in (5.10) subsequently reduces to [124, Eq. (3)] and reference therein.

5.3.2 Variable Gain Relay Scenario

Cumulative Distribution Function

It is well known that the CDF of the SNR, $\gamma = \min(\gamma_{SR}, \gamma_{RD})$, can be expressed as $F_\gamma(\gamma) = \Pr(\min(\gamma_{SR}, \gamma_{RD}) < \gamma)$. This expression can be re-written as [115, Eq. (4)]

$$F_\gamma(\gamma) = F_{\gamma_{SR}}(\gamma) + F_{\gamma_{RD}}(\gamma) - F_{\gamma_{SR}}(\gamma)\, F_{\gamma_{RD}}(\gamma). \tag{5.16}$$

The CDF of the first hop, $F_{\gamma_{SR}}(\gamma_{SR})$, with no interference from primary network, is given in (5.9) and the CDF of the second hop, $F_{\gamma_{RD}}(\gamma_{RD})$, can be easily derived by integrating the PDF in (5.3) as (2.12)

$$F_{\gamma_{RD}}(\gamma_{RD}) = \int_0^{\gamma_{RD}} f_{\gamma_{RD}}(t)\, dt = A\, \mathrm{G}_{r+1,3r+1}^{3r,1}\left[\frac{B}{\overline{\gamma}_{RD}}\, \gamma_{RD} \,\middle|\, \begin{matrix} 1, \kappa_1 \\ \kappa_2, 0 \end{matrix}\right], \tag{5.17}$$

where $A = \frac{r^{\alpha+\beta-2}\xi^2}{(2\,\pi)^{r-1}\Gamma(\alpha)\,\Gamma(\beta)}$, $B = \frac{(\alpha\,\beta)^r}{r^{2r}}$, $\kappa_1 = \frac{\xi^2+1}{r}, \ldots, \frac{\xi^2+r}{r}$ comprises of r terms, and $\kappa_2 = \frac{\xi^2}{r}, \ldots, \frac{\xi^2+r-1}{r}, \frac{\alpha}{r}, \ldots, \frac{\alpha+r-1}{r}, \frac{\beta}{r}, \ldots, \frac{\beta+r-1}{r}$ comprises of $3r$ terms. Now, with the help of some simple algebraic manipulations, the CDF of γ can be shown to be given after some simplifications by

$$\begin{aligned} F_\gamma(\gamma) = 1 - e^{-\gamma/P_n} \Big[1 - \gamma/\left(\psi + \gamma\right) e^{-\psi/P_n} \\ -A\left(1 - \frac{\gamma}{\psi+\gamma}\, e^{-\frac{\psi}{P_n}}\right) \mathrm{G}_{r+1,3r+1}^{3r,1}\left[\frac{B}{\overline{\gamma}_{RD}}\, \gamma \,\middle|\, \begin{matrix} 1, \kappa_1 \\ \kappa_2, 0 \end{matrix}\right]\Big]. \end{aligned} \tag{5.18}$$

In the absence of IT (i.e. non-cognitive scenario on the RF link wherein the user is always transmitting with constant (peak) power, P_n), the CDF in (5.18) simplifies to (4.31). This can be easily deduced as follows. When $\psi \to \infty$, the expression in (5.18) simply reduces to the non-CRN case.

Probability Density Function

Differentiating (5.18) with respect to γ, using the product rule then utilizing [62, Eq. (07.34.20.0001.01)], after some algebraic manipulations the PDF of the end-to-end SNR is obtained in exact closed-form in terms of Meijer's G functions as

$$\begin{aligned} f_\gamma(\gamma) = e^{-\frac{\gamma}{P_n}} \Bigg\{ & \frac{1}{P_n} - e^{-\frac{\psi}{P_n}} \left[\frac{\gamma}{(\psi+\gamma)^2} - \frac{1}{\psi+\gamma} + \frac{\gamma}{P_n(\psi+\gamma)} \right] \\ & + \frac{A}{\gamma} \left[1 - \frac{\gamma}{\psi+\gamma} e^{-\frac{\psi}{P_n}} \right] \mathrm{G}_{r,3r}^{3r,0} \left[\frac{B}{\overline{\gamma}_{RD}} \gamma \middle| \begin{matrix} \kappa_1 \\ \kappa_2 \end{matrix} \right] \\ & + A \Big[e^{-\psi/P_n} / (\psi+\gamma) \left(\gamma / (\psi+\gamma) - 1 \right) \\ & - \frac{1}{P_n} \left(1 - \frac{\gamma}{\psi+\gamma} e^{-\frac{\psi}{P_n}} \right) \Bigg] \mathrm{G}_{r+1,3r+1}^{3r,1} \left[\frac{B}{\overline{\gamma}_{RD}} \gamma \middle| \begin{matrix} 1, \kappa_1 \\ \kappa_2, 0 \end{matrix} \right] \Bigg\}. \end{aligned} \tag{5.19}$$

Similar to the CDF case, in the absence of IT from the RF link, the PDF in (5.19) simplifies to (4.32) for the non-CRN scenario.

Moment Generating Function

The MGF defined as $\mathcal{M}_\gamma(s) \triangleq \mathbb{E}\left[e^{-\gamma s}\right]$ where $\mathbb{E}\left[.\right]$ denotes the expectation operator, can be expressed, using integration by parts, in terms of the CDF as $\mathcal{M}_\gamma(s) = s \int_0^\infty e^{-\gamma s} F_\gamma(\gamma) d\gamma$. On placing (5.18) into this relation and expanding the brackets in order, five integrals are required to be solved to obtain the required result. Of these, the first three integrals are trivial. The fourth integral can be easily solved by utilizing [58, Eq. (7.813.1)]. Finally, for the fifth integral, the identity [114, p. 152] $(1+az)^{-b} = \frac{1}{\Gamma(b)} \mathrm{G}_{1,1}^{1,1}\left[az \middle| \begin{matrix} 1-b \\ 0 \end{matrix} \right]$ is first exploited to represent the fractional component in terms of Meijer's G function and then utilize the integral identity [69, Eq. (20)].

On combining all these terms, after some algebraic manipulations, the MGF of γ is obtained in terms of the EGBMGF (see [69] and references therein) as

$$\begin{aligned}\mathcal{M}_{\gamma}(s) &= 1 - s/\left(s + 1/P_n\right) + s\, e^{-\psi/P_n}\, \left[1/\left(s + 1/P_n\right)\right. \\ &\quad \left. - \psi\, e^{\psi(s+1/P_n)}\, \Gamma\left[0, \psi\left(s + 1/P_n\right)\right]\right] + A\, s/\left(s + 1/P_n\right) \\ &\quad \times \mathrm{G}_{r+2,3r+1}^{3r,2}\left[\frac{B}{\overline{\gamma}_{RD}(s + 1/P_n)}\,\middle|\, \begin{matrix} 0, 1, \kappa_1 \\ \kappa_2, 0 \end{matrix}\right] - \frac{A\, s\, \psi^{-1}}{\left(s + 1/P_n\right)^2} \\ &\quad \times e^{-\frac{\psi}{P_n}}\, \mathrm{G}_{1,0:1,1:\, r+1,3r+1}^{1,0:1,1:\, 3r,1}\left[\begin{array}{c|c|c|c} 2 & \begin{matrix} 0 \\ 0 \end{matrix} & \begin{matrix} 1, \kappa_1 \\ \kappa_2, 0 \end{matrix} & D_1, D_2 \end{array}\right],\end{aligned} \tag{5.20}$$

where $\Gamma\left[.,.\right]$ refers to incomplete Gamma function [58, Eq. (8.350.2)], $D_1 = 1/\left[\psi\left(s + 1/P_n\right)\right]$, and $D_2 = B/\left[\overline{\gamma}_{RD}\left(s + 1/P_n\right)\right]$. The expression in (5.20) can be easily and efficiently evaluated by utilizing the MATHEMATICA® implementation of the EGBMGF given in [69, Table II]. Additionally, similar to the CDF case, in absence of the IT from the RF link, the MGF in (5.20) simplifies to (4.33) for the non-CRN scenario.

Moments

The moments defined as $\mathbb{E}\left[\gamma^k\right]$ can be expressed in terms of the complementary CDF (CCDF) $F_{\gamma}^{c}(\gamma) = 1 - F_{\gamma}(\gamma)$, via integration by parts, as $\mathbb{E}\left[\gamma^k\right] = k\int_0^{\infty} \gamma^{k-1} F_{\gamma}^{c}(\gamma) d\gamma$. Now, placing (5.18) into this relation and utilizing [58, Eq. (7.813.1)], the moments are obtained as

$$\begin{aligned}\mathbb{E}\left[\gamma^k\right] &= k\, P_n^k\, \Gamma(k) - k\, \psi^k\, \Gamma\left(k+1\right)\, \Gamma\left[-k, \psi/P_n\right] - k\, A\, P_n^k \\ &\quad \times \mathrm{G}_{r+2,3r+1}^{3r,2}\left[\frac{B\, P_n}{\overline{\gamma}_{RD}}\,\middle|\, \begin{matrix} 1-k, 1, \kappa_1 \\ \kappa_2, 0 \end{matrix}\right] + \frac{k\, A\, P_n^{k+1}}{\psi}\, e^{-\frac{\psi}{P_n}} \\ &\quad \times \mathrm{G}_{1,0:1,1:\, r+1,3r+1}^{1,0:1,1:\, 3r,1}\left[\begin{array}{c|c|c|c} k+1 & \begin{matrix} 0 \\ 0 \end{matrix} & \begin{matrix} 1, \kappa_1 \\ \kappa_2, 0 \end{matrix} & \dfrac{P_n}{\psi}, \dfrac{B\, P_n}{\overline{\gamma}_{RD}} \end{array}\right].\end{aligned} \tag{5.21}$$

Similar to the CDF case, in absence of the IT from the RF link, the moments in (5.21) simplifies to (4.34) for non-CRN scenario since, as $\psi \to \infty$, $\Gamma[-k, \infty/P_n] \to 0$.

5.4 Applications

5.4.1 Fixed Gain Relay Scenario

Outage Probability

When the instantaneous output SNR γ falls below a given threshold γ_{th}, a situation labeled as outage is encountered and it is an important feature to study OP of a system. Hence, another important fact worth stating here is that the expression derived in (5.10) also serves the purpose for the expression of OP for this system or in other words, the probability that the SNR falls below a predetermined protection ratio γ_{th} can be simply expressed by replacing γ with γ_{th} in (5.10) as $P_{\text{out}}(\gamma_{\text{th}}) = F_{\gamma}(\gamma_{\text{th}})$.

5.4.2 Variable Gain Relay Scenario

Outage Probability

Similar to the fixed gain relay scenario, the expression of OP can be obtained by replacing γ with γ_{th} in (5.18) as $P_{\text{out}}(\gamma_{\text{th}}) = F_{\gamma}(\gamma_{\text{th}})$. [3]

Higher-Order AF

The AF is an important measure for the performance of a wireless communication system as it can be utilized to parameterize the distribution of the SNR of the received signal. In particular, the k^{th}-order AF for the instantaneous SNR γ is defined in [68, Eq. (3)]. Now, utilizing this equation by substituting (5.21) into it, the k^{th}-order

[3] In order to justify the behavior of the system, Meijer's G function can be expressed in terms of simpler elementary functions, under high SNR regime, via utilizing the asymptotic expansion of the Meijer's G function given in (A.1), Appendix.

AF can be obtained. Similarly, for $k = 2$ as a special case, the classical AF can be obtained.

Average BER

Substituting (5.18) into [69, Eq. (12)] and utilizing exactly the same procedure as employed in case of MGF, the average BER, $\overline{P}_b$, is obtained for a variety of binary modulations as

$$\begin{aligned}\overline{P}_b &= 1/2 - q^p/\left[2\left(q+1/P_n\right)^p\right] + p\,q^p\,\psi^p\,e^{q\,\psi}\,\Gamma\left[-p,\psi\left(q+1/P_n\right)\right]/2 \\ &\quad + A\,q^p/\left[2\,\Gamma(p)\left(q+1/P_n\right)^p\right]\,\mathrm{G}^{3r,2}_{r+2,3r+1}\left[\frac{B}{\overline{\gamma}_{RD}(q+1/P_n)}\,\middle|\,\begin{matrix}1-p,1,\kappa_1\\ \kappa_2,0\end{matrix}\right] \\ &\quad - \frac{A\,q^p}{2\,\Gamma(p)\,\psi\left(q+1/P_n\right)^{p+1}}\,e^{-\frac{\psi}{P_n}}\,\mathrm{G}^{1,0:1,1:3r,1}_{1,0:1,1:r+1,3r+1}\left[\begin{matrix}p+1\\ \\ 0\end{matrix}\,\middle|\,\begin{matrix}0\\ \\ 0\end{matrix}\,\middle|\,\begin{matrix}1,\kappa_1\\ \\ \kappa_2,0\end{matrix}\,\middle|\,D_3,D_4\right],\end{aligned} \tag{5.22}$$

where $D_3 = 1/\left[\psi\left(q+1/P_n\right)\right]$, $D_4 = B/\left[\overline{\gamma}_{RD}\left(q+1/P_n\right)\right]$, and the parameters p and q account for different modulation schemes. Similar to the moments case, in absence of the IT from the RF link, the average BER in (5.22) simplifies to (4.37) for the non-CRN scenario.

Average SER

In [78], the conditional SER has been presented in a desirable form and utilized to obtain the average SER of M-AM, M-PSK, and M-QAM. For example, for M-PSK the average SER $\overline{P}_s$ over generalized fading channels is given by [78, Eq. (41)]. Similarly, for M-AM and M-QAM, the average SER $\overline{P}_s$ over generalized fading channels is given by [78, Eq. (45)] and [78, Eq. (48)] respectively. On substituting (5.20) into [78, Eq. (41)], [78, Eq. (45)], and [78, Eq. (48)], the SER can be obtained for M-PSK, M-AM, and M-QAM, respectively. The analytical SER performance expressions obtained via the above substitutions are exact and can be easily estimated accurately by utilizing

the Gauss-Chebyshev Quadrature (GCQ) formula [79, Eq. (25.4.39)] that converges rapidly, requiring only few terms for an accurate result [80].

5.5 Results and Discussion

5.5.1 Fixed Gain Relay Scenario

The underlay cognitive SU transmission link (i.e. the RF link/S-R link) is modeled as Rayleigh fading channel and the FSO link (i.e. the R-D link) is modeled as Gamma-Gamma turbulence channel. The OP performance with IM/DD is presented in Fig. 5.2 for a range on the transmit power restriction on the SU, $P_n = -10 \rightarrow 30$ dB. The effect of the pointing error is varying ($\xi = 1.2, 6.7$) and so is the effect of in-

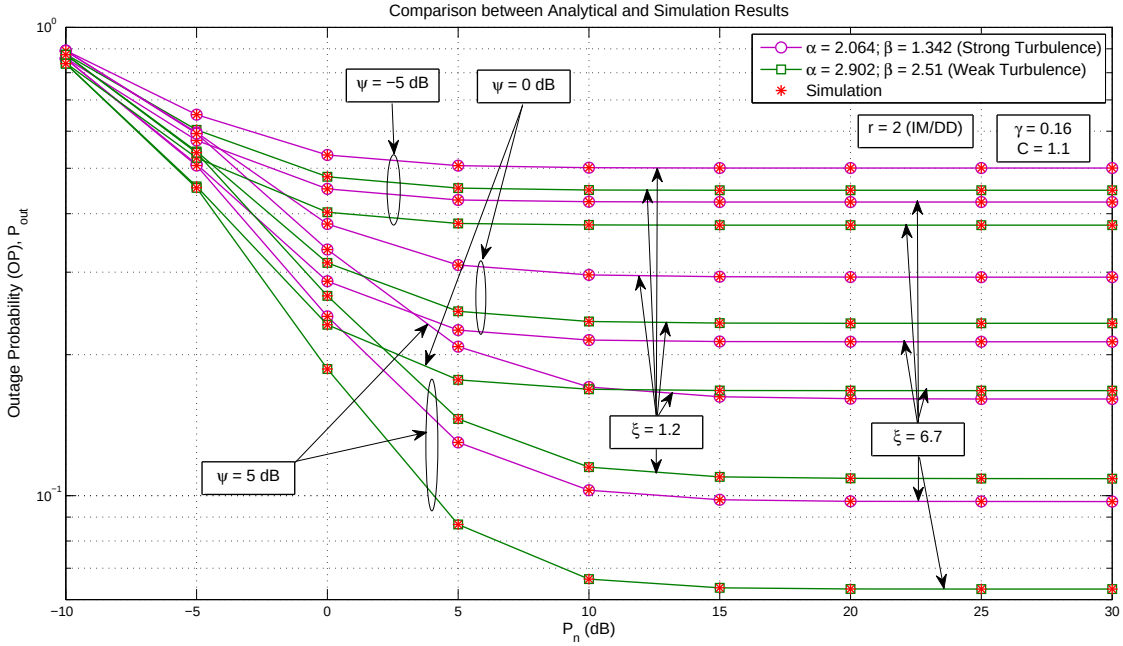

Figure 5.2: OP showing the performance of IM/DD technique over fixed gain relay with varying pointing errors (ξ's), IT's (ψ's), and scintillation parameters (α's and β's).

terference i.e. the IT ($\psi = -5, 0, 5$ dB). Hence, Fig. 5.2 demonstrates simultaneously

the effects of interference as well as pointing errors for weak ($\alpha = 2.902$; $\beta = 2.51$) and strong ($\alpha = 2.064$; $\beta = 1.342$) turbulence FSO channels [120, Table I]. The average SNR of the FSO link is arbitrarily set to $\overline{\gamma}_{RD} = 17$ dB, $C = 1.1$, and the threshold is set as $\gamma = 0.16$ all throughout. It can be seen that as the atmospheric turbulence conditions get severe, the OP starts increasing (i.e. the higher the values of α and β, the lower will be the OP). Also, similar results can be observed for the case of pointing errors i.e. as the pointing errors increase (i.e. the value of ξ decreases), the OP starts increasing and vice versa. Additionally it can be observed that as the IT increases, the OP performance starts getting better and the OP saturates while P_n keeps increasing as the performance is dominated by the IT condition. It can be observed from Fig. 5.2 that the Monte Carlo simulation results provide a perfect match to the analytical results obtained in this work. [4]

Fig. 5.3 demonstrates similar results as in Fig. 5.2 instead on the scale of a range of IT, $\psi = -10 \rightarrow 30$ dB with varying effects of maximum transmit power restriction ($P_n = 0, 5, \text{and } 10$ dB) and with the rest of the parameters being treated similar to Fig. 5.2. Similar results are observed and additionally it can be observed that as the transmit power restriction on the SU increases, the OP performance starts getting better.

5.5.2 Variable Gain Relay Scenario

The SU transmission link (i.e. the RF link/S-R link) are modeled as Rayleigh fading channel suffering interference and the FSO link (i.e. the R-D link) is modeled as Gamma-Gamma fading channel. The average BER performance of CBPSK ($p = 0.5$ and $q = 1$) with IM/DD is presented in Fig. 5.4 for a range on the transmit power

[4] It is important to note here that these values for the parameters were selected from the cited references subject to the standards to prove the validity of the obtained results and hence other specific values can be used to obtain the required results by design communication engineers before deployment.

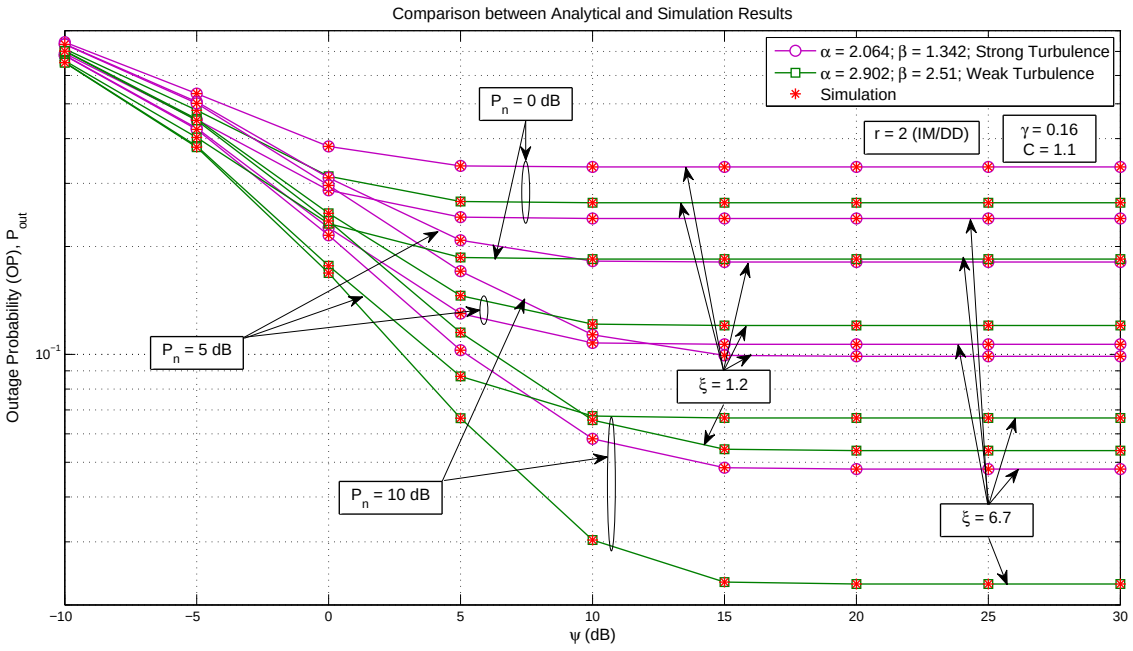

Figure 5.3: OP showing the performance of IM/DD technique over fixed gain relay with varying pointing errors (ξ's), transmit power restriction's on the SU (P_n's), and scintillation parameters (α's and β's).

restriction on the SU, $P_n = -10 \rightarrow 30$ dB. The effect of pointing error is varying ($\xi = 1.2, 6.7$) and so is the effect of interference i.e. the IT ($\psi = -5, 0, 5$ dB). Hence, Fig. 5.4 demonstrates simultaneously the effects of interference as well as pointing errors for weak ($\alpha = 2.902$; $\beta = 2.51$) and strong ($\alpha = 2.064$; $\beta = 1.342$) turbulence FSO channels. The average SNR of the FSO link is arbitrarily set as $\overline{\gamma}_{RD} = 17$ dB all throughout. It can be seen that as the atmospheric turbulence conditions get severe, BER starts increasing (i.e. the higher the values of α and β, the lower will be the BER). Also, similar results can be observed for the case of pointing errors i.e. as the pointing errors increase (i.e. the value of ξ decreases), BER starts increasing and vice versa. Additionally it can be observed that as the IT is increased, the BER performance starts getting better. It can be observed from Fig. 5.4 that the Monte Carlo simulation results provide a perfect match to the analytical results obtained in

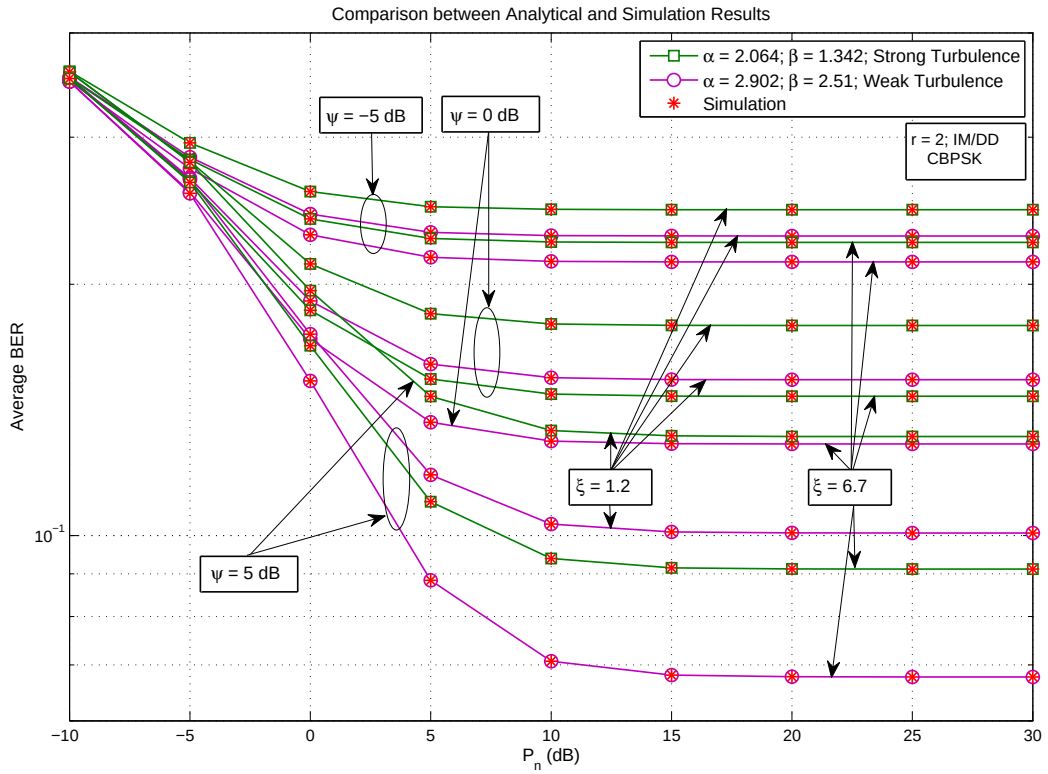

Figure 5.4: Average BER of CBPSK modulation scheme showing the performance of IM/DD technique over variable gain relay with varying pointing errors (ξ's), IT's (ψ's), and fading parameters (α's and β's).

this work. [5]

Fig. 5.5 demonstrates similar results as in Fig. 5.4 instead on the scale of a range of IT, $\psi = -10 \rightarrow 30$ dB with varying effects of maximum transmit power restriction ($P_n = 0, 5, \text{and } 10$ dB) and with the rest of the parameters being treated similar to Fig. 5.4. Similar results are observed and additionally it can be observed that as the transmit power restriction is increased on the SU, the BER performance starts getting better.

[5]It is important to note here that these values for the parameters were selected from the cited references subject to the standards to prove the validity of the obtained results and hence other specific values can be used to obtain the required results by design communication engineers before deployment.

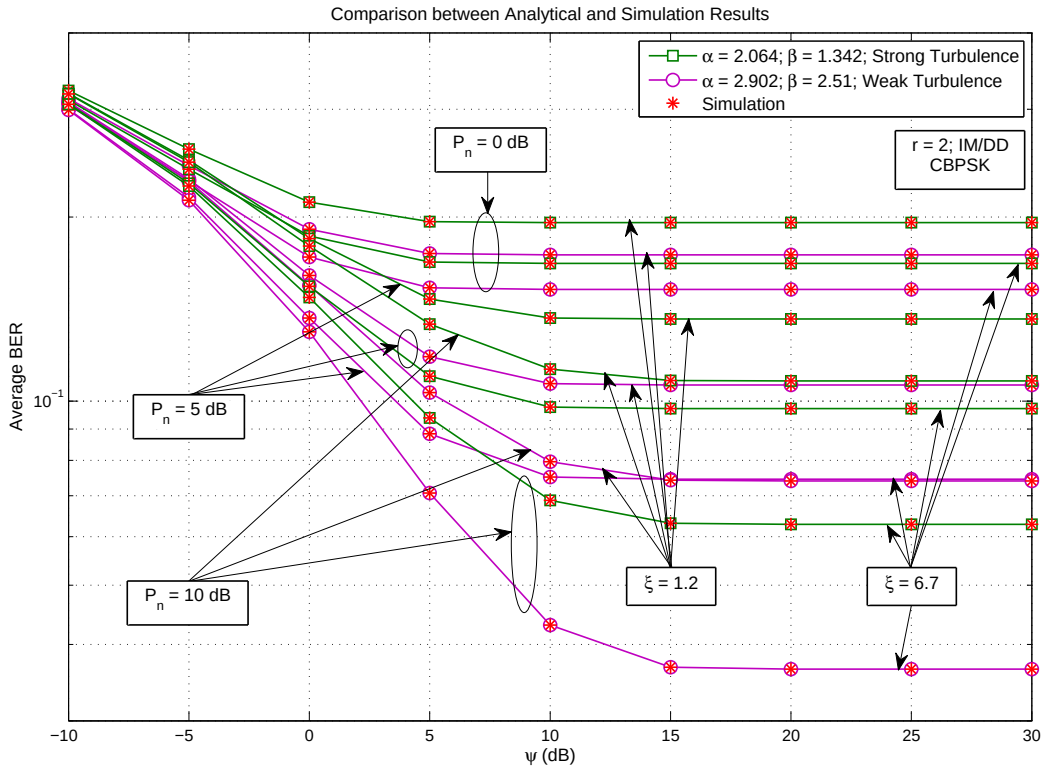

Figure 5.5: Average BER of CBPSK modulation scheme showing the performance of IM/DD technique over variable gain relay with varying pointing errors (ξ's), transmit power restriction's on the SU (P_n's), and fading parameters (α's and β's).

5.6 Concluding Remarks

Novel exact closed-form expression was derived for the outage probability of an asymmetric RF-FSO dual-hop transmission system with the RF link under the influence of interference (i.e. the secondary user transmission link is under interference constraint) with the relay being operated with fixed gain. The result was in terms of EGBFHF. Furthermore, novel exact closed-form expressions were derived for the CDF, the PDF, the MGF, and the moments of an asymmetric RF-FSO dual-hop transmission system with the RF link under the influence of interference (i.e. the SU transmission link is under interference constraint) with the relay being operated with variable gain. The results were obtained in terms of Meijer's G functions. Further, analytical expressions

were derived for various performance metrics for such a dual-hop transmission system including the OP, the higher-order AF, and the error rate of a variety of modulation schemes in terms of Meijer's G functions. In addition, this work presented simulation examples to validate and illustrate the mathematical formulation developed in this work to show the severity of the effects of the atmospheric turbulence conditions, the pointing errors in the free-space optical link, the interference temperature's set for the secondary user transmission, and the maximum transmit power restrictions on the secondary user, on the overall system performance.

Chapter 6

Concluding Remarks and Future Work

6.1 Summary

An extensive analysis was conducted on the performance of an asymmetric radio frequency (RF)-free-space optical (FSO) dual-hop transmission systems with various different developments towards generalization, unification, and practical applicability in each subsequent study/work relative to the previous one. At first, the single FSO link was unified by integrating all the previous related work on single FSO link into a single expression. This unification included both types of detection techniques i.e. heterodyne as well as intensity modulation/direct detection (IM/DD) and it also included the effect of pointing errors as well as negligible pointing errors. Specifically, the cumulative distribution function (CDF), the probability density function (PDF), the moment generating function (MGF), and the moments were derived. These lead to the derivation of the outage probability (OP), the higher-order amount of fading (AF), the average bit-error rate (BER) of binary modulation schemes, the average symbol error rate (SER) of M-ary amplitude modulation (M-AM), M-ary phase shift

keying (M-PSK) and M-ary quadrature amplitude modulation (M-QAM) schemes, and the ergodic capacity. Specifically, this analysis was focused on the Málaga ($\mathcal{M}$) atmospheric turbulence with zero boresight pointing errors.

A comprehensive ergodic capacity analysis was conducted over various atmospheric turbulences in composition with nonzero boresight pointing errors. These atmospheric turbulence included the log-normal (LN) turbulence, the Rician-LN (RLN) turbulence, and the $\mathcal{M}$ turbulence. It was concluded that finding exact closed-form solutions to the ergodic capacity's of these atmospheric turbulences along with in composition with nonzero boresight pointing errors is not possible and hence asymptotically very tight upper-bound approximations were demonstrated for the above. Many special cases, too, were derived and deduced based on the results obtained above.

Utilizing the unification for Gamma-Gamma turbulence demonstrated as a special case of the $\mathcal{M}$ turbulence, a simple asymmetric RF-FSO dual-hop was studied for amplify-and-forward relay schemes i.e. for both fixed gain relay as well as variable gain relay. This was followed by a diverse system having a direct RF link complementing the asymmetric RF-FSO dual-hop transmission system. Selection combining (SC) and maximal-ratio combining (MRC) schemes were assumed to study the performance of such a hybrid RF/RF-FSO transmission system with a direct RF link as well as an asymmetric RF-FSO dual-hop link. For all the above transmission systems under study, exact closed-form analytical expressions were derived for statistical characteristics such as the CDF, the PDF, the MGF, and the moments. These unified statistical characteristics were utilized to derive exact closed-form analytical expressions for the OP, the higher-order AF, the BER for various binary modulation schemes, the SER for various M-ary modulation schemes, and the ergodic capacity. It was satisfactorily demonstrated that the proposed hybrid RF/RF-FSO transmission system performed highly better than the traditional RF path.

Finally, the asymmetric RF-FSO dual-hop transmission system analyzed above was further enhanced via integrating it with the cognitive radio network (CRN) technology. Specifically, the RF end users were considered to be secondary (underlay cognitive) users in a cognitive setup and their performance to the destination via a relay and the FSO link was analyzed in terms of the OP and the BER for both fixed gain relay as well as variable gain relay.

A summary of the all the work presented in this thesis is tabulated in Table 6.1.

Table 6.1: Contributions to Mixed RF and FSO Transmission Systems

RF Link	**FSO Link**	**Pointing Errors**	**System Model**	**Performance Metrics**	**Publication**
-	$\mathcal{M}$	Zero Boresight	Heterodyne Detection & IM/DD	OP, AF, BER, SER, Capacity	[J.1]
-	GG	Zero Boresight	Heterodyne Detection & IM/DD	OP, AF, BER, SER, Capacity	[C.3]
-	LN, RLN, $\mathcal{M}$, & GG	Nonzero Boresight	Heterodyne Detection & IM/DD	Capacity	[J.2]
-	LN & RLN	Zero Boresight	Heterodyne Detection & IM/DD	Capacity	[C.7]
Rayleigh	GG	No	IM/DD, Fixed Gain	OP, AF, BER, SER, Capacity	[C.13]
Rayleigh	GG	Zero Boresight	IM/DD, Fixed Gain	OP, AF, BER, SER, Capacity	[J.7]
Rayleigh	GG	Zero Boresight	Heterodyne Detection & IM/DD, Variable Gain	OP, AF, BER, SER, Capacity	[C.12]
Rayleigh	GG	Zero Boresight	Heterodyne Detection & IM/DD, Direct+Fixed Gain, SC	OP, AF, BER, SER, Capacity	[C.15]
Rayleigh	GG	Zero Boresight	Heterodyne Detection & IM/DD, Direct+Variable Gain, SC	OP, AF, BER, SER, Capacity	[C.11]
Rayleigh	GG	Zero Boresight	Heterodyne Detection & IM/DD, Direct+Variable Gain, MRC	OP, BER, SER, Capacity	-
Rayleigh	GG	Zero Boresight	Heterodyne Detection & IM/DD, CRN & Fixed Gain	OP	[C.6]
Rayleigh	GG	Zero Boresight	Heterodyne Detection & IM/DD, CRN & Variable Gain	OP, BER	[C.9]

6.2 Future Research Work

The results presented on hybrid RF/RF-FSO transmission systems have indeed further motivated to explore and pursue the following possible venues for further research work with a practical application quite applicable to the region and globally. The different tasks possible are:

6.2.1 Performance Analysis of N-Best Select Users in Hybrid RF/RF-FSO Transmission Systems

Extending the basic work presented in Chapter 4, the performance of such a hybrid RF/RF-FSO may be improved manifolds. At present, the hybrid transmission system presented in Chapter 4 is losing on capacity since it is taking only a single RF (lesser bandwidth (BW)) user's message and transmitting over a high BW FSO link. The system may be improved by selecting N-best users i.e. N can be set in such a way that the high BW FSO link can be utilized to the maximum. Hence, N-best users may be selected based on certain SNR threshold and multiplexed together to be transmitted over the high BW FSO link ultimately utilizing one of the main advantages of a FSO link. This must definitely improve the performance and utility of such a hybrid RF/RF-FSO transmission system especially by utilizing the maximum possible capacity.

6.2.2 Performance Analysis of a Hybrid RF/RF-FSO transmission system with Incremental Relaying

At present, the hybrid transmission system presented in Chapter 4 is losing a time slot each time the relay is sending the RF message over the FSO link, assuming that the destination receives the message correctly via the direct RF link. To overcome this

issue, the relay can be made to transmit only in the case when the destination does not receives the transmitted message from the source as error-free. This will reduce the time loss that was caused due to unnecessary transmissions every time slot at the relay end ultimately improving the performance of such a hybrid RF/RF-FSO transmission system.

6.2.3 Performance Analysis of Asymmetric RF-FSO Dual-Hop Transmission Systems with Multiple Parallel Relays under Selective Relaying/Best Relay Selection

Considering a scenario wherein there are multiple parallel relays between the users and the BS and/or the internet backbone, there can be many possibilities of improving the performance of the system. Either all the relays may be utilized or just the best relay or may be N-best relays by setting a certain threshold. Besides this, if there is also a presence of direct RF path(s) between the users and BS then there can be a possibility of applying the diversity techniques to further improve the performance. Hence, in this way many possibilities are open for study to improve the performance of such asymmetric transmission systems.

NOTE: For proposed works in above three sections 6.2.1, 6.2.2, and 6.2.3, it is worth to note that the RF band is in any case free whenever the FSO link is under transmission (since FSO and RF operate on completely different set of frequency bands) and hence can yet be utilized by other surrounding users. Therefore, considering a vast heterogeneous (femto-cell) network, as can be extrapolated from Fig. 4.7, the performance of such a network must definitely improve.

6.2.4 Experimental Data Setup

It is worth mentioning that, since FSO is relatively a new technology, many research groups over the globe are investing their resources in acquiring experimental data to support the theoretical study. Authors in [125–128] have presented interesting results for European region and in [109] for Bangladesh. It is in plan to perform similar study for the Middle-East (ME) region where this region is more prone to fog and sandstorm instead of snow as is the case in the European region. The findings will be interesting for successful implementation of this technology.

The question one might ask is - where are we heading with all the above theoretical study? Since an uplink scenario is assumed all-throughout, therefore, one of the major application that is being targeted are the major oil-fields in the Middle-East (ME) region. In an oil-field, there are numerous oil-rigs spread around along with some BSs providing Wi-Fi connectivity to the oil-rigs for the data to be fed back to the central work environment (CWE)/central database. The oil-rigs too interact with each other for data exchange and other resources. Indeed there is huge amount of data being fed back to CWE as can be expected from such major oil-fields that are pumping millions of barrels of crude oil per day. The data being sent back also includes the live video feedback of the status of the oil-rigs for security and maintenance purposes. The performance of these oil-fields connected in wireless fashion can be improved via utilizing FSO technology. In Fig. 4.7, considering the buildings to be the BSs and the users as the oil-rigs, sets an exact example/scenario for this application. The oil-rigs can continue utilizing their RF Wi-Fi connectivity and keep interacting with their nearby oil-rigs and/or with the nearest BS. The BS can multiplex the data from all and/or most of the oil-rigs in its reach and then send it through high BW FSO link to the CWE either directly or maybe with the assistance of other BSs obviously equipped with FSO capability. Simultaneously, the oil-rigs can continue interacting

with their fellow oil-rigs since there will be no interference with the current FSO transmission. In this way, both the major features of a FSO link will be utilized i.e. the high capacity of FSO link and the fact that RF and FSO operate on completely different frequency bands. The major issue that arises is the distance that these FSO links can cover i.e. can they cover the distances of around 10 KMs between the BSs in an oil-field? If yes, then the solution is almost a perfect fit.

APPENDICES

Appendix A

Meijer's G Function Expansion

The Meijer's G function can be expressed, at a very high value of its argument, in terms of basic elementary functions via utilizing Meijer's G function expansion in [129, Theorem 1.4.2, Eq. (1.4.13)] and $\lim_{x\to 0^+} {}_cF_d\left[e; f; x\right] = 1$ [130] as

$$\begin{aligned}\lim_{z\to\infty^+} \mathrm{G}_{p,q}^{m,n}\left[z\,\middle|\begin{matrix}a_1,\ldots,a_n,\ldots,a_p\\ b_1,\ldots,b_m,\ldots,a_q\end{matrix}\right] &= \sum_{k=1}^{n} z^{a_k-1}\\ &\times \frac{\prod_{l=1;\,l\neq k}^{n}\Gamma(a_k-a_l)\prod_{l=1}^{m}\Gamma(1+b_l-a_k)}{\prod_{l=n+1}^{p}\Gamma(1+a_l-a_k)\prod_{l=m+1}^{q}\Gamma(a_k-b_l)},\end{aligned} \tag{A.1}$$

where $a_k - a_l \neq 0, \pm 1, \pm 2, \ldots; (k, l = 1, \ldots, n; k \neq l)$ and $a_k - b_l \neq 1, 2, 3, \ldots; (k = 1, \ldots, n; l = 1, \ldots, m)$.

Appendix B

Papers Accepted and Submitted

Journal Papers

[J.1] **I. S. Ansari**, F. Yilmaz, and M.-S. Alouini, "Performance analysis of free-space optical links over Málaga ($\mathcal{M}$) turbulence channels with pointing errors," under review in *IEEE Transactions on Wireless Communications*, Feb. 2015.

[J.2] **I. S. Ansari**, M.-S. Alouini, and J. Cheng, "On the capacity of FSO links under lognormal and composite-lognormal turbulences," under minor revision in *IEEE Transactions on Wireless Communications*, Aug. 2014.

[J.3] H. M. AlQuwaiee, **I. S. Ansari**, and M.-S. Alouini, "On the maximum and minimum of double generalized Gamma variates with applications to the performance of free-space optical communication systems," under review in *IEEE Transactions on Vehicular Technology*, Jul. 2014.

[J.4] H. M. AlQuwaiee, **I. S. Ansari**, and M.-S. Alouini, "On the performance of free-space optical communication systems over double generalized Gamma channel," under major revision in *IEEE Journal on Selected Areas in Communications*, Jun. 2014.

[J.5] E. Zedini, **I. S. Ansari**, and M.-S. Alouini, "On the performance of mixed Nakagami-m and Gamma-Gamma dual-hop transmission systems," *IEEE Photonics Journal*, vol. 7, no. 1, pp. , Dec. 2014.

[J.6] **I. S. Ansari**, F. Yilmaz, M.-S. Alouini, and O. Kucur, "New results on the sum of Gamma random variates with application to the performance of wireless communication systems over Nakagami-m fading channels," *Wiley Transactions on Emerging Technologies in Telecommunications*, vol. , no. , pp. , Nov. 2014.

[J.7] **I. S. Ansari**, F. Yilmaz, and M.-S. Alouini, "Impact of pointing errors on the performance of mixed RF/FSO dual-hop transmission systems," *IEEE Wireless Communications Letters*, vol. 2, no. 3, pp. 351-354, Jun. 2013.

[J.8] **I. S. Ansari**, S. Al-Ahmadi, F. Yilmaz, M.-S. Alouini, and H. Yanikomeroglu, "A new formula for the BER of binary modulations with dual-branch selection over generalized-K composite fading channels," *IEEE Transactions on Communications*, vol. 59, no. 10, pp. 2654-2658, Oct. 2011.

Conference Papers

[C.1] **I. S. Ansari** and M.-S. Alouini, "Asymptotic ergodic capacity analysis of composite lognormal shadowed channels," in *Proceedings of IEEE 81st Vehicular Technology Conference (VTC Spring' 2015)*, Glasgow, Scotland, May 2015.

[C.2] **I. S. Ansari** and M.-S. Alouini, "On the performance analysis of digital communications over Weibull-Gamma channels," in *Proceedings of IEEE 81st Vehicular Technology Conference (VTC Spring' 2015)*, Glasgow, Scotland, May 2015.

[C.3] **I. S. Ansari**, F. Yilmaz, and M.-S. Alouini, "A unified performance analysis of free-space optical links over Gamma-Gamma turbulence channels with pointing

errors," in *Proceedings of IEEE 81st Vehicular Technology Conference (VTC Spring' 2015)*, Glasgow, Scotland, May 2015.

[C.4] E. Zedini, **I. S. Ansari**, and M.-S. Alouini, "Unified performance analysis of mixed line of sight RF-FSO fixed gain dual-hop transmission systems," in *Proceedings of IEEE Wireless Communications and Networking Conference (WCNC' 2015)*, New Orleans, LA, USA, Mar. 2015.

[C.5] E. Zedini, **I. S. Ansari**, and M.-S. Alouini, "On the performance of hybrid line of sight RF and RF-FSO fixed gain dual-hop transmission systems," in *Proceedings of IEEE Global Communications Conference (GLOBECOM' 2014)*, Austin, TX, USA, Dec. 2014.

[C.6] **I. S. Ansari**, M. M. Abdallah, K. A. Qaraqe, and M.-S. Alouini, "Outage performance analysis of underlay cognitive RF and FSO wireless channels," in *Proceedings of 3rd International Workshop on Optical Wireless Communications (IWOW' 2014)*, Funchal, Madeira Islands, Portugal, Sep. 2014, pp. 6-10.

[C.7] **I. S. Ansari**, M.-S. Alouini, and J. Cheng, "On the capacity of FSO links under weak turbulence," in *Proceedings of IEEE 80th Vehicular Technology Conference (VTC Fall' 2014)*, Vancouver, Canada, Sep. 2014, pp. 1-6.

[C.8] H. M. AlQuwaiee, **I. S. Ansari**, and M.-S. Alouini, "On the maximum and minimum of two modified Gamma-Gamma variates with applications," in *Proceedings of IEEE Wireless Communications and Networking Conference (WCNC' 2014)*, Istanbul, Turkey, Apr. 2014, pp. 269-274.

[C.9] **I. S. Ansari**, M. M. Abdallah, M.-S. Alouini, and K. A. Qaraqe, "A performance study of two hop transmission in mixed underlay RF and FSO fading channels," in *Proceedings of IEEE Wireless Communications and Networking Conference (WCNC' 2014)*, Istanbul, Turkey, Apr. 2014, pp. 388-393.

[C.10] H. M. AlQuwaiee, **I. S. Ansari**, and M.-S. Alouini, "On the performance of free space optical wireless communication systems over double generalized Gamma fading channel," in *Proceedings of the 4th International Conference on Communications and Networking (COMNET' 2014)*, Hammamet, Tunisia, Mar. 2014.

[C.11] **I. S. Ansari**, F. Yilmaz, and M.-S. Alouini, "On the performance of hybrid RF and RF/FSO dual-hop transmission systems," in *Proceedings of 2nd International Workshop on Optical Wireless Communications (IWOW' 2013)*, Newcastle Upon Tyne, UK, Oct. 2013, pp. 45-59.

[C.12] **I. S. Ansari**, F. Yilmaz, and M.-S. Alouini, "On the performance of mixed RF/FSO variable gain dual-hop transmission systems with pointing errors," in *Proceedings of IEEE 78th Vehicular Technology Conference (VTC Fall' 2013)*, Las Vegas, USA, Sep. 2013.

[C.13] **I. S. Ansari**, F. Yilmaz, and M.-S. Alouini, "On the performance of mixed RF/FSO dual-hop transmission systems," in *Proceedings of IEEE 77th Vehicular Technology Conference (VTC Spring' 2013)*, Dresden, Germany, Jun. 2013.

[C.14] **I. S. Ansari**, F. Yilmaz, and M.-S. Alouini, "On the sum of squared eta-mu random variates with application to the performance of wireless communication systems," in *Proceedings of IEEE 77th Vehicular Technology Conference (VTC Spring' 2013)*, Dresden, Germany, Jun. 2013.

[C.15] **I. S. Ansari**, F. Yilmaz, and M.-S. Alouini, "On the performance of hybrid RF and RF/FSO fixed gain dual-hop transmission systems," in *Proceedings of The Second Saudi International Electronics, Communications and Photonics Conference (SIECPC' 2013)*, Riyadh, Saudi Arabia, Apr. 2013, pp. 1-6.

[C.16] **I. S. Ansari**, F. Yilmaz, and M.-S. Alouini, "On the sum of Gamma random variates with application to the performance of maximal ratio combining over

Nakagami-m fading channels," in *Proceedings of IEEE 13th Workshop on Signal Processing Advances in Wireless Communications (SPAWC' 2012)*, Cesme, Turkey, Jun. 2012, pp. 394-398.

[C.17] **I. S. Ansari**, S. Al-Ahmadi, F. Yilmaz, M.-S. Alouini, and H. Yanikomeroglu, "An exact closed-form expression for the BER of binary modulations with dual-branch selection over generalized-K fading," in *Proceedings of IEEE 73rd Vehicular Technology Conference (VTC Spring' 2011)*, Budapest, Hungary, May 2011.

[C.18] **I. S. Ansari**, "An implementation of traffic light system using multi-hop ad hoc networks," in *Proceedings of IEEE International Conference on Network-Based Information Systems (NBIS/ ISEUPS' 2009)*, Indianapolis, Indiana, US, Aug. 2009, pp. 177-181.

[C.19] **I. S. Ansari** and A. S. Qutbuddin, "Biometrics for home networks security," in *Proceedings of IEEE Student Conference on Research and Development 2009 (SCOReD' 2009)*, Malaysia, Nov. 2009, pp. 136-138.

BIBLIOGRAPHY

[1] J. B. Anderson, "Statistical distributions in mobile communications using multiple scattering," in *Proceedings of General Assembly International Union of Radio Sciences*, Maastricht, The Netherlands, Aug. 2002.

[2] A. Goldsmith, *Wireless Communications*. Cambridge. UK: Cambridge University Press, 2005.

[3] M. K. Simon and M.-S. Alouini, *Digital Communication over Fading Channels*, 2nd ed. Hoboken, New Jersey, USA: IEEE: John Wiley & Sons, Inc., 2005.

[4] S. M. Aghajanzadeh and M. Uysal, "Multi-hop coherent free-space optical communications over atmospheric turbulence channels," *IEEE Transactions on Communications*, vol. 59, no. 6, pp. 1657–1663, Jun. 2011.

[5] J. M. Romera-Jerez and A. J. Goldsmith, "Performance of multichannel reception with transmit antenna selection in arbitrarily distributed Nakagami fading channels," *IEEE Transactions on Wireless Communications*, vol. 8, no. 4, pp. 2006–2013, Apr. 2009.

[6] M. Z. Win and J. H. Winters, "Analysis of hybrid selection/maximal-ratio combining in Rayleigh fading," *IEEE Transactions on Communications*, vol. 47, no. 12, pp. 1773–1776, Dec. 1999.

[7] R. K. Mallik and M. Z. Win, "Analysis of hybrid selection/maximal-ratio combining in correlated Nakagami fading," *IEEE Transactions on Communications*, vol. 50, no. 8, pp. 1372–1383, Aug. 2002.

[8] R. K. Mallik, M. Z. Win, J. W. Shao, M.-S. Alouini, and A. Goldsmith, "Channel capacity of adaptive transmission with maximal ratio combining in correlated Rayleigh fading," *IEEE Transactions on Wireless Communications*, vol. 3, no. 4, pp. 1124–1133, Jul. 2004.

[9] D. G. Brennan, "Linear diversity combining techniques," *Proceedings of the IRE*, vol. 47, no. 6, pp. 1075–1102, Jun. 1959.

[10] ——, "Linear diversity combining techniques," *Proceedings of the IEEE*, vol. 91, no. 2, pp. 331–356, Feb. 2003.

[11] K. P. Peppas, F. Lazarakis, T. Zervos, A. Alexandridis, and K. Dangakis, "Sum of non-identical squared η-μ variates and applications in the performance analysis of DS-CDMA systems," *IEEE Transactions on Wireless Communications*, vol. 9, no. 9, pp. 2718–2723, Sep. 2010.

[12] M. Safari and M. Uysal, "Relay-assisted free-space optical communication," *IEEE Transactions on Wireless Communications*, vol. 7, no. 12, pp. 5441–5449, Dec. 2008.

[13] E. van der Meulen, "Transmission of information in a t-terminal discrete memoryless channel," Ph.D. dissertation, University of California, Berkeley, CA, USA, 1968.

[14] ——, "Three-terminal communication channels," *Advances in Applied Probability*, pp. 120–154, 1971.

[15] A. Sendonaris, E. Erkip, and B. Aazhang, "User cooperation diversity. Part I. System description," *IEEE Transactions on Communications*, vol. 51, no. 11, pp. 1927–1938, Nov. 2003.

[16] ——, "User cooperation diversity. Part II. Implementation aspects and performance analysis," *IEEE Transactions on Communications*, vol. 51, no. 11, pp. 1927–1938, Nov. 2003.

[17] J. Laneman, D. Tse, and G. Wornell, "Cooperative diversity in wireless networks: Efficient protocols and outage behavior," *IEEE Transactions on Information Theory*, vol. 50, no. 12, pp. 3062–3080, Dec. 2004.

[18] J. Laneman and G. Wornell, "Distributed space-time-coded protocols for exploiting cooperative diversity in wireless networks," *IEEE Transactions on Information Theory*, vol. 49, no. 10, pp. 2415–2425, Oct. 2003.

[19] R. Pabst, B. Walke, D. Schultz, P. Herhold, H. Yanikomeroglu, S. Mukherjee, H. Viswanathan, M. Lott, W. Zirwas, M. Dohler, H. Aghvami, D. Falconer, and G. Fettweis, "Relay-based deployment concepts for wireless and mobile broadband radio," *IEEE Communications Magazine*, vol. 42, no. 9, pp. 80–89, Sep. 2004.

[20] "IEEE standard for a local and metropolitan area networks, part 16: Air interface for fixed and mobile and mobile broadband wireless access systems: Multihop relay specification," *I.P802.16j*, vol. P802.16j/D3, Feb. 2008.

[21] M. O. Hasna and M.-S. Alouini, "A performance study of dual-hop transmissions with fixed gain relays," *IEEE Transactions on Wireless Communications*, vol. 3, no. 6, pp. 1963–1968, Nov. 2004.

[22] Y. Zhao, R. Adve, and T. J. Lim, "Improving amplify-and-forward relay networks: Optimal power allocation versus selection," *IEEE Transactions on Wireless Communications*, vol. 6, no. 8, pp. 3114–3123, Aug. 2007.

[23] P. Goetz, W. Rabinovich, R. Mahon, J. Murphy, M. Ferraro, M. Suite, W. Smith, B. Xu, H. Burris, C. Moore, W. Schultz, B. Mathieu, W. Freeman, S. Frawley, M. Colbert, and K. Reese, "Modulating retro-reflector lasercom systems at the naval research laboratory," in *Proceedings of Military Communications Conference (MILCOM' 10)*, Oct. 2010, pp. 1601–1606.

[24] I. K. Son, S. Kim, and S. Mao, "Building robust spanning trees in free space optical networks," in *Proceedings of Military Communications Conference (MILCOM' 10)*, Oct. 2010, pp. 1857–1862.

[25] T. Plank, E. Leitgeb, and M. Loeschnigg, "Recent developments on free space optical links and wavelength analysis," in *Proceedings of International Conference on Space Optical Systems and Applications (ICSOS' 11)*, May 2011, pp. 14–20.

[26] N. Nor, I. Rafiqul, W. Al-Khateeb, and S. Zabidi, "Environmental effects on free space earth-to-satellite optical link based on measurement data in Malaysia," in *Proceedings of International Conference on Computer and Communication Engineering (ICCCE' 12)*, Jul. 2012, pp. 694–699.

[27] M. Z. Win, "On the power spectral density of digital pulse streams generated by m-ary cyclostationary sequences in the presence of stationary timing jitter," *IEEE Transactions on Communications*, vol. 46, no. 9, pp. 1135–1145, Sep. 1998.

[28] M. Z. Win, C.-C. Chen, and R. A. Scholtz, "Optical phase-locked loop (OPLL) for an amplitude modulated communications link using solid state lasers," *IEEE*

Journal of Selective Areas in Communications, vol. SAC-13, no. 3, pp. 569–576, Apr. 1995.

[29] M. Z. Win, J. R. Lesh, C.-C. Chen, W. K. Marshall, M. D. Rayman, and R. A. Scholtz, "Optical phase-locked loop for optical communication," *NASA Tech Briefs*, Apr. 1992.

[30] M. Z. Win, "Estimation and tracking for deep-space optical communications," in *Proceedings of SPIE Space Sensing, Communications, and Networking*, vol. 1059, Jan. 1989, pp. 80–87.

[31] C.-C. Chen and M. Z. Win, "Frequency noise measurement of diode-pumped Nd:YAG ring lasers," *IEEE Photonics Journal*, vol. 2, no. 11, pp. 772–774, Nov. 1990.

[32] C.-C. Chen, D. Arbel, and M. Z. Win, "100-Mbps coherent optical link demonstration using frequency stabilized solid state lasers," in *Proceedings of SPIE Free-Space Laser Communication Technologies IV*, vol. 1635, Jan. 1991, pp. 215–224.

[33] C.-C. Chen and M. Z. Win, "Laser frequency stability requirements for coherent space communications," in *Proceedings of IEEE* 45*th Annual Symposium on Frequency Control*, May 1991, pp. 500–507.

[34] A. Yong, X. Zhun, C. Jin, Z. Fengxia, L. Yan, Z. Shancong, D. Ran, and X. Yongjun, "The analysis of 7.5 Gbps 40 Km FSO experiments," in *Proceedings of IEEE Photonics Society Summer Topical Meeting Series*, Jul. 2012, pp. 128–129.

[35] Y. Jahir, M. Atiquzzaman, H. Refai, and P. LoPresti, "Performance evaluation of AODVH: An ad hoc networking scheme for hybrid nodes," in *Proceedings*

of the 13th International Conference on Computer and Information Technology (ICCIT' 10), Dec. 2010, pp. 165–169.

[36] N. Agrawal, C. Davis, and S. Milner, "Free space optical sensor networking for underwater sensing applications," in *Proceedings of International conference on Intelligent Sensors, Sensor Networks and Information Processing (ISSNIP' 09)*, Dec. 2009, pp. 475–480.

[37] W. O. Popoola and Z. Ghassemlooy, "BPSK subcarrier intensity modulated free-space optical communications in atmospheric turbulence," *IEEE/OSA Journal of Lightwave Technology*, vol. 27, no. 8, pp. 967–973, Apr. 2009.

[38] L. C. Andrews, R. L. Phillips, and C. Y. Hopen, *Laser Beam Scintillation with Applications*. Bellingham, WA: SPIE, 2001.

[39] K. P. Peppas and C. K. Datsikas, "Average symbol error probability of general-order rectangular quadrature amplitude modulation of optical wireless communication systems over atmospheric turbulence channels," *IEEE/OSA Journal of Optical Communications and Networking*, vol. 2, no. 2, pp. 102–110, Feb. 2010.

[40] J. Park, E. Lee, and G. Yoon, "Average bit error rate of the Alamouti scheme in Gamma-Gamma fading channels," *IEEE Photonics Technology Letters*, vol. 23, no. 4, pp. 269–271, Feb. 2011.

[41] S. M. Navidpour, M. Uysal, and M. Kavehrad, "BER performance of free-space optical transmission with spatial diversity," *IEEE Transactions on Wireless Communications*, vol. 6, no. 8, pp. 2813–2819, Aug. 2007.

[42] S. Zabidi, W. Al-Khateeb, M. Islam, and W. Naji, "The effect of weather on free space optics communication (FSO) under tropical weather conditions and

a proposed setup for measurement," in *Proceedings of International Conference on Computer and Communication Engineering (ICCCE' 10)*, May 2010, pp. 1–5.

[43] S. Milner, S. Trisno, C. Davis, B. Epple, and H. Henniger, "A cross-layer approach to mitigate fading on bidirectional free space optical communication links," in *Proceedings of Military Communications Conference (MILCOM' 08)*, Nov. 2008, pp. 1–6.

[44] V. Khare and D. Chandra, "Extended Alamouti space time coding scheme with turbo coding for free space optical communication," in *Proceedings of International Conference on Computational Intelligence and Communication Networks (CICN' 11)*, Oct. 2011, pp. 359–362.

[45] E. Bayaki and R. Schober, "Performance and design of coherent and differential space-time coded FSO systems," *IEEE/OSA Journal of Lightwave Technology*, vol. 30, no. 11, pp. 1569–1577, Jun. 2012.

[46] C. Abou-Rjeily, "On the optimality of the selection transmit diversity for MIMO-FSO links with feedback," *IEEE Communications Letters*, vol. 15, no. 6, pp. 641–643, Jun. 2011.

[47] H. Moradi, H. Refai, and P. LoPresti, "Circular MIMO FSO nodes with transmit selection and receive generalized selection diversity," *IEEE Transactions on Vehicular Technology*, vol. 61, no. 3, pp. 1174–1181, Mar. 2012.

[48] H. G. Sandalidis, T. A. Tsiftsis, and G. K. Karagiannidis, "Optical wireless communications with heterodyne detection over turbulence channels with pointing errors," *Journal of Lightwave Technology*, vol. 27, no. 20, pp. 4440–4445, Oct. 2009.

[49] H. G. Sandalidis, T. A. Tsiftsis, G. K. Karagiannidis, and M. Uysal, "BER performance of FSO links over strong atmospheric turbulence channels with pointing errors," *IEEE Communications Letters*, vol. 12, no. 1, pp. 44–46, Jan. 2008.

[50] W. Gappmair, "Further results on the capacity of free-space optical channels in turbulent atmosphere," *IET Communications*, vol. 5, no. 9, pp. 1262–1267, Jun. 2011.

[51] T. A. Tsiftsis, "Performance of heterodyne wireless optical communication systems over Gamma-Gamma atmospheric turbulence channels," *Electronics Letter*, vol. 44, no. 5, pp. 372–373, Feb. 2008.

[52] C. Liu, Y. Yao, Y. Sun, and X. Zhao, "Average capacity for heterodyne FSO communication systems over Gamma-Gamma turbulence channels with pointing errors," *Electronics Letters*, vol. 46, no. 12, pp. 851–853, Jun. 2010.

[53] E. Lee, J. Park, D. Han, and G. Yoon, "Performance analysis of the asymmetric dual-hop relay transmission with mixed RF/FSO links," *IEEE Photonics Technology Letters*, vol. 23, no. 21, pp. 1642–1644, Nov. 2011.

[54] S. Haykin, "Cognitive radio: Brain-empowered wireless communications," *IEEE Journal on Selected Areas in Communications*, vol. 23, no. 2, pp. 201–220, Feb. 2005.

[55] S. Ekin, M. M. Abdallah, K. A. Qaraqe, and E. Serpedin, "Random subcarrier allocation in OFDM-based cognitive radio networks," *IEEE Transactions on Signal Processing*, vol. 60, no. 9, pp. 4758–4774, Sep. 2012.

[56] A. J.-Navas, J. M. G.-Balsells, J. F. Paris, and A. P.-Notario, "A unifying statistical model for atmospheric optical scintillation," in *Numerical Simulations of Physical and Engineering Processes*, J. Awrejcewicz, Ed., Intech, 2011, ch.8.

[57] A. J.-Navas, J. M. G.-Balsells, J. F. Paris, M. C.-Vazquez, and A. P.-Notario, "Impact of pointing errors on the performance of generalized atmospheric optical channels," *Optics Express*, vol. 20, no. 11, pp. 12 550–12 562, May 2012.

[58] I. S. Gradshteyn and I. M. Ryzhik, *Table of Integrals, Series and Products*. New York: Academic Press, 2000.

[59] A. Farid and S. Hranilovic, "Outage capacity optimization for free-space optical links with pointing errors," *IEEE/OSA Journal of Lightwave Technology*, vol. 25, no. 7, pp. 1702–1710, Jul. 2007.

[60] M. Niu, J. Cheng, and J. F. Holzman, "Error rate performance comparison of coherent and subcarrier intensity modulated optical wireless communications," *IEEE/OSA Journal of Optical Communications and Networking*, vol. 5, no. 10, pp. 554–564, Jun. 2013.

[61] H. Samimi and M. Uysal, "End-to-end performance of mixed RF/FSO transmission systems," *IEEE/OSA Journal of Optical Communications and Networking*, vol. 5, no. 11, pp. 1139–1144, Nov. 2013.

[62] I. Wolfram Research, *Mathematica Edition: Version 8.0*. Champaign, Illinois: Wolfram Research, Inc., 2010.

[63] H. E. Nistazakis, T. A. Tsiftsis, and G. S. Tombras, "Performance analysis of free-space optical communication systems over atmospheric turbulence channels," *IET Communications*, vol. 3, no. 8, pp. 1402–1409, Aug. 2009.

[64] M. Feng, J.-B. Wang, M. Sheng, L.-L. Cao, X.-X. Xie, and M. Chen, "Outage performance for parallel relay-assisted free-space optical communications in strong turbulence with pointing errors," in *Proceedings of International Conference on Wireless Communications and Signal Processing (WCSP' 2011)*, Nanjing, China, Nov. 1990, pp. 1–5.

[65] H. Li-Qiang, W. Qi, and S. Katsunori, "Outage probability of free space optical communication over atmosphere turbulence," in *Proceedings of WASE International Conference on Information Engineering (ICIE' 2010)*, Beidaihe, Hebei, China, Aug. 2010, pp. 127–130.

[66] M. D. Springer, *The Algebra of Random Variables*. New York: Wiley, Apr. 1979.

[67] C. K. Datsikas, K. P. Peppas, N. C. Sagias, and G. S. Tombras, "Serial free-space optical relaying communications over Gamma-Gamma atmospheric turbulence channels," *IEEE/OSA Journal of Optical Communications and Networking*, vol. 2, no. 8, pp. 576–586, Aug. 2010.

[68] F. Yilmaz and M.-S. Alouini, "Novel asymptotic results on the high-order statistics of the channel capacity over generalized fading channels," in *Proceedings of IEEE* 13^{th} *International Workshop on Signal Processing Advances in Wireless Communications (SPAWC' 2012)*, Cesme, Turkey, Jun. 2012, pp. 389–393.

[69] I. S. Ansari, S. Al-Ahmadi, F. Yilmaz, M.-S. Alouini, and H. Yanikomeroglu, "A new formula for the BER of binary modulations with dual-branch selection over generalized-K composite fading channels," *IEEE Transactions on Communications*, vol. 59, no. 10, pp. 2654–2658, Oct. 2011.

[70] N. C. Sagias, D. A. Zogas, and G. K. Kariaginnidis, "Selection diversity receivers over nonidentical Weibull fading channels," *IEEE Transactions on Vehicular Technology*, vol. 54, no. 6, pp. 2146–2151, Nov. 2005.

[71] A. H. Wojnar, "Unknown bounds on performance in Nakagami channels," *IEEE Transactions on Communications*, vol. 34, no. 1, pp. 22–24, Jan. 1986.

[72] I. S. Ansari, F. Yilmaz, M.-S. Alouini, and O. Kucur, "New results on the sum of Gamma random variates with applications to the performance of wireless

communication systems over Nakagami-m fading channels," *Wiley Transactions on Emerging Technologies in Telecommunications*, pp. –, Nov. 2014.

[73] ——, "On the sum of Gamma random variates with application to the performance of maximal ratio combining over Nakagami-m fading channels," in *Proceedings of IEEE* 13^{th} *International Workshop on Signal Processing Advances in Wireless Communications (SPAWC' 2012)*, Cesme, Turkey, Jun. 2012, pp. 394–398.

[74] X. Song, M. Niu, and J. Cheng, "Error rate of subcarrier intensity modulations for wireless optical communications," *IEEE Communications Letters*, vol. 16, no. 4, pp. 540–543, Apr. 2012.

[75] M. Niu, X. Song, J. Cheng, and J. F. Holzman, "Performance analysis of coherent wireless optical communications with atmospheric turbulence," *Optics Express*, vol. 20, no. 6, pp. 6515–6520, Mar. 2012.

[76] Z. Wang and G. B. Giannakis, "A simple and general parameterization quantifying performance in fading channels," *IEEE Transactions on Communications*, vol. 51, no. 8, pp. 1389–1398, Aug. 2003.

[77] E. Bayaki, R. Schober, and R. K. Mallik, "Performance analysis of MIMO free-space optical systems in Gamma-Gamma fading," *IEEE Transactions on Communications*, vol. 57, no. 11, pp. 3415–3424, Nov. 2009.

[78] M.-S. Alouini and A. J. Goldsmith, "A unified approach for calculating error rates of linearly modulated signals over generalized fading channels," *IEEE Transactions on Communications*, vol. 47, no. 9, pp. 1324–1334, Sep. 1999.

[79] M. Abramowitz and I. A. Stegun, *Handbook of Mathematical Functions*, 10th ed. New York: Dover, Dec. 1972.

[80] F. Yilmaz, O. Kucur, and M.-S. Alouini, "A novel framework on exact average symbol error probabilities of multihop transmission over amplify-and-forward relay fading channels," in *Proceedings of* 7^{th} *International Symposium on Wireless Communication Systems (ISWCS' 2010)*, York, U.K., Nov. 2010, pp. 546–550.

[81] A. Lapidoth, S. M. Moser, and M. A. Wigger, "On the capacity of free-space optical intensity channels," *IEEE Transactions on Information Theory*, vol. 55, no. 10, pp. 4449–4461, Oct. 2009.

[82] S. Arnon, *et.al., eds.*, *Advanced Optical Wireless Communications Systems*. Cambridge University Press, 2013.

[83] V. S. Adamchik and O. I. Marichev, "The algorithm for calculating integrals of hypergeometric type functions and its realization in reduce system," in *Proceedings of International Symposium on Symbolic and Algebraic Computation (ISSAC' 1990)*, New York, USA, 1990, pp. 212–224.

[84] C. Liu, Y. Yao, Y. Sun, and X. Zhao, "Analysis of average capacity for free space optical links with pointing errors over Gamma-Gamma turbulence channels," *Chinese Optics Letters*, vol. 8, no. 6, pp. 537–540, Jun. 2010.

[85] H. E. Nistazakis, E. A. Karagianni, A. D. Tsigopoulos, M. E. Fafalios, and G. S. Tombras, "Average capacity of optical wireless communication systems over atmospheric turbulence channels," *IEEE/OSA Journal of Lightwave Technology*, vol. 27, no. 8, pp. 974–979, Apr. 2009.

[86] Y. Ren, A. Dang, B. Luo, and H. Guo, "Capacities for long-distance free-space optical links under beam wander effects," *IEEE Photonics Technology Letters*, vol. 22, no. 14, pp. 1069–1071, Jul. 2010.

[87] D. L. Fried, "Optical heterodyne detection of an atmospherically distroted signal wave front," *Proceedings of the IEEE*, vol. 55, no. 1, pp. 57–67, Jan. 1967.

[88] M. Niu, J. Cheng, and J. F. Holzman, "Terrestrial coherent free-space optical communication systems," in *Optical Communication*, J. Awrejcewicz, Ed., Intech, 2012, ch.8.

[89] X. Zhu and J. M. Kahn, "Free-space optical communication through atmospheric turbuelnce channels," *IEEE Transactions on Communications*, vol. 50, no. 8, pp. 1293–1300, Aug. 2002.

[90] M. Cheng, C. Chen, J. Gao, C. Si, and Y. Zhang, "Capacity of wander and spread beams in log-normal distribution non-Kolmogorov turbulence optical links," *Elsevier Optik - International Journal of Light Electron Optics*, vol. PP, 2014, http://dx.doi.org/10.1016/j.ijleo.2014.01.127.

[91] X. Liu, C. Chen, Z. Hu, L. Zhang, Y. Zhu, and Y. Zhang, "Average capacity of ground-to-train log-normal wireless optical interconnects," *Elsevier Optik - International Journal of Light Electron Optics*, vol. PP, 2014, http://dx.doi.org/10.1016/j.ijleo.2014.01.121.

[92] F. Yang and J. Cheng, "Coherent free-space optical communications in lognormal-Rician turbulence," *IEEE Communications Letters*, vol. 16, no. 11, pp. 1872–1875, Nov. 2012.

[93] J. H. Churnside and S. F. Clifford, "Log-normal Rician probability-density function of optical scintillations in the turbulent atmosphere," *OSA Journal of Optical Society of America A*, vol. 4, no. 10, pp. 1923–1930, Oct. 1987.

[94] X. Song and J. Cheng, "Joint estimation of the lognormal-Rician atmospheric turbulence model by the generalized method of moments," *Elsevier Optics Communications*, vol. 285, pp. 4727–4732, Aug. 2012.

[95] F. Yang, J. Cheng, and T. A. Tsiftsis, "Free-space optical communication with nonzero boresight pointing errors," *IEEE Transactions on Communications*, vol. 62, no. 2, pp. 713–725, Feb. 2014.

[96] J. M. G.-Balsells, A. J.-Navas, J. F. Paris, M. C.-Vazquez, and A. P.-Notario, "On the capacity of $\mathcal{M}$-distributed atmospheric optical channels," *Optics Letters*, vol. 38, no. 20, pp. 3984–3987, Oct. 2013.

[97] J.-Y. Wang, J.-B. Wang, M. Chen, Y. Tang, and Y. Zhang, "Outage analysis for relay-aided free-space optical communications over turbulence channels with nonzero boresight pointing errors," *IEEE Photonics Journal*, vol. 6, no. 4, pp. 1–15, Aug. 2014.

[98] D. Kedar and S. Arnon, "Urban optical wireless communication networks: The main challenges and possible solutions," *IEEE Communications Magazine*, vol. 42, no. 5, pp. S2–S7, May 2004.

[99] H. G. Sandalidis and T. A. Tsiftsis, "Outage probability and ergodic capacity of free-space optical links over strong turbulence," *Electronics Letters*, vol. 44, no. 1, pp. 46–47, Jan. 2008.

[100] N. Wang and J. Cheng, "Moment-based estimation for the shape parameters of the Gamma-Gamma atmospheric turbulence model," *Optics Express*, vol. 18, no. 12, pp. 12 824–12 831, Jun. 2010.

[101] M. Rao, F. J. L.-Martinez, M.-S. Alouini, and A. Goldsmith, "MGF approach to the analysis of generalized two-ray fading models," *Submitted to IEEE Transactions on Wireless Communications*, 2014, available in arxiv.org at http://arxiv.org/abs/1406.5101.

[102] L. U. Ancarani and G. Gasaneo, "Derivatives of any order of the confluent hypergeometric function ${}_1F_1(a, b, z)$ with respect to the parameter a or b," *Journal of Mathematical Physics*, vol. 49, no. 6, pp. 063 508(1–16), 2008.

[103] S.-D. Lin, Y.-S. Chao, and H. M. Srivastava, "Some expansions of the exponential integral in series of the incomplete Gamma function," *Elsevier Applied Mathematics Letters*, vol. 28, no. 5, pp. 513–520, 2005.

[104] Y. Zhu, Y. Xin, and P.-Y. Kam, "Outage probability of Rician fading relay channels," *IEEE Transactions on Vehicular Technology*, vol. 57, no. 4, pp. 2648–2652, Jul. 2008.

[105] S. N. Datta, S. Chakrabarti, and R. Roy, "Error analysis of non coherent FSK with variable gain relaying in dual-hop Nakagami-m relay fading channel," in *Proceedings of 2010 International Conference on Signal Processing and Communications (SPCOM' 2010)*, Bangalore, India, Jul. 2010, pp. 1–5.

[106] H. A. Suraweera, R. H. Y. Louie, Y. Li, G. K. Karagiannidis, and B. Vucetic, "Two hop amplify-and-forward transmission in mixed Rayleigh and Rician fading channels," *IEEE Communication Letters*, vol. 13, no. 4, pp. 227–229, Apr. 2009.

[107] A. K. Gurung, F. S. Al-Qahtani, Z. M. Hussain, and H. Alnuweiri, "Performance analysis of amplify-forward relay in mixed Nakagami-m and Rician fading channels," in *Proceedings of 2010 International Conference on Advanced Technologies for Communications (ATC' 2010)*, Ho Chi Minh City, Vietnam, Oct. 2010, pp. 321–326.

[108] F. Yilmaz and M.-S. Alouini, "Product of the powers of generalized Nakagami-m variates and performance of cascaded fading channels," in *Proceedings of*

IEEE Global Telecommunications Conference (GLOBECOM' 2009), Honolulu, Hawaii, US, Nov.-Dec. 2009, pp. 1–8.

[109] N. Saquib, M. S. R. Sakib, A. Saha, and M. Hussain, "Free space optical connectivity for last mile solution in Bangladesh," in *Proceedings of* 2^{nd} *International Conference on Education Technology and Computer (ICETC' 2010)*, Shanghai, China, Jun. 2010, pp. 484–487.

[110] S. Ikki and M. H. Ahmed, "Performance analysis of dual-hop relaying communications over generalized Gamma fading channels," in *Proceedings of IEEE Global Telecommunications Conference (GLOBECOM' 2007)*, Washington DC, USA, Nov. 2007, pp. 3888–3893.

[111] S. S. Ikki and S. Aissa, "Performance evaluation and optimization of dual-hop communication over Nakagami-m fading channels in the presence of co-channel interferences," *IEEE Communications Letters*, vol. 16, no. 8, pp. 1149–1152, Aug. 2012.

[112] U. Charash, "Reception through Nakagami fading multipath channels with random delays," *IEEE Transactions on Communications*, vol. 27, no. 4, pp. 657–670, Apr. 1979.

[113] A. Annamalai, R. C. Palat, and J. Matyjas, "Estimating ergodic capacity of cooperative analog relaying under different adaptive source transmission techniques," in *Proceedings of 2010 IEEE Sarnoff Symposium*, Princeton, NJ, Apr. 2010, pp. 1–5.

[114] A. M. Mathai and R. K. Saxena, *The H-Function with Applications in Statistics and Other Disciplines*. New York: Wiley Eastern, 1978.

[115] S. S. Ikki and S. Aissa, "A study of optimization problem for amplify-and-forward relaying over Weibull fading channels with multiple antennas," *IEEE Communications Letters*, vol. 15, no. 11, pp. 1148–1151, Nov. 2011.

[116] Y.-C. Ko, M.-S. Alouini, and M. K. Simon, "Outage probability of diversity systems over generalized fading channels," *IEEE Transactions on Communications*, vol. 48, no. 11, pp. 1783–1787, Nov. 2000.

[117] M.-S. Alouini and M. K. Simon, "An MGF-based performance analysis of generalized selection combining over Rayleigh fading channels," *IEEE Transactions on Communications*, vol. 48, no. 3, pp. 401–415, Mar. 2000.

[118] M. D. Renzo, F. Graziosi, and F. Santucci, "Channel capacity over generalized fading channels: A novel MGF-based approach for performance analysis and design of wireless communication systems," *IEEE Transactions on Vehicular Technology*, vol. 59, no. 1, pp. 127–149, Jan. 2010.

[119] F. Yilmaz and M.-S. Alouini, "A unified MGF-based capacity analysis of diversity combiners over generalized fading channels," *IEEE Transactions on Communications*, vol. 60, no. 3, pp. 862–875, Mar. 2012.

[120] X. Tang, Z. Ghassemlooy, S. Rajbhandari, W. O. Popoola, and C. G. Lee, "Coherent polarization shift keying modulated free space optical links over a Gamma-Gamma turbulence channel," *American Journal of Engineering and Applied Sciences*, vol. 4, no. 4, pp. 520–530, 2011.

[121] P. K. Mittal and K. C. Gupta, "An integral involving generalized function of two variables," *Proceedings of the Indian Academy of Sciences-Section A*, vol. 75, no. 3, pp. 117–123, Mar. 1972.

[122] K. P. Peppas, A. N. Stassinakis, G. K. Topalis, H. E. Nistazakis, and G. S. Tombras, "Average capacity of optical wireless communication systems over IK

atmospheric turbulence channels," *IEEE/OSA Journal of Optical Communications and Networking*, vol. 4, no. 12, pp. 1026–1032, Dec. 2012.

[123] S. C. Gupta, "Integrals involving products of G-functions," *Proceedings of the National Academy of Sciences, India*, vol. 39(A), no. II, 1969.

[124] I. S. Ansari, F. Yilmaz, and M.-S. Alouini, "Impact of pointing errors on the performance of mixed RF/FSO dual-hop transmission systems," *IEEE Wireless Communications Letters*, vol. 2, no. 3, pp. 351–354, Jun. 2013.

[125] N. D. Chatzidiamantis, K. G. Karagiannidis, E. E. Kriezis, and M. Matthaiou, "Diversity combining in hybrid RF/FSO systems with PSK modulation," in *Proceedings of IEEE International Conference on Communications (ICC' 2011)*, Kyoto, Japan, Jun. 2011, pp. 1–6.

[126] J. Libich, M. Mudroch, P. Dvorak, and S. Zvanovec, "Performance analysis of hybrid FSO/RF link," in *Proceedings of* 6^{th} *European Conference on Antennas and Propagation (EUCAP' 2012)*, Prague, Mar. 2012, pp. 1235–1238.

[127] F. Nadeem, E. Leitgeb, M. S. Awan, and G. Kandus, "FSO/RF hybrid network availability analysis under different weather condition," in *Proceedings of Third International Conference on Next Generation Mobile Applications, Services and Technologies (NGMAST' 2009)*, Cardiff, Wales, Sep. 2009, pp. 239–244.

[128] F. Nadeem, V. Kvicera, M. S. Awan, E. Leitgeb, S. S. Muhammad, and G. Kandus, "Weather effects on hybrid FSO/RF communication link," *IEEE Journal on Selected Areas in Communications*, vol. 27, no. 9, pp. 1687–1697, Dec. 2009.

[129] A. M. Mathai and R. K. Saxena, *Generalized Hypergeometric Functions with Applications in Statistics and Physical Sciences,* Lecture Notes in Mathematics, vol. 348. Springer-Verlang, 1973.

[130] M. D. Renzo, A. Guidotti, and G. E. Corazza, "Average rate of downlink heterogeneous cellular networks over generalized fading channels: a stochastic geometry approach," *IEEE Transactions on Communications*, vol. 61, no. 7, pp. 3050–3071, Jul. 2013.